GIVING SHAPE TO GENOMIC REGULATORY NETWORKS CONTROLLING CRANIOFACIAL AND ASYMMETRIC ORGAN MORPHOGENESIS

A Dissertation

Presented to the Faculty of the Graduate School

of Cornell University

In Partial Fulfillment of the Requirements for the Degree of

Doctor of Philosophy

by

Ian C. Welsh

February 2016

GIVING SHAPE TO GENOMIC REGULATORY NETWORKS CONTROLLING CRANIOFACIAL AND ASYMMETRIC ORGAN MORPHOGENESIS

Ian C. Welsh, Ph.D.

Cornell University 2016

Morphogenesis is the most critical and dynamic utilization of genomic information in the life history of an organism and a powerful system for advancing our understanding of genomic regulation and function. Stereotyped morphogenic processes provide an invaluable system for directly visualizing the functional activity of the genome via our ability to position its operational components relationally in space and time through the techniques of experimental embryology, molecular biology, and transcriptome analysis. Developmental genomics seeks to establish *in vivo* models to provide a cellular context where the causal relationships between the expression of key morphoregulatory genes, their transcriptional targets, and the morphogenic cellular behaviors that they control are easily determined, quantifiable, and amenable to experimental manipulation. In pursuit of this challenge, I have developed and characterized gene regulatory network models focused on two critical morphogenic processes, craniofacial development and asymmetric organ morphogenesis.

Formation of the vertebrate face requires the coordinated outgrowth and fusion of multiple paired prominences. How morphogenetic domains are integrated to coordinate craniofacial development is an important question, and while a number of

genes and pathways important for palate development have been identified, an understanding of how these signals are organized and integrated to achieve precise control of craniofacial development has been lacking. My analysis identifies a previously unrecognized growth zone responsible for periodic signaling center formation and the modular organization of developmentally important signaling genes and transcription factors (e.g. *Shh, Bmp4, Msx1, and Barx1*) in the developing palate. This newly identified growth zone provides a distributed system of common instructional cues that maintain growth of the secondary palate in proper registration with the surrounding elements of the upper jaw.

Patterning of the embryonic left-right axis is essential to directing the asymmetric growth and morphology of individual organs. Overall body situs and asymmetry of organ morphology is critical to normal function and regulated by the homeobox transcription factor *Pitx2*. Importantly however, the gene targets and cellular behaviors controlled by *Pitx2* to manifest asymmetry remain obscure. Using transcriptomics of the simple binary left-right organization of the dorsal mesentery (DM), I have elaborated and functionally characterized *Pitx2* dependent asymmetric cellular processes acting on very different scales of biological organization. At the tissue level I show that regulation of asymmetric intercellular signaling is a conserved mechanism through with Pitx2 manifests differential cellular behavior to achieve asymmetric organ growth. At the chromatin level, I have leveraged the novel finding that genes physically linked to Pitx2 exhibit complementary right-specific expression relative to left-sided Pitx2 in order to characterized the relationship between 3D chromatin folding and asymmetric gene expression from the *Pitx2* locus itself.

BIOGRAPHICAL SKETCH

Ian Welsh, better known as Oko to his beloved nieces Leilani and Violet, was born in Quincy Massachusetts but spent what he believes to be formative years living in the Middle East and traveling, for which he is grateful to his parents. Upon returning to the United States and completing high school on Cape Cod, he joined the United States Air Force when he realized that to pursuing an engineering degree was not likely to be a prudent use of time or money. In the Air Force, Ian was fortunate to be trained in nuclear chemistry and serve as an airborne scientific lab technician conducting special operations aerial sampling missions in support of nuclear test ban treating monitoring and ballistic missile tests, maintaining a Top Secret security clearance and deploying in support of Operation Desert Storm. While the travel, adventure, and camaraderie of the military was enjoyable, finding radioactive clouds to fly through and warheads to fly under did not seem viable long-term career goals. Following his discharge, Ian supported himself through his undergraduate education where he found a genuine interest in pursuit of the biological sciences. This interest became considerably more focused towards developmental genetics when given the opportunity to pursue an unprecedented level of independent research while working as a technician at the Jackson Laboratory in the lab of Tim O'Brien. Ian's career in science began at the dawn of the genomic era, and at this juncture he is both amazed and grateful to be in position to continue his exploration of processes through which a genome propagates life.

DEDICATION

I dedicate the work presented in this dissertation to my family: Robert and Nina who within in me mix and who've given me life, love, and the world; Kevin my brother, whose intelligence, vocabulary, and motorcycle I've always been trying to catch up to; my sister-in-law Jessica, a deeply caring and patient heart, and mother to my beautiful, endearingly individual, and intrepid nieces Leilani Jane and Violet Kailani.

ACKNOWLEDGMENTS

I am immensely grateful for Natasza Kurpios, my advisor and supplier of caffeine and fine Polish smoked sausage. Natasza provided me with a home in a lab when I needed one and opened doors I wouldn't otherwise have approached, her enthusiasm and passion for science, her patience, humor, and tremendous support have given me the confidence and encouragement to make the most of the opportunities I've been given.

I am also deeply appreciative of the other members of my committee, John Lis, Drew Noden, and John Schimenti, for their mentorship and willingness to share their time and tremendous wealth of intellectual and technical knowledge and academic insight.

TABLE OF CONTENTS

CHAPTER 1

Introduction

1.1 Preface

Morphogenesis represents the most critical and dynamic utilization of genomic information in the life history of an organism and thus a powerful system for advancing our understanding of genomic regulation and function. The author presents the following dissertation to represent his efforts to establish morphogenetic model systems to contribute to this understanding. The three main chapters represent independent manuscripts that have been submitted to peer reviewed journals for publication. The research presented in these manuscripts was performed by the author in the laboratories of two separate thesis advisors, each with distinct research programs. Therefore, preceding these main chapters is a background section summarizing the scientific perspective and conceptual framework that has guided the author in pursuit of his dissertation research. A concluding chapter follows the relatively stand-alone main chapters, in order to relate the work presented in the preceding chapters to outstanding questions and avenues of further investigation.

1.2 Background

The field of genetics is fundamentally the science of biological information. This information shapes the physical and physiological characteristics of individuals and is passed from parent to offspring to effect the characteristics of succeeding generations. Thus appropriately, genetic information has long been referred to as a blueprint or program for life itself. Indeed, Erwin Schrödinger originally referred to the nature of the genetic material as a “code-script” in his prescient “What is Life” lectures originally delivered 1943, well prior to the identification and elucidation of

the structure of DNA and subsequent eras of molecular genetics and genomics (Schrödinger 1944). Nowhere is this analogy more appreciable than during the process of embryonic development of multicellular organisms. During development, this genetic program directs the generation from a single cell, the fertilized egg, a myriad of cell types, each with specialized function but shared genetic material (Wolpert 1984). Ultimately, execution of this program choreographs the precise spatial organization of these cells in order to assemble the tissues, organs, and species-specific bauplan of an organism that is itself endowed with the capacity to propagate this genetic program to subsequent generations. Accordingly, failure to properly execute this program during development has serious consequences including aborted development, birth defects, disease, and cancer, while modulation of its deployment, within a constrained parameter space, provides the basis for deriving evolutionary novelty (Peter and Davidson 2011; Klingenberg 2010; Hall 2003).

With the advent of the era of molecular genetics, the functional output of the genome was largely viewed within the conceptual framework provided by the central dogma (DNA➔RNA➔Protein) (Crick 1970). Thus efforts of developmental geneticists to understand how genetic information directs the biological processes of embryonic development predominantly focused on the annotation and functional characterization of individual protein coding genes. This approach provided critical advances in our understanding of the mechanisms through which genetic information directs the elaboration of complex animal morphology. First applied to invertebrate model systems (i.e. *Drosophila melanogaster*), the program directing development could now be seen to be executed via the spatiotemporally ordered expression of

functionally diverse genes (i.e. transcription factors, intercellular signaling molecules, or structural proteins), whose activity is required for the patterning of the body plan and step-wise formation of individual body parts (Nüsslein-Volhard and Wieschaus 1980). Building on this work, vertebrate embryologists subsequently established that many developmental regulatory genes discovered in fly had identifiable homologs in human and mouse that played functionally conserved roles in the patterning and morphogenesis, even for that of analogous organs and body parts (Akam 1989; Rossant and Joyner 1989; Lu et al. 2000; Rincón-Limas et al. 1999; Chisaka and Capecchi 1991; Jordan et al. 1992).

Importantly, molecular genetics provided a basis for understanding of the mechanisms through which the cellular and tissue interactions illuminated by experimental embryologists a century earlier, coordinate morphogenesis in the developing embryo. Critical morphogenic interactions such as induction and competency could be characterized on the basis of protein function and molecular activity (Hamburger 1988). Moreover the concept of positional information, the spatial cues that are differentially interpreted across a field of cells as a means to generate complex morphological pattern (Wolpert 1969), could now be defined in terms of differential gene expression that establishes both morphogen gradients and threshold dependent responses in order to organize differential cellular behavior (Wolpert 1984, 2011; Green and Smith 1991). It is interesting to note that at the cellular level, the process of embryonic development ultimately involves only a handful of fundamentally different cellular behaviors (Fig. 1.1). During development cells can proliferate or die, maintain a progenitor state or differentiate, migrate,

adhere, or condense, undergo changes in shape or size, and remodel their extracellular environment (Kolega 1986; Chant and Stowers 1995; Dressler 2006; Harrison 1989; Wang and Steinbeisser 2009). The formation of individual body parts is defined by a distinct combination and ordering of these behaviors and it is differential gene expression that regulates the ability of cells to perform these behaviors and choreographs their execution in a precise temporal and spatial order.

An additional critical role of differential gene expression in regulating cellular

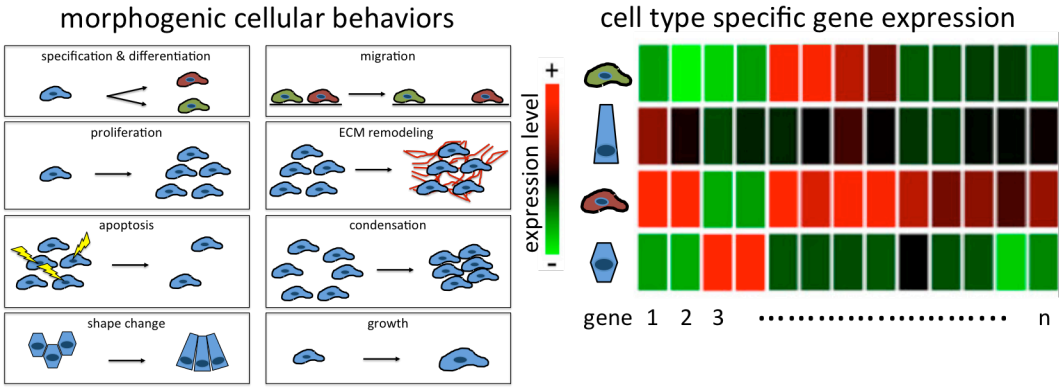

Figure 1.1 The generation of shape during development is derived from combinatorial deployment of only a handful of different cellular behaviors. Control of distinct cellular behavior is the result of differential gene expression.

behavior is establishing the spatial organization of core components of a handful of evolutionarily conserved developmental signaling pathways (Hedgehog (Hh), Wnt, receptor tyrosine kinase (RTK), TGF-β, nuclear receptor, Jak/STAT, and Notch) which are deployed repeatedly during development to coordinate intercellular communication and direct cellular behavior across a range of morphogenic contexts (Barolo and Posakony 2002). The localized expression of signaling pathway components (ligands, receptors, extracellular co-factors, and intracellular signaling intermediates and effectors) across a field of cells dictates what signals any given cell

can receive and/or transmit and thus which cells may be coupled via intercellular signaling (Jamora et al. 2003; Voas and Rebay 2004; Hubaud and Pourquie 2014; Brazil et al. 2015). Such communication is essential for regulating both protein activity and modulation of gene expression in space and time. Therefore, differential gene expression and intercellular signaling represent a major source of the cellular dynamics driving morphogenic processes (Barolo and Posakony 2002; Perrimon et al. 2012; Brazil et al. 2015).

Decades of experimental genetic analysis, performed in a host of model organisms and morphogenetic contexts has identified and functionally characterized a significant number of genes whose protein products are essential for normal embryonic development (Sönnichsen et al. 2005; Miklos and Rubin 1996; Spradling et al. 1999; Hentges et al. 2007). However, while individual genes may be critically required for normal development, it is clear that no single gene's function can entirely accomplish the task of directing development and that protein coding potential alone fails to fully define how the program directing development is physically manifest via information stored in DNA (Clamp et al. 2007; Taft et al. 2007). It is of note that protein coding genes represent less than 2% of most vertebrate genomes and of this, approximately 30% of genes are estimated to be of essential function (Clamp et al. 2007; Hentges et al. 2007). Interestingly, essential genes are disproportionately enriched for genes with developmental, transcriptional regulatory or cell signaling function, which as noted previously are used repeatedly during development and therefore exhibit complex spatiotemporal expression patterns (Davidson 2001). Significantly, loci with complex expression are characteristically associated with an

increased amount of flanking genomic real estate containing extensive blocks of evolutionary conserved noncoding sequence, implying functionally constrained sequence turnover (Nobrega et al. 2003; Ovcharenko et al. 2005; Narlikar and Ovcharenko 2009; Nelson et al. 2004; Siepel et al. 2005; Ponting and Hardison 2011). Indeed, experimental analyses routinely assigns cis-regulatory function to many conserved noncoding sequences, often as transcriptional enhancers with cell type specific activity related to the spatial expression of genes in the region (Pennacchio and Rubin 2001; Visel et al. 2007; Narlikar and Ovcharenko 2009).

Directing the expression of genes with critical developmental function typically involves the activity of multiple enhancer elements that individually contribute qualitative or quantitative input, and collectively define a gene's spatiotemporal expression pattern in toto (Bagheri-Fam et al. 2006; Montavon et al. 2011; Marinić et al. 2013). Moreover, while null coding mutations often highlight the pleiotropic function of developmentally essential genes, mutation of individual regulatory elements can have very targeted phenotypic consequences related to a restricted expression domain of a gene, further demonstrating the modular nature of cis-regulatory control (Shapiro et al. 2004, 2006). Importantly, cis-regulatory elements such as enhancers can be positioned at considerable distance from their target genes and function via looping of intervening chromatin to contact target promoters. The cis-regulatory genome therefore shapes not only spatial gene expression in the developing embryo but also the spatial organization of DNA within nuclei (de Laat and Duboule 2013; Phillips-Cremins et al. 2013; Bonora et al. 2014) and thus represents an essential source of genetic information integral the control of normal embryonic development.

Finally, the cis-regulatory genome is a largely unexplored landscape for understanding human disease (Bernstein et al. 2012; Weinhold et al. 2014), and provides a means to dissect mechanisms leading to the evolution of adaptive morphology (Wang and Chamberlin 2002; Wray 2007; Cleves et al. 2014), the conservation of regulatory function in the face of sequence variation (Tümpel et al. 2002; Stergachis et al. 2014; Cheng et al. 2014), and the paradoxical lack of correlation between organismal complexity and protein coding complexity (Taft et al. 2007).

This introduction began with restating the observation that hardwired within the sequence of a genome is the information necessary to encode the program of life and noting that the embryonic stages of an organism present the clearest manifestation of this program in action. When executed, this program directs the stereotyped development of structurally complex and species-specific morphology with remarkable fidelity and reproducibly across individual embryos of a given species. Dating back as far as Aristotle, the process of embryonic development has long held the fascination of man (Green and Sharpe 2015). During the late 1800's to early 1900's tremendous conceptual advances were made in the classical field of experimental embryology that subsequently yielded to the mechanistic insight of modern developmental biology and genetics. The former was characterized by a holistic approach with the ultimate goal of assigning causality to the self-organizing processes of embryogenesis (Hamburger 1988), and thus experimental embryologists were ostensibly early systems biologists. Developmental genetics on the other hand arose from the application of an increasingly reductionist approach to biological research fostered by molecular biology and biochemistry. We now possess a rich

catalogue of functionally annotated genomic sequences that contribute to embryonic development, attesting to the success of developmental genetics in the post-genomic era. However, the outstanding question remains, how might this extensive parts list be assembled into a rigorous representation of genomic information processing and the regulatory program controlling development?

The work of Eric Davidson stands out as notably prescient effort to synthesize a theoretical and experimental framework to understand the integrated regulation of genomic information and codify the physical basis of regulatory programs controlling animal development (Britten and Davidson 1969; Davidson and Britten 1971). Davidson's concept of developmental gene regulatory networks (GRNs) provides the means to make explicit the physical and logic processing components, akin to a computer's hardware and software, in terms of trans-regulatory factor activity, cis-regulatory inputs and processing, differential gene expression, and spatially regulated morphogenic cellular behavior (Davidson 2010).

The morphogenetic program directed by a GRN is accessed and deployed through the information encoded in DNA sequence in the form of protein coding genes, noncoding RNAs, and cis-regulatory elements (e.g. transcription factor binding sites, promoters, enhancers, and boundary or structural elements) that physically interact within the 3D space of the nucleus to coordinate transcription. Flanking each gene populating a GRN, individual cis-regulatory modules perform Boolean logic operations based on the binding of sequence specific regulatory proteins (i.e. cell type specific and signal dependent transcription factors) within in the network (Barolo and Posakony 2002; Stathopoulos and Levine 2005; Davidson 2010). The combinatorial

activity all cis-regulatory modules flanking a gene collectively define AND, OR, and NOT logic gates and thereby make explicit the conditional logic controlling the dynamic expression of a gene in a given developmental context or point in time (Yuh et al. 1998). The structure of GRNs can be represented in circuit wiring diagrams that capture the directionality of trans-regulatory interactions and cis-regulatory logic operations that define the dynamic behavior of a morphogenetic program (Fig. 1.2) and provide a rich source of testable hypotheses that may not be otherwise apparent.

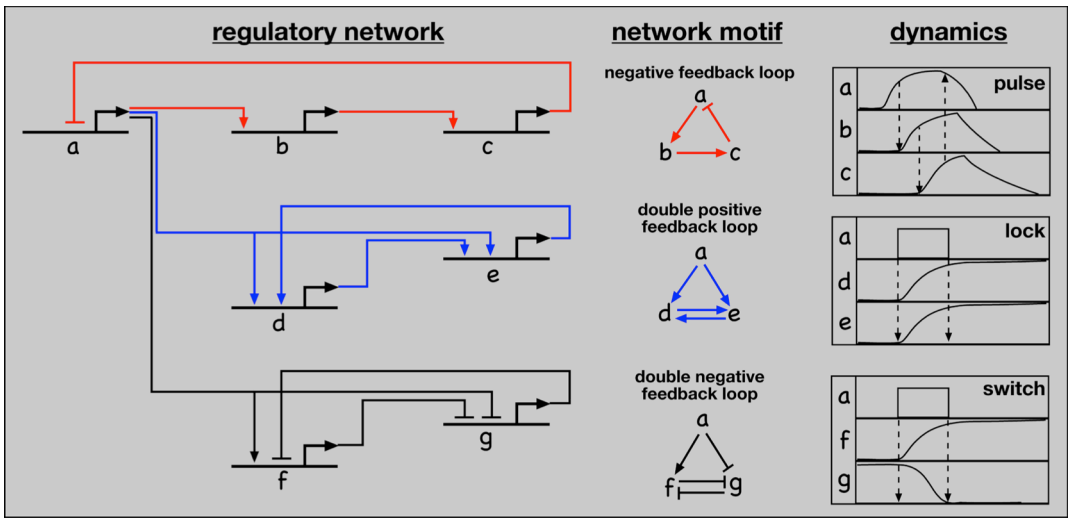

Figure 1.2. GRN circuits, logic processing, and the resulting gene expression dynamics.

Functionally, gene regulatory networks integrate cellular patterning and dynamic intercellular signaling, received as input from the network, and upon some logic operation, define the output of the genome in the form of quantifiable changes in the composition of a cell's transcriptome (Istrail and Davidson 2005). Importantly, GRNs define the regulatory interactions not only within a cell, but also the regulatory influence between cells. Hence, GRNs function during morphogenesis to integrate intercellular communication and patterning information at a local level to modulate global spatial gene expression and morphogenic cellular behavior and thereby direct

the step-wise formation of structure. In this way, development can be viewed to progress via a series of regulatory states, the sum of active transcriptional regulatory proteins in a cell at a given time. This regulatory state defines the gene expression profile and the morphogenic cellular behavior of the developing structure, which in turn influences the subsequent regulatory state to drive morphogenesis inexorably forward.

In pursuit of my dissertation research, I have worked to apply a GRN level perspective in the development and analysis of models of genomic regulation of morphogenesis. Importantly, it is the stereotyped morphogenic processes within the developing embryo that provides an essential 3-dimensional reference frame with which to bring into coherent resolution spatially and temporally distributed GRN activity. The techniques of experimental embryology, molecular biology, genetics, and transcriptome analysis provide the ability to map regulatory activity and transcriptional output onto anatomically referenced cellular behavior and tissue level dynamics of a developing structure.

In application this approach aims establish how genomic information is deployed and processed by defining the spatial organization of lineage restricted transcription factor and intercellular signaling component expression, and if available, the activity of associated cis-regulatory elements. The spatial organization and regulatory hierarchy of this genomic activity informs and is informed by differential cellular behavior in relation to the anatomical organization of the developing structure. The application of this experimental approached is exemplified in chapters 2-4. Finally, the stereotypical nature of morphogenesis allows the temporal dynamics of

the developing system to be revealed via the generation of reconstructed time series from multiple embryos of incrementally advanced stages, an approach highlighted in chapter 2.

1.3 Rationale

Signaling interactions and the coordinated control of craniofacial development

Orofacial anomalies and cleft palate are among the most common birth defects, affecting over 6,000 newborns in the U.S. each year (www.marchofdimes.com). The association of facial clefting with a large number of syndromes, along with high sporadic incidence, emphasizes the sensitivity of craniofacial development to genetic and environmental insults and reflects a complex series of morphogenic movements and tissue interactions. A common strategy during morphogenesis, including that of the head and face, is to organize signaling dynamics into spatial domains defined by reciprocal interactions between adjacent epithelial and mesenchymal tissues (Gritli-Linde 2007). Craniofacial morphogenesis requires coordination between a surface layer of epithelium covering the predominantly cranial neural crest (CNC) derived mesenchyme of the pharyngeal arches, paired structures that will form the bulk of the face, jaw, and neck.

A network of signaling interactions instructs the outgrowth and midline fusion of these paired facial primordia as well as the movements and shape changes that accompany the growth of paired maxillary shelves that will form the secondary palate. Initially, the palatal shelves extend vertically to flank the tongue. Subsequent rotation, elevation, and medially directed growth bring the bilateral shelves in contact at the

midline where they fuse to separate the oral and nasal cavities. Importantly, the medial growth of the palatal shelves must also be coordinated with the elongation and patterning of the upper jaw. Thus, development of the face and palate requires the integration of the three dimensional outgrowth of multiple primordia with orchestrated movements that bring these structures together to complete the formation of the head and face. Alteration of the temporal control of the outgrowth and movement of these structures results in defects in craniofacial morphogenesis.

Studies have advanced the idea that regional differences in gene expression and signaling responsiveness along the anterior posterior axis of the palatal shelf play a critical role in patterning and coordinating growth (Hilliard et al. 2005). However, how the expression of genes with critical function during palate development is globally organized and its relationship to regional patterning and coordination of palate and facial development has been lacking. Furthermore, the cellular and genomic regulatory basis of these regional differences is poorly understood.

Building on initial observations published in 2007 (Welsh et al. 2007), work presented in Chapter 2 reports the systematic study of spatial gene expression in the palate which led to the identification and genetic characterization of a previously unrecognized morphogenetic domain of secondary palate, the rugae growth zone (Welsh and O'Brien 2009). It is demonstrated that this region of the palate functions to integrate intercellular signaling in order to generate a reiterated pattern of *Shh* expressing signaling centers called rugae. The periodic formation of these signaling centers coincides with the anterior growth of the mid-facial complex. Importantly, it is also shown that a network of genes, known to play critical roles in the three

dimensional growth and patterning of the palatal shelves, is organized into complementary rugae and inter-rugae expression domains. This segmental organization arises from epithelial mesenchymal interactions that direct periodic cell cycle exit and signaling center formation within the rugae growth zone. It is proposed that the periodic formation and modular organization of rugae signaling domains provides a distributed system of common instructional cues that maintain growth of the secondary palate in proper registration with the surrounding elements of the upper jaw.

Pitx2 dependent tissue and chromatin level asymmetries associated with left-right organ morphogenesis

During morphogenesis, interactions between the gut endoderm and lateral splanchnic mesoderm generates the form and function of the majority of organs within the body cavity. The anterior-posterior patterned endoderm defines the A-P position of organ primordia, while the left-right patterned lateral mesoderm instructs the asymmetry of organ form and its placement within the body cavity (Zorn and Wells 2009; Burn and Hill 2009). The transcriptional and signaling interactions that direct patterning and subsequent differentiation of individual organ primordia have been extensively elaborated (Kim et al. 2005; van den Brink 2007). Less well understood are the cellular mechanisms that sculpt individual organ shape, where advancement is hampered by a lack of experimentally accessible models and the complex 3-dimensional growth of many organs (Zorn and Wells 2009; Shiratori and Hamada 2006; Shiratori et al. 2006).

The gastrointestinal (GI) tract develops with a characteristic left-right asymmetry that is critical for normal organ function and body situs. Failure to achieve proper gut chirality can have serious consequences, resulting in gut malrotation and life threatening birth defects such as midgut volvulus (Applegate et al. 1999; Applegate 2009). The dorsal mesentery (DM), which suspends the gut tube from the dorsal body wall, consists of four cellular compartments readily identifiable in their distribution across the left-right (L-R) axis. Left-right differences in cell shape and behavior in these compartments are downstream of the left-specific transcription factor *Pitx2* and play a central role in the transfer of asymmetric patterning information from the lateral plate mesoderm (LPM) to the developing gut tube that is required for establishing proper gut situs (Davis et al. 2008; Kurpios et al. 2008). Significantly, although over a decade's worth of research has extensively elaborated the early molecular cascades responsible for patterning the left-right axis and despite the seriousness of birth defects that arise from failure to establish proper body situs, the cellular mechanisms responsible for translating L-R patterning into asymmetric organ growth are largely unknown (Shiratori and Hamada 2006).

In the lab of Natasza Kurpios, I have taken advantage of the unique features of the DM, where focus is efficiently placed on binary left versus right differences in the development and function of readily identifiable cellular compartments, to further define the molecular composition of the DM and identify the cellular mechanisms through which *Pitx2* drives asymmetric organ development. In order to define the molecular and cellular mechanisms through which *Pitx2* directs asymmetry, Natasza has previously generated microarray profiles of the cellular compartments comprising

the DM. My research based on these data provides novel insight into mechanisms, acting on very different scales of organization, which produce morphological asymmetry.

Chapter 3 details the tissue level organization and functionally characterization of a network of genes involved in Wnt signaling which that is differentially organized across the L-R axis of the DM (Welsh et al. 2013). Seeking to understand how intercellular communication is organized in the DM, from the microarray data I found that expression of genes involved in the activation and cellular response to noncanonical WNT signaling, is exclusive to the left DM. Conversely, expression of the secreted WNT antagonists is restricted to the right DM. Using targeted gene misexpression and genetic analyses, I show that genes which positively regulate noncanonical Wnt signaling are *Pitx2* targets. Through these targets, *Pitx2* potentiates Wnt dependent activation of the formin protein Daam2, a regulator of actin cytoskeleton and key Wnt effector. Experiments in vivo and in vitro of Daam2 link actin dynamics to cadherin-

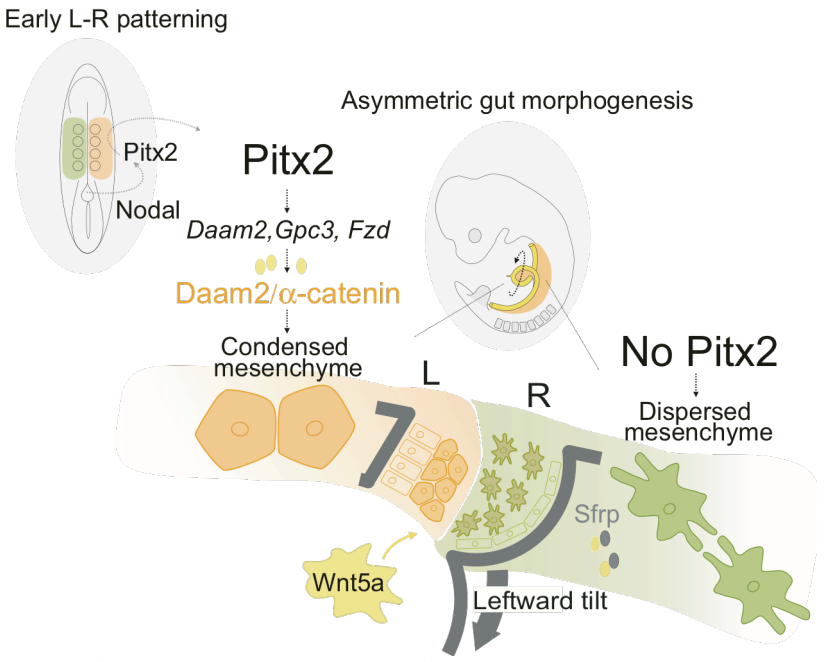

Figure 1.3. Tissue level integration of L-R patterning and WNT signaling drives cellular asymmetry in the DM.

based junctions, to drive asymmetric cell adhesion in the DM (Fig 1.3). This work highlights a conserved tissue level integration of L-R patterning with intercellular signaling that provides a mechanism through which *Pitx2* physically manifests L-R differences in cellular architecture to orchestrate asymmetric organ growth.

Arising from the identification of an unexpected and novel pattern of complementary spatial expression across the L-R axis of genes from the *Pitx2* locus itself, Chapter 4 characterizes the chromosomal level organization of asymmetric gene expression (Welsh et al., in review Developmental Cell). Remarkably, genes physically linked to *Pitx2*, including an uncharacterized gene proximally positioned at the boundary of a large (~600kb) gene desert flanked distally by *Pitx2*, exhibit right specific expression relative to left-specific expression of *Pitx2*. GRO-seq analysis of nascent transcription of the locus in the left vs right DM identified a unique regulatory element, e926, with binary left-right activity, acting as a left-specific enhancer and a right-specific promoter for a conserved long noncoding RNA (lncRNA) whose expression is negatively regulated by *Pitx2*. Fluorescent in situ hybridization (FISH), demonstrates the binary L-R cellular organization and asymmetric gene expression of the DM is mirrored by subtle *Pitx2* dependent differences in 3D nuclear architecture. This work establishes the *Pitx2* locus as a powerful experimental system for studying the structural and regulatory genomic basis of L-R patterning, currently an entirely unexplored avenue of research. For example, mutations within the human *PITX2* gene are associated with Axenfeld-Rieger Syndrome (ARS) characterized by mental retardation, craniofacial birth defects and umbilical hernias. Importantly, screening of ARS patients has identified individuals who possess no mutations in *PITX2* coding

sequences but who harbor lesions within the adjacent gene desert devoid of coding genes, supporting an essential role for cis-regulatory sequences within the desert in driving *PITX2* expression.

REFERENCES

Akam M. 1989. Hox and HOM: homologous gene clusters in insects and vertebrates. *Cell* **57**: 347–349.

Anderson E, Devenney PS, Hill RE, Lettice LA. 2014. Mapping the Shh long-range regulatory domain. *Development*. http://dev.biologists.org/content/early/2014/09/24/dev.108480.abstract.

Applegate K. 2009. Evidence-based diagnosis of malrotation and volvulus. *Pediatr Radiol* **39**: 161–163. http://dx.doi.org/10.1007/s00247-009-1177-x.

Applegate KE, Goske MJ, Pierce G, Murphy D. 1999. Situs Revisited: Imaging of the Heterotaxy Syndrome. *RadioGraphics* **19**: 837–852. http://dx.doi.org/10.1148/radiographics.19.4.g99jl31837.

Attanasio C, Nord AS, Zhu Y, Blow MJ, Li Z, Liberton DK, Morrison H, Plajzer-Frick I, Holt A, Hosseini R, et al. 2013. Fine tuning of craniofacial morphology by distant-acting enhancers. *Science* **342**: 1241006. http://www.pubmedcentral.nih.gov/articlerender.fcgi?artid=3991470&tool=pmcentrez&rendertype=abstract.

Bagheri-Fam S, Barrionuevo F, Dohrmann U, Günther T, Schüle R, Kemler R, Mallo M, Kanzler B, Scherer G. 2006. Long-range upstream and downstream enhancers control distinct subsets of the complex spatiotemporal Sox9 expression pattern. *Dev Biol* **291**: 382–397.

Barolo S, Posakony JW. 2002. Three habits of highly effective signaling pathways: principles of transcriptional control by developmental cell signaling. *Genes Dev* **16** : 1167–1181. http://genesdev.cshlp.org/content/16/10/1167.short.

Bernstein BE, Birney E, Dunham I, Green ED, Gunter C, Snyder M. 2012. An integrated encyclopedia of DNA elements in the human genome. *Nature* **489**: 57–74. http://dx.doi.org/10.1038/nature11247.

Biswas D, Milne TA, Basrur V, Kim J, Elenitoba-Johnson KSJ, Allis CD, Roeder RG. 2011. Function of leukemogenic mixed lineage leukemia 1 (MLL) fusion proteins through distinct partner protein complexes. *Proc Natl Acad Sci* **108**: 15751–15756.

Bitoun E, Oliver PL, Davies KE. 2007. The mixed-lineage leukemia fusion partner AF4 stimulates RNA polymerase II transcriptional elongation and mediates coordinated chromatin remodeling. *Hum Mol Genet* **16**: 92–106.

Bonn S, Zinzen RP, Girardot C, Gustafson EH, Perez-Gonzalez A, Delhomme N, Ghavi-Helm Y, Wilczyński B, Riddell A, Furlong EEM. 2012. Tissue-specific analysis of chromatin state identifies temporal signatures of enhancer activity during embryonic development. *Nat Genet* **44**: 148–156.

Bonora G, Plath K, Denholtz M. 2014. A mechanistic link between gene regulation and genome architecture in mammalian development. *Curr Opin Genet Dev* **27**: 92–101.

Brazil DP, Church RH, Surae S, Godson C, Martin F. 2015. BMP signalling: agony and antagony in the family. *Trends Cell Biol* **25**: 249–264. http://www.sciencedirect.com/science/article/pii/S0962892414002141.

Britten RJ, Davidson EH. 1969. Gene Regulation for Higher Cells: A Theory. *Sci* **165** : 349–357. http://www.sciencemag.org/content/165/3891/349.short.

Burn SF, Hill RE. 2009. Left-right asymmetry in gut development: What happens next? *BioEssays* **31**: 1026–1037.

Cajiao I, Zhang A, Yoo EJ, Cooke NE, Liebhaber SA. 2004. Bystander gene activation by a locus control region. *EMBO J* **23**: 3854–3863.

Chant J, Stowers L. 1995a. GTPase cascades choreographing cellular behavior: Movement, morphogenesis, and more. *Cell* **81**: 1–4. http://www.sciencedirect.com/science/article/pii/0092867495903631.

Cheng Y, Ma Z, Kim B-H, Wu W, Cayting P, Boyle AP, Sundaram V, Xing X, Dogan N, Li J, et al. 2014. Principles of regulatory information conservation between mouse and human. *Nature* **515**: 371–375. http://dx.doi.org/10.1038/nature13985.

Chisaka O, Capecchi MR. 1991. Regionally restricted developmental defects resulting from targeted disruption of the mouse homeobox gene hox-1.5. *Nature* **350**: 473–479.

Clamp M, Fry B, Kamal M, Xie X, Cuff J, Lin MF, Kellis M, Lindblad-Toh K, Lander ES. 2007. Distinguishing protein-coding and noncoding genes in the human genome. *Proc Natl Acad Sci U S A* **104**: 19428–19433.

Cleves PA, Ellis NA, Jimenez MT, Nunez SM, Schluter D, Kingsley DM, Miller CT. 2014. Evolved tooth gain in sticklebacks is associated with a cis-regulatory allele of Bmp6. *Proc Natl Acad Sci* **111** : 13912–13917. http://www.pnas.org/content/111/38/13912.abstract.

Core LJ, Martins AL, Danko CG, Waters CT, Siepel A, Lis JT. 2014. Analysis of nascent RNA identifies a unified architecture of initiation regions at mammalian promoters and enhancers. *Nat Genet* **46**: 1311–1320. http://dx.doi.org/10.1038/ng.3142.

Core LJ, Waterfall JJ, Lis JT. 2008. Nascent RNA sequencing reveals widespread pausing and divergent initiation at human promoters. *Science* **322**: 1845–1848.

Creyghton MP, Cheng AW, Welstead GG, Kooistra T, Carey BW, Steine EJ, Hanna J, Lodato MA, Frampton GM, Sharp PA, et al. 2010. Histone H3K27ac separates active from poised enhancers and predicts developmental state. *Proc Natl Acad Sci U S A* **107**: 21931–21936.

Crick F. 1970. Central dogma of molecular biology. *Nature* **227**: 561–563.

Danko CG, Hyland SL, Core LJ, Martins AL, Waters CT, Lee HW, Cheung VG, Kraus WL, Lis JT, Siepel A. 2015. Identification of active transcriptional regulatory elements from GRO-seq data. *Nat Meth* **12**: 433–438. http://dx.doi.org/10.1038/nmeth.3329.

Davidson EH. 2001. *Genomic Regulatory Systems: In Development and Evolution*. Elsevier Science https://books.google.com/books?id=jC3h4teINFoC.

Davidson EH. 2010. *The Regulatory Genome: Gene Regulatory Networks In Development And Evolution*. Elsevier Science http://books.google.com/books?id=F2ibJj1LHGEC.

Davidson EH, Britten RJ. 1971. Note on the control of gene expression during development. *J Theor Biol* **32**: 123–130. http://www.sciencedirect.com/science/article/pii/0022519371901408.

Davis NM, Kurpios NA, Sun X, Gros J, Martin JF, Tabin CJ. 2008. The Chirality of Gut Rotation Derives from Left-Right Asymmetric Changes in the Architecture of the Dorsal Mesentery. *Dev Cell* **15**: 134–145.

De Laat W, Duboule D. 2013. Topology of mammalian developmental enhancers and their regulatory landscapes. *Nature* **502**: 499–506. http://www.ncbi.nlm.nih.gov/pubmed/24153303.

Dixon JR, Selvaraj S, Yue F, Kim A, Li Y, Shen Y, Hu M, Liu JS, Ren B. 2012. Topological domains in mammalian genomes identified by analysis of chromatin interactions. *Nature* **485**: 376–380.

Dressler GR. 2006. The cellular basis of kidney development. *Annu Rev Cell Dev Biol* **22**: 509–529.

Drissen R, Palstra R-J, Gillemans N, Splinter E, Grosveld F, Philipsen S, de Laat W. 2004. The active spatial organization of the beta-globin locus requires the transcription factor EKLF. *Genes Dev* **18**: 2485–2490.

Duboc V, Röttinger E, Lapraz F, Besnardeau L, Lepage T. 2005. Left-right asymmetry in the sea urchin embryo is regulated by nodal signaling on the right side. *Dev Cell* **9**: 147–58. http://www.sciencedirect.com/science/article/pii/S1534580705001772 (Accessed September 16, 2014).

Flajollet S, Rachez C, Ploton M, Schulz C, Gallais R, Métivier R, Pawlak M, Leray A, Issulahi AA, Héliot L, et al. 2013. The Elongation Complex Components BRD4 and MLLT3/AF9 Are Transcriptional Coactivators of Nuclear Retinoid Receptors. *PLoS One* **8**.

Flomen RH, Vatcheva R, Gorman PA, Baptista PR, Groet J, Barišić I, Ligutic I, Nižetić D. 1998. Construction and Analysis of a Sequence-Ready Map in 4q25: Rieger Syndrome Can Be Caused by Haploinsufficiency of RIEG, but Also by Chromosome Breaks ≈90 kb Upstream of This Gene. *Genomics* **47**: 409–413. http://www.sciencedirect.com/science/article/pii/S0888754397951272.

Franco D, Campione M. 2003. The role of Pitx2 during cardiac development: Linking left-right signaling and congenital heart diseases. *Trends Cardiovasc Med* **13**: 157–163.

Ghavi-Helm Y, Klein FA, Pakozdi T, Ciglar L, Noordermeer D, Huber W, Furlong EEM. 2014. Enhancer loops appear stable during development and are associated with paused polymerase. *Nature*. http://www.ncbi.nlm.nih.gov/pubmed/25043061.

Green JB, Smith JC. 1991. Growth factors as morphogens: do gradients and thresholds establish body plan? *Trends Genet* **7**: 245–250.

Green JBA, Sharpe J. 2015. Positional information and reaction-diffusion: two big ideas in developmental biology combine. *Dev* **142** : 1203–1211. http://dev.biologists.org/content/142/7/1203.abstract.

Gritli-Linde A. 2007. Molecular control of secondary palate development. *Dev Biol* **301**: 309–326.

Grote P, Herrmann BG. 2013. The long non-coding RNA Fendrr links epigenetic control mechanisms to gene regulatory networks in mammalian embryogenesis. *RNA Biol* **10**: 1579–1585. http://www.ncbi.nlm.nih.gov/pubmed/24036695.

Grote P, Wittler L, Hendrix D, Koch F, Währisch S, Beisaw A, Macura K, Bläss G, Kellis M, Werber M, et al. 2013. The Tissue-Specific lncRNA Fendrr Is an Essential Regulator of Heart and Body Wall Development in the Mouse. *Dev Cell* **24**: 206–214.

Hall BK. 2003. Evo-Devo: evolutionary developmental mechanisms. *Int J Dev Biol* **47**: 491–495. http://www.ncbi.nlm.nih.gov/entrez/query.fcgi?cmd=Retrieve&db=PubMed&dopt=Citation&list_uids=14756324.

Hamburger V. 1988. *The Heritage of Experimental Embryology: Hans Spemann and the Organizer*. Oxford University Press http://books.google.com/books?id=4vBqAAAAMAAJ.

Hamburger V, Hamilton HL. 1951. A series of normal stages in the development of the chick embryo. *J Morphol* **88**: 49–92.

Harrison F. 1989. The extracellular matrix and cell surface, mediators of cell interactions in chicken gastrulation. *Int J Dev Biol* **33**: 417–438.

Hentges KE, Pollock DD, Liu B, Justice MJ. 2007. Regional variation in the density of essential genes in mice. *PLoS Genet* **3**: 661–664.

Hilliard SA, Yu L, Gu S, Zhang Z, Chen YP. 2005. Regional regulation of palatal growth and patterning along the anterior-posterior axis in mice. *J Anat* **207**: 655–667.

Hubaud A, Pourquie O. 2014. Signalling dynamics in vertebrate segmentation. *Nat Rev Mol Cell Biol* **15**: 709–721. http://dx.doi.org/10.1038/nrm3891.

Istrail S, Davidson EH. 2005. Logic functions of the genomic cis-regulatory code. *Proc Natl Acad Sci U S A* **102**: 4954–4959.

Jamora C, DasGupta R, Kocieniewski P, Fuchs E. 2003. Links between signal transduction, transcription and adhesion in epithelial bud development. *Nature* **422**: 317–322.

Jin F, Li Y, Dixon JR, Selvaraj S, Ye Z, Lee AY, Yen C-A, Schmitt AD, Espinoza C a, Ren B. 2013. A high-resolution map of the three-dimensional chromatin interactome in human cells. *Nature* **503**: 290–4. http://www.pubmedcentral.nih.gov/articlerender.fcgi?artid=3838900&tool=pmcentrez&rendertype=abstract.

Jones B, Su H, Bhat A, Lei H, Bajko J, Hevi S, Baltus GA, Kadam S, Zhai H, Valdez R, et al. 2008. The histone H3K79 methyltransferase Dot1L is essential for mammalian development and heterochromatin structure. *PLoS Genet* **4**.

Jordan T, Hanson I, Zaletayev D, Hodgson S, Prosser J, Seawright A, Hastie N, van Heyningen V. 1992. *The human PAX6 gene is mutated in two patients with aniridia*.

Jugessur A, Murray JC. 2005. Orofacial clefting: Recent insights into a complex trait. *Curr Opin Genet Dev* **15**: 270–278.

Kagey MH, Newman JJ, Bilodeau S, Zhan Y, Orlando DA, van Berkum NL, Ebmeier CC, Goossens J, Rahl PB, Levine SS, et al. 2010. Mediator and cohesin connect gene expression and chromatin architecture. *Nature* **467**: 430–435.

Kampstra P. 2008. Beanplot : A Boxplot Alternative for Visual Comparison of Distributions. *J Stat Softw* **28**: 1–9. http://www.jstatsoft.org/v28/c01/paper.

Kikuta H, Laplante M, Navratilova P, Komisarczuk AZ, Engström PG, Fredman D, Akalin A, Caccamo M, Sealy I, Howe K, et al. 2007. Genomic regulatory blocks encompass multiple neighboring genes and maintain conserved synteny in vertebrates. *Genome Res* **17**: 545–555.

Kim BM, Buchner G, Miletich I, Sharpe PT, Shivdasani RA. 2005. The stomach mesenchymal transcription factor barx1 specifies gastric epithelial identity through inhibition of transient Wnt signaling. *Dev Cell* **8**: 611–622.

Kim SK, Jung I, Lee H, Kang K, Kim M, Jeong K, Kwon CS, Han YM, Kim YS, Kim D, et al. 2012. Human histone H3K79 methyltransferase DOT1L

methyltransferase binds actively transcribing RNA polymerase II to regulate gene expression. *J Biol Chem* **287**: 39698–39709.

Klingenberg CP. 2010. Evolution and development of shape: integrating quantitative approaches. *Nat Rev Genet* **11**: 623–635.

Kolega J. 1986. The cellular basis of epithelial morphogenesis. *Dev Biol (N Y 1985)* **2**: 103–143. http://www.ncbi.nlm.nih.gov/entrez/query.fcgi?cmd=Retrieve&db=PubMed&dopt=Citation&list_uids=3078113.

Kurpios NA, Ibañes M, Davis NM, Lui W, Katz T, Martin JF, Belmonte JCI, Tabin CJ. 2008. The direction of gut looping is established by changes in the extracellular matrix and in cell:cell adhesion. *Proc Natl Acad Sci* **105** : 8499–8506. http://www.pnas.org/content/105/25/8499.abstract.

Lettice LA, Horikoshi T, Heaney SJH, van Baren MJ, van der Linde HC, Breedveld GJ, Joosse M, Akarsu N, Oostra BA, Endo N, et al. 2002. Disruption of a long-range cis-acting regulator for Shh causes preaxial polydactyly. *Proc Natl Acad Sci U S A* **99**: 7548–7553.

Liu C, Liu W, Lu MF, Brown NA, Martin JF. 2001. Regulation of left-right asymmetry by thresholds of Pitx2c activity. *Development* **128**: 2039–2048.

Liu W, Ma Q, Wong K, Li W, Ohgi K, Zhang J, Aggarwal AK, Rosenfeld MG. 2013. Brd4 and JMJD6-associated anti-pause enhancers in regulation of transcriptional pause release. *Cell* **155**: 1581–1595.

Logan M, Pagán-Westphal SM, Smith DM, Paganessi L, Tabin CJ. 1998. The transcription factor pitx2 mediates situs-specific morphogenesis in response to left-right asymmetric signals. *Cell* **94**: 307–317.

Lu CH, Rincón-Limas DE, Botas J. 2000. Conserved overlapping and reciprocal expression of msh/Msx1 and apterous/Lhx2 in Drosophila and mice. *Mech Dev* **99**: 177–181.

Lu MF, Pressman C, Dyer R, Johnson RL, Martin JF. 1999. Function of Rieger syndrome gene in left-right asymmetry and craniofacial development. *Nature* **401**: 276–278.

Mahadevan A, Welsh IC, Sivakumar A, Gludish DWW, Shilvock ARR, Noden DMM, Huss D, Lansford R, Kurpios NAA. 2014. The Left-Right Pitx2 Pathway Drives Organ-Specific Arterial and Lymphatic Development in the Intestine. *Dev Cell* **31**: 690–706. http://www.cell.com/article/S1534580714006959/fulltext (Accessed December 11, 2014).

Marinić M, Aktas T, Ruf S, Spitz F. 2013. An Integrated Holo-Enhancer Unit Defines Tissue and Gene Specificity of the Fgf8 Regulatory Landscape. *Dev Cell* **24**: 530–542.

Melgar MF, Collins FS, Sethupathy P. 2011. Discovery of active enhancers through bidirectional expression of short transcripts. *Genome Biol* **12**: R113.

Miklos GLG, Rubin GM. 1996. The Role of the Genome Project in Determining Gene Function: Insights from Model Organisms. *Cell* **86**: 521–529. http://www.sciencedirect.com/science/article/pii/S0092867400801269.

Montavon T, Soshnikova N, Mascrez B, Joye E, Thevenet L, Splinter E, De Laat W, Spitz F, Duboule D. 2011. A regulatory archipelago controls hox genes transcription in digits. *Cell* **147**: 1132–1145.

Narlikar L, Ovcharenko I. 2009. Identifying regulatory elements in eukaryotic genomes. *Briefings Funct Genomics Proteomics* **8**: 215–230.

Nelson CE, Hersh BM, Carroll SB. 2004. The regulatory content of intergenic DNA shapes genome architecture. *Genome Biol* **5**: R25.

Nobrega MA, Ovcharenko I, Afzal V, Rubin EM. 2003. Scanning Human Gene Deserts for Long-Range Enhancers. *Sci* **302** : 413. http://www.sciencemag.org/content/302/5644/413.short.

Nora EP, Dekker J, Heard E. 2013. Segmental folding of chromosomes: A basis for structural and regulatory chromosomal neighborhoods? *BioEssays* **35**: 818–828.

Nüsslein-Volhard C, Wieschaus E. 1980. Mutations affecting segment number and polarity in Drosophila. *Nature* **287**: 795–801.

Ovcharenko I, Loots GG, Nobrega MA, Hardison RC, Miller W, Stubbs L. 2005. Evolution and functional classification of vertebrate gene deserts. *Genome Res* **15**: 137–145.

Pennacchio LA, Rubin EM. 2001. Genomic strategies to identify mammalian regulatory sequences. *Nat Rev Genet* **2**: 100–109. http://dx.doi.org/10.1038/35052548.

Perrimon N, Pitsouli C, Shilo B-Z. 2012. Signaling mechanisms controlling cell fate and embryonic patterning. *Cold Spring Harb Perspect Biol* **4**: a005975. http://www.pubmedcentral.nih.gov/articlerender.fcgi?artid=3405863&tool=pmcentrez&rendertype=abstract.

Peter IS, Davidson EH. 2011. Evolution of gene regulatory networks controlling body plan development. *Cell* **144**: 970–985.

Phillips-Cremins JE, Sauria MEG, Sanyal A, Gerasimova TI, Lajoie BR, Bell JSK, Ong CT, Hookway TA, Guo C, Sun Y, et al. 2013. Architectural protein subclasses shape 3D organization of genomes during lineage commitment. *Cell* **153**: 1281–1295.

Pina C, May G, Soneji S, Hong D, Enver T. 2008. MLLT3 Regulates Early Human Erythroid and Megakaryocytic Cell Fate. *Cell Stem Cell* **2**: 264–273.

Ponting CP, Hardison R. 2011. What fraction of the human genome is functional? *Genome Res* 1769–1776. http://www.ncbi.nlm.nih.gov/pubmed/21875934.

Rainger JK, Bhatia S, Bengani H, Gautier P, Rainger J, Pearson M, Ansari M, Crow J, Mehendale F, Palinkasova B, et al. 2014. Disruption of SATB2 or its long-range

cis-regulation by SOX9 causes a syndromic form of Pierre Robin sequence. *Hum Mol Genet* **23**. http://www.ncbi.nlm.nih.gov/pubmed/24363063.

Razin S V., Gavrilov AA, Pichugin A, Lipinski M, Iarovaia O V., Vassetzky YS. 2011. Transcription factories in the context of the nuclear and genome organization. *Nucleic Acids Res* **39**: 9085–9092.

Reis LM, Tyler RC, Volkmann Kloss BA, Schilter KF, Levin A V, Lowry RB, Zwijnenburg PJG, Stroh E, Broeckel U, Murray JC, et al. 2012. PITX2 and FOXC1 spectrum of mutations in ocular syndromes. *Eur J Hum Genet*.

Rincón-Limas DE, Lu CH, Canal I, Calleja M, Rodríguez-Esteban C, Izpisúa-Belmonte JC, Botas J. 1999. Conservation of the expression and function of apterous orthologs in Drosophila and mammals. *Proc Natl Acad Sci U S A* **96**: 2165–2170.

Rinn JL, Chang HY. 2012. Genome Regulation by Long Noncoding RNAs. *Annu Rev Biochem* **81**: 145–166.

Rossant J, Joyner AL. 1989. Towards a molecular-genetic analysis of mammalian development. *Trends Genet* **5**: 277–283.

Ryan AK, Blumberg B, Rodriguez-Esteban C, Yonei-Tamura S, Tamura K, Tsukui T, de la Peña J, Sabbagh W, Greenwald J, Choe S, et al. 1998. Pitx2 determines left-right asymmetry of internal organs in vertebrates. *Nature* **394**: 545–551.

Schaukowitch K, Joo J-Y, Liu X, Watts JK, Martinez C, Kim T-K. 2014. Enhancer RNA Facilitates NELF Release from Immediate Early Genes. *Mol Cell* **56**: 29–42. http://www.cell.com/article/S1097276514006789/fulltext (Accessed September 25, 2014).

Schrödinger E. 1944. *What is Life?: The Physical Aspect of the Living Cell*. The University Press http://books.google.com/books?id=154CAAAAMAAJ.

Semina E V, Reiter R, Leysens NJ, Alward WL, Small KW, Datson NA, Siegel-Bartelt J, Bierke-Nelson D, Bitoun P, Zabel BU, et al. 1996. Cloning and

characterization of a novel bicoid-related homeobox transcription factor gene, RIEG, involved in Rieger syndrome. *Nat Genet* **14**: 392–399.

Shapiro MD, Bell MA, Kingsley DM. 2006. Parallel genetic origins of pelvic reduction in vertebrates. *Proc Natl Acad Sci U S A* **103**: 13753–13758.

Shapiro MD, Marks ME, Peichel CL, Blackman BK, Nereng KS, Jónsson B, Schluter D, Kingsley DM. 2004. Genetic and developmental basis of evolutionary pelvic reduction in threespine sticklebacks. *Nature* **428**: 717–723.

Shen Y, Yue F, McCleary DF, Ye Z, Edsall L, Kuan S, Wagner U, Dixon J, Lee L, Lobanenkov V V., et al. 2012. A map of the cis-regulatory sequences in the mouse genome. *Nature* **488**: 116–120.

Shim EY, Walker AK, Shi Y, Blackwell TK. 2002. CDK-9/cyclin T (P-TEFb) is required in two postinitiation pathways for transcription in the C. elegans embryo. *Genes Dev* **16**: 2135–2146.

Shiratori H, Hamada H. 2006. The left-right axis in the mouse: from origin to morphology. *Development* **133**: 2095–2104.

Shiratori H, Sakuma R, Watanabe M, Hashiguchi H, Mochida K, Sakai Y, Nishino J, Saijoh Y, Whitman M, Hamada H. 2001. Two-step regulation of left-right asymmetric expression of Pitx2: Initiation by nodal signaling and maintenance by Nkx2. *Mol Cell* **7**: 137–149.

Shiratori H, Yashiro K, Shen MM, Hamada H. 2006. Conserved regulation and role of Pitx2 in situs-specific morphogenesis of visceral organs. *Development* **133**: 3015–3025.

Shopland LS, Lynch CR, Peterson KA, Thornton K, Kepper N, Von Hase J, Stein S, Vincent S, Molloy KR, Kreth G, et al. 2006. Folding and organization of a contiguous chromosome region according to the gene distribution pattern in primary genomic sequence. *J Cell Biol* **174**: 27–38.

Siepel A, Bejerano G, Pedersen JS, Hinrichs AS, Hou M, Rosenbloom K, Clawson H, Spieth J, Hillier LW, Richards S, et al. 2005. Evolutionarily conserved elements in vertebrate, insect, worm, and yeast genomes. *Genome Res* **15**: 1034–1050.

Sönnichsen B, Koski LB, Walsh A, Marschall P, Neumann B, Brehm M, Alleaume A-M, Artelt J, Bettencourt P, Cassin E, et al. 2005. Full-genome RNAi profiling of early embryogenesis in Caenorhabditis elegans. *Nature* **434**: 462–469.

Spitz F, Gonzalez F, Duboule D. 2003. A global control region defines a chromosomal regulatory landscape containing the HoxD cluster. *Cell* **113**: 405–417.

Splinter E, Heath H, Kooren J, Palstra RJ, Klous P, Grosveld F, Galjart N, De Laat W. 2006. CTCF mediates long-range chromatin looping and local histone modification in the ??-globin locus. *Genes Dev* **20**: 2349–2354.

Spradling AC, Stern D, Beaton A, Rhem EJ, Laverty T, Mozden N, Misra S, Rubin GM. 1999. The Berkeley Drosophila Genome Project gene disruption project: Single P-element insertions mutating 25% of vital Drosophila genes. *Genetics* **153**: 135–177.

Stathopoulos A, Levine M. 2005. Genomic regulatory networks and animal development. *Dev Cell* **9**: 449–462.

Steger DJ, Lefterova MI, Ying L, Stonestrom AJ, Schupp M, Zhuo D, Vakoc AL, Kim J-E, Chen J, Lazar MA, et al. 2008. DOT1L/KMT4 recruitment and H3K79 methylation are ubiquitously coupled with gene transcription in mammalian cells. *Mol Cell Biol* **28**: 2825–2839.

Stergachis AB, Neph S, Sandstrom R, Haugen E, Reynolds AP, Zhang M, Byron R, Canfield T, Stelhing-Sun S, Lee K, et al. 2014. Conservation of trans-acting circuitry during mammalian regulatory evolution. *Nature* **515**: 365–370. http://dx.doi.org/10.1038/nature13972.

Sutherland H, Bickmore WA. 2009. Transcription factories: gene expression in unions? *Nat Rev Genet* **10**: 457–466.

Taft RJ, Pheasant M, Mattick JS. 2007. The relationship between non-protein-coding DNA and eukaryotic complexity. *BioEssays* **29**: 288–299.

Tao Y, Zhang M, Li L, Bai Y, Zhou Y, Moon AM, Kaminski HJ, Martin JF. 2014. Pitx2, an atrial fibrillation predisposition gene, directly regulates ion transport and intercalated disc genes. *Circ Cardiovasc Genet* **7**: 23–32.

Tümpel S, Maconochie M, Wiedemann LM, Krumlauf R. 2002. Conservation and diversity in the cis-regulatory networks that integrate information controlling expression of Hoxa2 in hindbrain and cranial neural crest cells in vertebrates. *Dev Biol* **246**: 45–56.

Van de Werken HJG, Landan G, Holwerda SJB, Hoichman M, Klous P, Chachik R, Splinter E, Valdes-Quezada C, Öz Y, Bouwman BAM, et al. 2012. Robust 4C-seq data analysis to screen for regulatory DNA interactions. *Nat Methods* **9**: 969–972.

Van den Brink GR. 2007. Hedgehog signaling in development and homeostasis of the gastrointestinal tract. *Physiol Rev* **87**: 1343–1375.

Vance KW, Ponting CP. 2014. Transcriptional regulatory functions of nuclear long noncoding RNAs. *Trends Genet* **30**: 348–355. http://www.sciencedirect.com/science/article/pii/S0168952514000869.

Visel A, Minovitsky S, Dubchak I, Pennacchio LA. 2007. VISTA Enhancer Browser - A database of tissue-specific human enhancers. *Nucleic Acids Res* **35**.

Voas MG, Rebay I. 2004. Signal integration during development: insights from the Drosophila eye. *Dev Dyn* **229**: 162–175. http://www.ncbi.nlm.nih.gov/entrez/query.fcgi?cmd=Retrieve&db=PubMed&dopt=Citation&list_uids=14699588.

Volkmann BA, Zinkevich NS, Mustonen A, Schilter KF, Bosenko D V., Reis LM, Broeckel U, Link BA, Semina E V. 2011. Potential novel mechanism for Axenfeld-Rieger syndrome: Deletion of a distant region containing regulatory elements of PITX2. *Investig Ophthalmol Vis Sci* **52**: 1450–1459.

Waite MR, Skidmore JM, Micucci JA, Shiratori H, Hamada H, Martin JF, Martin DM. 2013. Pleiotropic and isoform-specific functions for Pitx2 in superior colliculus and hypothalamic neuronal development. *Mol Cell Neurosci* **52**: 128–139.

Wang J, Bai Y, Li N, Ye W, Zhang M, Greene SB, Tao Y, Chen Y, Wehrens XHT, Martin JF. 2014. Pitx2-microRNA pathway that delimits sinoatrial node development and inhibits predisposition to atrial fibrillation. *Proc Natl Acad Sci U S A* **111**: 9181–6. http://www.ncbi.nlm.nih.gov/pubmed/24927531.

Wang X, Chamberlin HM. 2002. Multiple regulatory changes contribute to the evolution of the Caenorhabditis lin-48 ovo gene. *Genes Dev* **16**: 2345–2349.

Wang Y, Steinbeisser H. 2009. Molecular basis of morphogenesis during vertebrate gastrulation. *Cell Mol Life Sci* **66**: 2263–2273.

Watanabe H, Schmidt HA, Kuhn A, Hoger SK, Kocagoz Y, Laumann-Lipp N, Ozbek S, Holstein TW. 2014. Nodal signalling determines biradial asymmetry in Hydra. *Nature* **advance on**. http://dx.doi.org/10.1038/nature13666.

Weinhold N, Jacobsen A, Schultz N, Sander C, Lee W. 2014. Genome-wide analysis of noncoding regulatory mutations in cancer. *Nat Genet* **46**: 1160–1165. http://dx.doi.org/10.1038/ng.3101.

Welsh IC, Hagge-Greenberg A, O'Brien TP. 2007. A dosage-dependent role for Spry2 in growth and patterning during palate development. *Mech Dev* **124**: 746–61. http://www.pubmedcentral.nih.gov/articlerender.fcgi?artid=2043129&tool=pmcentrez&rendertype=abstract (Accessed April 1, 2014).

Welsh IC, O'Brien TP. 2009. Signaling integration in the rugae growth zone directs sequential SHH signaling center formation during the rostral outgrowth of the palate. *Dev Biol* **336**: 53–67. http://www.pubmedcentral.nih.gov/articlerender.fcgi?artid=2789450&tool=pmcentrez&rendertype=abstract (Accessed April 1, 2014).

Welsh IC, Thomsen M, Gludish DW, Alfonso-Parra C, Bai Y, Martin JF, Kurpios N a. 2013. Integration of left-right Pitx2 transcription and Wnt signaling drives

asymmetric gut morphogenesis via Daam2. *Dev Cell* **26**: 629–44. http://www.ncbi.nlm.nih.gov/pubmed/24091014 (Accessed March 27, 2014).

Williamson I, Berlivet S, Eskeland R, Boyle S, Illingworth RS, Paquette D, Dostie J, Bickmore WA. 2014. Spatial genome organization: contrasting views from chromosome conformation capture and fluorescence in situ hybridization. *Genes Dev* **28** : 2778–2791. http://genesdev.cshlp.org/content/28/24/2778.abstract.

Wolpert L. 1984. DNA AND ITS MESSAGE. *Lancet* **324**: 853–856. http://www.sciencedirect.com/science/article/pii/S0140673684908857.

Wolpert L. 2011. Positional information and patterning revisited. *J Theor Biol* **269**: 359–365.

Wolpert L. 1969. Positional information and the spatial pattern of cellular differentiation. *J Theor Biol* **25**: 1–47.

Wray GA. 2007. The evolutionary significance of cis-regulatory mutations. *Nat Rev Genet* **8**: 206–216.

Yuh CH, Bolouri H, Davidson EH. 1998. Genomic cis-regulatory logic: experimental and computational analysis of a sea urchin gene. *Science* **279**: 1896–1902.

Zorn AM, Wells JM. 2009. Vertebrate endoderm development and organ formation. *Annu Rev Cell Dev Biol* **25**: 221–251.

Zuniga A, Michos O, Spitz F, Haramis A-PG, Panman L, Galli A, Vintersten K, Klasen C, Mansfield W, Kuc S, et al. 2004. Mouse limb deformity mutations disrupt a global control region within the large regulatory landscape required for Gremlin expression. *Genes Dev* **18**: 1553–1564.

CHAPTER 2

Manuscript #1

Signaling integration in the rugae growth zone directs sequential SHH signaling center formation during the rostral outgrowth of the palate

Signaling integration in the rugae growth zone directs sequential SHH signaling center formation during the rostral outgrowth of the palate

Ian C. Welsh[1] and Timothy P. O'Brien[1,2]

[1]Department of Biomedical Sciences, Cornell University, Ithaca NY 14853

[2]Corresponding Author: Timothy P. O'Brien

Department of Biological Sciences

Cornell University

Ithaca, NY 14853

tpo5@cornell.edu

(607) 253-4326

Running title: Periodic rugae formation and palate outgrowth

Keywords: craniofacial evolution; palate development; periodic patterning; developmental module; signaling network; FGF; BMP; SHH; p63

2.2 Abstract

Evolution of facial morphology arises from variation in the activity of developmental regulatory networks that guide the formation of specific craniofacial elements. Importantly, the acquisition of novel morphology must be integrated with a phylogenetically inherited developmental program. We have identified a unique region of the secondary palate associated with the periodic formation of rugae during the rostral outgrowth of the face. Rugae function as SHH signaling centers to pattern the elongating palatal shelves and we have found that a network of signaling genes and transcription factors is spatially organized relative to palatal rugae. Additionally, the first formed ruga is strategically positioned at the presumptive junction of the future hard and soft palate that defines anterior-posterior differences in regional growth, mesenchymal gene expression and cell fate. We propose a molecular circuit integrating FGF and BMP signaling to control proliferation and differentiation during the sequential formation of rugae and inter-rugae domains in the palatal epithelium. Epithelial expression of p63 and the BMP antagonist Sostdc1 is lost in Fgf10 mutants and results in failed rugae differentiation and loss of coordinating epithelial mesenchymal signaling. Our results establish a genetic program that reiteratively organizes signaling domains to coordinate the growth of the secondary palate with the elongating midfacial complex.

2.3 Introduction

Craniofacial development requires the outgrowth and precisely choreographed movements of multiple facial primordia. Bilateral maxillary and mandibular prominences fuse along the midline with the frontonasal process to frame the jaw and face. Outgrowth and patterning of the facial prominences depends on the immigration of cranial neural crest (CNC) cells that delaminate from the neural folds at the time of neural tube closure. Fate mapping and heterospecific transplantation studies show that distinct populations of CNC cells, defined by rostro-caudal level of origin and path of migration, are prepatterned as to the skeletal elements into which they will ultimately differentiate (Lee et al., 2004; Noden, 1983; Santagati and Rijli, 2003; Schneider and Helms, 2003). Conversely, evidence from genetic studies indicate a critical role for epithelial signals and support that refinement of facial form is derived from local tissue interactions between CNC and surface epithelia (Haworth et al., 2004; Haworth et al., 2007; Shigetani et al., 2000; Tyler and Koch, 1977; Yamagishi et al., 2006). These local interactions regulate cellular behaviors such as proliferation, migration, apoptosis, and differentiation within individual facial primordia and are mediated by developmental signaling pathways including the Bone morphogenic protein (BMP), Sonic hedgehog (SHH), Fibroblast growth factor (FGF), Retinoic acid, and WNT pathways (Ahlgren and Bronner-Fraser, 1999; He et al., 2008; Hu and Helms, 1999; Jeong et al., 2004; Liu et al., 2005; Schneider et al., 2001; Szabo-Rogers et al., 2008).

While critical roles have been demonstrated for individual transcription factors and signaling molecules, developmental control of craniofacial morphogenesis is achieved through the integration of molecular activity within transiently organized signaling centers. Mutations in genes which result in altered craniofacial development

are often associated with syndromes that affect the formation of other anatomical structures such as the limb, pointing to a conservation of underlying regulatory interactions and morphogenetic processes that define the activity of signaling centers (Barrow et al., 2002; Ibrahimi et al., 2001; Schneider et al., 1999; Stanier and Moore, 2004). Studies support that species-specific craniofacial morphology is generated by spatiotemporal differences in the activity of discrete signaling centers within individual facial primordia (Abzhanov et al., 2004; Wu et al., 2006b). For example, reciprocal FGF/SHH/BMP interactions establish the frontonasal ectodermal zone (FEZ), a signaling center positioned at the distal tip of the frontonasal mass that guides outgrowth of the midfacial complex (Abzhanov et al., 2007; Hu et al., 2003; Marcucio et al., 2005). The FEZ is organized relative to the adjacent expression domains of *Shh* and *Fgf8* and the mutual antagonism between these two pathways (Abzhanov et al., 2007; Hu and Marcucio, 2009a). Signals from the FEZ also regulate *Bmp4* expression within the adjacent mesenchyme, thereby directing CNC proliferation that sculpts the final size and shape of the upper jaw (Hu and Marcucio, 2009a; Hu and Marcucio, 2009b; Hu et al., 2003). Importantly, differences in the spatial organization of the FEZ and its associated signaling correlate with species-specific patterns of growth and final shape of the midfacial complex (Abzhanov et al., 2004; Hu and Marcucio, 2009b; Wu et al., 2006a; Wu et al., 2006b).

Many vertebrates, notably mammals, generate a derivative of the maxillary prominences, the secondary palate that separates the oral and nasal cavities. Palate development involves a series of rotation and elevation movements that accompany the outgrowth of the bilateral palatal shelves that meet and fuse along the midline to

form the roof of the oral cavity. The molecular and genetic basis of medial outgrowth and fusion of the palatal shelves has been studied extensively (Gritli-Linde, 2007; Lan et al., 2004; Stanier and Moore, 2004). However, less is known about growth control and patterning during the anterior extension of the palate. The anterior and posterior palate have been shown to exhibit differential competence to respond to signaling input, the anterior palate is BMP responsive whereas the posterior palate is considered to be permissive to FGF signaling (Shigetani et al., 2000; Zhang et al., 2002). Gene expression patterns also highlight molecular differences between the anterior and posterior palate (He et al., 2008; Hilliard et al., 2005; Li and Ding, 2007). In the mesenchyme, signaling and transcription factors including *Bmp4*, *Fgf10*, *Msx1* and *Shox2* are expressed in anterior domains while *Barx1, Tbx22,* and *Mn1* expression is restricted to posterior domains (Liu et al., 2008; Welsh et al., 2007; Yu et al., 2005). These regional differences in signaling and gene expression are ultimately translated into differences in cell fate, whereby the anterior mesenchyme differentiates to form the bony hard palate while posterior mesenchyme gives rise to the muscular soft palate.

Reciprocal signaling between mesenchyme and the overlying epithelium also plays a critical role in growth of the secondary palate (Gritli-Linde, 2007; Rice et al., 2004; Tyler and Koch, 1977). Both *Fgf10* and *Bmp4* are required for the epithelial expression of *Shh*, which is in turn involved in a cascade directing proliferation of the underlying mesenchyme (Rice et al., 2004; Zhang et al., 2002). *Shh* expression is restricted to the palatal rugae, epithelial thickenings that form the transverse ridges on the roof of the oral cavity (Bitgood and McMahon, 1995). Finally, highlighting the

role of epithelial-mesenchymal feedback in integrated signaling and tissue patterning, recent work by Lan and Jiang demonstrates that epithelial SHH signaling acts to restrict *Bmp4* expression but is required to maintain *Fgf10* expression in the mesenchyme (Lan and Jiang, 2009).

Importantly, the elongation of the secondary palate must coincide with the rostral extension of the midfacial complex. However, a defined domain of molecular interactions that pattern the outgrowth of the secondary palate, comparable to the FEZ, has not been appreciated. Our previous finding that the anterior growth of the palate involves periodic addition of *Shh* expressing rugae suggests that outgrowth is guided by a dynamic sequence of interactions between a regionalized mesenchyme and a highly patterned surface epithelium (Welsh et al., 2007). In this study we define a region of critical morphogenetic activity positioned at the junction of the future anterior-posterior (A-P) palate that serves to integrate FGF/SHH/BMP signaling to direct the differentiation of rugae signaling centers during the outgrowth of the anterior palate. The periodic formation of rugae provides a novel reference frame for studies of the spatial and temporal organization of a network of signaling genes and transcription factors that direct patterning and growth of the secondary palate.

2.4 Results

2.4.1 Periodic rugae formation during outgrowth of the anterior palate

A significant number of genes are known to be required for palate development. However, the lack of orienting landmarks has made interpreting the

integrated expression patterns of these genes difficult. In this study we have used rugae formation as a reference to examine the spatiotemporal dynamics of gene expression in the secondary palate. Rugae, which are formed in a defined sequence during the anterior extension of the palate, act as SHH signaling centers involved in epithelial-mesenchymal interactions required to coordinate palate outgrowth and patterning (Lan and Jiang, 2009; Pantalacci et al., 2008; Welsh et al., 2007). A first stripe of *Shh* rugae expression (R1) is evident at E12.0 and by E15.5, as the palatal shelves contact and fuse, the full complement of 8 rugae have formed (Fig. 2.1). In order to better appreciate the temporal dynamics of rugae formation in relation to palate development, we used *in situ* hybridization to generate a reconstructed time series. The number of rugae present and the extent of nascent *Shh* expression provide a proxy for ordering the developmental progression of a collection of palatal shelves. From 134 samples, dissected between E12.0 and E15.5 of development and hybridized for *Shh* expression, we ordered a series of 45 palates that capture the sequential formation of R1-R8. This reconstructed time series represents the full sequence of

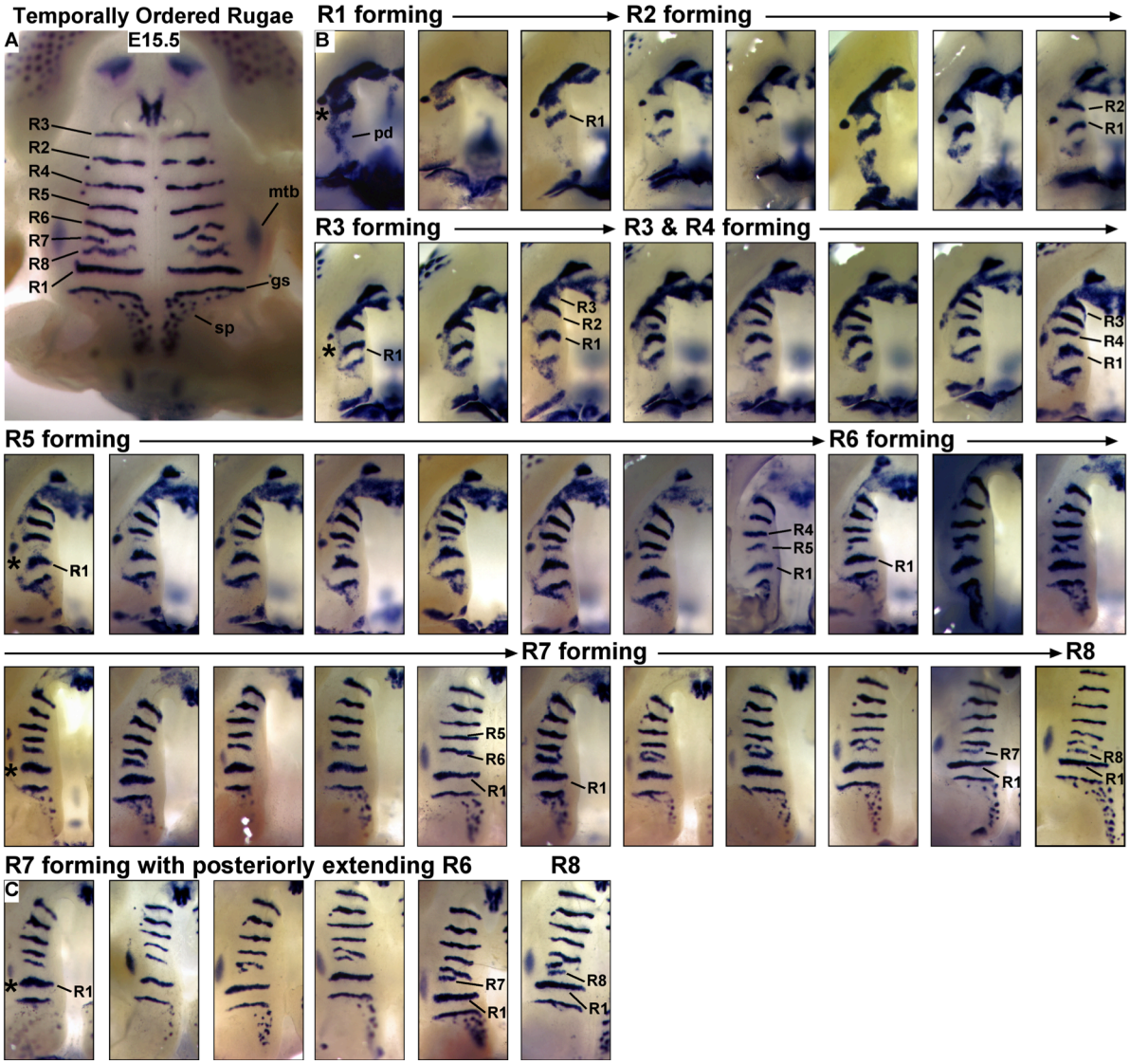

Figure 2.1. Periodic rugae formation and rostral growth of the palate. (**A**) *Shh* expression marking rugae at E15.5 (oral view of palates, anterior is towards top). Rugae (R1-R8) are labeled with respect to the order of their formation (shown in **B**). *Shh* expression posterior to the first formed rugae gives rise to a lateral line of taste buds termed the geschmacksstreifen and punctate *Shh* domains in developing sensory papilla overlaying the posterior soft palate. (**B**) A reconstructed time series showing the formation of R1-R8 highlights regional differences in the growth of the anterior and posterior palate. Around E12.0, the R1 ruga arises as a distinct band of *Shh* expression immediately posterior to the forming molar tooth bud signaling center. During rostral extension of the palate, the spatial relationship between R1 and the developing molar tooth bud remains unchanged (asterisks in left most panel of each row). Following the formation of R1, the remaining rugae (R2-R8) are generated anterior to R1. R3 and R4 form in quick succession anterior and posterior to R2 respectively. The domain of R4-R8 formation can be referenced to three distinct landmarks: anterior to R1; posterior to the most recently formed ruga; and medial to the molar tooth bud. (**C**) Variation in the morphology of R7 and R8 appears to be associated with the extent to which R6 extends posteriorly. gs, geschmacksstreifen; mtb, molar tooth bud; pd, posterior domain of *Shh* expression; sp, sensory papilla.

rugae formation during the anterior extension, medially directed outgrowth, and midline fusion of the palatal shelves (Fig. 2.1B and C).

This data set demonstrates that at approximately E12.0, the first ruga (R1) arises as a distinct band of *Shh* expression that separates posteriorly from the forming molar tooth bud (mtb) signaling center. This molecular data supports earlier observations of Peterkova based on detailed histological analysis that suggest the rugae and teeth share a common developmental origin in the odontogenic epithelium (Peterkova, 1985). Following the formation of R1, the remaining rugae (R2-R8) are generated anterior to R1. Furthermore, with the exception of R3, new rugae formation occurs via an interposition process (Fig. 2.1B). R3 actually forms anterior to R2 but is closely followed by the formation of R4 between R1 and R2. All subsequent rugae form between R1 and the most recently formed ruga (R1+n). Previously, rugae have been numbered relative to their position along the A-P axis of the palate, with the anterior most ruga labeled as R1 (Peterkova, 1985). However, the labeling of rugae, numbered in the order in which they are formed would result in the sequence: anterior<R3, R2, R4, R5, R6, R7, R8, R1>posterior.

The domain of periodic rugae formation can be referenced to three distinct landmarks: anterior to R1; medial to the position of the mtb; and posterior to R1+n (Fig. 2.1B). Following formation at this site, each new ruga is displaced with the anterior elongation of the palate. Thus, periodic rugae formation is localized to a specific domain and is intimately associated with the rostral outgrowth of the anterior palate. We refer to this distinct region of the palate as the rugae growth zone (RGZ).

Shh expression in R1 exhibits a characteristic morphology and dynamic that is distinct from the remaining rugae. R1 initiates as a posteriorly angled band of expression (during R2-R3 formation) that then becomes broader and chevron shaped (during R4-R5 formation) prior to flattening along its A-P axis (during R6-R8 formation). This flattening of R1is accompanied by the posterior regression of the site of nascent rugae formation with respect to the mtb such that R4 forms at the anterior limit of the mtb, while R7 and R8 form at the mid-posterior level of the mtb. The increasingly posterior formation of R7 and R8 is accompanied by the elongation of the *Shh* expression domain in the mtb as well as the flattening of R1. Variability in the morphology of R7 and R8 has been noted previously. It is interesting to speculate that the position of nascent rugae induction and the variability in R7/R8 morphology may be related to the dynamics and interplay between three signaling domains, R1, the mtb, and R1+n. This hypothesis is supported by the observation that the formation of a posteriorly angled R6 is associated with a laterally shortened R7 ruga (Fig. 2.1C).

2.4.2 A network of genes is organized about rugae signaling centers

The dynamics of *Shh* expression demonstrate that periodic patterning generates a series of signaling domains in the epithelium of the elongating palatal shelves. To further investigate patterning in relation to rugae formation and the anterior extension of the palatal shelves, we surveyed the expression of a number of key signaling molecules and transcription factors. Regionally restricted expression of genes such as *Wnt5a*, *Twist1*, *Pax9*, *Tbx22*, *Tgf-b3*, and *Sox9* along the anterior-posterior and medial-lateral axis, highlight the spatial heterogeneity of gene expression in the

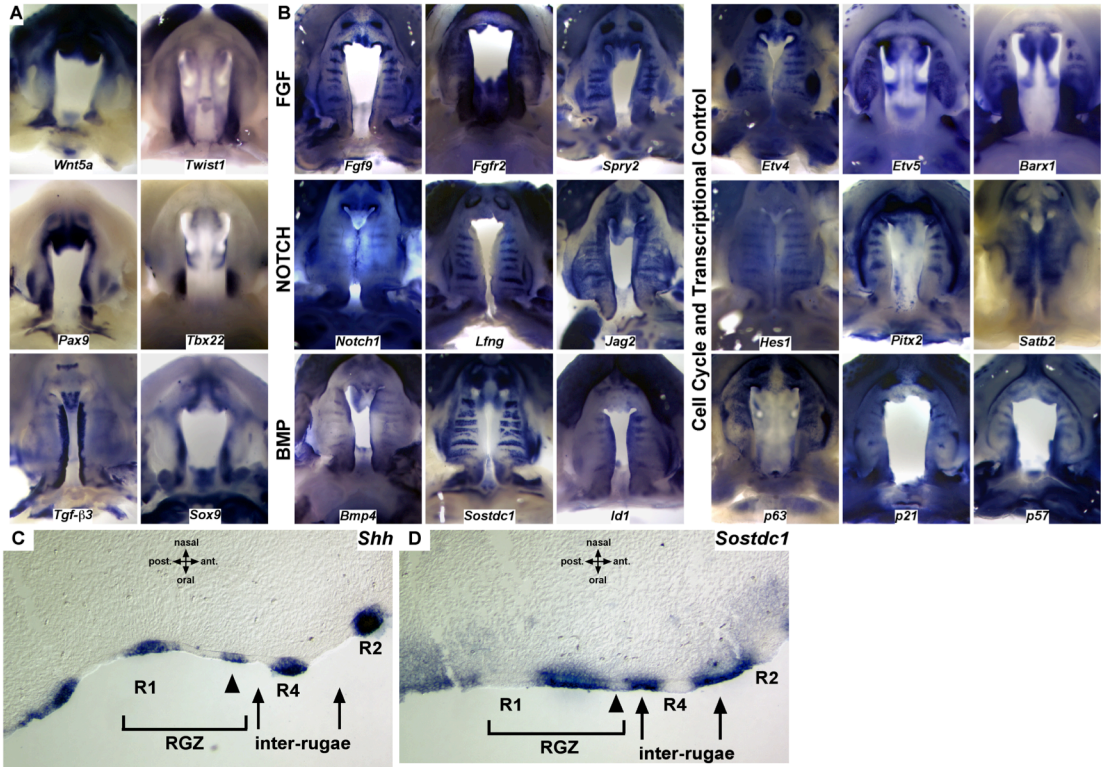

Figure 2.2. A survey of spatial gene expression during the outgrowth and fusion of the palate. (**A**) Regional differences in expression domains, particularly with respect to the anterior-posterior and medial-lateral axes, highlight domains of expression in the developing palate. (**B**) Gene expression domains in the developing palate are organized relative to the developing rugae. In addition to SHH, multiple components of a network of signaling genes and transcription factors that are critical for palate development, including the FGF, NOTCH, and BMP pathways, exhibit restricted expression to either rugae or inter-rugae expression domains. The distribution of rugae signaling centers, generated during anterior growth, provide a mechanism to integrate A-P differences in gene expression with localized sources of patterning information. (**C**) Sagittal section *in situ* showing *Shh* expression restricted to the thickened epithelium of established rugae as well as the anterior edge of the RGZ epithelium prior to epithelial thickening. (**D**) Epithelial expression of the dual BMP/WNT antagonist *Sostdc1* is restricted to the RGZ epithelium and inter-rugae domains but is downregulated at the site of rugae formation (arrowheads in **C** and **D**).

developing palate (Fig. 2.2A). Significantly, we also found that the expression of a number of transcription factors and members of several developmental signaling pathways (FGF, BMP, SHH, and NOTCH) is segmentally organized with respect to rugae and inter-rugae domains in the developing palate (Fig. 2.2B-D). Restricted

expression within rugae has been reported for components of the SHH pathway as well as *Barx1*, *Etv5,* and *Bmp4* (Rice et al., 2006; Welsh et al., 2007; Lee et al., 2007).

However, the segmental expression of genes critical for orofacial development such as *Jag2, Fgfr2*, and *Pitx2* has not been reported (Casey et al., 2006; Liu et al., 2003; Rice et al., 2004). Our survey demonstrates that several components of the FGF, BMP, and NOTCH signaling pathways exhibit expression that is restricted to either rugae (*Fgf9*, *Spry2*, *Etv4*, *Notch1*, *Lfng*, *Hes1*) or inter-rugae domains (*Fgfr2*, *Etv5*, *Sostdc1*, *Id1*) in the palatal epithelium or mesenchyme (Fig. 2.2B). The complementary organization of gene expression domains for components of these signaling pathways and transcription factors provide information of the directionality of cellular signaling acting during palate development. For example, the NOTCH receptor *Notch1*, its signaling modulator *Lfng*, and downstream transcriptional mediator *Hes1* are all expressed within rugae, whereas the ligand *Jag2* is expressed in the adjacent inter-rugae domains.

We also note that the segmental expression of certain genes appears to be stage specific. For example at E12.5 and E13.5, transcripts for *Notch1*, *Bmp4*, and the transcription factor *Satb2* appear to be broadly distributed in the palate (data not shown) however, beginning at ~E14.5 expression becomes rugae associated (Fig. 2.2B). Moreover, changes in the epithelial expression of *Etv5* during rugae formation and maturation point to dynamic epithelial-mesenchymal signaling along the A-P axis of the palate (data not shown). Our expression survey uncovers a previously unappreciated organization of gene expression and signaling domains in the developing palate. Further studies to localize and refine gene expression domains with

respect to the RGZ, rugae, and inter-rugae domains will provide additional insights into the spatial organization of genetic networks in the palate.

2.4.3 The R1 ruga coincides with gene expression domains defining anterior and posterior palate

Our expression studies reveal that molecular signals in the palate are organized relative to the developing rugae. We next investigated the spatial relationship between the region of rugae formation and A-P domains in the developing palate. Prior to the formation of the secondary palate, mesenchyme of the maxillary prominence is patterned into anterior *Msx1* and posterior *Barx1* expression domains (Barlow et al., 1999; Zhang et al., 2002). We found that A-P differences in the expression of *Msx1* and *Barx1* are maintained from the earliest stages of the secondary palatal shelf development as they form along the medial aspect of the maxillary prominence (Fig. 2.3). At E11.5, restricted *Msx1* expression in the anterior most aspect of the palatal shelf is initiated coincident with the formation of the primary choanae on the roof of the stomodeum (Fig. 2.3A, D). Choanae are bilateral involutions that will form the nasal cavity and provide landmarks for the junction between the primary and secondary palate (Tamarin, 1982). At E11.5, the mesenchymal expression of *Barx1* extends nearly along the entire length of the palatal shelf and abuts the posterior limit of the primary choanae (Fig. 2.3B, E). Significantly, the site of R1 formation is positioned at the junction of the mesenchymal expression domains of *Msx1* and *Barx1* at the posterior limit of the choanae (Fig. 2.3C&F). As previously reported, epithelial expression of *Barx1* is restricted to the inter-rugae domains of the anterior palate

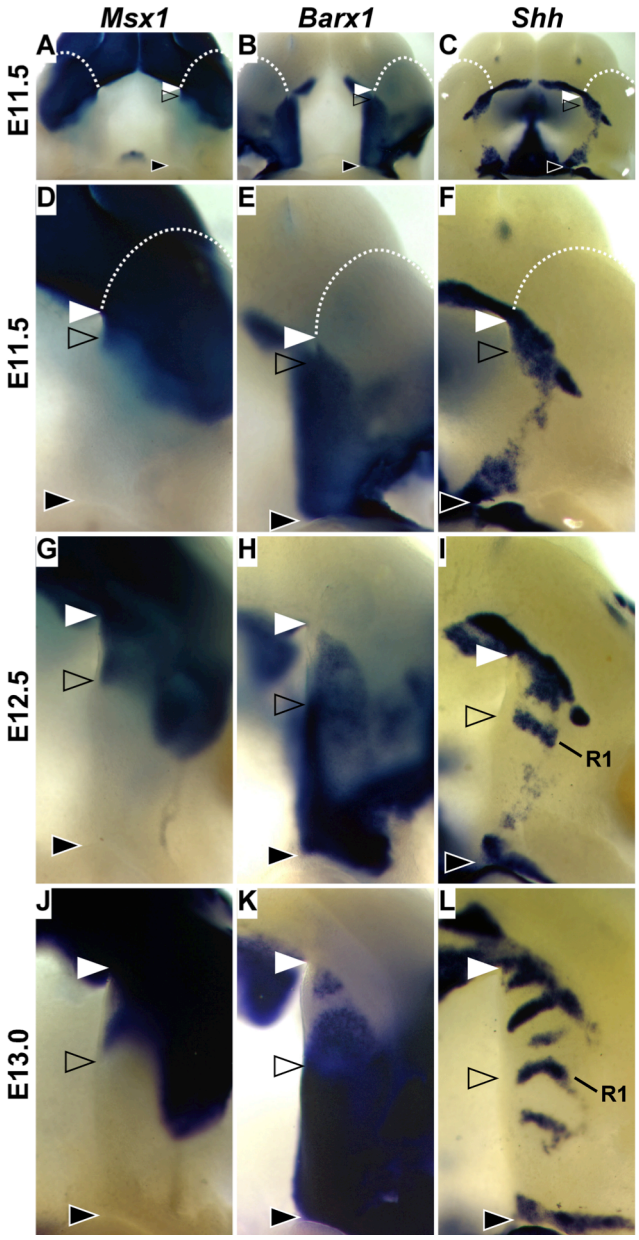

Figure 2.3. The first formed ruga (R1) highlights regional growth of the anterior palate and is coincident with anterior-posterior differences in mesenchymal gene expression. (**A-C**) Oral view of E11.5 wildtype embryos hybridized for *Msx1* (**A**), *Barx1* (**B**), and *Shh* (**C**). White dashed line marks the lamboidal junction between the maxillary process and the frontonasal mass. White and black filled arrowheads mark the anterior and posterior limit of the palatal process respectively. Mesenchyme of the maxillary prominence is patterned into anterior *Msx1* (**A**, **D**, **G**, **J**, between white and open arrowheads) and posterior *Barx1* (**B**, **E**, **H**, **K**, between open and black arrowheads) expression domains. *Shh* expression (**C**, **F**, **I**, **L**) in R1 is coincident with the mesenchymal boundary between *Msx1* and *Barx1* (open arrowheads) and provides a landmark to visualize the anterior outgrowth of the *Msx1* positive palate (region between white and open arrowheads). Restricted inter-rugae expression of *Barx1* in the epithelium expands with the elongating anterior palate (**H** and **K**) whereas the posterior mesenchymal domain remains a constant size (region between open and black arrowheads)

(Welsh et al., 2007). As palate development progresses, growth of the palate along the A-P axis results in the relative expansion of the mesenchymal *Msx1* and inter-rugae *Barx1* expression domains anterior to R1 compared to the mesenchymal domain of *Barx1* posterior to R1 (Fig. 2.3G-L). Up to E12.5, mesenchymal *Msx1* and *Barx1* share a posterior and anterior boundary respectively with R1 (Fig. 2.3G, H, I). However, by E13.5 continued expansion of the mesenchyme anterior to R1 begins to shift the posterior boundary of *Msx1* expression away from R1 (Fig. 2.3J, K, L). Therefore, the RGZ and the sequential formation of rugae signaling centers provide a reference frame to directly visualize the formation of the anterior palate as it extends away from R1 at the boundary of the presumptive soft palate.

The directed growth of the anterior palate away from R1 correlates with known differences in signaling responsiveness and cell fate (Hilliard et al., 2005; Yu et al., 2005; Zhang et al., 2002). To further investigate the relationship between A-P patterning in relation to the position of R1, we compared the expression of *Barx1* with that of *Shox2,* a marker of the anterior palate, between E12.5 and E15.5 (Li and Ding, 2007; Yu et al., 2005). Similar to *Msx1,* the expression of *Shox2* is initiated in the anterior-most mesenchyme upon rostral extension of the anterior palate (Yu et al., 2005). In contrast to the posterior expansion of *Shox2* expression reported by Li and Ding, we found that the posterior boundary of *Shox2* remains coincident with R1 and the anterior boundary of mesenchymal *Barx1* expression throughout palate development (Fig. 2.4). Interestingly, expression of *Shox2* in the anterior mesenchyme is dependent on BMP signaling, while *Barx1* expression is inhibited by BMP signaling (Yu et al., 2005). Consistent with the differential regulation of *Shox2* and *Barx1* by

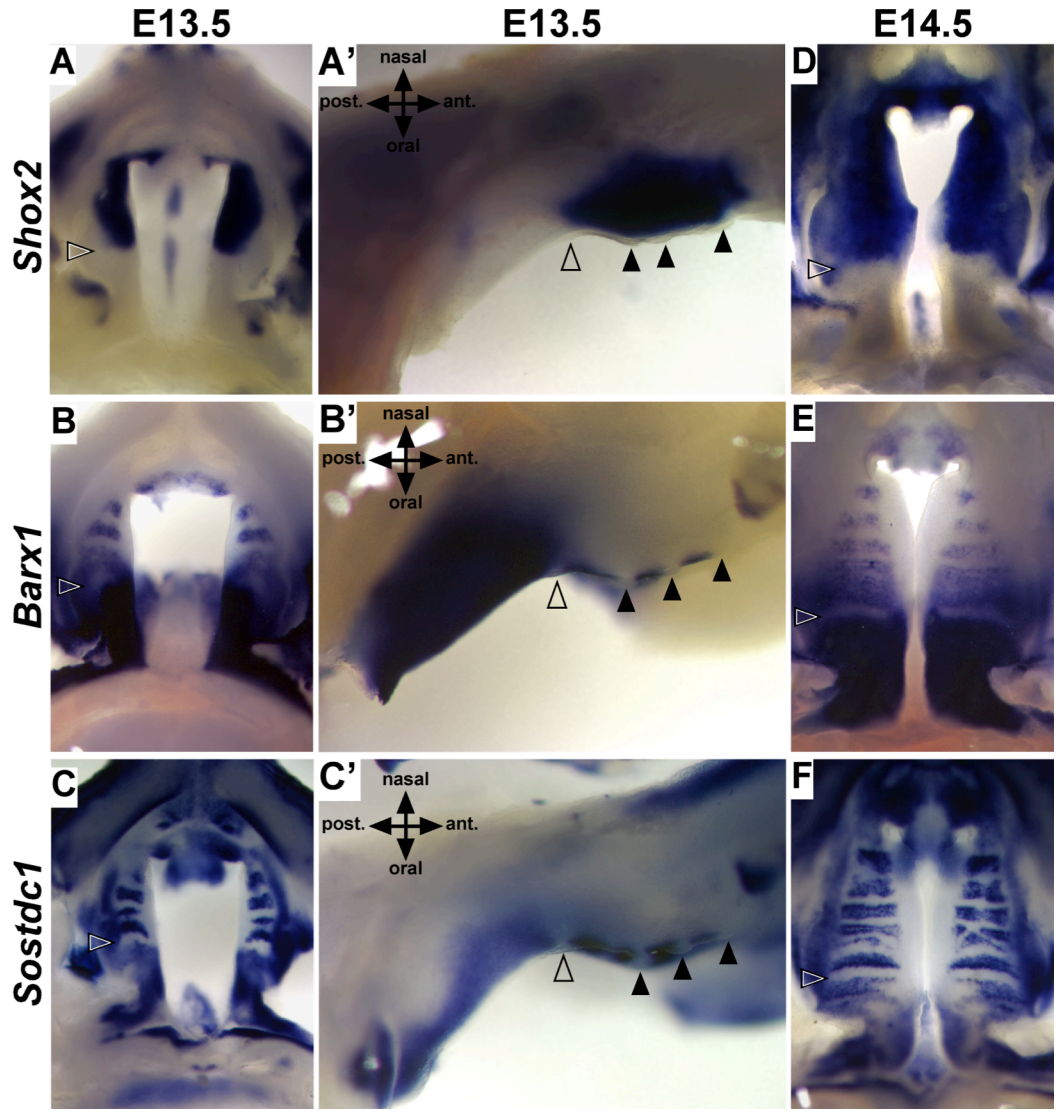

Figure 2.4. R1 marks the anterior-posterior boundary of mesenchymal cell fate. During the outgrowth (E13.5) and fusion (E14.5) of the palatal shelves, the mesenchymal expression of *Shox2* (**A**,**A'**, and **D**) and *Barx1* (**B**,**B'**, and **E**) share a common boundary defined by the location of R1 (open arrowheads) in the overlying epithelium. Expression of *Shox2* and *Barx1* is positively or negatively regulated by BMP signaling respectively. The expression of the BMP signaling antagonist *Sostdc1* is consistent with the establishment of BMP permissive or restricted signaling domains in both the anterior and posterior palate (**C**,**C'**, and **F**). Black arrowheads mark position of anterior rugae.

BMP signaling, we found the expression of the BMP signaling antagonist *Sostdc1*, is also spatially organized relative to R1. Similar to *Barx1*, *Sostdc1* is expressed in the mesenchyme posterior to R1, while anterior expression is restricted to domains of inter-rugae epithelium (Fig. 2.4C,C', and F). These data support that R1 and the RGZ are key features defining differences in patterning, signaling competence, and growth along the A-P axis of the palatal shelves.

2.4.4 Mesenchymal Fgf10 is expressed in a posterior-anterior gradient adjacent to the RGZ

The sequential generation and relative spacing of rugae are consistent with an activation-inhibition mechanism that regulates the formation and patterning of ectodermal appendages (Pispa and Thesleff, 2003). Mesenchyme often provides the first instructive signal for the formation of ectodermal organs that develop through reciprocal epithelial and mesenchymal interactions. Previously, we demonstrated that *Shh* expression, rugae morphology and palate closure are disrupted in mice lacking the FGF signaling antagonist *Spry2* (Welsh et al., 2007). Therefore, we examined *Fgf10* expression in the mesenchyme adjacent to the RGZ. We performed whole mount *in situ* hybridization of *Shh* and *Fgf10* on paired sets of right and left palatal shelves from individual embryos as well as on adjacent serial frontal and sagittal sections. These data show that contrary to the findings of Pantalacci *et el.* nascent *Shh* expression at the anterior edge of the RGZ actually precedes the overt epithelial thickening that defines rugae (Fig. 2.5A-C) (Pantalacci et al., 2008). Surprisingly, we found that *Fgf10* expression forms a gradient within the mesenchyme of the RGZ. *Fgf10* is most

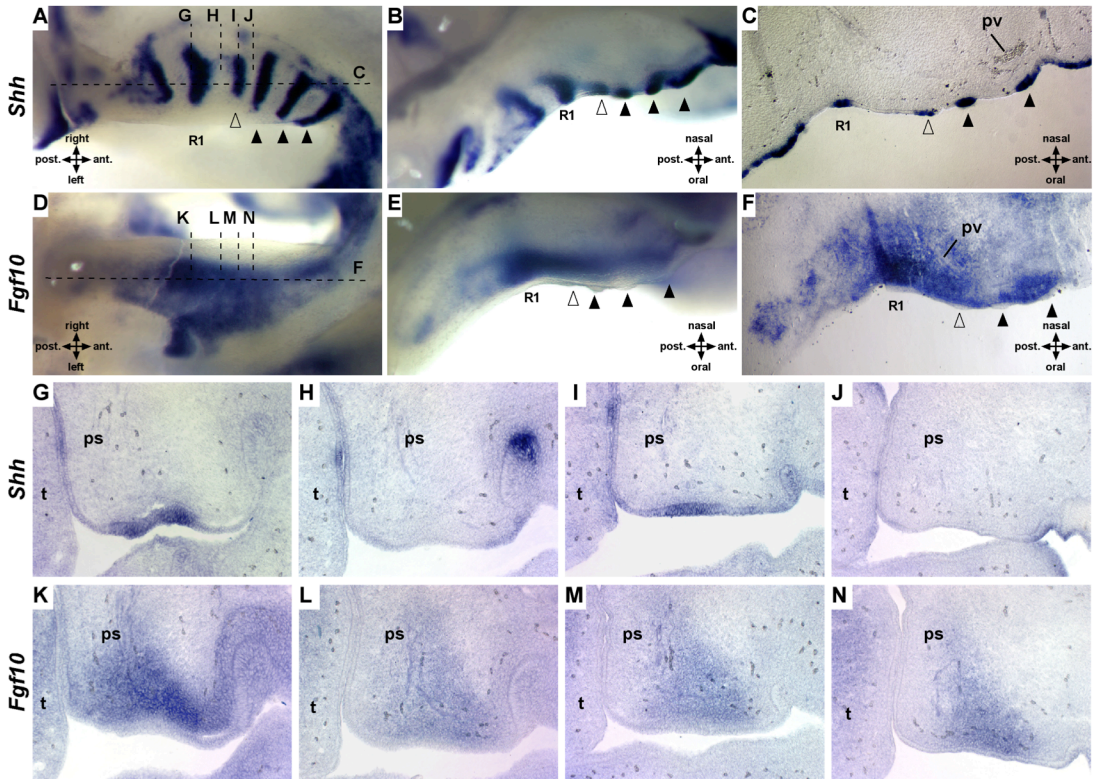

Figure 2.5. *Fgf10* is expressed in a gradient defined by R1 and the site of nascent *Shh* expression at the anterior of the RGZ. Whole mount *in situ* hybridization on the palatal shelves of a single embryo detecting expression of *Shh* (right shelf, **A** and **B**) or *Fgf10* (left shelf, **D** and **E**). Dashed horizontal and vertical lines indicate approximate plane of section shown in **C** and **F** or **G-N** respectively (open arrowheads mark nascent ruga, black arrowheads mark definitive rugae). Section *in situ* hybridization for *Shh* and *Fgf10* on adjacent sagittal (**C** and **F**) or serial frontal sections (**G-N**) of E13.5 wildtype palates show robust posterior expression of *Fgf10* in the mesenchyme adjacent to *Shh* in R1 compared to the mid-RGZ (**H** and **L**), anterior RGZ (**I** and **M**), and recently formed inter-rugae domain (**J** and **N**). ps, palatal shelf; pv, palantine vein; t, tongue.

highly expressed in the condensed mesenchyme directly adjacent to R1 but expression diminishes anteriorly towards the site of nascent rugae formation (Fig. 2.5). Consistent with the recently demonstrated positive feedback of *Fgf10* expression by epithelial SHH signaling (Lan and Jiang, 2009), *Fgf10* expression is again upregulated anterior to the R1+n rugae, although not to the level seen adjacent to R1 (Fig. 2.5F).

Analysis of H&E stained sections through the RGZ show that compared to the thickened and protruding epithelium of mature rugae and the markedly thinner abutting inter-rugae domain, the oral epithelium throughout the RGZ adjacent to the

Fgf10 gradient is of an intermediate thickness forming a placode that extends anteriorly from R1 (Fig. 2.6A). We also note that mesenchymal cells corresponding to the domain of highest levels of *Fgf10* expression exhibit a distinct polarity orthogonal to adjacent epithelium of R1 (Fig. 2.6B). Therefore, the RGZ is not only defined by distinct gene expression domains but also unique differences in the cellular organization of both the mesenchyme and epithelium. Thus, a gradient of FGF10 signaling potentially provides an important inductive cue from the mesenchyme that together with inhibitory signals from the epithelium control the timing and spatial positioning of epithelial differentiation to establish rugae and inter-rugae domains. A candidate source for an inhibitory signal is the R1+n ruga that moves away from the RGZ during palate elongation (Pantalacci et al., 2008).

2.4.5 Molecular signals maintaining proliferation versus cell cycle exit during rugae differentiation

We considered that rugae differentiation involves an FGF10-dependent program that triggers *Shh* expression and cell cycle exit in a localized population of cells within the RGZ. In a series of BrdU labeling experiments, we confirmed that epithelial cell proliferation is diminished in established rugae, including R1 and the most recently formed rugae (R1+n). In contrast, inter-rugae epithelium, including the domain between the anterior boundary of the RGZ and the R1+n rugae display high levels of proliferation. Notably, we detected non-uniform proliferation within the RGZ (Fig. 2.6C, D). Epithelial cells within the posterior half of the RGZ adjacent to R1 exhibit an elevated mitotic index relative to that of cells in the anterior half of the

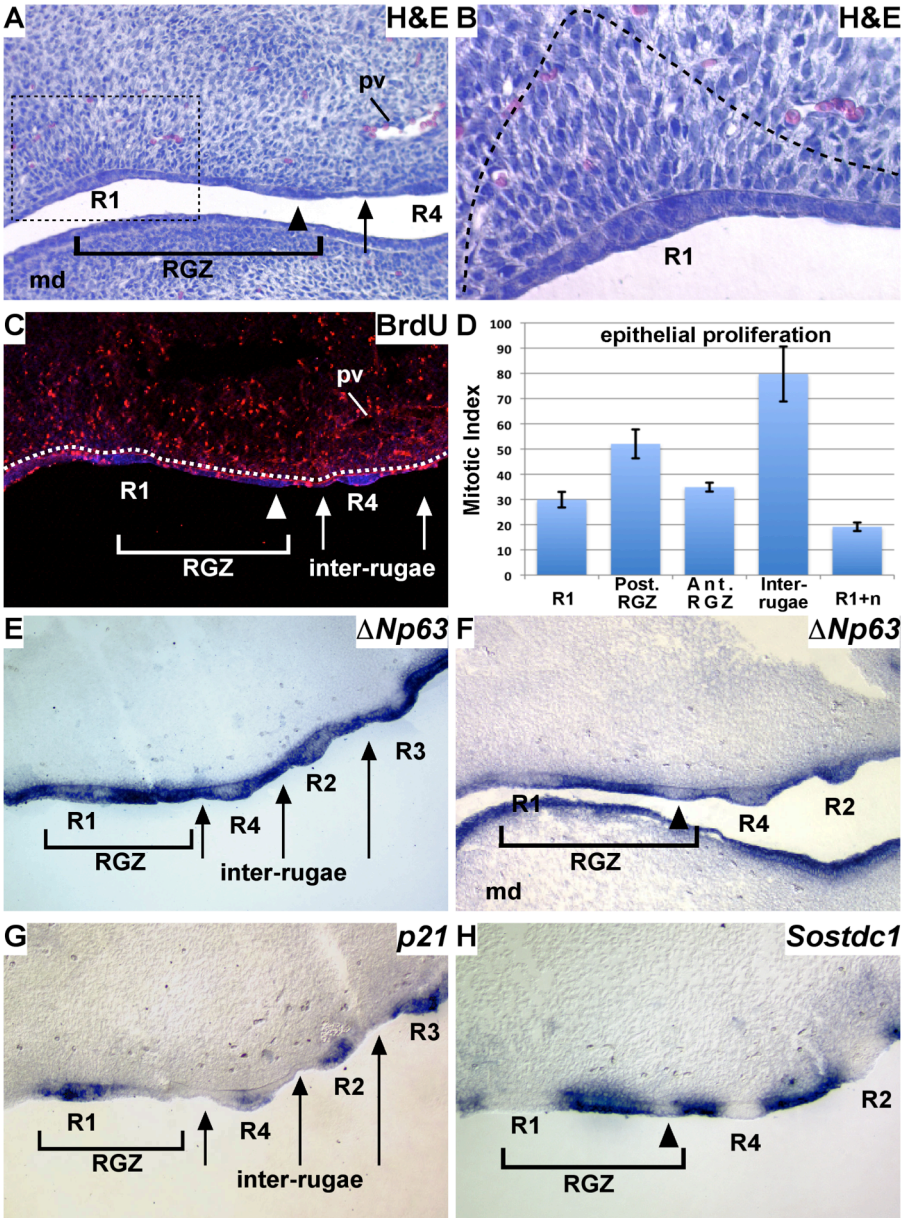

Figure 2.6. Domains of cell proliferation and gene expression associated with rugae formation in the RGZ. (**A**) H&E stained sagittal section of an E13.5 palate shows differences in the organization of both the mesenchyme and epithelium in the region of the RGZ. The epithelium within the RGZ is of an intermediate thickness to that in rugae and inter-rugae domains (arrow) that extends anteriorly from R1 (arrowhead marks anterior RGZ and site of rugae formation). The condensed mesenchyme adjacent to R1 shows a polarity orthogonal relative to the epithelium (dashed box enlarged in **B**). (**C**) Cell proliferation detected by BrdU incorporation (BrdU: red, nuclei counterstained with DAPI (blue), dashed white line separates mesenchyme and epithelium) is uniform in the palatal mesenchyme. Proliferation is high in inter-rugae domains (arrows) and in the posterior RGZ and reduced in the thickened epithelium of rugae and nascent rugae (white arrowhead). (**D**) Summary of regional differences in epithelial proliferation in the E13.5 palate (error bars represent SEM, n=4). Sagittal sections of E13.5 palates hybridized for *DNp63* (**E** and **F**) *p21* (**G**) and *Sostdc1* (**H**) expression supports that rugae morphogenesis involves cell cycle exit. Within the RGZ, *DNp63* is strongly expressed immediately anterior to R1 (**E**) but is periodically downregulated at the site of nascent rugae formation (arrowhead, **F**). Expression of *DNp63* (**E** and **F**) and the cell cycle inhibitor *p21* (**G**) becomes progressively upregulated in maturing rugae. (**H**) *Sostdc1* expression overlaps with *DNp63* within the RGZ and is also periodically downregulated at the site of rugae formation (arrowhead) but is restricted to inter-rugae domains in the anterior palate. Abbreviations: md, mandible; pv, palatine vessel.

RGZ. Significantly, this region of diminished proliferation within the RGZ corresponds to cells that initiate *Shh* expression prior to the overt epithelial differentiation into rugae (see Fig. 2.5).

The proliferation pattern within the RGZ suggests that rugae and inter-rugae domains are established through the spatial organization of molecular signals controlling cell cycle exit and maintenance, respectively. The *p53* related factor *p63* is thought to integrate the activity of multiple signaling pathways and act as a switch to regulate molecular cascades that promote the maintenance of epithelial progintors versus cell cycle exit and differentiation (Yang et al., 1999). *p63* has been shown to maintain epithelial cell "stemness" through the positive regulation of *Fgfr2b* and *Jag2* (Candi et al., 2007). We established that *Fgfr2b* and *Jag2* expression is localized to inter-rugae domains (see Fig. 2.2). Complex regulation of the *p63* locus results in the expression of at least six protein variants exhibiting distinct and often opposing regulation of target genes (Vigano et al., 2006; Wu et al., 2003; Yang et al., 1998). Alternative promoter usage generates two N-terminal isoforms, a longer transactivating (TA) domain containing *TAp63* and a truncated *DNp63* lacking the TA domain, while alternative splicing of the C-terminus generates a, b, and g isoforms. Notably, the *DNp63* isoform has been shown to be the predominant isoform expressed during craniofacial development and to be required for the differentiation and maintenance of signaling centers in the oral epithelium (Laurikkala et al., 2006; Mikkola, 2007; Mills et al., 1999). Furthermore, FGF10 has been shown to be a potent inducer of *p63* during ectodermal organogenesis and the periodic patterning of skin

appendages (Tao et al., 2002). Therefore, we examined the spatial organization of *DNp63* expression in the developing palate epithelium.

We found that in the developing palate, *DNp63* expression is notably dynamic with respect to the sequence of rugae induction and maturation. *DNp63* is not expressed in R1 or the R1+n rugae but its expression becomes rugae specific in more mature anterior rugae. Significantly *DNp63* is strongly expressed within the RGZ epithelium immediately anterior to R1, however as the R1+n rugae is displaced by the expansion of the newly formed inter-rugae domain, expression is downregulated at the site of nascent rugae formation (Fig. 2.6E and F). *DNp63* has been shown to inhibit the expression of the cell cycle regulator *p21*, a factor induced by BMP4 that promotes growth arrest during signaling center formation (Jernvall et al., 1998; Nguyen et al., 2006; Okuyama et al., 2007). Our expression analysis demonstrates that *p21* is strongly expressed in R1 but is excluded from the RGZ epithelium, a pattern complementary to that of *DNp63*. Interestingly, similar to *DNp63* in R1+n and more mature anterior rugae, *p21* expression becomes progressively upregulated (Fig. 2.6G). In the developing tooth bud, BMP4 induces its own antagonist *Sostdc1*, and expression of *Shh* and *p21* (Laurikkala et al., 2003). *Sostdc1* acts to inhibit BMP4 signaling, while SHH signaling acts to locally inhibit the expression of *Sostdc1*. In this way, reciprocal epithelial-mesenchymal signaling serves to restrict the field of cells competent to respond to a BMP threshold dependent induction of signaling center differentiation. Similar to *DNp63* and consistent with its role in tooth development, *Sostdc1* is also periodically down regulated at the site of rugae induction (Fig. 6H). Therefore, within the RGZ *DNp63* is coexpressed with *Sostdc1*, while in established

rugae expression overlaps with *p21*. Thus, while *p63* expression within the RGZ likely inhibits *p21* expression to sustain the cell cycle, periodic down regulation of *DNp63* and *Sostdc1* expression at the anterior RGZ may facilitate growth arrest and signaling center differentiation. These data suggest that during the rostral extension of the anterior palate, a dynamic molecular circuit coordinates the sequential formation of both rugae and inter-rugae epithelium from a common precursor population in the RGZ.

2.4.6 Loss of Fgf10 results in failure to maintain the RGZ and loss of coordinating epithelial-mesenchymal signaling

Our data suggest that *p63* expression and rugae morphogenesis are dependent on FGF10 signaling from the mesenchyme. The targeted disruption of *Fgf10* in mice results in cleft palate and loss of *Shh* expression (Alappat et al., 2005; Rice et al., 2004). We sought to further examine palate defects in *Fgf10* mutants with respect to signaling in the RGZ. Using QRT-PCR analysis, we compared the palatal expression of several genes proposed to mediate rugae morphogenesis between E13.5 wildtype (n=3) and *Fgf10* mutants (n=4) (Fig. 2.7). Consistent with its role as a mediator of FGF signaling during craniofacial development and dynamic epithelial expression in the palate (Firnberg and Neubuser, 2002) we found that *Etv5* expression is reduced to approximately 50 percent wildtype levels in *Fgf10* mutant palates. Laurikkala et al previously showed that *DNp63* is the predominant isoform of *p63* expressed in the oral epithelium during development (Laurikkala et al., 2006). We detected no significant differences in the expression levels of the *TAp63* isoform, however, *DNp63*

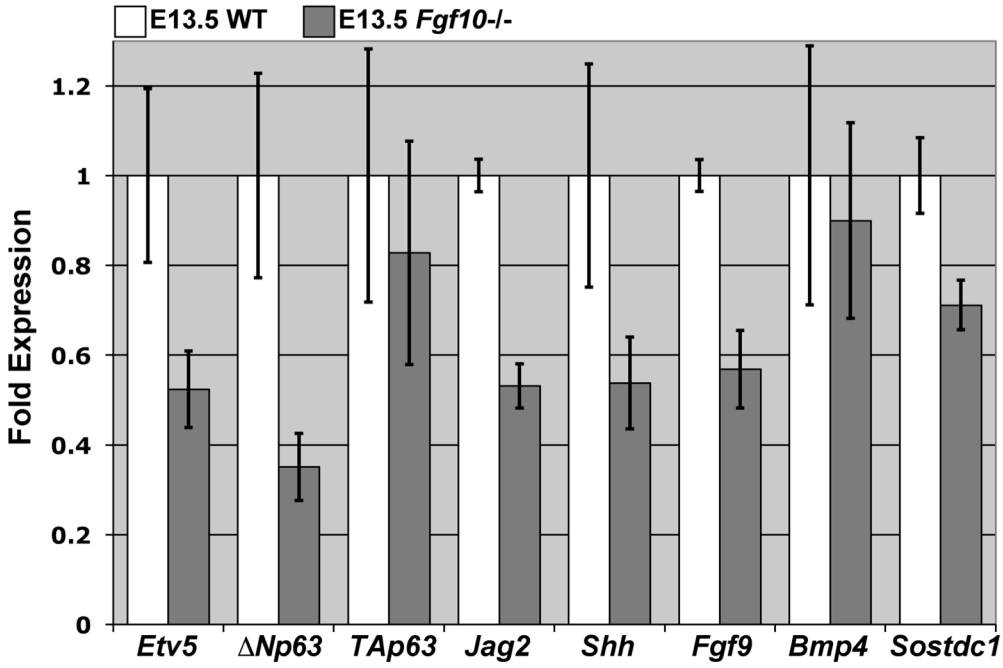

Figure 7. QRT-PCR analysis detects altered expression of both rugae and inter-rugae specific genes in *Fgf10* mutant palates. Relative to wildtype (n=3), E13.5 *Fgf10* mutants (n=4) exhibit reduced expression of *Etv5, DNp63*, *Jag2*, *Shh* and *Fgf9*, and *Sostdc1,* but not the TA isoform of *p63* or *Bmp4* (error bars represent SEM).

expression is significantly reduced in the palate of *Fgf10* mutants. Furthermore, expression levels of *Jag2*, a *p63* target expressed in the inter-rugae epithelium, as well as *Fgf9* that is coexpressed with *Shh*, are also reduced. Interestingly, although we detected normal levels of *Bmp4* expression in the palates of E13.5 *Fgf10* mutants, we detected a consistent reduction in the expression levels of the dual BMP/WNT antagonist *Sostdc1*.

We next sought to investigate the impact of these quantitative changes in gene expression on the spatial organization of the RGZ and rugae development. Consistent with the QRT-PCR data, *in situ* hybridization confirmed that rugae formation is severely disrupted in the *Fgf10* mutant palate. The organized *Shh* expression domains that highlight established and forming rugae progressively deteriorate between E13.5 -

E14.5 (Fig. 2.8A, B). Furthermore, the expression of both *Etv5* and *DNp63* is specifically lost in the epithelium of the palatal shelves of *Fgf10* mutants, while *Etv5* expression in the mesenchyme of the medial palatal shelf appears unaffected (Fig. 2.8C, D). Although QRT-PCR indicated a moderate reduction in expression levels, we found that *Sostdc1* expression in the anterior epithelium to be completely lost (Fig. 2.8E). Surprisingly, we also detected significant upregulation of *Sostdc1* in the mesenchyme posterior to R1 and in the molar tooth bud, suggesting a loss of coordinated epithelial-mesenchymal signaling via the BMP and possibly WNT pathways in *Fgf10* mutant palates (Fig. 2.8E).

Significantly, loss of *p63* function has recently been shown to result in failed outgrowth of the anterior palate and is associated with elevated levels of *Bmp4* and loss of *Shh* expression in the maxillary process (Thomason et al., 2008). During tooth development, *Sostdc1* integrates the BMP, SHH, and FGF pathways and is required to regulate epithelial responsiveness to *Bmp4* induction of *Shh* and *p21* expressing signaling centers (Kassai et al., 2005; Laurikkala et al., 2003). Furthermore, Sostdc1 (also called *Wise*, *Ectodin*, and USAG-1) has recently been shown to coordinate the BMP and WNT pathways via its interaction with the WNT co-receptor *Lrzp4* (Ohazama et al., 2008). In order to determine whether *Sostdc1* plays a similar role during rugae formation we analyzed *Shh* expression in the palates of *Sostdc1*^{Shk} (Sharkey) mutants. Sharkey was recovered as a spontaneous mutation resulting in supernumerary teeth, a phenotype associated with the targeted disruption of *Sostdc1*. Characterization by The Jackson Laboratory Craniofacial Mutant Resource group confirmed Sharkey as a new null mutation in *Sosdtc1* resulting from a single base pair

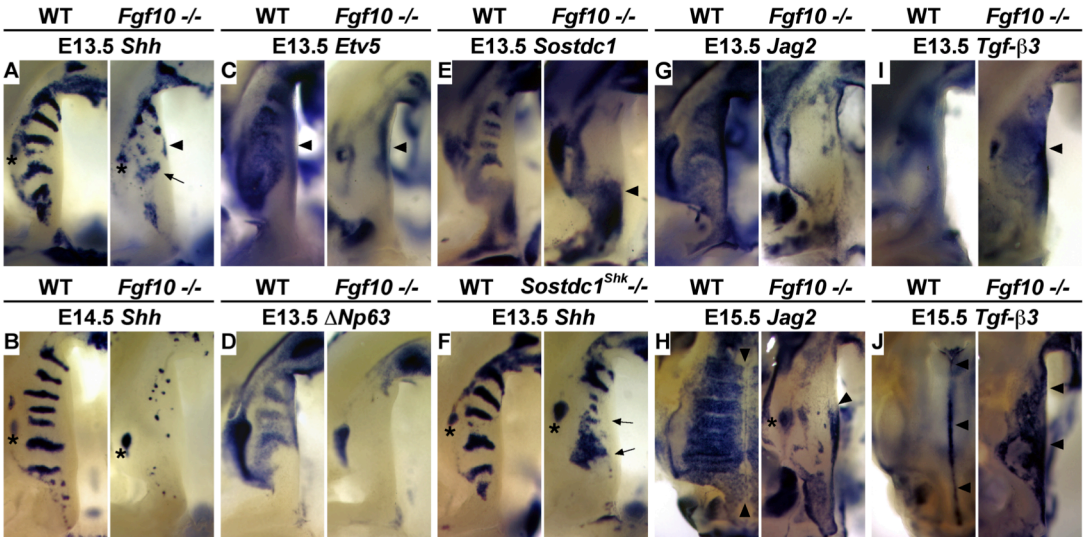

Figure 2.8. Altered patterning of the palatal epithelium associated with loss of the RGZ in *Fgf10* mutants. **(A)** The RGZ is reduced in size (distance between R1 and the molar tooth bud) and *Shh* expression in R1 (arrow) is diminished in E13.5 *Fgf10* mutant palates. *Shh* is highly disorganized in the anterior palate and ectopically expressed in the medial edge epithelium (arrowheads). (**B**) In the E14.5 *Fgf10* mutant, *Shh* expression is reduced to small puncta of expression in the anterior palate and all evidence of R1 and the RGZ has been lost. At E13.5 *Fgf10* mutants exhibit specific loss of gene expression in the RGZ and inter-rugae epithelium of the anterior palate including that of: (**C**) *Etv5,* a transcriptional mediator of the FGF/MAPK pathway (arrowheads mark expression in the mesenchyme), (**D**) *DNp63*, and (**E**) *Sostdc1*, a negative feedback inhibitor of BMP signaling. Mesenchymal expression of *Sostdc1* (**E**) in the presumptive soft palate and adjacent tooth anlage is elevated (arrowhead). (**F**) Loss of *Sostdc1* function in the spontaneous mutant Sharky (*Sostdc1*^{Shk}), results in expanded expression of *Shh* in the molar tooth bud (asterisk), ectopic expression throughout the RGZ (arrows), and an increased distance between these two expression domains. (**G-J**) Patterning of the medial edge epithelium (MEE) is also altered in Fgf10 mutants. (**G**) In E13.5 wildtype, *Jag2* is expressed in inter-rugae domains of the anterior palate and the medial edge epithelium (MEE) but excluded from rugae. *Jag2* expression is absent within the RGZ and anterior oral epithelium of E13.5 *Fgf10* mutants but weak expression is seen medially. (**H**) *Jag2* expression is downregulated within the MEE of E15.5 wildtype palates and the medial boundary of inter-rugae *Jag2* expression abuts the MEE (arrowheads). In E15.5 *Fgf10* mutants, *Jag2* is ectopically expressed in the MEE (arrowhead) with an anterior boundary that is aligned with the normal anterior extent of the RGZ (asterisk marks the molar tooth bud). (**I**) *Tgf-b3* expression is significantly upregulated in *Fgf10* mutant palates at E13.5, particularly in the MEE adjacent to the region of the RGZ (arrowhead). (**J**) In the fusing palates of E15.5 wildtype embryos, *Tgf-b3* expression is restricted to the medial epithelial seem (MES) (arrowheads). *Tgf-b3* expression in E15.5 *Fgf10* mutants is ectopically expressed across the oral surface of the palatal shelf but reduced in the region showing highest levels of precocious expression at E13.5 and ectopic *Jag2* at E15.5 (arrowheads).

deletion in exon 2 (Craniofacial Resource, The Jackson Laboratory, www.jax.org/cranio/index.html). Significantly, we found that *Shh* is ectopically expressed throughout the RGZ of *Sostdc1*^{Shk} mutant palates at E13.5 (Fig. 2.8F). This

data supports that similar to its role in tooth cusp patterning, *Sostdc1* in the palate acts to regulate induction of signaling centers.

The epithelial patterning defects in *Fgf10* mutants are not limited to the organization of gene expression domains along the A-P axis of the palate. We note that from E14.5 to E15.5 as the palatal shelves make contact and fuse, the medial edge of palatal rugae share a common boundary with the lateral extent of medial edge epithelia (MEE). Only after shelf fusion at E16.5 do the anterior-most rugae (R3, R2, and R4) fuse across the midline. Down-regulation of *Jag2* and the restricted expression of *Tgf-b3* within the medial edge MEE is part of an intrinsic program to pattern palatal epithelium and localize the tissue remodeling that promotes shelf fusion in the region of midline contact (Jin et al., 2008). Interestingly, we found that the inter-rugae expression of *Jag2* is lost in *Fgf10* mutants but is expressed ectopically in the MEE (Fig. 8G, H) while *Tgf-b3* is precociously and ectopically expressed across the oral epithelium of *Fgf10* mutant palates (Fig. 8I, J). Therefore, failed rugae morphogenesis and altered epithelial patterning resulting from loss of *Fgf10* impacts both the anterior-posterior and medial-lateral axis of the palatal shelves.

Collectively our data suggests that a highly integrated molecular circuit coordinates epithelial-mesenchymal signaling within the RGZ in order to direct the periodic differentiation of SHH expressing signaling centers during palate outgrowth. Mesenchymal *Fgf10* acting upstream of both *p63* and *Sostdc1* thus provides a mechanism to couple both FGF10 and BMP4 regulation of *Shh* expression by restricting induction of *Shh* expression to the anterior edge of the *Fgf10* gradient in the RGZ.

2.5 Discussion

2.5.1 The RGZ and spatial organization of a network of genes that directs palate development

In this study we have identified a novel region of morphogenetic activity, the RGZ, that functions to integrate multiple signaling pathways critical for guiding palate morphogenesis. Signaling via the FGF, BMP, and SHH pathways is essential for multiple aspects of craniofacial development (Abzhanov and Tabin, 2004; Hu and Helms, 1999; Kim et al., 1998; Trumpp et al., 1999). The spatial organization of molecular interactions amongst these pathways has been shown to establish the frontonasal ectodermal zone (FEZ) that directs mid-facial outgrowth (Abzhanov et al., 2007; Abzhanov et al., 2004; Hu et al., 2003). In the secondary palate, both *Fgf10* and *Bmp4* are required for the expression of *Shh* (Rice et al., 2004; Zhang et al., 2002). However, a mechanism explaining their combined regulation of *Shh* has been lacking. We propose a molecular model involving *p63* and *Sostdc1* that integrates FGF10 and BMP4 signaling that balances epithelial proliferation and differentiation to control the sequential induction of *Shh* expression in the palate (Fig. 2.9A). Epithelial SHH signaling to the mesenchyme completes a positive feedback loop that maintains *Fgf10* expression and is required for directing patterning and outgrowth of the palate (Lan and Jiang, 2009). In this way, the periodic formation of rugae signaling centers supplies a register of signaling cues to the underlying mesenchyme as the palate extends anteriorly. The periodicity of rugae formation will facilitate a more detailed

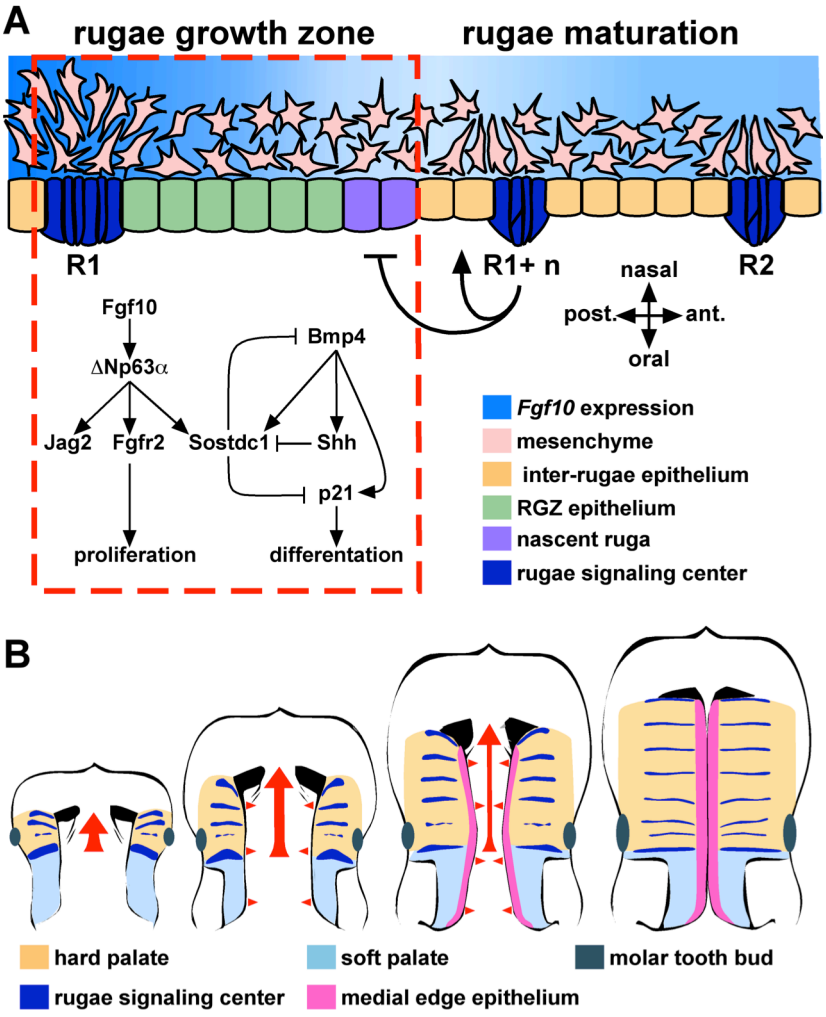

Figure 2.9. Models of the molecular and morphogenetic activity associated with the RGZ. (**A**) We suggest a model of molecular interactions integrating FGF10 and BMP4 signaling during rugae formation within the RGZ. Both *Fgf10* and *Bmp4* are required for epithelial expression of *Shh*. The RGZ acts as a source of both rugae and inter-rugae epithelium. Within the RGZ, *Fgf10* is expressed in a gradient extending from R1 to the site of nascent rugae formation. We propose that FGF10 signaling, mediated through *DNp63a* and its targets *Jag2* and *Fgfr2b*, maintains proliferation of epithelial progenitors at the posterior end of the RGZ. Epithelial expression of the *Bmp4* antagonist *Sostdc1* in the anterior palate also requires *Fgf10*. We found that similar to its role in tooth cusp patterning, *Sostdc1* acts to restrict induction of *Shh* in the RGZ. We propose that the relative balance between FGF10 and BMP4 signaling is one component defining the A-P position of rugae formation. Induction of *Shh* and *p21* expression results in cell cycle exit and epithelial differentiation while continued proliferation of inter-rugae epithelium moves the R1+n rugae away from the RGZ. Signals from the R1+n rugae (bar and arrow) are also proposed to influence the fate of RGZ epithelium. (**B**) The anterior growth of the anterior palate (tan) proceeds from the first formed rugae (red arrow) and is coincident with the establishment of segmental signaling domains (rugae). Fusion of the bilateral shelves requires medially directed growth (red arrowheads) and patterning of the medial edge epithelium (MEE, pink). The lateral boundary of the MEE coincides with the medial edge of the rugae, suggesting that signals from the rugae also participate in the intrinsic program that patterns the MEE. Thus, rugae and the RGZ provide a reference frame for visualizing the organization of signaling domains with respect to the anterior–posterior and medial-lateral patterning and growth of the palatal shelves.

dissection of the timing of molecular and cellular events that establish and maintain this critical epithelial-mesenchymal feedback loop.

The early disorganized and ectopic expression of *Shh* in *Fgf10* mutant palates, followed by progressive loss of *Shh* expression, demonstrates that *Shh* is not directly dependent on *Fgf10*. Instead, our data indicates that mesenchymal *Fgf10* is required to organize and maintain the RGZ and rugae morphogenesis, possibly through *p63* mediated maintenance of an epithelial progenitor population in the posterior RGZ (Harada et al., 2002). In addition to *Shh*, loss of RGZ activity in *Fgf10* mutants results in the absence or altered expression of *Etv5*, *p63*, and *Fgf9*. Similar to *p63*, epithelial expression of the BMP signaling antagonist *Sostdc1* is completely lost in the anterior palate while expression posterior to the RGZ and in the molar tooth bud is actually elevated. Loss of *p63* results in elevated BMP4 signaling, loss of *Shh* expression and failed outgrowth of the anterior palate (Thomason et al., 2008). Altered expression in *Fgf10* mutants suggest that *Sostdc1* is a downstream target through which *p63* regulates *Bmp4*.

We have identified complementary rugae and inter-rugae specific expression of ligands, receptors, and transcriptional mediators in both the epithelium and mesenchyme providing new insight into the directionality, organization, and spatial integration of signaling interactions that guide palate morphogenesis. For example, both loss and gain of function mutations of *Fgf9* have been reported to result in cleft palate, however the etiology underlying the defect has not been analyzed (Colvin et al., 2001; Harada et al., 2009; Murakami et al., 2002). Rugae specific expression of *Fgf9* in the epithelium along with *Etv4* (*Pea3*) in the underlying mesenchyme suggests

the presence of a reciprocal epithelial-mesenchymal FGF feedback loop commonly observed during the development of other structures (del Moral et al., 2006; Sun et al., 2000; Zhang et al., 2006). Our data support a model where rugae signaling centers, established through the dynamic activity of the RGZ, provide a framework to organize a network of genes that pattern the three dimensional growth and patterning of the palatal shelves (Fig. 2.9B).

2.5.2 The RGZ and regional differences in A-P growth of the palate

The RGZ, positioned at the A-P junction of the future soft and elongating hard palate, provides a landmark for understanding regional differences in palate outgrowth and patterning. Elongation of the maxillary prominence is accompanied by growth of the anterior palate. A recent report from Li and Ding compared the dynamic expression of anteriorly restricted *Shox2* with *Meox2*, a marker of posterior palatal fate, during A-P elongation of the palatal shelves (Jin and Ding, 2006; Li and Ding, 2007). Focusing on the changes in the relative size of the *Shox2* and *Meox2* expression domains during palate development, the authors argue that the growth of the anterior palate involves a posteriorly directed expansion of *Shox2* expression and conversion of once posterior *Meox2* expressing cells into an anterior fate. However, in the present study we demonstrate that the position of R1 remains constant relative to *Shox2* and *Barx1* expression, markers of anterior and posterior mesenchymal fate respectively. This observation is inconsistent with a posteriorly directed expansion of the *Shox2* expression domain. Furthermore, we show that rostral extension of the anterior epithelium is achieved by interposition of additional rugae and inter-rugae domains

between R1 and the R1+n rugae, implying the presence of an epithelial progenitor population in the posterior RGZ that is maintained by high levels of FGF10 (Harada et al., 2002). Differences in mesenchymal proliferation rates along the A-P axis of the palate have not been documented (Li and Ding, 2007; Liu et al., 2008). This suggests that an alternative mechanism provides a source of mesenchyme to accompany the growth of the anterior palate immediately anterior to R1.

Recent analysis of cleft palate in *Wnt5a* mutants identified the presence of directed cell migration in the developing palate (He et al., 2008; Li and Ding, 2007; Liu et al., 2008). Isotopic grafting of EGFP expressing anterior or posterior palatal mesenchyme into wildtype or *Wnt5a* mutant palates demonstrated that posterior palatal mesenchyme preferentially migrates anteriorly whereas anterior mesenchyme tends to migrate towards the lateral palate. Interestingly, the authors showed that directed migration is dependent on a *Wnt5a* expression gradient in the anterior palate that is complementary to the *Fgf10* gradient that we report here. Furthermore, in addition to *Wnt5a* He et al. found that FGF10 also acts as a potent chemoattractant for palatal mesenchyme. Therefore, the strong expression domain of *Fgf10* at the junction of the anterior and posterior palate and the complementary *Wnt5a* expression gradient in the anterior palate (see Fig. 2A) suggest that a complex and combinatorial control of cell movements may be involved in the rostral outgrowth of the palatal shelves. Further investigation of the differences in migratory behavior between anterior and posterior palatal mesenchyme in reference to the landmarks provided by the RGZ will likely prove informative.

2.5.3 Modularity and integration of signaling domains during craniofacial outgrowth

Craniofacial development involves the precisely coordinated outgrowth and midline fusion of multiple bud-like prominences and requires positional and patterning information provided by spatially separated signaling centers. In avians and mammals, formation of the beak or nasal capsule and primary palate is coordinated by FEZ signals that direct the growth of the frontonasal mass (Hu and Marcucio, 2009b; Wu et al., 2006b). The mammalian secondary palate represents an elaboration of the skeletodontal elements of the upper jaw within the vertebrate craniofacial body plan. We have identified the RGZ, strategically positioned relative to the A-P axis of the palate, as the location of periodic generation of signaling centers during the rostral outgrowth of the palate. We observe that at E11.5 *Shh* expression in the FEZ is contiguous with the adjacent region of the maxillary prominence that will give rise to R1 (see Fig. 3C and F). During the initial stages of secondary palate development, the site of R1 formation is closely associated with the formation of the primary choanae that presages the site of fusion between the primary palate with the anterior secondary palate (Tamarin, 1982). Therefore, growth of the anterior hard palate occurs via the expansion of the domain intervening the FEZ and R1. How these two morphogenetic domains may be integrated to coordinate craniofacial development is an important question with the potential to significantly advance our understanding of the etiology of an important class of birth defects, clefting of the primary and secondary palate (cleft lip and cleft palate).

To address the question of coordination between morphogenic domains during craniofacial development, Depew and Simpson have proposed a “hinge and caps”

model to explain how spatially distributed sources of positional information may be integrated to achieve a "global" solution to the outgrowth of the numerous facial primordia that form the oral cavity in gnathostomes (Depew and Simpson, 2006). This model is based upon the interplay between prepatterned populations of CNC with the activity of proximo-distal positioned epithelial signaling centers. In the model, proximal "hinge" and distal "caps" derived signals coordinate the outgrowth and patterning of intervening tissue to achieve midline fusion of paired facial primordia as well as maintain proper registration between elements of the upper and lower jaws (Depew and Compagnucci, 2008; Depew and Simpson, 2006). "Hinge" defining signals, including *Fgf8*, *Ptx2*, and the nested expression of the *Dlx* gene family members, emanate from the junction of the maxillary and mandibular components of the first branchial arch. "Caps" are sources of positional information located most distally from the "hinge" region, such as the distal mandibular arch of the lower jaw and the lamboidal junction between the distal maxillary arch and frontonasal mass of the upper jaw (i.e. the FEZ). The juxtaposition of proximal and distal sources of positional information imposes an inherent polarity upon the developing facial primordia. A prediction that follows from this model is the potential to establish coordinating domains or "developmental modules" within the facial prominences that are defined in response to "hinge" and "caps" signaling. Such "developmental modules" would provide a mechanism for coordinating the growth of autonomous components of the upper and lower jaw.

The FEZ-directed rostral growth of the midfacial complex is accompanied by the extension of the anterior palate. We propose that the modularity of rugae signaling

domains provides a distributed system of common instructional cues that maintain growth of the secondary palate in proper registration with the surrounding elements of the upper jaw. Furthermore, integration of the unique periodic activity of the RGZ within the hierarchy of the "hinge and caps" model would also provide a mechanism to maintain evolutionary plasticity while meeting the morphogenic requirements specific to palate closure. If RGZ dynamics are coupled with adjacent "hinge and caps" signaling domains, evolutionary variation in facial form resulting from species-specific activity of the FEZ would conceivably be accompanied by corresponding output from the RGZ. As evidence in support of this hypothesis, we note that species-specific variations in rugae number from 3-4 in human, 8 in mouse, and 18 in the horse correlate with striking differences in the rostral extension of the face and the underlying skeletal elements. Therefore, signaling dynamics within the RGZ potentially provide a readily modulated mechanism that satisfies the need to coordinate a phylogenetically inherited body plan for skull development with the palate morphogenetic program while also accommodating evolutionary adaptation of facial form.

2.6 Materials and methods

Mice

Fgf10 +/- mice, originally described by Sekine (Sekine et al., 1999), were provided by Dr. J. Greer (University of Alberta, Canada) and maintained on a C57Bl/6J background. Genomic DNA from tail biopsies was isolated for genotyping mice with

the following primers: wildtype fwd., (5'-CTTCCAGTATGTTCCTTCTGATGAGAC-3'); wildtype rev., (5'-GTACGGACAGTCTTCTTCTTGGTCCC-3'); mutant fwd., (5'-ACGACGGGCGTTCCTTGCGCAGCTGTG-3'); mutant rev., (5'-TCAGAAGAACCGTCAAGAAGGCGATA-3'). Occasional ectopic fusions of the palate to the tongue or mandible in *Fgf10* mutants were noted at the time of dissection and only samples without fusions were selected for expression analysis. The *Sostdc1*^{shk}/J (Sharkey) mouse is a spontaneous mutation resulting from a single base pair deletion in exon 2 of *Sostdc1* which introduces a premature stop codon. Sharkey mice were acquired from the craniofacial mutant resource at the Jackson Laboratory (Bar Harbor, Maine) and maintained as a homozygous population.

RNA isolation and Quantitative RT-PCR

Individual palatal shelves were dissected free of surrounding tissue including the molar tooth bud, snap frozen in RNAlater (Invitrogen), and stored at -80^{o}C until processing. RNA from each palatal shelf was purified using the RNeasy Micro kit (Qiagen) and RNA yield and quality were assessed via Nanodrop UV spectrophotometry. Individual cDNAs were generated from each sample via reverse transcription of 1.0 mg of total RNA using the ABI high capacity archive kit. Quantitative real-time PCR on an ABI 7500 platform was carried out on triplicate reactions of each sample using 5.0 ng of cDNA template. b-Actin expression was used as an endogenous control and cDNA derived from a pool of 1.0 mg each of E8.5-E18.5 whole embryo RNA was used to calibrate relative expression levels in both

wildtype (n=3) and mutant (n=4). The following ABI TaqMan probes were used in this analysis: *Bmp4*, Mm_00432087_m1; *Etv5*, Mm_00465816_m1; *Fgf9*, 00442759_m1; *Jag2*, Mm_00439935_m1; *DNp63*, Mm_01169470_m1; *Tap63*, Mm_01150797_m1; *Shh*, Mm_00436527_m1; *Sostdc1*, Mm_00840254_m1.

In situ hybridization

Whole mount and section *in situ* hybridization was performed with digoxygenin (DIG) or dinitrophenol (DNP) labeled antisense riboprobes. Processing of whole mount samples was carried out on an Intavis InsituPro VS robotic platform. Samples for section *in situ* were fresh frozen in OCT compound and sectioned at 20 mm thickness. For experiments involving mutants, wildtype and mutants were processed together and detected for an identical period. Gene expression was analyzed in 3 wildtype and 4 mutant samples. Detailed protocols and a complete list of sequences cloned to generate *in situ* probes are available upon request.

BrdU labeling

Embryos were labeled with BrdU (Roche) by injecting pregnant females with 10mM BrdU (20ml/gram of body weight) 1 hour prior to sacrifice. Heads were embedded in paraffin and serial 6 mm sagittal sections collected. DNA was denatured with 2N HCl for one hour prior to incubation with anti-BrdU (Roche) followed by Cy3 (Molecular Probes) and counterstaining with DAPI. 3 sections through the region of the RGZ of E13.5 embryos (n=4) were used to count the number of BrdU positive cells and the total number of cells to determine the mitotic index for each domain. The RGZ was

divided into two equal domains defined by drawing a vertical line midway between the anterior extent of R1 and the posterior boundary of the first inter-rugae domain.

2.7 Acknowledgements

We thank Drs. Mark Roberson, Kevin Peterson and Randal Babiuk for critical reading of the manuscript along with Jim Hagarman for helpful discussions and Yingying Zhao for technical assistance. We thank Dr. Leah-Rae Donahue and Julie Hurd at the Craniofacial Mutant Resource at The Jackson Laboratory for assistance with Sharkey mice. This work was supported by National Institutes of Health (NIH) HD41066 (T.P.O.) and a Presidential Life Sciences fellowship from Cornell University (I.C.W.).

REFERENCES

Abzhanov, A., Cordero, D. R., Sen, J., Tabin, C. J., Helms, J. A., 2007. Cross-regulatory interactions between Fgf8 and Shh in the avian frontonasal prominence. Congenit Anom (Kyoto). 47**,** 136-48.

Abzhanov, A., Protas, M., Grant, B. R., Grant, P. R., Tabin, C. J., 2004. Bmp4 and morphological variation of beaks in Darwin's finches. Science. 305**,** 1462-5.

Abzhanov, A., Tabin, C. J., 2004. Shh and Fgf8 act synergistically to drive cartilage outgrowth during cranial development. Dev Biol. 273**,** 134-48.

Ahlgren, S. C., Bronner-Fraser, M., 1999. Inhibition of sonic hedgehog signaling in vivo results in craniofacial neural crest cell death. Curr Biol. 9**,** 1304-14.

Alappat, S. R., Zhang, Z., Suzuki, K., Zhang, X., Liu, H., Jiang, R., Yamada, G., Chen, Y., 2005. The cellular and molecular etiology of the cleft secondary palate in Fgf10 mutant mice. Dev Biol. 277**,** 102-13.

Barlow, A. J., Bogardi, J. P., Ladher, R., Francis-West, P. H., 1999. Expression of chick Barx-1 and its differential regulation by FGF-8 and BMP signaling in the maxillary primordia. Dev Dyn. 214**,** 291-302.

Barrow, L. L., van Bokhoven, H., Daack-Hirsch, S., Andersen, T., van Beersum, S. E., Gorlin, R., Murray, J. C., 2002. Analysis of the p63 gene in classical EEC syndrome, related syndromes, and non-syndromic orofacial clefts. J Med Genet. 39**,** 559-66.

Bitgood, M. J., McMahon, A. P., 1995. Hedgehog and Bmp genes are coexpressed at many diverse sites of cell-cell interaction in the mouse embryo. Dev Biol. 172**,** 126-38.

Candi, E., Rufini, A., Terrinoni, A., Giamboi-Miraglia, A., Lena, A. M., Mantovani, R., Knight, R., Melino, G., 2007. DeltaNp63 regulates thymic development through enhanced expression of FgfR2 and Jag2. Proc Natl Acad Sci U S A. 104**,** 11999-2004.

Casey, L. M., Lan, Y., Cho, E. S., Maltby, K. M., Gridley, T., Jiang, R., 2006. Jag2-Notch1 signaling regulates oral epithelial differentiation and palate development. Dev Dyn. 235**,** 1830-44.

Colvin, J. S., White, A. C., Pratt, S. J., Ornitz, D. M., 2001. Lung hypoplasia and neonatal death in Fgf9-null mice identify this gene as an essential regulator of lung mesenchyme. Development. 128**,** 2095-106.

del Moral, P. M., De Langhe, S. P., Sala, F. G., Veltmaat, J. M., Tefft, D., Wang, K., Warburton, D., Bellusci, S., 2006. Differential role of FGF9 on epithelium and mesenchyme in mouse embryonic lung. Dev Biol. 293**,** 77-89.

Depew, M. J., Compagnucci, C., 2008. Tweaking the hinge and caps: testing a model of the organization of jaws. J Exp Zoolog B Mol Dev Evol. 310**,** 315-35.

Depew, M. J., Simpson, C. A., 2006. 21st century neontology and the comparative development of the vertebrate skull. Dev Dyn. 235**,** 1256-91.

Firnberg, N., Neubuser, A., 2002. FGF signaling regulates expression of Tbx2, Erm, Pea3, and Pax3 in the early nasal region. Dev Biol. 247**,** 237-50.

Gritli-Linde, A., 2007. Molecular control of secondary palate development. Dev Biol. 301**,** 309-26.

Harada, H., Toyono, T., Toyoshima, K., Yamasaki, M., Itoh, N., Kato, S., Sekine, K., Ohuchi, H., 2002. FGF10 maintains stem cell compartment in developing mouse incisors. Development. 129**,** 1533-41.

Harada, M., Murakami, H., Okawa, A., Okimoto, N., Hiraoka, S., Nakahara, T., Akasaka, R., Shiraishi, Y., Futatsugi, N., Mizutani-Koseki, Y., Kuroiwa, A., Shirouzu, M., Yokoyama, S., Taiji, M., Iseki, S., Ornitz, D. M., Koseki, H.,

2009. FGF9 monomer-dimer equilibrium regulates extracellular matrix affinity and tissue diffusion. Nat Genet. 41**,** 289-98.

Haworth, K. E., Healy, C., Morgan, P., Sharpe, P. T., 2004. Regionalisation of early head ectoderm is regulated by endoderm and prepatterns the orofacial epithelium. Development. 131**,** 4797-806.

Haworth, K. E., Wilson, J. M., Grevellec, A., Cobourne, M. T., Healy, C., Helms, J. A., Sharpe, P. T., Tucker, A. S., 2007. Sonic hedgehog in the pharyngeal endoderm controls arch pattern via regulation of Fgf8 in head ectoderm. Dev Biol. 303**,** 244-58.

He, F., Xiong, W., Yu, X., Espinoza-Lewis, R., Liu, C., Gu, S., Nishita, M., Suzuki, K., Yamada, G., Minami, Y., Chen, Y., 2008. Wnt5a regulates directional cell migration and cell proliferation via Ror2-mediated noncanonical pathway in mammalian palate development. Development. 135**,** 3871-9.

Hilliard, S. A., Yu, L., Gu, S., Zhang, Z., Chen, Y. P., 2005. Regional regulation of palatal growth and patterning along the anterior-posterior axis in mice. J Anat. 207**,** 655-67.

Hu, D., Helms, J. A., 1999. The role of sonic hedgehog in normal and abnormal craniofacial morphogenesis. Development. 126**,** 4873-84.

Hu, D., Marcucio, R. S., 2009a. A SHH-responsive signaling center in the forebrain regulates craniofacial morphogenesis via the facial ectoderm. Development. 136**,** 107-16.

Hu, D., Marcucio, R. S., 2009b. Unique organization of the frontonasal ectodermal zone in birds and mammals. Dev Biol. 325**,** 200-10.

Hu, D., Marcucio, R. S., Helms, J. A., 2003. A zone of frontonasal ectoderm regulates patterning and growth in the face. Development. 130**,** 1749-58.

Ibrahimi, O. A., Eliseenkova, A. V., Plotnikov, A. N., Yu, K., Ornitz, D. M., Mohammadi, M., 2001. Structural basis for fibroblast growth factor receptor 2 activation in Apert syndrome. Proc Natl Acad Sci U S A. 98**,** 7182-7.

Jeong, J., Mao, J., Tenzen, T., Kottmann, A. H., McMahon, A. P., 2004. Hedgehog signaling in the neural crest cells regulates the patterning and growth of facial primordia. Genes Dev. 18**,** 937-51.

Jernvall, J., Aberg, T., Kettunen, P., Keranen, S., Thesleff, I., 1998. The life history of an embryonic signaling center: BMP-4 induces p21 and is associated with apoptosis in the mouse tooth enamel knot. Development. 125**,** 161-9.

Jin, J. Z., Ding, J., 2006. Analysis of Meox-2 mutant mice reveals a novel postfusion-based cleft palate. Dev Dyn. 235**,** 539-46.

Jin, J. Z., Li, Q., Higashi, Y., Darling, D. S., Ding, J., 2008. Analysis of Zfhx1a mutant mice reveals palatal shelf contact-independent medial edge epithelial differentiation during palate fusion. Cell Tissue Res. 333**,** 29-38.

Kassai, Y., Munne, P., Hotta, Y., Penttila, E., Kavanagh, K., Ohbayashi, N., Takada, S., Thesleff, I., Jernvall, J., Itoh, N., 2005. Regulation of mammalian tooth cusp patterning by ectodin. Science. 309**,** 2067-70.

Kim, H. J., Rice, D. P., Kettunen, P. J., Thesleff, I., 1998. FGF-, BMP- and Shh-mediated signalling pathways in the regulation of cranial suture morphogenesis and calvarial bone development. Development. 125**,** 1241-51.

Lan, Y., Jiang, R., 2009. Sonic hedgehog signaling regulates reciprocal epithelial-mesenchymal interactions controlling palatal outgrowth. Development. 136**,** 1387-96.

Lan, Y., Ovitt, C. E., Cho, E. S., Maltby, K. M., Wang, Q., Jiang, R., 2004. Odd-skipped related 2 (Osr2) encodes a key intrinsic regulator of secondary palate growth and morphogenesis. Development. 131**,** 3207-16.

Laurikkala, J., Kassai, Y., Pakkasjarvi, L., Thesleff, I., Itoh, N., 2003. Identification of a secreted BMP antagonist, ectodin, integrating BMP, FGF, and SHH signals from the tooth enamel knot. Dev Biol. 264**,** 91-105.

Laurikkala, J., Mikkola, M. L., James, M., Tummers, M., Mills, A. A., Thesleff, I., 2006. p63 regulates multiple signalling pathways required for ectodermal organogenesis and differentiation. Development. 133**,** 1553-63.

Lee, J. M., Kim, J. Y., Cho, K. W., Lee, M. J., Cho, S. W., Zhang, Y., Byun, S. K., Yi, C. K., Jung, H. S., 2007. Modulation of cell proliferation during palatogenesis by the interplay between Tbx3 and Bmp4. Cell Tissue Res. 327**,** 285-92.

Lee, S. H., Bedard, O., Buchtova, M., Fu, K., Richman, J. M., 2004. A new origin for the maxillary jaw. Dev Biol. 276**,** 207-24.

Li, Q., Ding, J., 2007. Gene expression analysis reveals that formation of the mouse anterior secondary palate involves recruitment of cells from the posterior side. Int J Dev Biol. 51**,** 167-72.

Liu, W., Lan, Y., Pauws, E., Meester-Smoor, M. A., Stanier, P., Zwarthoff, E. C., Jiang, R., 2008. The Mn1 transcription factor acts upstream of Tbx22 and preferentially regulates posterior palate growth in mice. Development. 135**,** 3959-68.

Liu, W., Selever, J., Lu, M. F., Martin, J. F., 2003. Genetic dissection of Pitx2 in craniofacial development uncovers new functions in branchial arch morphogenesis, late aspects of tooth morphogenesis and cell migration. Development. 130**,** 6375-85.

Liu, W., Sun, X., Braut, A., Mishina, Y., Behringer, R. R., Mina, M., Martin, J. F., 2005. Distinct functions for Bmp signaling in lip and palate fusion in mice. Development. 132**,** 1453-61.

Marcucio, R. S., Cordero, D. R., Hu, D., Helms, J. A., 2005. Molecular interactions coordinating the development of the forebrain and face. Dev Biol. 284**,** 48-61.

Mikkola, M. L., 2007. p63 in skin appendage development. Cell Cycle. 6**,** 285-90.

Mills, A. A., Zheng, B., Wang, X. J., Vogel, H., Roop, D. R., Bradley, A., 1999. p63 is a p53 homologue required for limb and epidermal morphogenesis. Nature. 398**,** 708-13.

Murakami, H., Okawa, A., Yoshida, H., Nishikawa, S., Moriya, H., Koseki, H., 2002. Elbow knee synostosis (Eks): a new mutation on mouse Chromosome 14. Mamm Genome. 13**,** 341-4.

Nguyen, B. C., Lefort, K., Mandinova, A., Antonini, D., Devgan, V., Della Gatta, G., Koster, M. I., Zhang, Z., Wang, J., Tommasi di Vignano, A., Kitajewski, J., Chiorino, G., Roop, D. R., Missero, C., Dotto, G. P., 2006. Cross-regulation between Notch and p63 in keratinocyte commitment to differentiation. Genes Dev. 20**,** 1028-42.

Noden, D. M., 1983. The role of the neural crest in patterning of avian cranial skeletal, connective, and muscle tissues. Dev Biol. 96**,** 144-65.

Ohazama, A., Johnson, E. B., Ota, M. S., Choi, H. Y., Porntaveetus, T., Oommen, S., Itoh, N., Eto, K., Gritli-Linde, A., Herz, J., Sharpe, P. T., 2008. Lrp4 modulates extracellular integration of cell signaling pathways in development. PLoS One. 3**,** e4092.

Okuyama, R., Ogawa, E., Nagoshi, H., Yabuki, M., Kurihara, A., Terui, T., Aiba, S., Obinata, M., Tagami, H., Ikawa, S., 2007. p53 homologue, p51/p63, maintains the immaturity of keratinocyte stem cells by inhibiting Notch1 activity. Oncogene. 26**,** 4478-88.

Pantalacci, S., Prochazka, J., Martin, A., Rothova, M., Lambert, A., Bernard, L., Charles, C., Viriot, L., Peterkova, R., Laudet, V., 2008. Patterning of palatal rugae through sequential addition reveals an anterior/posterior boundary in palatal development. BMC Dev Biol. 8**,** 116.

Peterkova, R., 1985. The common developmental origin and phylogenetic aspects of teeth, rugae palatinae, and fornix vestibuli oris in the mouse. J Craniofac Genet Dev Biol. 5**,** 89-104.

Pispa, J., Thesleff, I., 2003. Mechanisms of ectodermal organogenesis. Dev Biol. 262**,** 195-205.

Rice, R., Connor, E., Rice, D. P., 2006. Expression patterns of Hedgehog signalling pathway members during mouse palate development. Gene Expr Patterns. 6**,** 206-12.

Rice, R., Spencer-Dene, B., Connor, E. C., Gritli-Linde, A., McMahon, A. P., Dickson, C., Thesleff, I., Rice, D. P., 2004. Disruption of Fgf10/Fgfr2b-coordinated epithelial-mesenchymal interactions causes cleft palate. J Clin Invest. 113**,** 1692-700.

Santagati, F., Rijli, F. M., 2003. Cranial neural crest and the building of the vertebrate head. Nat Rev Neurosci. 4**,** 806-18.

Schneider, R. A., Helms, J. A., 2003. The cellular and molecular origins of beak morphology. Science. 299**,** 565-8.

Schneider, R. A., Hu, D., Helms, J. A., 1999. From head to toe: conservation of molecular signals regulating limb and craniofacial morphogenesis. Cell Tissue Res. 296**,** 103-9.

Schneider, R. A., Hu, D., Rubenstein, J. L., Maden, M., Helms, J. A., 2001. Local retinoid signaling coordinates forebrain and facial morphogenesis by maintaining FGF8 and SHH. Development. 128**,** 2755-67.

Sekine, K., Ohuchi, H., Fujiwara, M., Yamasaki, M., Yoshizawa, T., Sato, T., Yagishita, N., Matsui, D., Koga, Y., Itoh, N., Kato, S., 1999. Fgf10 is essential for limb and lung formation. Nat Genet. 21**,** 138-41.

Shigetani, Y., Nobusada, Y., Kuratani, S., 2000. Ectodermally derived FGF8 defines the maxillomandibular region in the early chick embryo: epithelial-mesenchymal interactions in the specification of the craniofacial ectomesenchyme. Dev Biol. 228**,** 73-85.

Stanier, P., Moore, G. E., 2004. Genetics of cleft lip and palate: syndromic genes contribute to the incidence of non-syndromic clefts. Hum Mol Genet. 13 Spec No 1**,** R73-81.

Sun, X., Lewandoski, M., Meyers, E. N., Liu, Y. H., Maxson, R. E., Jr., Martin, G. R., 2000. Conditional inactivation of Fgf4 reveals complexity of signalling during limb bud development. Nat Genet. 25**,** 83-6.

Szabo-Rogers, H. L., Geetha-Loganathan, P., Nimmagadda, S., Fu, K. K., Richman, J. M., 2008. FGF signals from the nasal pit are necessary for normal facial morphogenesis. Dev Biol. 318**,** 289-302.

Tamarin, A., 1982. The formation of the primitive choanae and the junction of the primary and secondary palates in the mouse. Am J Anat. 165**,** 319-37.

Tao, H., Yoshimoto, Y., Yoshioka, H., Nohno, T., Noji, S., Ohuchi, H., 2002. FGF10 is a mesenchymally derived stimulator for epidermal development in the chick embryonic skin. Mech Dev. 116**,** 39-49.

Thomason, H. A., Dixon, M. J., Dixon, J., 2008. Facial clefting in Tp63 deficient mice results from altered Bmp4, Fgf8 and Shh signaling. Dev Biol. 321**,** 273-82.

Trumpp, A., Depew, M. J., Rubenstein, J. L., Bishop, J. M., Martin, G. R., 1999. Cre-mediated gene inactivation demonstrates that FGF8 is required for cell survival and patterning of the first branchial arch. Genes Dev. 13**,** 3136-48.

Tyler, M. S., Koch, W. E., 1977. In vitro development of palatal tissues from embryonic mice. III. Interactions between palatal epithelium and heterotypic oral mesenchyme. J Embryol Exp Morphol. 38**,** 37-48.

Vigano, M. A., Lamartine, J., Testoni, B., Merico, D., Alotto, D., Castagnoli, C., Robert, A., Candi, E., Melino, G., Gidrol, X., Mantovani, R., 2006. New p63 targets in keratinocytes identified by a genome-wide approach. EMBO J. 25**,** 5105-16.

Welsh, I. C., Hagge-Greenberg, A., O'Brien, T. P., 2007. A dosage-dependent role for Spry2 in growth and patterning during palate development. Mech Dev. 124**,** 746-61.

Wu, G., Nomoto, S., Hoque, M. O., Dracheva, T., Osada, M., Lee, C. C., Dong, S. M., Guo, Z., Benoit, N., Cohen, Y., Rechthand, P., Califano, J., Moon, C. S., Ratovitski, E., Jen, J., Sidransky, D., Trink, B., 2003. DeltaNp63alpha and TAp63alpha regulate transcription of genes with distinct biological functions in cancer and development. Cancer Res. 63**,** 2351-7.

Wu, P., Jiang, T. X., Shen, J. Y., Widelitz, R. B., Chuong, C. M., 2006a. Morphoregulation of avian beaks: Comparative mapping of growth zone activities and morphological evolution. Developmental Dynamics. 235**,** 1400-1412.

Wu, P., Jiang, T. X., Shen, J. Y., Widelitz, R. B., Chuong, C. M., 2006b. Morphoregulation of avian beaks: comparative mapping of growth zone activities and morphological evolution. Dev Dyn. 235**,** 1400-12.

Yamagishi, C., Yamagishi, H., Maeda, J., Tsuchihashi, T., Ivey, K., Hu, T., Srivastava, D., 2006. Sonic hedgehog is essential for first pharyngeal arch development. Pediatr Res. 59**,** 349-54.

Yang, A., Kaghad, M., Wang, Y., Gillett, E., Fleming, M. D., Dotsch, V., Andrews, N. C., Caput, D., McKeon, F., 1998. p63, a p53 homolog at 3q27-29, encodes multiple products with transactivating, death-inducing, and dominant-negative activities. Mol Cell. 2**,** 305-16.

Yang, A., Schweitzer, R., Sun, D., Kaghad, M., Walker, N., Bronson, R. T., Tabin, C., Sharpe, A., Caput, D., Crum, C., McKeon, F., 1999. p63 is essential for regenerative proliferation in limb, craniofacial and epithelial development. Nature. 398**,** 714-8.

Yu, L., Gu, S., Alappat, S., Song, Y., Yan, M., Zhang, X., Zhang, G., Jiang, Y., Zhang, Z., Zhang, Y., Chen, Y., 2005. Shox2-deficient mice exhibit a rare type of incomplete clefting of the secondary palate. Development. 132**,** 4397-406.

Zhang, X., Stappenbeck, T. S., White, A. C., Lavine, K. J., Gordon, J. I., Ornitz, D. M., 2006. Reciprocal epithelial-mesenchymal FGF signaling is required for cecal development. Development. 133**,** 173-80.

Zhang, Z., Song, Y., Zhao, X., Zhang, X., Fermin, C., Chen, Y., 2002. Rescue of cleft palate in Msx1-deficient mice by transgenic Bmp4 reveals a network of BMP and Shh signaling in the regulation of mammalian palatogenesis. Development. 129**,** 4135-46.

CHAPTER 3

Manuscript #2

Integration of L-R Pitx2 transcription and Wnt signaling drives asymmetric gut morphogenesis via Daam2

Integration of L-R *Pitx2* transcription and Wnt signaling drives asymmetric gut morphogenesis via Daam2

Ian C. Welsh[1], Michael Thomsen[1], David W. Gludish[1], Catalina Alfonso-Parra[1], Yan Bai[2], James F. Martin[2], and Natasza A. Kurpios[1*]

[1]Department of Molecular Medicine, College of Veterinary Medicine, Cornell University, Ithaca, NY 14853, USA

[2]Department of Molecular Physiology and Biophysics, Baylor College of Medicine, Houston, TX 77030, USA

*Author for correspondence: natasza.kurpios@cornell.edu, phone: 607-253-4452; fax: 607-253-3659

Running title: The Wnt effector Daam2 drives L-R gut development

3.2 Abstract

A critical aspect of gut morphogenesis is initiation of a leftward tilt. Failure to do so leads to gut malrotation and volvulus. The direction of tilt is specified by asymmetric cell behaviors within the dorsal mesentery (DM), which suspends the gut tube, and is downstream of *Pitx2*, the key transcription factor responsible for the transfer of left-right (L-R) information from early gastrulation to morphogenesis. Although *Pitx2* is a master regulator of L-R organ development, its cellular targets that drive asymmetric morphogenesis are not known. Using laser microdissection and targeted gene misexpression in the chicken DM, we show that *Pitx2*-specific effectors mediate Wnt signaling to activate the formin Daam2, a key Wnt effector and itself a Pitx2 target, linking actin dynamics to cadherin-based junctions, to ultimately generate asymmetric cell behaviors. Our work highlights how integration of two conserved cascades may be the ultimate force through which *Pitx2* sculpts L-R organs.

HIGHLIGHTS

- *Daam2* is a cellular target of Pitx2 required for L-R asymmetric gut morphogenesis
- Pitx2 target genes *Frizzled*, *Daam2* and *Gpc3* mediate noncanonical Wnt signaling
- Daam2 binds a-catenin and N-Cadherin to drive adhesion in the gut dorsal mesentery
- Pitx2 and noncanonical Wnt signaling provide a mechanism for L-R gut morphogenesis

3.3 Introduction

The generation of asymmetry is fundamental to vertebrate development. Most organs develop with a characteristic left-right (L-R) anatomy that is critical to function and coordination of overall organ situs within the body cavity. How global L-R information is translated into asymmetries of cell behavior and coordinated with organ polarity is largely unknown (Gray et al., 2011). Initial L-R symmetry-breaking decisions are made at the primitive node and lead to left-sided expression of the highly conserved, TGFb-related Nodal throughout the left splanchnic mesoderm (Levin et al., 1995). While this restricted expression is transient, Nodal induces the homeobox transcription factor *Pitx2*, whose expression persists to maintain left-side identity of all organ primordia to which the splanchnic mesoderm contributes. This *Pitx2*-driven asymmetry is evolutionarily conserved, and altered *Pitx2* activity disrupts L-R patterning resulting in reversed or isomerised growth of organs. In spite of enormous progress made towards understanding upstream patterning events, mechanisms by which *Pitx2* expression leads to asymmetric changes in tissue organization remain largely unknown (Shiratori and Hamada, 2006). Focusing on the midgut, our goal has been to define the transcriptional targets and cellular mechanisms through which *Pitx2* manifests asymmetric morphogenesis in higher vertebrates.

The primitive gut, a straight epithelial tube surrounded by mesenchymal cells (Fig. 3.1A, yellow), is divided into foregut, midgut, and hindgut along the rostral-caudal axis. Importantly, the midgut lengthens disproportionately to the embryo, resulting in the formation of a primary midgut loop, which herniates ventrally into the

base of the umbilicus (in mammals) or yolk stalk (in birds). A highly conserved counterclockwise rotation accompanies midgut herniation (Fig. 3.1A, curved arrow). This carries the caudal half of the loop cranially on the left, then across the abdomen, before it again passes caudally on the right side, completing a total rotation through 270 degrees. This asymmetric rotation brings the future intestines into the familiar adult position upon retraction into the abdomen.

Chiral midgut rotation in mammals and birds is driven by asymmetric cellular behavior within the dorsal mesentery (DM, Fig. 3.1AB), a bridge of mesoderm connecting the gut tube along its entire axial length to the dorsal body wall (Davis et al., 2008; Hecksher-Sorensen et al., 2004; Kurpios et al., 2008). The embryonic DM consists of four juxtaposed and molecularly distinct cellular compartments: left epithelium, left mesenchyme, right mesenchyme, and right epithelium (Fig. 3.1C). Subsequent cellular changes in each compartment are required to initiate gut rotation. In the chicken, DM forms on day 3 (Hamburger-Hamilton [HH] stage 19) (Hamburger and Hamilton, 1992), and initially these compartments are bilaterally symmetric. However, within 10-12 hours (HH21) DM cells rapidly reorganize via a combination of epithelial shape changes and mesenchymal condensation (left) or expansion (right). Consequently, relative to the dorsal-ventral (D-V) axis the left DM shortens while the right side lengthens, deforming the DM and shifting the attached gut tube to the left (Fig. 3.1C). This leftward tilt provides a directional L-R bias for counterclockwise gut rotation. Importantly, there are no asymmetries in cell number, proliferation or cell

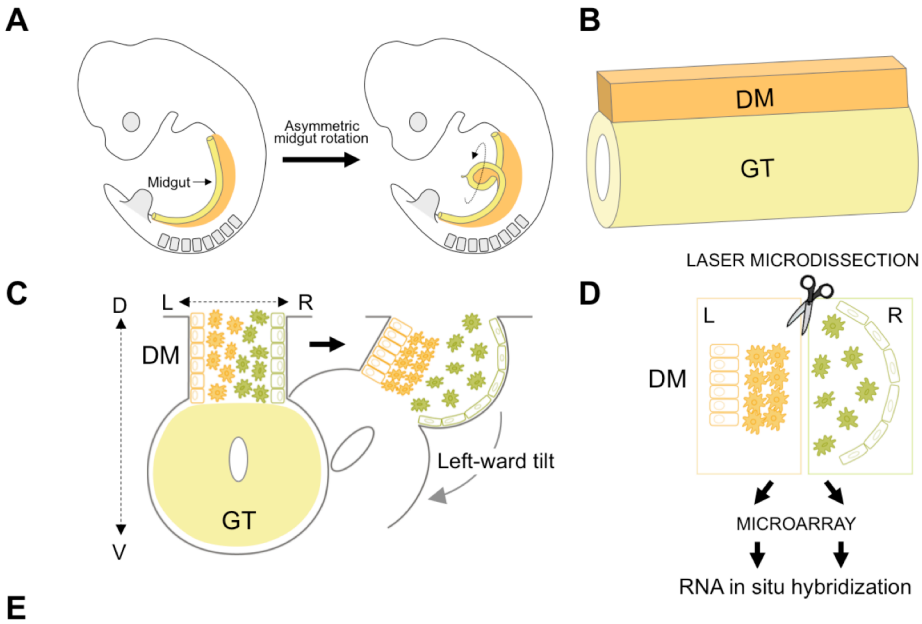

E

	Gene	LE	LM	RM	RE	LE	LM	RM	RE	Significant	Genbank
L	**PITX2**	1.9	1.8	0.3	0.1	5541.1	5204.9	910.8	401.6	Yes	BX935055.1
	DAAM2	1.6	1.3	0.5	0.6	182.5	150.7	64.5	76.8	Yes	ENSGALT00000016348.1
	GPC3	1.5	1.5	0.6	0.4	518.2	547.2	198.3	147.9	Yes	ENSGALT00000009820.1
	FZD8	1.4	1.5	0.6	0.7	74.0	80.7	33.0	35.7	Yes	BX259135
	FZD4	1.2	1.0	0.6	1.0	827.8	679.2	401.3	673.7	Yes	NM_204099.1
	ISL1	1.6	2.2	0.4	0.3	358.0	479.6	93.8	74.3	Yes	NM_205414.1
	WNT5A	1.0	0.8	1.0	1.5	79.2	62.2	85.2	117.1	No	NM_204887.1
R	**SFRP1**	1.0	0.6	1.2	1.1	303.1	180.0	377.3	344.7	Yes	NM_204553.1
	PRICKLE1	0.8	0.6	1.2	1.2	638.6	438.3	894.6	895.4	Yes	ENSGALT00000015558.1
	SFRP2	0.7	0.9	1.1	1.5	330.7	384.7	494.5	677.1	Yes	NM_204773.1
	TBX18	0.4	0.7	1.8	1.5	275.7	407.8	1139.2	941.7	Yes	NM_204453.1

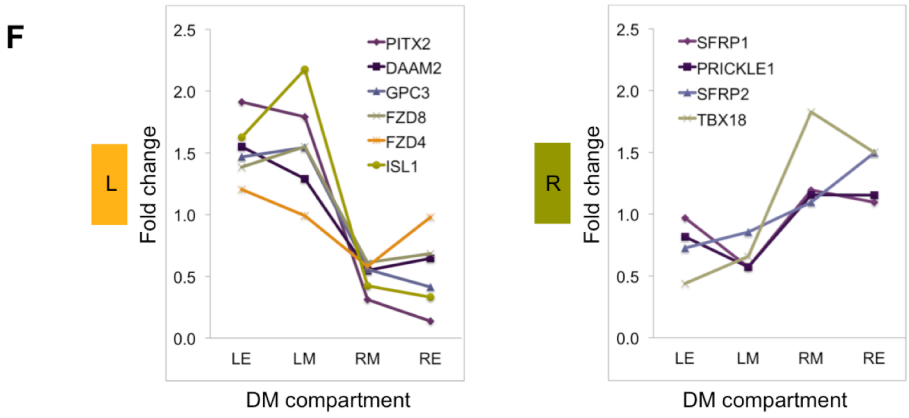

FIG. 3.1. DM and laser capture microdissection (LCM). **A** Gut tube (GT, *yellow*; chicken HH20; mouse E10.0) undergoes counterclockwise rotation at HH21. **B** Gut tube is suspended by DM (*orange*) along the D-V axis. **C** Pitx2-driven deformation of DM at HH21 along the L-R axis initiates gut rotation. **D** LCM of the DM. **E** Selected microarray expression values from epithelium (E) and mesenchyme (M) of the Left (L) or Right (R) chicken DM (at HH21). Raw and normalized expression values are shown. Left genes (*orange)*, right (*green)*, and unbiased (*yellow)* are grouped. **F** Plot of normalized expression fold changes across the L-R axis.

death within the DM showing that gut rotation is strictly a consequence of differential cell behavior across the L-R axis.

Previous studies in birds and mice have established that *Pitx2* is essential to induce the left-specific gene expression and cell behavior within the DM (Davis et al., 2008; Kurpios et al., 2008). Pitx2-null mice are unable to generate the leftward tilt and exhibit randomized chirality of gut rotation (Davis et al., 2008; Shiratori and Hamada, 2006). These studies highlight the DM as a central player in the transfer of early L-R patterning, but leave unresolved the mechanisms by which this initial molecular asymmetry leads to asymmetric cell behavior.

Towards defining these processes, we made use of the binary cellular organization of the DM and its accessibility in ovo and performed laser capture microdissection (LCM) and microarray analysis of the left (*Pitx2* positive) and right (*Pitx2* negative) chicken mesenteric compartments (Fig. 3.1D). This indicated that genes involved in both positive and negative regulation of the Wnt pathway were differentially expressed across the L-R axis. RNA in situ hybridization (ISH) validated the spatial accuracy of these data and highlighted gradients of gene expression along the L-R and orthogonal D-V axis of the DM. Using targeted gene misexpression studies in the chicken DM and mouse genetics, we demonstrate that expression of the formin *Daam2*, a key cellular effector of Wnt signal transduction, is a downstream target of *Pitx2*, that is both necessary and sufficient for Pitx2-directed cell behavior in the mesenchyme of the left DM. We propose a model for *Pitx2* regulation of asymmetric organ morphogenesis: *Pitx2* potentiates asymmetric Wnt signaling via

Daam2 activation, to induce polarized condensation in the left DM necessary to initiate gut rotation.

3.4 Results

3.4.1 Asymmetric organization of a Wnt signaling network across the L-R axis of the DM

Our objective was to identify cellular effectors in the chicken DM that exhibit a spatial expression profile similar to *Pitx2* and which may therefore represent *Pitx2* targets responsible for the cellular behavior in the left DM (Fig. 3.1D). The detailed methodology of LCM together with the microarray data will be described elsewhere. Implicating the role of Wnt signaling, many of the most asymmetric gene expression profiles were those of the Wnt pathway (Fig. 3.1EF). Using ISH, we confirmed that the *Frizzled* (*Fzd*) receptors *Fzd4* and *Fzd8* are exclusively left-sided (Fig. 3.2AB, purple). Moreover, *Fzd4*/*8* are expressed in a nested pattern within the left DM, with *Fzd4* expressed in a broader domain that encompasses the more ventrally restricted *Fzd8*, suggesting a gradient of signaling potential exists along the D-V axis of the left DM (Fig. 3.2AB). The specific combination of *Fzd4/8* has been shown to cooperatively mediate noncanonical Wnt signaling during development (Ye et al., 2011). Whereas we also identified a number of *Fzd* receptors that exhibit bilateral expression in the DM (such as *Fzd1*, Fig. S3.1A), notably, we found no *Fzd* receptors expressed only on the right.

Wnt signaling is spatially modulated by heparan sulfate proteoglycans (Yan and Lin, 2009). For example, Wnt signaling is positively regulated by *Gpc3*

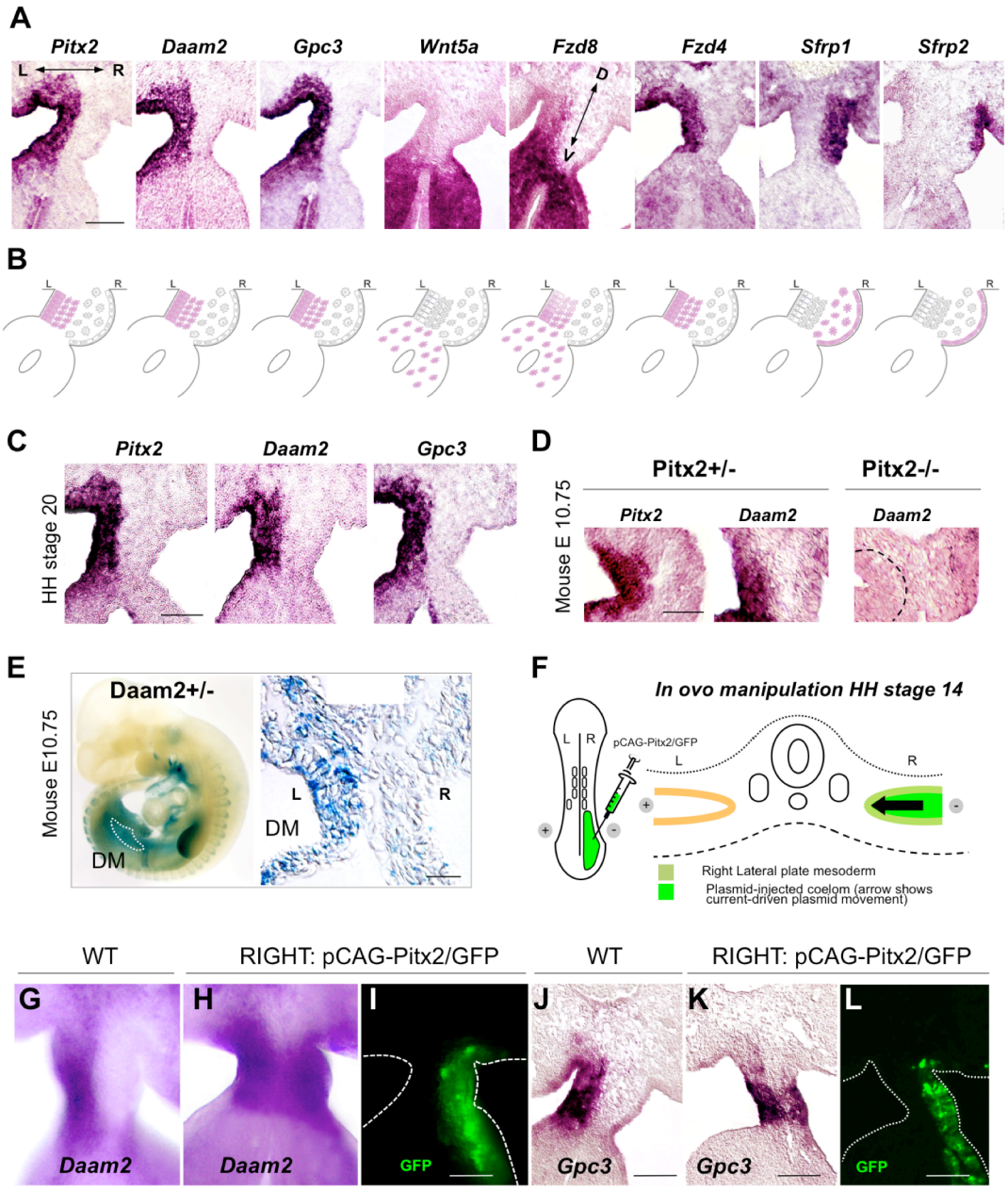

FIG. 3.2. Asymmetric organization of a Wnt signaling network across the L-R DM. **A** ISH, *purple* reveals positive (*Daam2*, *Gpc3*, *Wnt5a*, *Fzd8*, *Fzd4)* and negative (*Sfrp1*, and *Sfrp2)* Wnt pathway components in the DM and gut. **B** Gene expression schematic from **A**. Also see Fig. **S1**. **C** Left-sided *Daam2* and absence of *Daam2* in *Pitx2*-/- DM. **D** Left-sided *Daam2* and *Gpc3* prior to tilt. **E** *Daam2*$^{tm1a(KOMP)Wtsi}$ mice shows left-specific b-galactosidase activity. **F** Schematic of in ovo electroporation: DNA microinjected into the coelomic cavity (HH14) and electroporated to target the right splanchnic mesoderm (see **IL**). Arrow represents current-driven plasmid movement. **G** WT left-sided *Daam2* expression. **H** pCAG-Pitx2 induces right-sided *Daam2,* marked by GFP in **I**. **J** WT left-sided *Gpc3* expression. **K** pCAG-Pitx2 induces right-sided *Gpc3*, marked by GFP in **L.** Scale bars: **A** (100 mm); **CIJKL** (100 mm); **D** (50 mm); **E** (20 mm). See also Figure S1.

(Capurro et al., 2005b; De Cat et al., 2003; Song et al., 2005; Stigliano et al., 2009), a member of the glypican family that is mutated in Simpson-Golabi-Behmel syndrome (Pilia et al., 1996). *Gpc3* is one of the most differentially expressed genes on the left side of the DM (Fig. 3.1E) and ISH on adjacent sections for *Pitx2* and *Gpc3* revealed striking similarities in expression pattern at the time of tilting (HH21, Fig. 3.2AB) and just prior to it (HH19-20, Fig. 3.2C). The clinical features of Simpson-Golabi-Behmel syndrome include instances of gut malrotation and other intestinal defects both in human and in *Gpc3*-null mice (Cano-Gauci et al., 1999; Golabi and Rosen, 1984). Importantly, *Gpc3*-null mice exhibit elevated canonical but reduced noncanonical Wnt signaling in vivo (Capurro et al., 2005a; Song et al., 2005) suggesting *Gpc3* in the left midgut DM may act as a positive modulator of noncanonical Wnt signaling to establish the asymmetric cell behaviors of the leftward tilt, a finding supported by the combined expression of *Fzd4* and *Fzd8* in the same domain (Fig. 3.2AB) (Ye et al., 2011).

The dishevelled associated activator of morphogenesis (Daam) family of formin homology proteins consists of *Daam1* (Habas et al., 2001; Khadka et al., 2009; Li et al., 2011; Miller et al., 2011; Nishimura et al., 2012; Sato et al., 2006; Zhu et al., 2012) and the largely uncharacterized *Daam2* (Lee and Deneen, 2012). Daam1/2 are key intracellular effectors of Wnt signal transduction. We found that *Daam2* expression is restricted to the left mesenteric compartment undergoing mesenchymal condensation (Fig. 3.2AB). ISH on adjacent sections for *Pitx2*, *Gpc3* and *Daam2* both prior to (HH19-20, Fig. 3.2C) and during the leftward tilt (HH21, Fig. 3.2AB) highlights expression overlap. Upon signal dependent activation, formins polymerize unbranched

filamentous actin (F-actin) and form stress fibers necessary for cell polarity, cytoskeletal rearrangements, and adhesion (Habas et al., 2001; Kobielak et al., 2004; Liu et al., 2008). We hypothesized that Daam2-dependent regulation of the actin cytoskeleton drives mesenchymal condensation and thus provides the key missing link in the transmission of early L-R patterning signals to the forces driving gut rotation.

The secreted Frizzled-related proteins (Sfrp), which share structural homology to the Wnt binding domain of *Fzd* but are not membrane bound, compete for ligand binding and function to spatially attenuate Wnt signaling (Moon et al., 1997; Wolf et al., 2008). We found that expression of *Sfrp1* and *Sfrp2* is exclusive to the right side of the DM (Fig. 3.2AB). Interestingly, the noncanonical Wnt/PCP core gene *Prickle-1* (Gray et al., 2011) was expressed in a decreasing R-to-L gradient (Fig. S3.1B). Collectively, this complementary left vs. right expression pattern of positive and negative Wnt pathway components establish differentially permissive environments for Wnt signaling via asymmetric responsiveness to Wnt signaling cues. For example, the expression of *Fzd4/8*, *Gpc3* and *Daam2* on the left side may function to potentiate Wnt signaling, leading to Wnt activation of Daam2 and condensation of the left mesenchyme. Simultaneously, these effects may be antagonized within the right DM by the presence of Wnt inhibitors *Sfrp1* and *Sfrp2*, whereas graded *Prickle-1* expression may further modulate Wnt output (Carreira-Barbosa et al., 2003; Chan et al., 2006; Veeman et al., 2003b).

Wnt5a, considered a prototypical noncanonical Wnt ligand, is expressed in the adjacent midgut at the onset of its morphogenesis (Cervantes et al., 2009; Yamaguchi et al., 1999). Whereas Wnt5a is critical for elongation of the midgut, whether it plays a

role during L-R gut morphogenesis isn't known. We hypothesized that *Wnt5a* expression in the midgut is the source of directional Wnt ligand responsible for Daam2 activation in the left DM (Liu et al., 2008). Indeed, *Wnt5a* was not found in the DM but was robustly expressed immediately ventral to the DM in the midgut mesenchyme (Fig. 3.2AB). We also observed that the most dorsal domain of *Wnt5a* expression overlaps with the most ventral domain of left-sided *Fzd8* and *Gpc3* (Fig. 3.2AB). We reasoned that mesenchymal cells on the left undergo condensation and drive the tilt in response to Wnt5a secreted from the adjacent gut mesenchyme, a mechanism that may temporally coordinate intestinal elongation and coincident looping morphogenesis.

3.4.2 Oriented mesenchymal condensation underlies the leftward tilt of the midgut

Specific Wnt-Fzd complex activation of canonical vs. noncanonical Wnt signaling is both highly context dependent and influenced by multiple factors (van Amerongen and Nusse, 2009; Veeman et al., 2003a). Noncanonical Wnt signaling primarily alters cellular behavior whereas the canonical pathway induces changes in cell proliferation and differentiation (Veeman et al., 2003a). We previously showed that there are no asymmetries in cell number, proliferation or cell death within the four mesenteric compartments at the time of tilting (Davis et al., 2008), arguing against a role of canonical signaling during gut tilting. Furthermore, formation of the leftward tilt involves polarized cell shape changes of the left epithelial compartment (Davis et al., 2008). While this observation favors noncanonical Wnt signaling, whether the condensing mesenchymal compartment of the left DM exhibits signs of tissue polarity characteristic of a noncanonical Wnt response isn't known. To resolve this, we used

cell polarity XY vectors defined by the location of the golgi apparatus (GM130/Golga2 staining) relative to the nucleus (DAPI, Fig. 3.3AB) in the DM. This analysis confirmed previously identified apical-basal polarity in the left epithelium compared to the random polarity of the right (Fig. 3.3B; n=75 L-side, n=70; R-side, p value < 0.0001). Moreover, we now show that left mesenchymal cells are oriented to the left across the L-R axis of the DM (Fig. 3.3B; n=322; p<0.009). In contrast, right mesenchymal cells show no significant orientation bias (Fig. 3.3B; n=270; p<0.6).

Our results support active noncanonical Wnt signaling in the DM and agree well with previous reports showing a lack of TOPGAL activity during midgut morphogenesis (Cervantes et al., 2009; Matsuyama et al., 2009). However, to rule out canonical Wnt activity in the DM, we employed three widely published b-catenin dependent Wnt reporters in vivo (Barolo, 2006; Biechele et al., 2009). All three reporters showed no activity in the left or right DM by comparison to report in tissues known to undergo canonical Wnt signaling (dorsal neural tube, the yolk sac, and neural ectoderm (Griffin et al., 2011; Lassiter et al., 2007; Lee and Deneen, 2012) (Fig. 3.3C-E and Fig. S3.3AB). These results argue against canonical Wnt activity during asymmetric gut rotation and favor a model where *Pitx2* asymmetrically induces *Fzd4*/*8*, *Gpc3* and *Daam2,* enabling the DM to respond to noncanonical Wnt.

3.4.3 Wnt components in the DM are conserved downstream of Pitx2

The asymmetric architecture and molecular readout of the DM are evolutionarily conserved among birds and mice. In *Pitx2* mutant mice, the left DM fails to condense (Davis et al., 2008) and we therefore asked whether this defect is

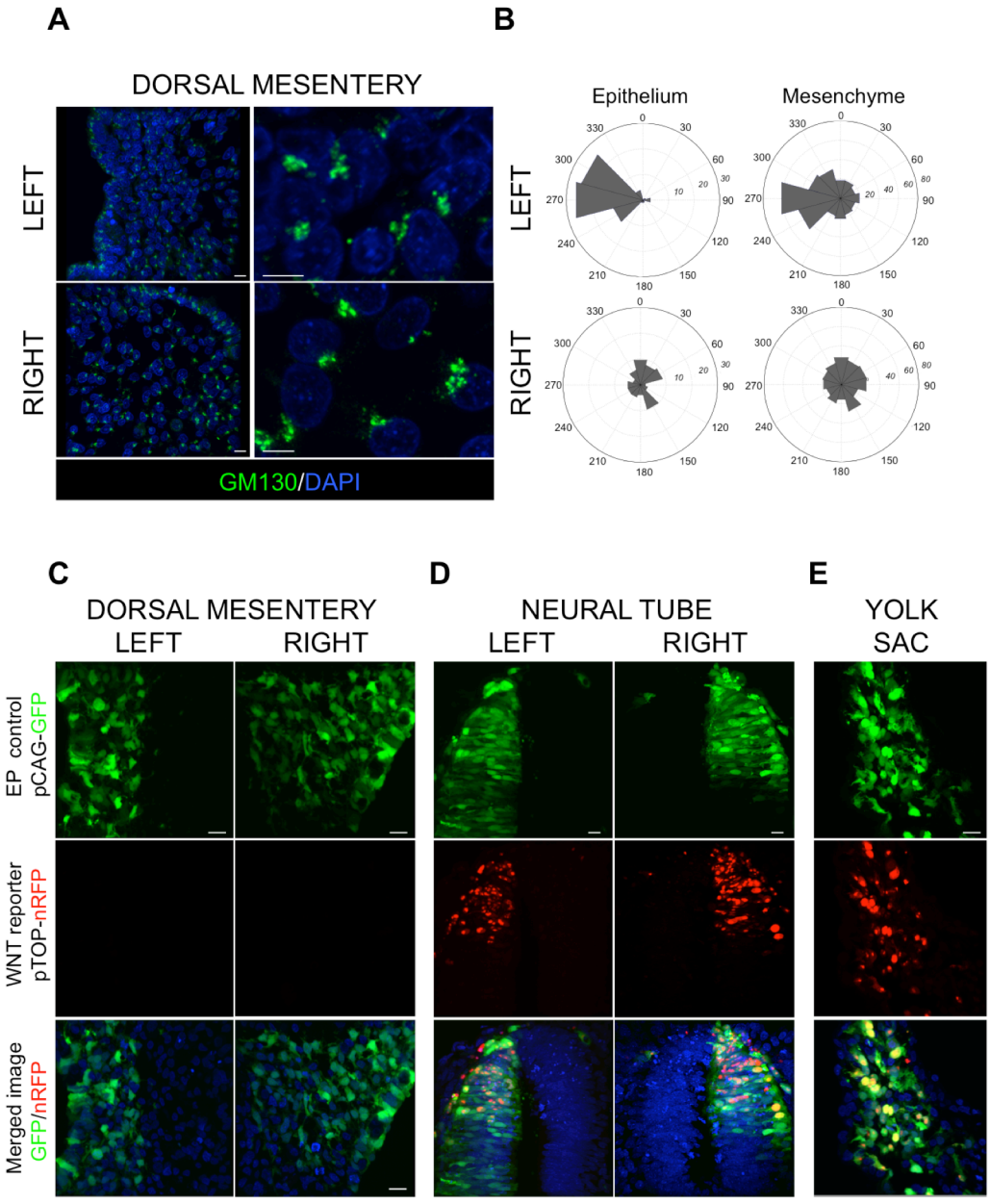

FIG. 3.3. Cellular behavior in the DM is polarized. **A** WT left and right DM stained with GM130 (golgi) and DAPI. **B** Cell orientation measured by the angle of the golgi with respect to the nucleus (X-axis: L-R, Y-axis: D-V, Radial-axis: number of cells per bin). Polarized left mesenchyme is oriented to the left (L: $p<0.009$; R: $p<0.6$). For L vs. R epithelium: p value < 0.0001). **C** Electroporation of pTOP-nRFP (*red*) into (**C**) the left and right DM; (**D**) neural tube; and (**E**) yolk sack (Also see Fig. **S2**). GFP identifies electroporated cells. *Blue* is DAPI. Scale bars: **A** (10 mm; insets are 5 mm); **C** (10mm).

associated with altered expression of *Daam2*. At E10.75, we observed left-sided *Daam2* expression in WT mouse DM, akin to that observed in the chick (Fig. 3.2D). Importantly, expression of *Daam2* was lost in the DM of *Pitx2*-/- mutant embryos (Fig. 3.2D, dotted line).

We have generated *Daam2*$^{tm1a(KOMP)Wtsi}$ mice harboring a targeted disruption of *Daam2*; the complete characterization of these mice will be reported independently. However, this allele harbors an insertion of lacZ under control of the endogenous *Daam2* promoter, and whole mount b-galactosidase assays confirm left-restricted expression of Daam2 in the DM of Daam2+/- embryos (Fig. 3.2E), further arguing for a conserved role of Daam2 in L-R asymmetric gut morphogenesis.

To learn whether Pitx2 is sufficient to drive *Daam2* expression we induced ectopic Pitx2 using in ovo DNA electroporation (Davis et al., 2008; Kurpios et al., 2008) (Fig. 3.2F). We found that Pitx2 strongly induced Wnt signaling components on the right side, including both *Daam2* and *Gpc3* (Fig. 3.2G-L).

In an effort to discern between direct and indirect Pitx2-dependent transcription, we performed comparative genomics and computational sequence analysis to search for highly conserved Pitx2 binding sites in the promoters of candidate Pitx2 targets. We confirmed Pitx2 binding sites at known Pitx2 targets and predicted conserved Pitx2 binding sites at *Gpc3*, *Fzd4* and *Daam2* (Fig. S3.2).

3.4.4 Daam2 activation is required for mesenchymal condensation in the DM

Daam1 and *Daam2* contain identical structural domains and share a high degree of protein similarity (Nakaya et al., 2004). In the absence of signaling, Daam

proteins are autoinhibited by interactions between their N-terminal GTPase binding domain (GBD), located within the diaphanous inhibitory domain (DID), and a C-terminal diaphanous autoinhibitory domain (DAD; Fig. 3.4A) (Habas et al., 2001). Wnt signal-dependent binding of Dishevelled to the DAD domain is a key step in Daam1 activation (Liu et al., 2008). To address the function of Daam2 during L-R gut morphogenesis, we generated protein truncation mutants (Fig. 3.4A) based upon the previous functional dissection of Daam1 (Habas et al., 2001). Mutants consisting of the N-terminus alone (N-Daam1) exhibit dominant-negative activity (Habas et al., 2001; Liu et al., 2008), whereas mutants missing only the GBD domain (CA-Daam1) are constitutively active even in the absence of Wnt signaling. The ability of activated Daam1 (and CA-Daam1) to elicit specific cytoskeletal changes in cultured cells such as polarized stress fiber formation has been well documented. Briefly, CA-Daam1 enhances, whereas N-Daam1 disrupts, the formation of actin stress fibers. We employed similar in vitro analysis to validate the utility our CA-Daam2 and N-Daam2 mutant constructs for the functional dissection of Daam2 during gut morphogenesis (Fig. S4 and Methods).

To learn whether Daam2 activation is required for mesenchymal condensation, we initially introduced CA-Daam2 into the right DM (Fig. 3.4B). This induced robust aggregation of mesenchymal cells (Fig. 4DEP; $n=5$; $p<0.006$) similar to that normally seen on the left side (Fig. 3.4CP), while non-electroporated right-sided cells remained dispersed (Fig. 3.4DE). Furthermore, compared to non-electroporated cells and consistent with the role of formins in regulating the actin cytoskeleton (Habas et al., 2001; Kobielak et al., 2004; Liu et al., 2008) CA-Daam2-positive cells exhibited

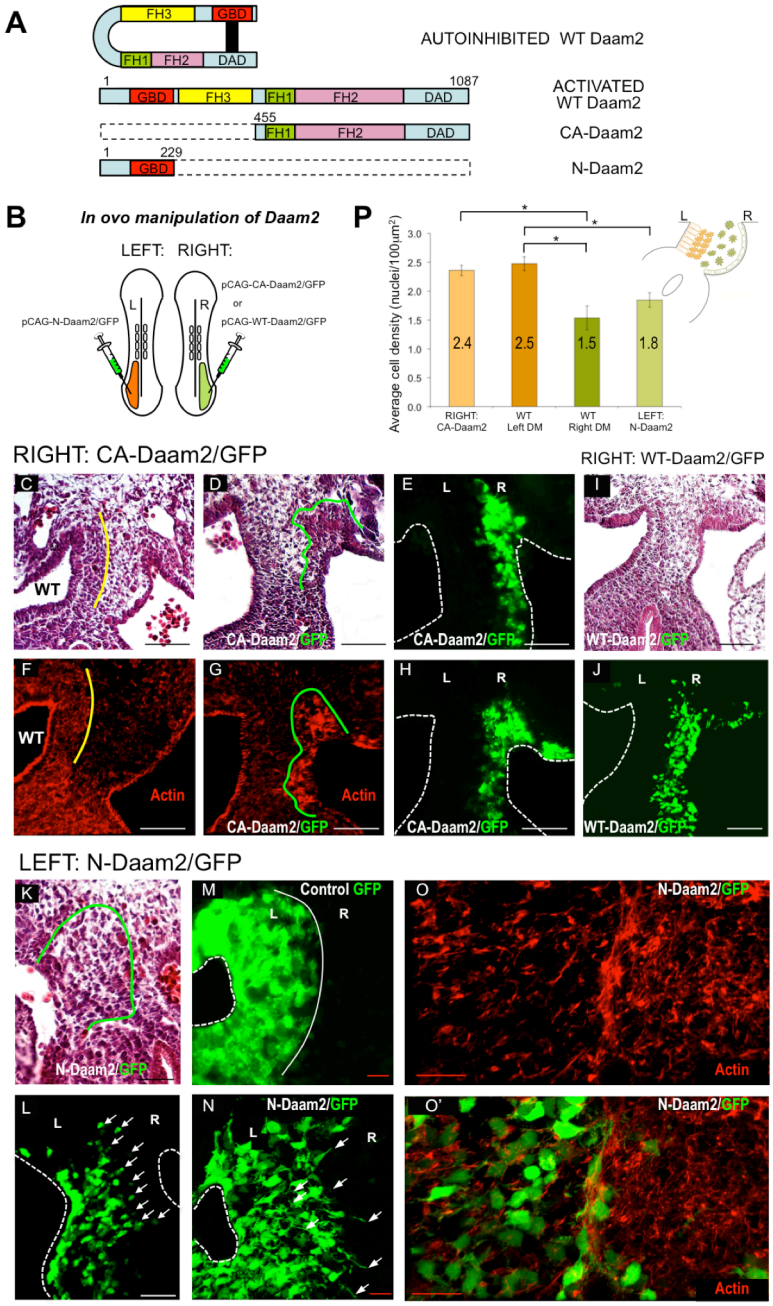

FIG. 3.4. Daam2 activation is required for mesenchymal condensation in the DM. **A** Wnt signal-dependent binding of Dishevelled to DAD activates Daam. **B** In ovo electroporations: N-Daam2 is targeted to the left, CA-Daam2 to the right (See also Fig. **S4** for construct validation). **C-H** CA-Daam2 targeting of the right DM: **C** WT DM with left-specific condensation (*yellow* line) with asymmetric F-actin (red in **F**, Phalloidin); **D** CA-Daam2 induces condensation (*green* line, GFP coelectroporated in **E**) and **(G)** increased F-actin (GFP coelectroporated in **H**). **I** Right-sided Daam2 electroporation in the DM has no effect on condensation, marked by GFP in **J**. **K-O'** N-Daam2 targeting of the left DM. **K** Loss of condensation (*green* boundary from **L**). *White* arrows in **L** show N-Daam2-electroporated cells separating from the left. **M** Control (pCAG-GFP) highlights tightly compacted cells compared to dispersed cells expressing N-Daam2 (**N**), which produce filopodia-like extensions (*white* arrows) and (O) exhibit decreased F-actin (*red*, Phalloidin). **P** Calculated mesenchymal cell densities of WT and electroporated tissue sections (mean ± SEM, all p-values <0.0155). Scale bars: **C-H** (50 mm); **I-J** (100 mm); **K-L** (50 mm); **M-O'** (15mm). *, p<0.05. See also Figure S4-7.

increased F-actin staining (Fig. 3.4F-H), an effect also observed in vitro (not shown). Electroporation of WT Daam2 into the right side had no effect on cell behavior in the DM (Fig. 3.4IJ; n=7), in agreement with the autoinhibition of Daam proteins in the absence of Wnt, further arguing that the right DM is a non-permissive environment for Wnt signaling.

To confirm the requirement for Daam2 during condensation, we introduced N-Daam2 to the left DM (Fig. 3.4B). This disrupted condensation (Fig. 3.4KLP; n=3; $p<0.05$) and was accompanied by reduced levels of F-actin (Fig. 3.4OO'; n=6). In contrast to extensive cell-cell compaction and a well-defined L-R boundary in WT (Fig. 3.4C) or control GFP-electroporated left mesenchyme (Fig. 3.4M), cells expressing N-Daam2 remained dispersed (Fig. 3.4N vs. Fig. 3.4M) and were often found separating from the left compartment (Fig. 3.4L, arrows). Moreover, long, filopodia extensions were present on Daam2-inhibited cells, mimicking the normal behavior of right-sided mesenchyme (Fig. 3.4N, arrows), while co-electroporation of the right DM with both N-Daam2 and Pitx2 interferes with the cellular effects of misexpressed Pitx2 alone in the right DM suggesting that epistatically, Daam2 is functionally downstream of Pitx2 (Fig. S3.7). Our experiments suggest the ability of N-Daam2 electroporated mesenchymal cells to maintain cell-cell contact was severely compromised. We also noted that N-Daam2 electroporated epithelial cells lost their columnar organization (Fig. S3.5). This is consistent with the previously characterized role of the actin cytoskeleton in the DM epithelial compartment (Davis et al., 2008; Plageman et al., 2011).

To confirm that the effects of N-Daam2 electroporation are a direct consequence of perturbed Daam2 function, we performed Daam2 knockdown experiments with the use of a previously published RCAS-shRNA system (Deneen et al., 2006). The effect of knockdown of endogenous Daam2 was verified using ISH (Fig. S3.6A-C'). Electroporating a scrambled shRNA had no effect on expression of endogenous Daam2 (Fig. S3.6BB' vs. S6A) and did not alter condensation in the DM (Fig. S3.6EE'I vs. S6DD'I; n=3). In contrast, electroporating Daam2-shRNA perturbed mesenchymal condensation, consistent with our N-Daam2 results (Fig. S3.6FF'I vs. S3.6EE'I, n=6; $p< 0.005$). Hence, N-Daam2 interferes with the cellular effects of Pitx2 supporting that Daam2 is a key mediator of Pitx2 during mesenchymal condensation.

3.4.5 Daam2 affects mesenchymal condensation by lengthening cadherin-based junctions

Asymmetric cell behaviors in the DM depend in part on the cell adhesion molecule N-cadherin (Kurpios et al., 2008; Plageman et al., 2011). We therefore asked whether differences exist in the organization of cell-cell junctions in the L-R mesenchymal compartments, and whether such differences are dependent on Daam2. Scanning and transmission electron microscopy (EM) highlighted that cell-cell junctions differed markedly on the two sides of the DM (Fig. 3.5A-C). We observed extensive membrane contacts between adjacent mesenchymal cells on the left (Fig. 3.5B, yellow arrowhead), while junctions between cells on the right consisted of thin filopodia extensions (Fig. 3.5C). We used transmission EM to count and measure the

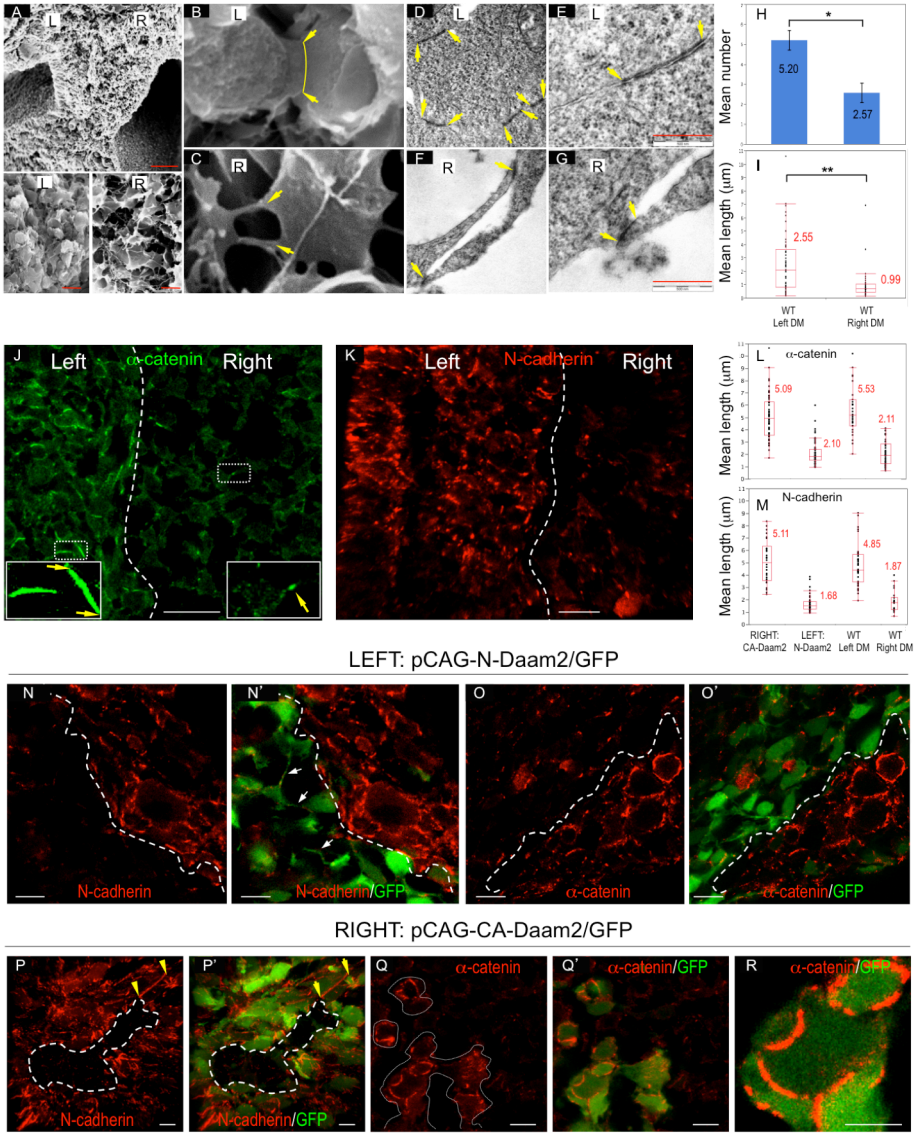

FIG. 3.5. Daam2 lengthens cell-cell junctions. **A-G** Scanning (**A-C**) and transmission (**D-G**) EM show differences in left (**ABDE**) vs. right (**ACFG**) mesenchymal cell junction morphologies (*yellow* arrowheads). **HI** Cell-cell contacts on the left are increased in number (**H,** mean ± SEM) and length (**I**) vs. the right ($p<0.05$ & <0.01, respectively). (**JK**) Differences in cell junction organization highlighted by a-catenin *(green*, **J)** and N-cadherin staining (*red*, **K**, high magnifications inset); L-R boundary indicated (dotted line). **LM** Morphometric analysis of mean cell junction lengths in WT and electroporated tissues stained with a-catenin (*top*) and N-cadherin (*bottom*). Right-sided CA-Daam2 promotes lengthened junctions ($p<0.0001$) not statistically different from WT left cells ($p>0.17$), while left-sided N-Daam2 reduces junction length ($p<0.0001$) to resemble right-sided WT cells ($p>0.59$). **N-O'** N-Daam2 (left) impairs adhesion and accumulation of both N-cadherin (*red*, **NN'**, note filopodia-like extensions, *white* arrows in **N'**) and a-catenin (*red*, **OO'**) to cell-cell contacts (GFP-marked electroporation boundary depicted). **P-R** CA-Daam2 (right) induces accumulation of both N-cadherin (*red*, **PP'**, *yellow* arrowheads) and a-catenin (*red*, **Q-R**). Scale bars: **A** (30mm top and 5mm bottom panels); **EG** (500nm); **JK** (10mm); **NO'** (10mm); **PP'** (5mm); **QQ'** (10mm); **R** (5mm). Boxplots represent quartiles and median of the data, whiskers indicate extreme values. *, $p<0.05$, **, $p<0.001$.

length of cell-cell contacts in the DM (Fig. 3.5D-G). We found an increased number of contacts per cell on the left vs. right side (Fig. 3.5DFH; 5.2 vs. 2.6 cell contacts; n=5 left and n=7 right; $p<0.05$). Moreover, there was a significant increase in the length of the left-sided contacts compared to the right (Fig. 3.5EGI; 2.55 vs. 0.99 μm, n=49 left and n=35 right; $p<0.01$).

α-Catenin is an adherens junction (AJ) protein that binds to b-catenin and is necessary for AJ formation and maintenance (Vasioukhin et al., 2000). Localization of a-catenin (Fig. 3.5J) and N-cadherin (Fig. 3.5K) in the DM highlights differences in the length of junctions across the L-R axis. We measured the length of junctions on the left vs. the right DM using fluorescently labeled cell junction complexes (Fig. 3.5L, a-catenin; Fig. 3.5M, N-cadherin). Consistent with EM data, the length of contacts on the left was ~2.6 (2.62, 2.59 vs. 2.57 [EM]) fold higher by comparison to the right (Fig. 3.5LM; n=11; $p< 0.0001$).

To determine whether junctions are dependent on Daam2, we introduced N-Daam2 to the left DM and followed with morphometric analyses as described above (Fig. 3.5LM). This significantly perturbed intercellular adhesion and resulted in a failure to accumulate both N-cadherin (Fig. 3.5NN') and a-catenin (Fig. 3.5OO'L) to points of cell-cell contact. Moreover, the length of N-cadherin- or a-catenin-labeled cell junctions was significantly reduced in cells electroporated with N-Daam2 by comparison to non-electroporated cells (Fig. 3.5LM, n=6, $p< 0.0001$, N-cadherin; $p< 0.0001$, a-catenin). Long, filopodial cell-cell contacts were present between Daam2-inhibited left mesenchymal cells, mimicking the normal appearance of right-sided mesenchyme (Fig. 3.5N', white arrows). In contrast, electroporation of CA-Daam2

into the right DM resulted in accumulation of N-cadherin (Fig. 3.5PP') and a-catenin (Fig. 3.5QR) at cell-cell contacts and significantly increased the length of junctions (Fig. 3.5LM, n=5, $p<0.0001$, N-cadherin; $p<0.0001$, a-catenin). We conclude that Daam2 directs the formation and size of cadherin-based junctions during mesenchymal condensation.

3.4.6 Daam2 physically interacts with a-catenin and N-cadherin

Formin-1 (Fmn1), the founding member of the formin superfamily, is a critical binding partner for a-catenin in the skin, linking actin cytoskeleton to AJs (Kobielak et al., 2004). The modulation of junctions containing a-catenin downstream of Daam2 activation prompted us to determine whether Daam2 protein is physically associated with these junctions and to explore whether, like Fmn1, Daam2 and a-catenin physically interact. We turned first to the localization of Daam2 and a-catenin in mammalian cells, and show that Flag-Daam2 is found both in the cytoplasm and at cell borders (Fig. 3.6A), and co-localizes with staining for endogenous a-catenin (Fig. 3.6A, rectangles). To test whether Daam2 and a-catenin physically interact, we transfected 293T cells with either Daam2, Fmn1, or with CA-Daam2 (all Flag-tagged). As expected, Fmn1 immunoprecipitated in a complex with antibodies against a-catenin (Fig. 3.6B). Importantly, both Daam2 and CA-Daam2 co-immunoprecipitated with endogenous a-catenin (Fig. 6B). Furthermore, endogenous Daam2 co-immunoprecipitated with endogenous a-catenin and N-cadherin in untransfected 293T cells (Fig. 3.6C). Together, these data reveal that Daam2 is a binding partner of a-

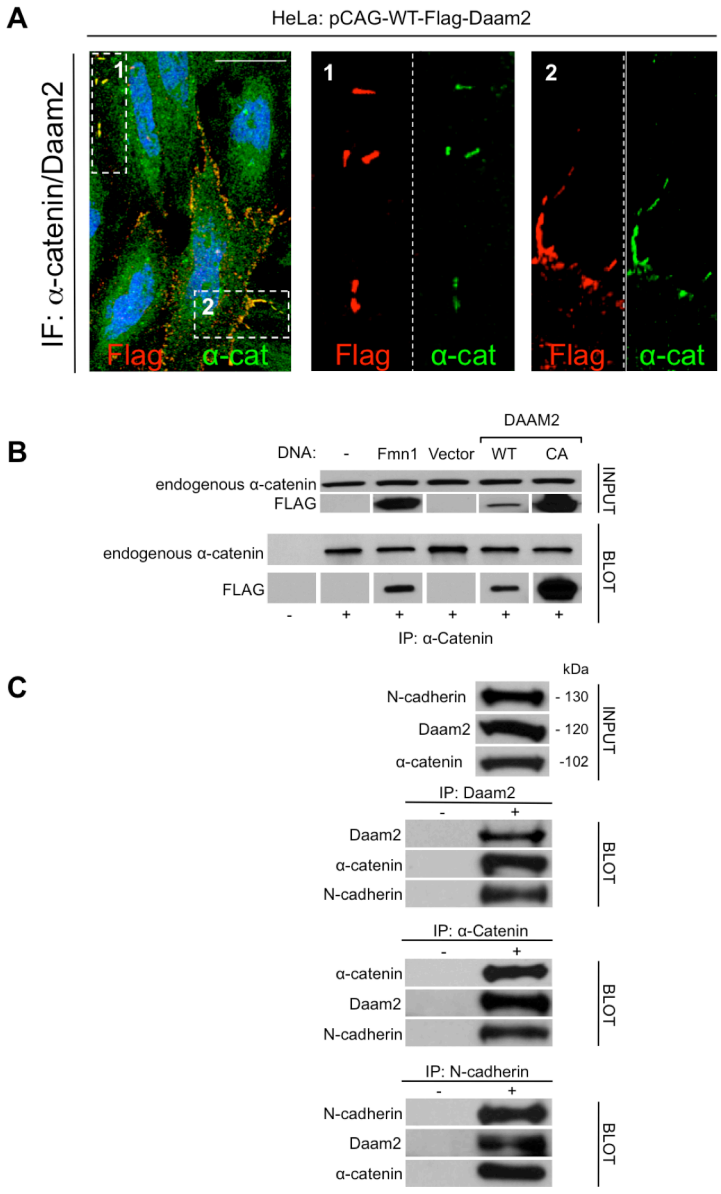

FIG. 3.6. Daam2 physically interacts with junctional proteins. **A** Flag-Daam2 (*red*) and endogenous a-catenin (*green*) co-localize at the cell surface in HeLa cells. Dotted rectangles (1 and 2) are magnified. **B** Overexpressed WT- and CA-Daam2, and positive control Fmn1 bind endogenous a-catenin. **C** Reciprocal IP experiments show Daam2 interacts with both a-catenin and N-cadherin (endognous, untransfected lysates). Scale bars: **A** (10mm).

catenin and N-cadherin, and suggest that the Daam2/a-catenin interaction is cadherin-complex dependent and likely to occur at the cell membrane.

3.4.7 Wnt5a-/- embryos fail to initiate the leftward tilt of the midgut

Wnt5a is required for ventral closure of the primitive gut and for subsequent midgut elongation, independent of canonical Wnt/β-catenin (Cervantes et al., 2009; Yamaguchi et al., 1999). To determine if *Wnt5a* is also required in the DM we examined this structure in *Wnt5a*-/- mutants (Fig. 3.7A-E'). While the DM formed in *Wnt5a*-/- embryos, its ventral outgrowth was arrested (Fig. 3.7FG, n=6/6, dotted rectangles). Importantly, the gut tube of *Wnt5a*-/- mutants also failed to initiate the asymmetric leftward tilt (Fig. 3.7F-I, n=6/6, single arrow). These defects were not accompanied by changes in cell proliferation or cell death in the DM, or *Pitx2* expression (Fig. S3.8; Fig. S3.1C).

In WT mice, elongation of the midgut to form the primary ventral loop is preceded by ventral closure and occurs concurrently with outgrowth of the DM (Fig. 3.7N, WT, curved arrows). Our data provide further insight into the etiology of intestinal defects in Wnt5a-/- mutants, suggesting that arrested DM outgrowth (Fig. 3.7N, Wnt5a-/-, straight arrows) imposes a restriction that, accompanied by delayed ventral closure of the midgut, forces the elongating gut tube to form a branch rather than a midgut loop as previously reported (Cervantes et al., 2009) (Fig. 3.7N). This agrees with the described physical restraint placed on the lengthening gut tube by the DM, a process required for the proper topology of intestinal loops during later stages (Savin et al., 2011).

Importantly, in some Wnt5a-null embryos there was defective remodeling of the lining of the coelomic cavity involving aberrant foldings and adhesions of serosal

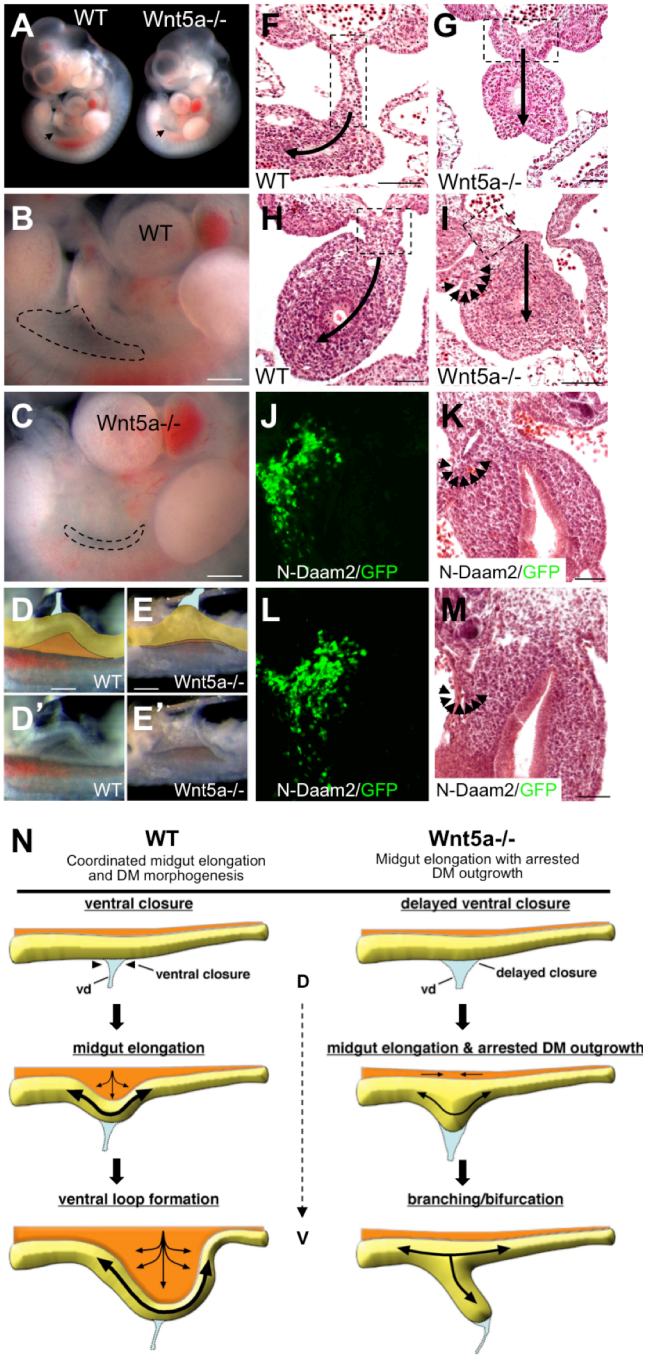

FIG. 7. Wnt5a-/- embryos fail to initiate the leftward tilt of the midgut. **A** Wnt5a-/- and WT embryos (E10.5, arrow marks DM). **BC** Higher magnification of **A** highlights arrested DM development in Wnt5a-/- embryo (**C**, dotted lines). **D-E'** Dissection of embryos from **A** highlights DM (orange) and midgut (yellow). **FH** Normal leftward tilt (arrow) and loss of tilt in Wnt5a-/- embryo (**GI**). Dotted rectangles highlight arrested ventral outgrowth of the DM at the level of the midgut (**F**, WT; **G**, Wnt5a-/-) and defective morphology of the DM (**H**, WT; **I**, Wnt5a-/-) posterior to the midgut. **J-M** Chicken DM with N-Daam2 on the left (**JL**, GFP, electroporated). **KM** Coelomic cavity defects (*black* arrows) in N-Daam2 electroporated chick embryos are reminiscent of Wnt5a-/- embryos (**I,** *black* arrows). **N** Model for the role of Wnt5a in midgut loop formation: Ventral closure of the gut occurs at the initiation of midgut elongation and results in formation of the vitelline duct (vd). Delayed closure and arrested DM outgrowth in Wnt5a-/- forces the elongating midgut to branch rather than loop. Scale bars: **B-E'** (500 mm); **F** (100 mm); **GH** (50 mm); **I** (100 mm); **J-M** (50 mm). See also Figure S5 and S1.

epithelial layers (Fig. 3.7I, arrowheads), a phenotype also noted in the left DM of some chick embryos electroporated with N-Daam2 (Fig. 3.7J-M, arrows). The results of these experiments demonstrate a requirement for Wnt5a to initiate asymmetric gut morphogenesis in mice and suggest that Wnt5a in the gut is the noncanonical signal required to activate Daam2 in the DM (Fig. 3.8).

3.5 Discussion

The goal of this research has been to define the transcriptional targets and cellular mechanisms through which *Pitx2* manifests asymmetric gut morphogenesis in higher vertebrates. Although *Pitx2* has been thoroughly studied in development, its downstream targets are unknown. Leveraging the binary L-R organization of the DM, we performed laser microdisection of the left and right to identify *Fzd4*, *Gpc3* and *Daam2* as downstream *Pitx2* targets. We show that positive regulation of these genes by *Pitx2* acts to potentiate asymmetric Wnt signaling via Daam2 activation, inducing polarized condensation in the left DM necessary to initiate gut rotation. Conversely, these effects are antagonized within the right DM by the presence of the Wnt inhibitors *Sfrp1* and *Sfrp2.* This work provides new insight into the molecular effectors of gut morphogenesis and uncovers an important link between the earliest L-R signals initiated during gastrulation, and Daam2 activation downstream of Wnt signaling, as the ultimate driving force through which *Pitx2* initiates asymmetric development (Fig. 3.8).

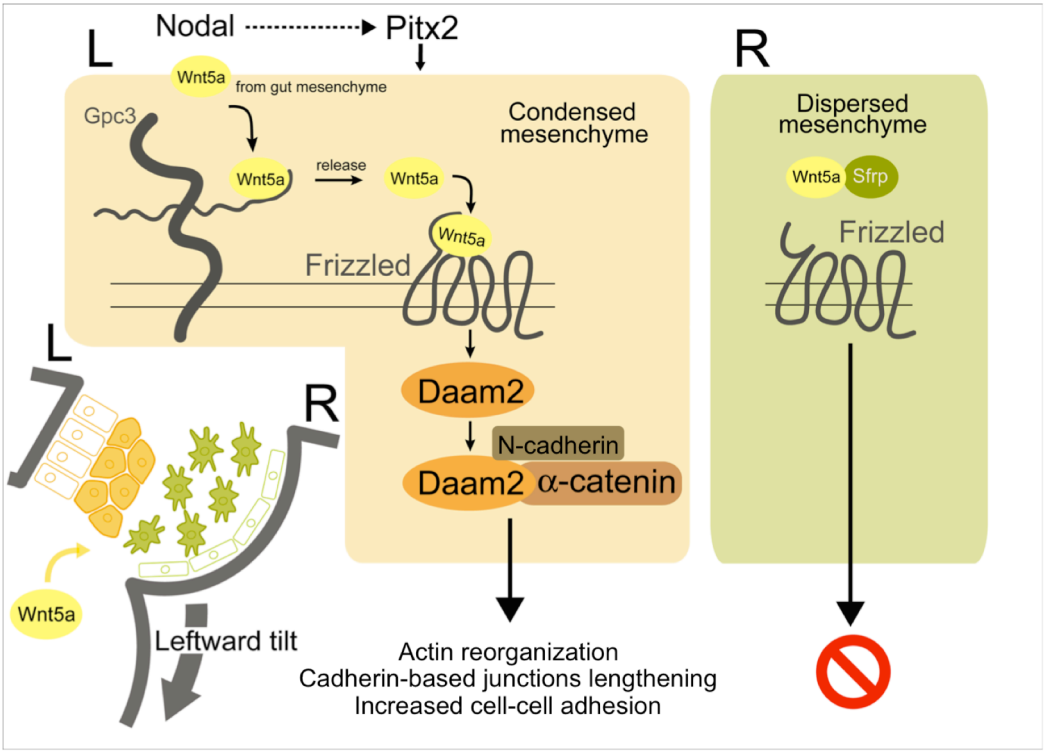

FIG. 3.8. Model for L-R gut rotation. Transcriptional regulation of Wnt pathway genes by Pitx2 leads to Daam2 activation. Daam2 mediates adhesion at cell junctions by binding a-catenin and N-cadherin. Subsequent actin remodeling and lengthening of junctions cause left condensation. Wnt5a produced in the adjacent gut orients condensation relative to the D-V axis. Antagonized Wnt signaling causes right mesenchymal cells to remain dispersed.

2.5.1 The role of noncanonical Wnt signaling in L-R gut morphogenesis

The mammalian Wnt signaling family consists of 19 ligands and 10 receptors (van Amerongen and Nusse, 2009). The ability of specific Wnt-Frizzled complexes to activate canonical vs. noncanonical signaling is inherently complex and depends heavily on cellular context including the composition of co-receptors at the cell surface, the presence of extracellular antagonists, and the intracellular expression of various signaling intermediates (van Amerongen and Nusse, 2009). Components at almost every level of the Wnt pathway have been shown to affect both b-catenin-

dependent and -independent responses. Ultimately, signal integration determines the appropriate cell behavior in response. In the midgut DM, we show left-sided expression of *Fzd4*/*8*, *Gpc3*, and *Daam2* (Wnt-permissive) with contrasting expression of Wnt antagonists *Sfrp1* and *Sfrp2* on the right. Not surprisingly, all of these genes have been linked to canonical and noncanonical Wnt signaling (Capurro et al., 2005a; Chan et al., 2006; Song et al., 2005; Veeman et al., 2003b; Wawrzak et al., 2007; Ye et al., 2011). The noncanonical pathway primarily affects cellular behavior such as shape, adhesion and polarity, whereas the canonical Wnt pathway influences cell fate decisions and changes in cell proliferation and differentiation. We rule out canonical signaling in the DM by reporting an absence of any asymmetry in conventional metrics of β-catenin-dependent signaling: cell number, proliferation or cell death within the DM are equal, while several widely used canonical Wnt reporters show no activity in the DM. Instead, we show that the leftward tilt is initiated by Daam2-dependent regulation of the actin cytoskeleton and cadherin-based cell adhesion leading directly to changes in cell behavior that manifest as greater or lesser cell packing on the left or right sides, respectively. Hence, the left-specific expression of *Fzd4/8*, *Gpc3* and *Daam2* likely functions via noncanonical Wnt signaling to establish asymmetric cell behaviors underlying the leftward tilt.

Our evidence that noncanonical Wnt signaling is responsible for the L-R asymmetries includes the demonstration that Daam2-positive mesenchymal cells are oriented to the left across the L-R embryonic axis. In contrast, Daam2-negative cells of the right show no specific orientation. Tissue polarity is a key cellular feature of noncanonical Wnt/PCP signaling in both vertebrates and invertebrates (Gray et al.,

2011). Whereas in Drosophila much has been learned of the PCP pathway (Vladar et al., 2009), in vertebrates the definition of what constitutes PCP signaling, particularly in mesenchymal cells, is not entirely clear (Wallingford, 2012). Interestingly, our work revealed that one of the components of the PCP pathway, *Prickle-1*, is asymmetrically expressed in a R-L gradient in the DM. In Drosophila wing disc, *Prickle* (*Pk*) is asymmetrically localized across the intercellular proximal-distal interface to antagonize Fzd receptor activity and to generate asymmetry of Fzd-Dishevelled activity across each proximal-distal cell boundary during PCP signaling (Tree et al., 2002). In zebrafish, the asymmetric localization of Pk and Dishevelled fusion proteins to the anterior and posterior cell edges (Yin et al., 2008) parallels localization of these proteins in Drosophila. At present, the subcellular localization of Prickle-1, Dishevelled or other core PCP proteins in the DM has not been explored and the mechanistic function of this restricted right-sided expression remains unclear. It is attractive to speculate that in the DM, *Prickle-1* may function either upstream or in parallel to Daam2 to establish the distinct mesenchymal cell orientation during the leftward tilt of the midgut.

2.5.2 Coordinating cell behaviors in the DM with embryonic polarity

Expression of Wnt5a in the adjacent gut mesenchyme raises the possibility that Wnt5a diffusion may form a gradient, coordinating the D-V outgrowth of the DM with the establishment of L-R asymmetry. Indeed, the L-R changes in the DM are oriented relative to the orthogonal D-V axis such that the left side shortens while the right side lengthens. Among the genes whose expression we have examined in situ, *Fzd8*, *Gpc3*,

and *Islet1* (Davis et al., 2008), show a D-V bias, i.e. closer to the source of Wnt5a. A likely candidate responsible for Wnt5a extracellular distribution and gradient formation is *Gpc3*. Glypicans modulate Wnt signaling and this is highly dependent on complex post-translational modifications of the core Gpc protein (Yan and Lin, 2009).

We have recently identified the left-specific, ventrally restricted expression of enzymes involved in biosynthesis and posttranslational modification of Gpc3 at the time when the DM deforms (unpublished), raising the possibility that functional editing of Gpc3 serves to concentrate diffusible Wnt5a. Indeed, in vitro studies have shown that Gpc3 binds Wnt5a with high affinity and enhances Wnt5a-dependent Jnk activation in mesothelioma cells and in mice (Song et al., 2005). In zebrafish, *Gpc4* ortholog *knypek* is part of the Wnt/PCP pathway required to establish polarized cell behaviors underlying convergent extension (Topczewski et al., 2001). Interestingly, Drosophila homologs of *Gpc3/4*, *Dally* and *Dally*-like, respectively, play an important role in organizing the cellular distribution of extracellular Wnt/Wingless (Baeg et al., 2001). Future work will be necessary to establish the relationship between mammalian glypicans, their subcellular localization, and the noncanonical Wnt/PCP pathway to understand how glypicans can impact global tissue morphogenesis in higher vertebrates.

Wnt5a itself is required for midgut morphogenesis (Cervantes et al., 2009; Yamaguchi et al., 1999). We show that DM morphogenesis and initiation of asymmetric gut rotation is also disrupted in Wnt5a-/- mutants, arguing that Wnt5a links the morphogenetic program of these two adjacent tissues. These defects occur precisely in the region that forms a branch instead of a midgut loop in Wnt5a-/-

embryos (Cervantes et al., 2009), suggesting that disrupted ventral outgrowth of the DM contributes to the formation of the aberrant branch (Fig. 3.6N). This combination of orthogonal D-V and L-R morphogenic defects in *Wnt5a*-/- embryos supports our model where Wnt5a in the gut mesenchyme provides a directional cue linking the D-V axis with L-R patterning in order to coordinate morphogenesis of the DM with developing midgut. Conserved looping morphogenesis depends on physical interaction between the growing gut tube and DM (Savin et al., 2011) underscoring the importance of coordinated growth of these adjacent tissues.

Examples of noncanonical Wnt/PCP-mediated molecular crosstalk between embryonic axes are few. Most recently, PCP signaling has been shown to position basal bodies of cilia at the posterior margin of node cells and Kupffer's vesicle, providing the posterior tilt and thus leftward fluid flow it generates to bathe the left lateral plate with the Nodal ligand (Hashimoto and Hamada, 2010). This provided a partial answer to how anterior-posterior information is translated into L-R organ polarity. However, how established L-R patterning information is further translated into asymmetries of cell behavior and coordinated with organ polarity has remained elusive. Here we begin to answer this question, showing that integration of noncanonical Wnt signaling with embryonic polarity may be a general mechanism through which *Pitx2* sculpts the growth of asymmetric organs, a mechanism warranting further investigation in other L-R asymmetric viscera.

2.5.3 Role of the formin Daam2 in the DM

Our data show that cadherin-based junctions involving a-catenin and N-cadherin are primary candidates responsible for the asymmetric condensation in the DM. Cadherin-based junctions are dynamic, and their stability arises from the coordinated assembly, remodeling, and recycling of junctional proteins that interact with the actin cytoskeleton. For example Dia1 (Diaphanous), the founding member of the subfamily of formins to which Daam2 belongs, is required for both the stability and length of AJs at points of cell-cell contact (Carramusa et al., 2007). Moreover, Formin-1 is recruited to nascent AJs via interaction with a-catenin, and this recruitment is required for intercellular adhesion in the skin (Kobielak et al., 2004). We show that Daam2 similarly interacts with both a-catenin and N-cadherin, while Daam2 activity is required for cell-cell adhesion, organizing N-cadherin and a-catenin at cell junctions. These data raise the possibility that individual formin proteins, as nucleators of filamentous actin, may function broadly during development as tissue-specific modulators of cell adhesion via their interaction with junctional complex proteins.

Daams have also been shown to regulate small GTPases such as RhoA to influence cytoskeletal architecture (Habas et al., 2001). However, debate continues as to whether Daams act upstream, downstream, or in parallel to small GTPases (Aspenstrom et al., 2006; Higashi et al., 2008). While mutation of mouse Daam1 results in neonatal lethality (Li et al., 2011), the disruption of cytoskeletal architecture due to Daam1 mutation is independent of RhoA, Rac1, or Cdc42. Instead, Daam1 organizes N-cadherin-dependent adhesion of cardiomyocytes during heart

morphogenesis (Li et al., 2011). Interestingly, Daam2 was recently shown to mediate formation of Dvl3/Axin signaling complexes required for patterning the dorsal neural tube downstream of canonical Wnt signaling (Lee and Deneen, 2012), highlighting a diverse Daam signaling repertoire during vertebrate development that depends heavily on cellular context. Thus the specific contribution of these related formins to L-R laterality in other organ systems is of great interest.

2.5.4 Midgut rotation and clinical implications

Midgut malrotation is a birth defect of unknown genetic origin predisposing affected babies to catastrophic volvulus (Lampl et al., 2009). Understanding how L-R asymmetry is initiated and executed during gut rotation may shed light onto the origin of midgut malrotation and other classes of human gut disorders. Our work has shown that mutations in two genes associated with gut malrotation in humans are differentially expressed in the DM: transcription factor *PITX2*, which causes Rieger syndrome (Lu et al., 1999), and *GPC3*, which causes Simpson-Golabi-Behmel syndrome (Pilia et al., 1996). Both disorders are pleiotropic and difficult to study in humans. Thus the ability to isolate and perturb these genes and their downstream targets in vivo is a singular advantage of the DM, enabling us to link genetic cause with anatomic outcome. Moreover, lessons learned from these experiments will impact the study of other regions of the gut, and other tubular organs, some of which share strikingly similar features of morphogenesis and genetic patterning with the vertebrate midgut.

3.6 Material and Methods

Animals

Mouse embryos, with the morning of the plug defined as E0.5, were collected from *Pitx2*^{hd} allele (Lu et al., 1999), *Wnt5a* mutant B6:129S7-*Wnt5a*^{tm1Amc}/J (Yamaguchi et al., 1999), and Daam2-/- (Daam2$^{tm1a(KOMP)Wtsi}$). BAT-GAL reporter mice were generously provided by Dr. Courtney Griffin (Griffin et al., 2011). See Supplemental Material for more information. Fertile White Leghorn eggs from the Cornell Poultry Research Farm were incubated at 38°C and staged (Hamburger and Hamilton, 1992).

In Ovo Electroporation

Plasmid DNA (0.6-3.0mg/ml) was microinjected into the left or right coelomic cavity of HH14 chicken embryos (Kurpios et al., 2008), with coelectroporated pCAG-GFP or mCherry to visualize targeted cells. Platinum electrodes delivered 3 sequential 10 ms pulses of 50V delivered from a BTX electroporator. RNAi was performed using described reagents (Deneen et al., 2006; Lee and Deneen, 2012). The effect of knockdown using RCAS-Daam2-shRNA electroporation was verified using ISH compared to a mutant shRNA control with 5bp substitutions.

RNA in Situ Hybridization

250mm thick embryo slices for whole mount ISH was performed as described (Brent et al., 2003). Section ISH was performed as described (http://geisha.arizona.edu/geisha/protocols.jsp) using chromogenic detection.

Electron Microscopy

EM specimens were dissected, fixed ON with either 4% PFA and 2.5% glutaraldehyde in 0.1M Sodium Cacodylate (SC) buffer, pH 7.4 (TEM) or with 2.0% glutaraldehyde in 0.05M SC buffer, pH7.4 (SEM). Several washes with 0.1M SC were followed by 1.5% Osmium Tetroxide (OsO_4) staining. SEM samples were EtOH-dehydrated, subjected to critical point drying with CO_2, mounted on stubs and sputter coated with gold/palladium. Following OsO_4 staining, TEM samples were stained with 2% Uranyl Acetate, embedded in LX 112 resin (Ladd Research), and ultrathin sections were collected. Electron micrographs were acquired with a Leica 440 scanning EM or a FEI T12 Spirit transmission EM (Cornell).

Cell Behavior Quantification

Transmission electron micrographs in which the cell body and nucleus were completely in frame were used to estimate the mean number and length of cell-cell contacts within each compartment. Measurements (Imaris) were normalized relative to the scale bar. Cell behavior was quantified from 15μm sections of WT and electroporated embryos stained with DAPI and antibodies to α-catenin or N-cadherin. Fluorescently labeled cell junctions were measured (ImageJ) for electroporated (GFP) and non-electroporated cell contacts (control). Condensation was quantified (ImageJ) as nuclei per $100\mu m^2$ within WT or electroporated tissue. Cell polarity was scored from z-stacks of 20mm paraffin sections stained with DAPI and anti-GM130 (golgi). Vectors were drawn (Imaris) from the center of mass of the nucleus (point A) to that of the golgi (point B). XY-plane vector coordinates were transformed into unit

vectors, combined, and plotted on an angle histogram with point A at the center. Vectors were grouped in 30^0 "bins" based on angle of orientation across the L-R axis (L, 225-315°; R, 45-135°).

Statistical Analysis

Student's t-test was used to compare means; error bars are standard error of the mean.

Cloning, Plasmids, and Oligonucleotides

cDNAs and probes for RNA ISH were TA-cloned using oligo-dT primed cDNA reverse transcription from pooled RNA of chicken (HH19 and 21) or mouse (E8.5-18.5). Cloned DNA was sequence-verified. Chicken EST clones (ChESTs) were generously provided by Amitabha Bandyopadhyay and Jonaki Sen; pCMV-Fmn1(IV)-Flag by Elaine Fuchs (Kobielak et al., 2004), pTOP-nRFP, RCAS-Daam2-shRNA, RCAS-RNA-mut-shRNA by Benjamin Deneen (Lee & Deneen, 2012), and pBS-BARvs by Randall Moon (Biechele et al., 2009). See Supplemental Material for more information.

Transfections, IP, and Blotting

Cells were cultured in DMEM containing 10% fetal bovine serum, under humidified conditions in 5% CO_2 at 37°C. 293FT or HeLa cells were transfected with Lipofectamine 2000 (Invitrogen). Cells were washed twice with PBS and lysates prepared in the presence of protease inhibitors (Roche). For IP, 1.0mg of lysate was cleared with protein G sepharose (GE) for 1 hour at 4°C then incubated ON with

protein G sepharose and either 8.0mg of a-catenin (Thermo MA1-2000), 7.0 mg of N-cadherin (BD Sciences, 610921), or 7.0mg of Daam2 antibodies (LSBio LS-C100232). Primary antibodies for immunoblotting: Flag (1:15,000), a-catenin (1:1000), N-cadherin (1:4000), or Daam2 antibodies (1:5000). Signal was detected with a 1:15,000 dilution of anti-mouse (GE Healthcare) or anti-rabbit IgG HRP (Invitrogen) and ECL Select reagent (GE).

Immunofluorescence

Frozen sections or cultured cells were permeabilized with 0.1% Triton X-100/PBS, blocked in 3% BSA/PBS, and incubated with antibodies (primary at 4°C ON, secondary for 1 hour at RT) using standard protocols. Primary antibodies used: a-catenin (Sigma, C2081), N-cadherin (DSHB, clone 6b3 or BD Biosciences, 610921), GFP (Abcam, ab290), Flag (Agilent, 200472), phospho-Histone-H3 (Abcam, ab5176), GM-130 (BD, 610822) and cleaved-Caspase3 (Millipore, AB3623). Samples were incubated with mouse or rabbit Alexa Fluor 488 or Alexa Fluor 594 secondary antibodies, counterstained with Phalloidin and DAPI and mounted with Prolong Gold antifade (all Invitrogen). Confocal images were acquired using identical exposures within the same staining experiment. Confocal z-stacks were acquired with a Zeiss LSM 710. Imaris (Bitplane) was used for images and z-stack analyses. Bright field micrographs were acquired with a Zeiss Observer.Z1 and AxioCam HRc camera.

3.7 Acknowledgements

We thank Drs. Drew Noden and Randall Moon for reading the manuscript and helpful suggestions. We thank Dr. Richard Maas for access to Laser Microdissection; Drs. Habas, Fuchs, Griffin, Bandyopadhyay, Sen and Deneen for reagents described above; and Megan Carpenter and Kate Lew for technical assistance. This work was supported by Cornell Comparative Cancer Biology Training Program, I.C.W.; March of Dimes, N.A.K. (1-FY11-520); NSF CU-ADVANCE, N.A.K. (0547373); NIH, N.A.K. (R01 DK092776), and NIH institutional support for I.C.W. (HD057854).

Daam2$^{tm1a(KOMP)Wtsi}$ targeted ES cells were funded by NIH grants to Velocigene (U01HG004085) and the CSD Consortium (U01HG004080).

REFERENCES

Aspenstrom, P., Richnau, N., and Johansson, A. S. (2006). The diaphanous-related formin DAAM1 collaborates with the Rho GTPases RhoA and Cdc42, CIP4 and Src in regulating cell morphogenesis and actin dynamics. *Exp Cell Res* **312,** 2180-2194.

Baeg, G. H., Lin, X., Khare, N., Baumgartner, S., and Perrimon, N. (2001). Heparan sulfate proteoglycans are critical for the organization of the extracellular distribution of Wingless. *Development* **128,** 87-94.

Barolo, S. (2006). Transgenic Wnt/TCF pathway reporters: all you need is Lef? *Oncogene* **25,** 7505-7511.

Biechele, T. L., Adams, A. M., and Moon, R. T. (2009). Transcription-based reporters of Wnt/beta-catenin signaling. *Cold Spring Harbor protocols* 2009**,** pdb prot5223.

Brent, A. E., Schweitzer, R., and Tabin, C. J. (2003). A somitic compartment of tendon progenitors. *Cell* **113,** 235-248.

Cano-Gauci, D. F., Song, H. H., Yang, H., McKerlie, C., Choo, B., Shi, W., Pullano, R., Piscione, T. D., Grisaru, S., Soon, S., et al. (1999). Glypican-3-deficient mice exhibit developmental overgrowth and some of the abnormalities typical of Simpson-Golabi-Behmel syndrome. *J Cell Biol* **146,** 255-264.

Capurro, M. I., Shi, W., Sandal, S., and Filmus, J. (2005a). Processing by convertases is not required for glypican-3-induced stimulation of hepatocellular carcinoma growth. *J Biol Chem* **280,** 41201-41206.

Capurro, M. I., Xiang, Y. Y., Lobe, C., and Filmus, J. (2005b). Glypican-3 promotes the growth of hepatocellular carcinoma by stimulating canonical Wnt signaling. *Cancer Res* **65,** 6245-6254.

Carramusa, L., Ballestrem, C., Zilberman, Y., and Bershadsky, A. D. (2007). Mammalian diaphanous-related formin Dia1 controls the organization of E-cadherin-mediated cell-cell junctions. *J Cell Sci* **120,** 3870-3882.

Carreira-Barbosa, F., Concha, M. L., Takeuchi, M., Ueno, N., Wilson, S. W., and Tada, M. (2003). Prickle 1 regulates cell movements during gastrulation and neuronal migration in zebrafish. *Development* **130,** 4037-4046.

Cervantes, S., Yamaguchi, T. P., and Hebrok, M. (2009). Wnt5a is essential for intestinal elongation in mice. *Dev Biol **326,*** 285-294.

Chan, D. W., Chan, C. Y., Yam, J. W., Ching, Y. P., and Ng, I. O. (2006). Prickle-1 negatively regulates Wnt/beta-catenin pathway by promoting Dishevelled ubiquitination/degradation in liver cancer. *Gastroenterology* **131,** 1218-1227.

Davis, N. M., Kurpios, N. A., Sun, X., Gros, J., Martin, J. F., and Tabin, C. J. (2008). The chirality of gut rotation derives from left-right asymmetric changes in the architecture of the dorsal mesentery. *Dev Cell* **15,** 134-145.

De Cat, B., Muyldermans, S. Y., Coomans, C., Degeest, G., Vanderschueren, B., Creemers, J., Biemar, F., Peers, B., and David, G. (2003). Processing by proprotein convertases is required for glypican-3 modulation of cell survival, Wnt signaling, and gastrulation movements. *J Cell Biol* **163,** 625-635.

Deneen, B., Ho, R., Lukaszewicz, A., Hochstim, C. J., Gronostajski, R. M., and Anderson, D. J. (2006). The transcription factor NFIA controls the onset of gliogenesis in the developing spinal cord. *Neuron* **52,** 953-968.

Golabi, M., and Rosen, L. (1984). A new X-linked mental retardation-overgrowth syndrome. Am *J Med Genet* **17,** 345-358.

Gray, R. S., Roszko, I., and Solnica-Krezel, L. (2011). Planar cell polarity: coordinating morphogenetic cell behaviors with embryonic polarity. *Dev Cell* **21,** 120-133.

Griffin, C. T., Curtis, C. D., Davis, R. B., Muthukumar, V., and Magnuson, T. (2011). The chromatin-remodeling enzyme BRG1 modulates vascular Wnt signaling at two levels. *Proc Natl Acad Sci U S A* **108,** 2282-2287.

Habas, R., Kato, Y., and He, X. (2001). Wnt/Frizzled activation of Rho regulates vertebrate gastrulation and requires a novel Formin homology protein Daam1. *Cell* **107,** 843-854.

Hamburger, V., and Hamilton, H. L. (1992). A series of normal stages in the development of the chick embryo. 1951. *Dev Dyn* **195,** 231-272.

Hashimoto, M., and Hamada, H. (2010). Translation of anterior-posterior polarity into left-right polarity in the mouse embryo. *Curr Opin Genet Dev* **20,** 433-437.

Hecksher-Sorensen, J., Watson, R. P., Lettice, L. A., Serup, P., Eley, L., De Angelis, C., Ahlgren, U., and Hill, R. E. (2004). The splanchnic mesodermal plate directs spleen and pancreatic laterality, and is regulated by Bapx1/Nkx3.2. *Development* **131,** 4665-4675.

Higashi, T., Ikeda, T., Shirakawa, R., Kondo, H., Kawato, M., Horiguchi, M., Okuda, T., Okawa, K., Fukai, S., Nureki, O., et al. (2008). Biochemical characterization of the Rho GTPase-regulated actin assembly by diaphanous-related formins, mDia1 and Daam1, in platelets. *J Biol Chem* **283,** 8746-8755.

Khadka, D. K., Liu, W., and Habas, R. (2009). Non-redundant roles for Profilin2 and Profilin1 during vertebrate gastrulation. *Dev Biol* **332,** 396-406.

Kobielak, A., Pasolli, H. A., and Fuchs, E. (2004). Mammalian formin-1 participates in adherens junctions and polymerization of linear actin cables. *Nat Cell Biol* **6,** 21-30.

Kurpios, N. A., Ibanes, M., Davis, N. M., Lui, W., Katz, T., Martin, J. F., Izpisua Belmonte, J. C., and Tabin, C. J. (2008). The direction of gut looping is established by changes in the extracellular matrix and in cell:cell adhesion. *Proc Natl Acad Sci U S A* **105,** 8499-8506.

Lampl, B., Levin, T. L., Berdon, W. E., and Cowles, R. A. (2009). Malrotation and midgut volvulus: a historical review and current controversies in diagnosis and management. *Pediatr Radiol* **39,** 359-366.

Lassiter, R. N., Dude, C. M., Reynolds, S. B., Winters, N. I., Baker, C. V., and Stark, M. R. (2007). Canonical Wnt signaling is required for ophthalmic trigeminal placode cell fate determination and maintenance. *Dev Biol* **308,** 392-406.

Lee, H. K., and Deneen, B. (2012). Daam2 is required for dorsal patterning via modulation of canonical Wnt signaling in the developing spinal cord. *Dev Cell* **22,** 183-196.

Levin, M., Johnson, R. L., Stern, C. D., Kuehn, M., and Tabin, C. (1995). A molecular pathway determining left-right asymmetry in chick embryogenesis. *Cell* **82,** 803-814.

Li, D., Hallett, M. A., Zhu, W., Rubart, M., Liu, Y., Yang, Z., Chen, H., Haneline, L. S., Chan, R. J., Schwartz, R. J., et al. (2011). Dishevelled-associated activator of morphogenesis 1 (Daam1) is required for heart morphogenesis. *Development* **138,** 303-315.

Liu, W., Sato, A., Khadka, D., Bharti, R., Diaz, H., Runnels, L. W., and Habas, R. (2008). Mechanism of activation of the Formin protein Daam1. *Proc Natl Acad Sci U S A* **105,** 210-215.

Lu, M. F., Pressman, C., Dyer, R., Johnson, R. L., and Martin, J. F. (1999). Function of Rieger syndrome gene in left-right asymmetry and craniofacial development. Nature **401,** 276-278.

Matsuyama, M., Aizawa, S., and Shimono, A. (2009). Sfrp controls apicobasal polarity and oriented cell division in developing gut epithelium. *PLoS Genet* **5,** e1000427.

Miller, R. K., Canny, S. G., Jang, C. W., Cho, K., Ji, H., Wagner, D. S., Jones, E. A., Habas, R., and McCrea, P. D. (2011). Pronephric tubulogenesis requires Daam1-mediated planar cell polarity signaling. *J Am Soc Nephrol* **22,** 1654-1664.

Moon, R. T., Brown, J. D., Yang-Snyder, J. A., and Miller, J. R. (1997). Structurally related receptors and antagonists compete for secreted Wnt ligands. *Cell* **88,** 725-728.

Nakaya, M. A., Habas, R., Biris, K., Dunty, W. C., Jr., Kato, Y., He, X., and Yamaguchi, T. P. (2004). Identification and comparative expression analyses of Daam genes in mouse and Xenopus. *Gene Expr Patterns* **5,** 97-105.

Nishimura, T., Honda, H., and Takeichi, M. (2012). Planar cell polarity links axes of spatial dynamics in neural-tube closure. *Cell* **149,** 1084-1097.

Pilia, G., Hughes-Benzie, R. M., MacKenzie, A., Baybayan, P., Chen, E. Y., Huber, R., Neri, G., Cao, A., Forabosco, A., and Schlessinger, D. (1996). Mutations in GPC3, a glypican gene, cause the Simpson-Golabi-Behmel overgrowth syndrome. *Nat Genet* **12,** 241-247.

Plageman, T. F., Jr., Zacharias, A. L., Gage, P. J., and Lang, R. A. (2011). Shroom3 and a Pitx2-N-cadherin pathway function cooperatively to generate asymmetric cell shape changes during gut morphogenesis. *Dev Biol* **357,** 227-234.

Sato, A., Khadka, D. K., Liu, W., Bharti, R., Runnels, L. W., Dawid, I. B., and Habas, R. (2006). Profilin is an effector for Daam1 in non-canonical Wnt signaling and is required for vertebrate gastrulation. *Development* **133,** 4219-4231.

Savin, T., Kurpios, N. A., Shyer, A. E., Florescu, P., Liang, H., Mahadevan, L., and Tabin, C. J. (2011). On the growth and form of the gut. *Nature* **476,** 57-62.

Shiratori, H., and Hamada, H. (2006). The left-right axis in the mouse: from origin to morphology. *Development* **133,** 2095-2104.

Song, H. H., Shi, W., Xiang, Y. Y., and Filmus, J. (2005). The loss of glypican-3 induces alterations in Wnt signaling. *J Biol Chem* **280,** 2116-2125.

Stigliano, I., Puricelli, L., Filmus, J., Sogayar, M. C., Bal de Kier Joffe, E., and Peters, M. G. (2009). Glypican-3 regulates migration, adhesion and actin cytoskeleton

organization in mammary tumor cells through Wnt signaling modulation. *Breast Cancer Res Treat* **114,** 251-262.

Topczewski, J., Sepich, D. S., Myers, D. C., Walker, C., Amores, A., Lele, Z., Hammerschmidt, M., Postlethwait, J., and Solnica-Krezel, L. (2001). The zebrafish glypican knypek controls cell polarity during gastrulation movements of convergent extension. *Dev Cell* **1,** 251-264.

Tree, D. R., Shulman, J. M., Rousset, R., Scott, M. P., Gubb, D., and Axelrod, J. D. (2002). Prickle mediates feedback amplification to generate asymmetric planar cell polarity signaling. *Cell* **109,** 371-381.

van Amerongen, R., and Nusse, R. (2009). Towards an integrated view of Wnt signaling in development. *Development* **136,** 3205-3214.

Vasioukhin, V., Bauer, C., Yin, M., and Fuchs, E. (2000). Directed actin polymerization is the driving force for epithelial cell-cell adhesion. *Cell* **100,** 209-219.

Veeman, M. T., Axelrod, J. D., and Moon, R. T. (2003a). A second canon. Functions and mechanisms of beta-catenin-independent Wnt signaling. *Dev Cell* **5,** 367-377.

Veeman, M. T., Slusarski, D. C., Kaykas, A., Louie, S. H., and Moon, R. T. (2003b). Zebrafish prickle, a modulator of noncanonical Wnt/Fz signaling, regulates gastrulation movements. *Current biology* : CB **13,** 680-685.

Vladar, E. K., Antic, D., and Axelrod, J. D. (2009). Planar cell polarity signaling: the developing cell's compass. *Cold Spring Harbor perspectives in biology* **1,** a002964.

Wallingford, J. B. (2012). Planar cell polarity and the developmental control of cell behavior in vertebrate embryos. *Annual review of cell and developmental biology* **28,** 627-653.

Wawrzak, D., Metioui, M., Willems, E., Hendrickx, M., de Genst, E., and Leyns, L. (2007). Wnt3a binds to several sFRPs in the nanomolar range. *Biochem Biophys Res Commun* **357,** 1119-1123.

Wolf, V., Endo, Y., and Rubin, J. S. (2008). Purification and Wnt-inhibitory activities of secreted frizzled-related proteins. *Methods Mol Biol* **468,** 31-44.

Yamaguchi, T. P., Bradley, A., McMahon, A. P., and Jones, S. (1999). A Wnt5a pathway underlies outgrowth of multiple structures in the vertebrate embryo. *Development* **126,** 1211-1223.

Yan, D., and Lin, X. (2009). Shaping morphogen gradients by proteoglycans. *Cold Spring Harbor perspectives in biology* **1,** a002493.

Ye, X., Wang, Y., Rattner, A., and Nathans, J. (2011). Genetic mosaic analysis reveals a major role for frizzled 4 and frizzled 8 in controlling ureteric growth in the developing kidney. *Development* **138,** 1161-1172.

Yin, C., Kiskowski, M., Pouille, P. A., Farge, E., and Solnica-Krezel, L. (2008). Cooperation of polarized cell intercalations drives convergence and extension of presomitic mesoderm during zebrafish gastrulation. *J Cell Biol* **180,** 221-232.

Zhu, Y., Tian, Y., Du, J., Hu, Z., Yang, L., Liu, J., and Gu, L. (2012). Dvl2-dependent activation of Daam1 and RhoA regulates Wnt5a-induced breast cancer cell migration. *PLoS One* **7,** e37823.

CHAPTER 4

Manuscript #3

Embryonic gut laterality is mirrored by asymmetric Pitx2 locus chromatin architecture dependent on Pitx2 and CTCF

Embryonic gut laterality is mirrored by asymmetric chromatin architecture at the Pitx2 locus dependent on Pitx2 and CTCF

Ian C. Welsh[1], Hojoong Kwak[2], Frances L. Chen[1], Melissa Werner[1], Lindsay S. Shopland[3], Charles G. Danko[4], John T. Lis[2] and Natasza A. Kurpios[1]*

[1]Department of Molecular Medicine, College of Veterinary Medicine, Cornell University, Ithaca, NY 14853, USA. [2]Department of Molecular Biology and Genetics, Cornell University, Ithaca, NY 14853, USA. [3]The Jackson Laboratory, Bar Harbor, ME, 04609, USA and Eastern Maine Medical Center Cancer Care, 33 Whiting Hill Rd. Brewer, ME 04412, USA. [4] Department of Biomedical Sciences, The Baker Institute for Animal Health, Cornell University, Ithaca, NY 14853, USA.

*Corresponding author: nk378@cornell.edu

Running title: *Pitx2* mediated left-right chromatin asymmetry

4.2 Abstract

Three-dimensional (3D) chromatin organization is fundamental for cell type-specific gene expression. The transcription factor Pitx2 is expressed on the left side of the early vertebrate embryo to pattern left-right (L-R) organs including the dorsal mesentery (DM), whose asymmetric cell behavior directs gut looping chirality. However, despite the critical importance of organ laterality, chromatin-level regulation of Pitx2 remains undefined. Here we show that genes immediately neighboring *Pitx2* on chicken chromosome 4 are expressed strictly on the right side of the DM, opposite left-sided *Pitx2*. Pitx2 represses right-sided genes, including a long noncoding RNA we have named *Playrr* (*Pitx2* locus asymmetric regulated RNA). Using 3D fluorescent in situ hybridization in chicken and mouse embryos, we find that long-range chromatin looping across a conserved gene desert generates constitutive *Pitx2* locus architecture dependent on the CCCTC-binding factor CTCF. We show that *Pitx2* is required for modest L-R changes in the positioning of genes within this constitutive architecture that accompany asymmetric transcription. Collectively, we demonstrate that transcriptional and morphological asymmetries driving gut looping are mirrored by chromatin architectural asymmetries at the *Pitx2* locus. We propose a model where minor changes in chromatin topology coordinate L-R transcription of this locus essential for asymmetric organogenesis.

4.3 Introduction

The external bilateral symmetry of vertebrates conceals the highly conserved left-right (L-R) asymmetries of the internal organs essential for their normal function and efficient packing within the body cavity. L-R patterning initiates early during gastrulation via transient signaling of the transforming growth factor b-related protein Nodal, which results in persistent expression of the homeobox transcription factor Pitx2 throughout the left lateral mesoderm (Logan et al. 1998; Shiratori et al. 2001). Subsequently, restricted *Pitx2* expression specifies the left identity of individual organ primordia (Ryan et al. 1998; Zorn and Wells 2009). The control of laterality by *Pitx2* represents a remarkably ancient function, as this pathway is required for normal asymmetric morphogenesis even in basal deuterostomes such as sea urchin and non-bilaterians such as hydra (Duboc et al. 2005; Watanabe et al. 2014).

Tissue-specific gene expression provides the basis for genetic control of morphogenesis and is central to human health and disease. The activity of intercellular signaling and transcription factors is integrated by cis-regulatory elements encoded in the genome to coordinate spatial gene expression and direct morphogenesis. However, genes and regulatory elements that must physically interact to drive tissue-specific expression are commonly distributed across large genomic intervals (Zuniga et al. 2004; Marinić et al. 2013; Lettice et al. 2002; Anderson et al. 2014). While it is now appreciated that genes cluster in the nucleus and form 3D topologically associating domains (TADs) of considerable (500 kb – 1 Mb) chromosomal sequence, how genes are regulated within this structural context is unknown (Shopland et al. 2006). Importantly, most information on gene regulation at the level of 3D nuclear structure

has been obtained from cells in culture (Sutherland and Bickmore 2009). Evaluating 3D chromatin structure *in situ*, in the 3D tissues in which cells differentiate, is important for understanding the role of chromatin 3D structure in tissue-specific gene regulation.

Indicative of the inherent complexity, a number of strategies to translate the 3D organization of the genome into cell type specific gene expression have been enumerated (reviewed in de Laat and Duboule 2013). Highlighting outstanding questions regarding the source of specificity of transcriptional control in vertebrates, such distributed regulatory landscapes can also influence "by-stander" genes within the genomic interval, while at other loci regulation is strictly independent (Spitz et al. 2003; Cajiao et al. 2004; Anderson et al. 2014; Marinić et al. 2013). While these few examples are instrumental, additional experimentally tractable models are needed to dissect, in the context of tissues and organs that a locus controls, the mechanisms through which 3D organization of the linear genome coordinates spatial gene expression.

Regulation of *Pitx2* in vertebrates is complex, involving multiple isoforms with unique and overlapping spatial expression and function. *Pitx2a* and *Pitx2b* are generated by alternative splicing and are expressed bilaterally, while *Pitx2c* is derived from an alternative promoter, and is exclusively left-sided (Shiratori et al. 2006; Liu et al. 2001). *Pitx2* null mice exhibit mid gestation lethality and global organ laterality defects (Lu et al. 1999). Moreover, mutations in the human *PITX2* gene are associated with Axenfeld-Rieger Syndrome (ARS) characterized by mental retardation, mandibular and ocular birth defects, as well as ventral body wall defects and umbilical

hernias (Semina et al. 1996). Importantly, screening of ARS patients has identified individuals who possess no mutations in *Pitx2* coding sequences but who harbor large lesions within an adjacent gene desert devoid of coding genes, suggesting an essential cis-regulatory role for elements within the desert in driving *Pitx2* expression (Flomen et al. 1998; Volkmann et al. 2011; Reis et al. 2012). Despite the wealth of available knowledge about early signaling events controlling laterality, the specific genomic mechanisms governing the expression of its master effector remain unexplored.

To this end, we make use of the dorsal mesentery (DM), a bridge of mesodermal tissue suspending the gut that possesses a unique binary (L vs. R) molecular and cellular asymmetry directed by left-sided *Pitx2* (Fig. 4.1A, top). The left compartment of the DM condenses while the right expands causing the DM to deform and tilt the gut tube leftward (Davis et al. 2008; Kurpios et al. 2008). This tilt provides a bias for asymmetric gut rotation, disruption of which randomizes gut looping (Davis et al. 2008) (Fig. 4.1A, top). To define the molecular composition of the DM, we recently completed a laser capture microdissection and microarray analysis of the left (*Pitx2*-positive) and right (*Pitx2*-negative) halves of the chicken DM at the critical time when L-R DM asymmetries are apparent (HH21, akin to mouse embryonic [E] day 10.5) (Hamburger and Hamilton 1951; Welsh et al. 2013). We report here our recent analyses of these data, which strikingly reveal that genes immediately neighboring *Pitx2* and positioned either proximally and distally to a large conserved gene desert flanking *Pitx2* are expressed in a right-specific pattern opposite to left-specific *Pitx2*. Moreover, positioned at the proximal end of the gene desert we

identified the conserved sequence element e926, with left-specific enhancer activity in the DM of transgenic mouse embryos. In contrast, our genome-wide global run-on

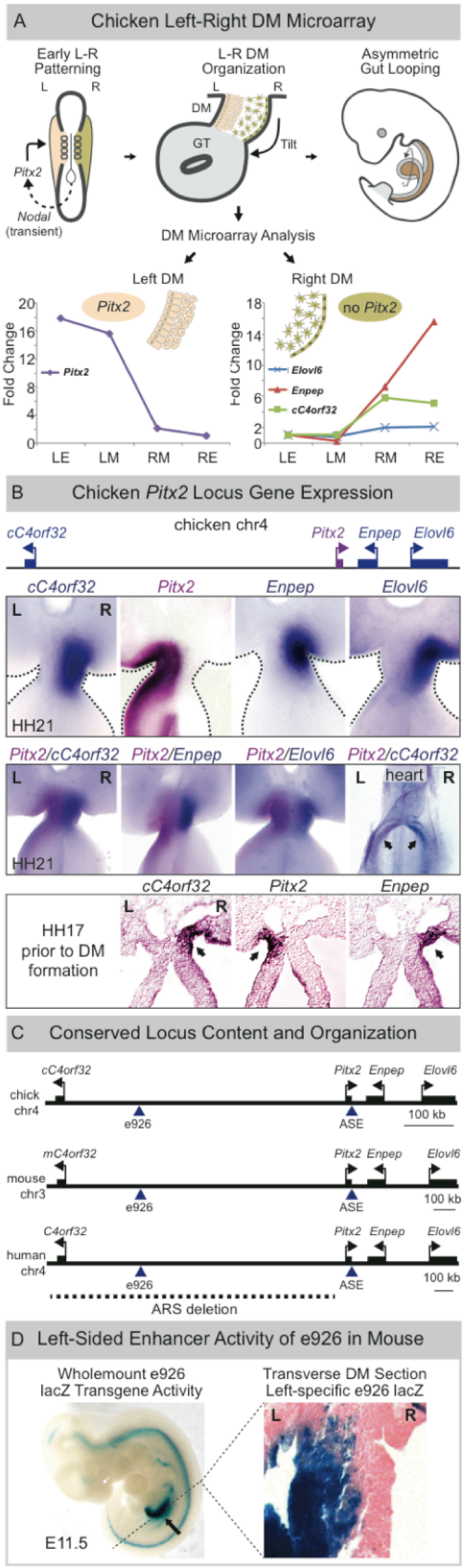

Figure 4.1. L-R asymmetric gene expression at the *Pitx2* locus (A) Nodal-induced *Pitx2* initiates gut looping directed by L-R changes in the DM cellular architecture (tan, left; green, right). DM microarray (LE, left epithelium, LM, left mesenchyme, RM, right mesenchyme, RE, right epithelium) identifies genes linked to *Pitx2* with right side-restricted expression, validated in (B) via whole mount double in situ hybridization (*Pitx2*, magenta, right-specific genes, blue) at HH21 (DM), at HH17 (lateral mesoderm, DM precursor, arrows) and at HH12 (sinus venosus of the primitive heart, arrows). (C) *Pitx2* locus conservation in chicken, mouse, and human (dashed line, human ARS deletion). Note, human locus is shown inverted relative to its orientation on chr4. (D) e926 directs left-specific reporter gene expression (LacZ) in the left DM of transgenic mouse embryos. See also Supplemental Figure 1.

sequencing, GRO-seq and dREG (discriminative Regulatory Element detection from GRO-seq) (Core et al. 2008; Danko et al. 2015) analysis of left and right DM samples found that e926 functions endogenously as a promoter for a conserved lncRNA exclusively transcribed in the right DM. We employed fluorescent in situ hybridization (FISH) to correlate this binary L-R expression of locus genes with nuclear architecture and discovered highly evolutionary conserved long-range chromatin looping in the left and right DM. Importantly, within this invariant 3D topology, we identified subtle but conserved L-R differences in proximity of these genes that are dependent on *Pitx2*. These data represent the first report of chromatin-level asymmetry during L-R organogenesis and suggest a model where tissue-specific cis-regulatory topology establishes L-R transcription among higher vertebrates.

4.4 Results

4.4.1 L-R asymmetric gene expression at the Pitx2 locus

We identified *Pitx2* as the most differentially expressed gene on the microarray, with ~19-fold higher expression in the left DM consistent with the central role of this gene in regulating asymmetric organogenesis (Welsh et al. 2013) (Fig. 4.1A, graph). Interestingly, our new analyses found that glutamyl aminopeptidase A (*Enpep*) is the most differentially expressed gene in the right DM, with ~17-fold higher expression (Fig. 4.1A, graph). Remarkably, these two genes exhibiting the highest fold differences in left vs. right-sided expression are located immediately adjacent to each other in the genome. On chicken chromosome 4, *Pitx2* is flanked proximally by a large (~600kb) gene desert and 27kb distally by the convergently

transcribed *Enpep* (Fig. 4.1B). RNA in situ hybridization confirmed these results and demonstrated that tissue asymmetry in the DM is mirrored by differences in expression of these linked genes across the L-R axis (Fig. 4.1B).

Intrigued, we asked whether additional genes neighboring the *Pitx2* locus also exhibit asymmetric expression in the DM and identified two additional genes with right-side restricted gene expression: fatty acid elongase, (Elovl6), the immediate neighbor of *Enpep*, and the ortholog of the uncharacterized human gene *C4ORF32*, *Loc422694* (*cC4orf32*) positioned at the proximal boundary of the gene desert (Fig. 4.1A-C). This novel pattern of asymmetric expression was not exclusive to the DM. We observed asymmetric expression of linked genes well prior to DM formation in the lateral mesoderm (precursor to the DM, Fig. 1B HH17), and in other asymmetric organs, such as the heart, where *Pitx2* plays an essential role (Fig. 4.1B, HH12) (Franco and Campione 2003). Consistent with the importance of this locus, its gene content, order, and orientation are highly conserved throughout vertebrate evolution (from human to frog), suggesting that functional and regulatory constraint acting across the locus maintains such synteny (Kikuta et al. 2007; Nobrega et al. 2003) (Fig. 4.1C).

4.4.2 Identification of asymmetric regulatory element e926 at the Pitx2 locus

Regulation of asymmetric *Pitx2c* expression requires the activity of the ASE enhancer element located in the last intron of *Pitx2* (Shiratori et al., 2006). The functional activity of this element is highly conserved and homologous ASE sequences from fish, frog, chicken, mouse, and human are able to drive left-specific

reporter gene activity in mice (Shiratori et al. 2001, 2006). We hypothesized that additional enhancer elements exist within the conserved gene desert that contribute to the robust L-R expression of genes at the *Pitx2* locus. Such deserts, devoid of protein coding genes, commonly harbor regulatory elements (REs) critical for coordinating spatiotemporal expression of nearby genes. Indeed, translocations and deletions within the desert flanking *Pitx2* found in ARS patients provide strong evidence for the cis-regulatory role at the *Pitx2* locus (Fig. 4.1C, human) (Rainger et al. 2014; Volkmann et al. 2011; Reis et al. 2012).

We searched the Vista Enhancer Browser and identified hs926, a human derived sequence located in the proximal third of the desert whose sequence is highly conserved among human, mouse, and chicken (Fig. S4.1) (Visel et al. 2007). Element 926 (e926) appeared to show enhancer like activity in the midgut of E11.5 transgenic reporter embryos (Fig. 1D, n=4/7 embryos assayed). Upon sectioning we found that e926 drove robust lacZ reporter activity specifically in the left DM (Fig. 4.1D). Thus, as assayed via transgenesis, e926 functions as an additional transcriptional enhancer responsive to the regulatory environment within the left DM.

4.4.3 Right-specific regulatory activity of e926 in vivo

To directly confirm the left-specific activity of e926 in vivo, we conducted a genome-wide global run-on sequencing, GRO-seq, of left vs. right derived DM samples (Fig. 4.2A) (Core et al. 2008). GRO-seq allows mapping of nascent transcription by engaged RNA polymerase II (RNA Pol II) and collects strand-specific reads that identify regions of divergent transcription shown to be a distinct signature of

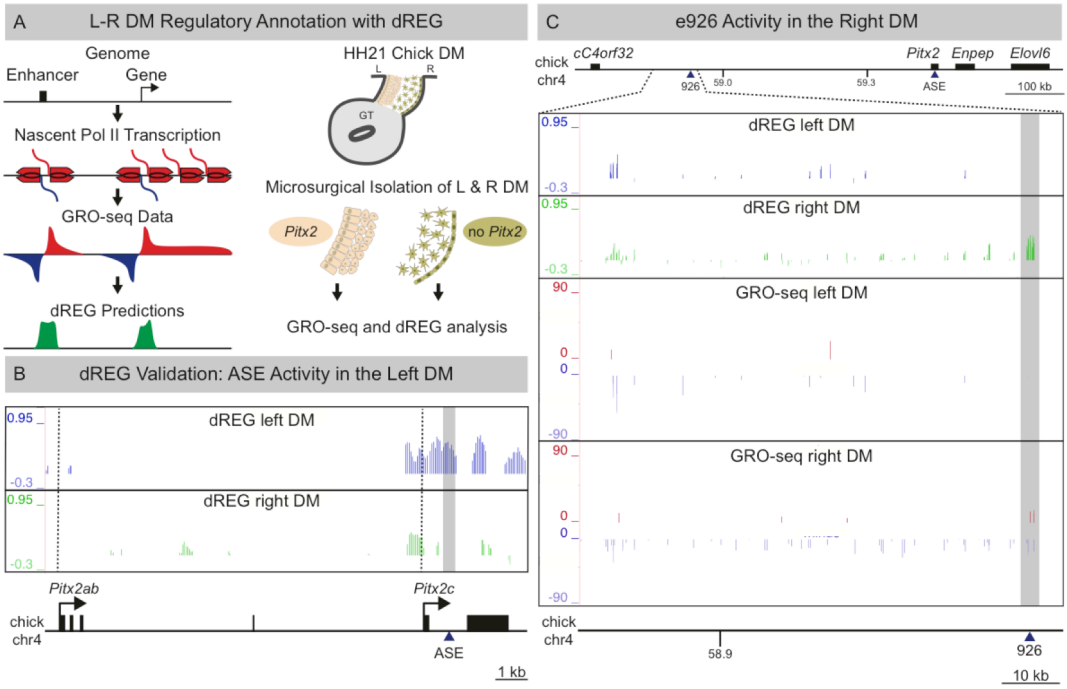

Figure 4.2. L-R DM GRO-seq/dREG analyses (A) Left: Overview of GRO-seq and dREG. Right: GRO-seq libraries were prepared from HH21 L-R DM samples (B) dREG peaks corresponding to ASE are exclusive to the left DM (grey box). Dashed vertical lines mark Pitx2a/b and Pitx2c TSS. (C) dREG peaks overlapping e926 are right-specific (grey box) in contrast to left-specific transgenic reporter gene activity driven by e926. GRO-seq detects asymmetric transcription from the minus strand at the proximal gene desert in the right DM.

active REs (Core et al. 2008; Melgar et al. 2011; Core et al. 2014). Moreover, a computational tool termed discriminative Regulatory Element detection from GRO-seq (dREG) recognizes the pattern of divergent transcription at active REs allowing characterization of the transcriptional regulatory state at the level of both nascent transcription and activation of associated REs (Fig. 4.2A, green) (Danko et al. 2015).

Consistent with our microarray data, both GRO-seq and dREG analysis confirmed the binary L-R gene expression from the *Pitx2* locus, readily apparent as differential transcription at the proximal and distal gene ends of desert in the left or right DM, respectively (Fig. S4.2). For example, GRO-seq reads mapped to the

asymmetric *Pitx2c* at the distal end demonstrate transcription in the left but not right DM samples, and dREG peaks overlapping the ASE enhancer were exclusively observed in the left DM samples (Fig. 4.2B, grey box; Fig. S4.3). In contrast, GRO-seq and dREG detected extensive transcription of the proximal desert preferentially in the right DM (Fig. 4.2C, Fig. S4.2) including dREG peaks directly overlapping the conserved e926 enhancer (Fig. 4.2C, grey box). Although this confirms e926 as an asymmetrically responsive cis-regulatory element, it stands in striking contrast to transgenesis data supporting the left-specific activity of e926 (Fig. 4.1D). These data are consistent with recent findings demonstrating that enhancers may act differently when tested in trans as single elements, vs. within the cis-context of the endogenous locus (Marinić et al. 2013).

4.4.4 Identification of a conserved lncRNA, Playrr, transcribed from e926 on the right

dREG identifies active REs as sites of divergent transcription occurring at both enhancers and promoters (Danko et al. 2014). Therefore, an alternative explanation for the discrepancy in asymmetric activity of e926 is that this regulatory element does not function as an enhancer but may act instead as a promoter in the right DM. However, there are currently no annotated genes in the chicken genome within the gene desert distal to *cC4orf32* and proximal to *Pitx2*. Interestingly, we noted that GRO-seq reads extend a considerable distance proximally from e926, suggesting the presence of a gene transcribed from the minus strand towards *cC4orf32* (Fig. 4.2C, GRO-seq right DM). Supporting this hypothesis, the syntenic region of the mouse genome is annotated with D030025E07Rik, a long noncoding RNA (lncRNA) with a

transcriptional start site (TSS) contained within e926 that is also transcribed from the minus strand of mouse chromosome 3 (Fig. 4.3A). To characterize the expression profile of this lncRNA in the chicken and mouse DM, we cloned D030025E07Rik and chicken ESTs corresponding to the transcribed region identified through GRO-seq. In both species, expression of this lncRNA was restricted to the right side of the DM consistent with the GRO-seq data (Fig. 4.3B). These results support the presence of a conserved lncRNA expressed contralateral to the left-specific enhancer activity of e926 from which it is derived. We refer to this novel lncRNA as *Playrr* (*Pitx2* locus asymmetric regulated RNA).

4.4.5 Pitx2 negatively regulates Playrr expression in vivo

We found conserved *Pitx2* binding sites within e926 suggesting that *Pitx2* regulates *Playrr* expression (Fig. 4.3C). To directly test this, we used a genetic approach and examined *Playrr* expression in *Pitx2*-/- mouse DM at E10.5. Strikingly, we found that in the absence of *Pitx2* on the left, *Playrr* is bilaterally expressed in the DM (Fig. 4.3B). This indicates that in the left DM, *Pitx2* represses *Playrr*.

4.4.6 Global and local chromatin looping of the Pitx2 locus in the chicken DM

The complementary expression of *Pitx2* and *Playrr*, and the evolutionary conservation of their arrangement in chromosomal sequence, suggest that their regulation may be coordinated by chromosome structure. Thus, to understand how binary L-R transcription relates to nuclear chromatin architecture we employed multi-color 3D fluorescent in situ hybridization on chicken DM sections (3D tissue-FISH).

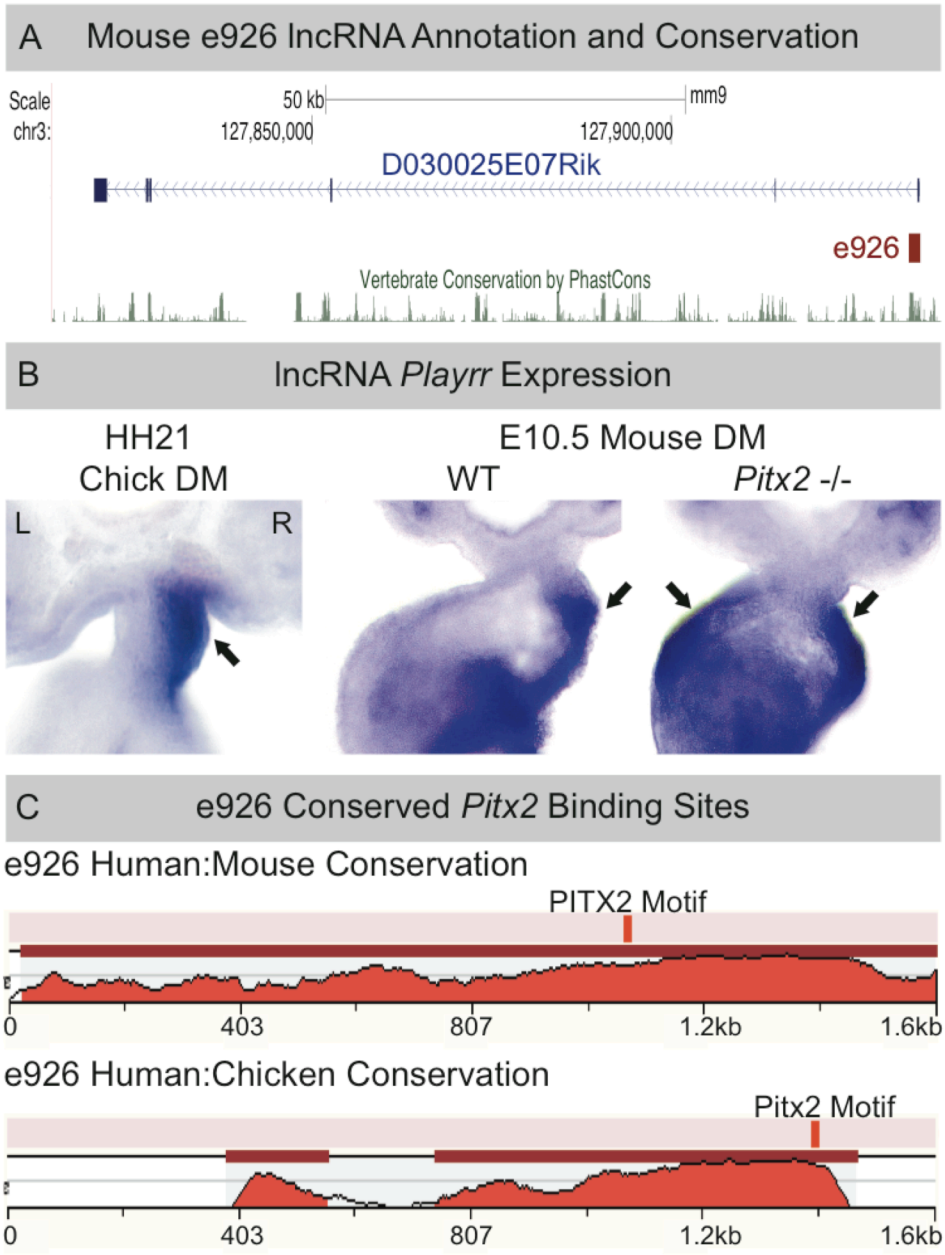

Figure 4.3. Identification of a conserved lncRNA, Playrr, asymmetrically transcribed from e926. (A) Annotation of mouse lncRNA *Playrr* (D030025E07Rik). (B) Whole mount in situ hybridization showing right-specific *Playrr* in WT HH21 chicken and E10.5 mouse embryos vs. bilateral Playrr expression in *Pitx2*-null mouse DM. (C) Prediction of *Pitx2* binding sites within e926 conserved between human and mouse (top) or human and chicken (bottom) (http://rvista.dcode.org/).

We hypothesized that looping interactions of the *Pitx2* locus organizes chromatin differentially in nuclei on the left vs. right. We used DNA probes to label *cC4orf32* (Cy5, blue) at the proximal boundary of the gene desert, *Playrr* (DIG, green) within the gene desert, and *Pitx2* (Cy3, red) at the distal end of the gene desert (Fig. 4.4A). Quantification of each pairwise interprobe distance (i.e. *cC4orf32-Playrr*, *cC4orf32-Pitx2*, and *Playrr-Pitx2*) was used to compare how these loci are positioned within the 3D space of the nucleus relative to each other and to the intervening gene desert (Table 4.1).

In the linear genome, *cC4orf32* and *Playrr* are nearest to each other, separated by ~162kb compared to the ~578kb separating *cC4orf32* and *Pitx2* or ~416kb separating *Playrr* and *Pitx2* (Fig. 4.4A). However, our FISH revealed that within the 3D nuclear space of the DM, both *cC4orf32* and *Playrr* were significantly closer to *Pitx2* than to each other (Table 4.1A). Our data therefore establish that long-range looping of the *Pitx2* locus positions the proximal and distal ends of the gene desert in close proximity within the 3D space of the nucleus. Interestingly, we found the global architecture of the locus was similarly organized in the left and right DM (Fig. 4.4BC). Importantly however, we identified subtle but statistically significant L-R differences in interprobe distances for both *cC4orf32-Pitx2* and *Playrr-Pitx2*, demonstrating that both *cC4orf32* and *Playrr* are positioned significantly closer to *Pitx2* in the left DM compared to the right (Fig. 4.4B, Fig. S4.4A, Table 4.1A). Left-right differences in the distributions of these loci were highly reproducible across five independent experiments (Fig. S4.4). Hence, mirroring the L-R asymmetric gene expression and cellular architecture within the DM, proximity of *cC4orf32*, *Playrr*, and *Pitx2* in nuclei

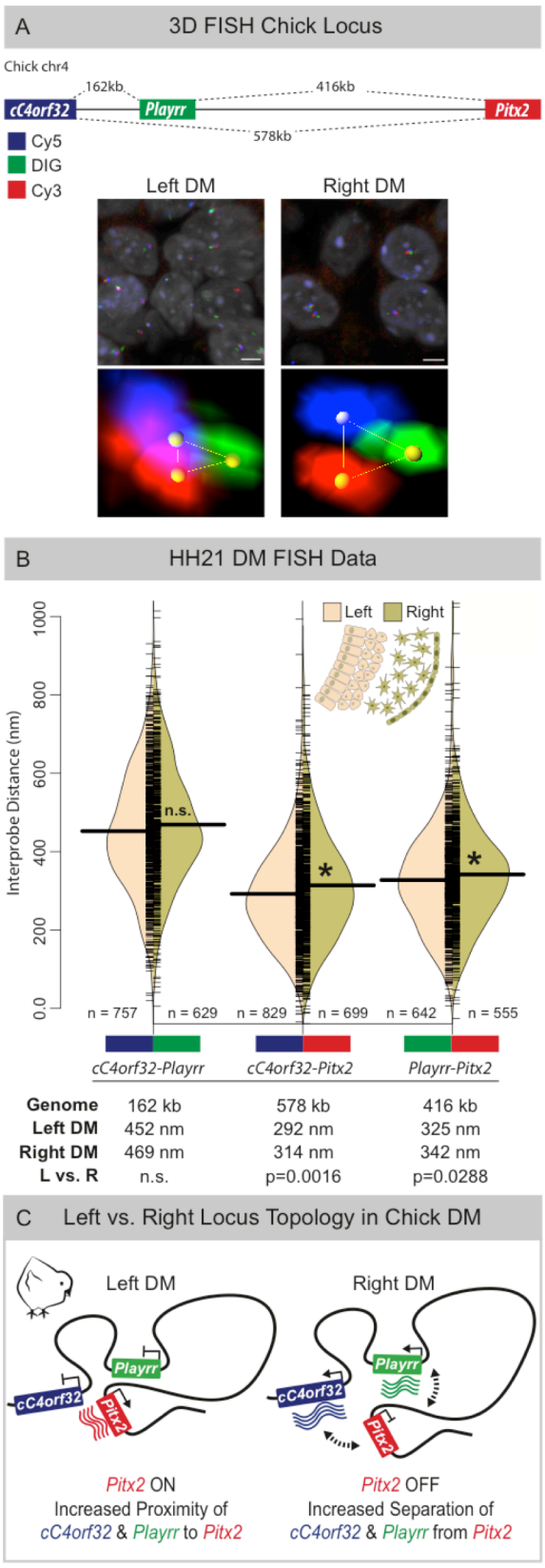

Figure 4.4. Global and local chromatin looping of the *Pitx2* locus in the chicken L-R DM (A) Right-specific *cC4orf32* and *Playrr*, and left-specific *Pitx2,* marked with Cy5, DIG, and Cy3 labeled DNA probes, respectively. (B) Split bean plots comparing distributions of interprobe distances for each probe pair between the left and right DM. Individual measurements are plotted as short horizontal ticks, the density trace and mean are plotted as the filled curve and large horizontal bar, respectively. Summary table below plots shows distance separating each probe pair in the genome or nucleus. (C) Model of *Pitx2* locus organization and resulting gene expression in nuclei of the left or right chicken DM. Scale bars in A, 2.0mm.

of the left DM is associated with preferential transcription of *Pitx2*. Conversely, in the right DM, where *cC4orf32* and *Playrr* are expressed, they are further separated from *Pitx2* (Fig. 4.4C). Thus, L-R differences in 3D looping of the *Pitx2* locus are characterized by subtle local shifts, rather than global differences, in the relative position of individual genes within a constant overall locus topology.

4.4.7 Spatial proximity of Playrr and Pitx2 is a conserved feature of locus topology

To address the degree to which asymmetric nuclear architecture of the chicken *Pitx2* locus is conserved, we used the same FISH labeling scheme on mouse DM sections and analyzed pairwise interprobe distances for 5730508B09Rik (*mC4orf32*, the mouse ortholog of *C4ORF32*, Cy5, blue) at the proximal end of the desert, *Playrr* (DIG, green) within the desert, and *Pitx2* (Cy3, red) at the distal end of the desert (Fig. 4.5A). In the mouse genome, the linear genomic distance separating the FISH probe pairs *mC4orf32-Playrr*, *mC4orf32-Pitx2*, and *Playrr-Pitx2* is 380kb, 1.36Mb, and 980kb respectively (Table 4.1B).

Consistent with our analysis of chicken DM nuclei, long-range looping across the mouse gene desert positions both *mC4orf32* and *Playrr* in significantly closer proximity to *Pitx2* than to each other (Fig. 4.5B, Table 4.1B). Remarkably, although in the mouse *Playrr* is located nearly twice the genomic distance proximal to *Pitx2* compared to chicken, the interprobe distance measured for *Playrr-Pitx2* was nearly identical to that measured in chicken (Table 4.1B). Moreover, the difference between *Playrr-Pitx2* spatial proximity in the left vs. the right DM was maintained in the mouse, further highlighting our observation that proximity of *Playrr* and *Pitx2* in

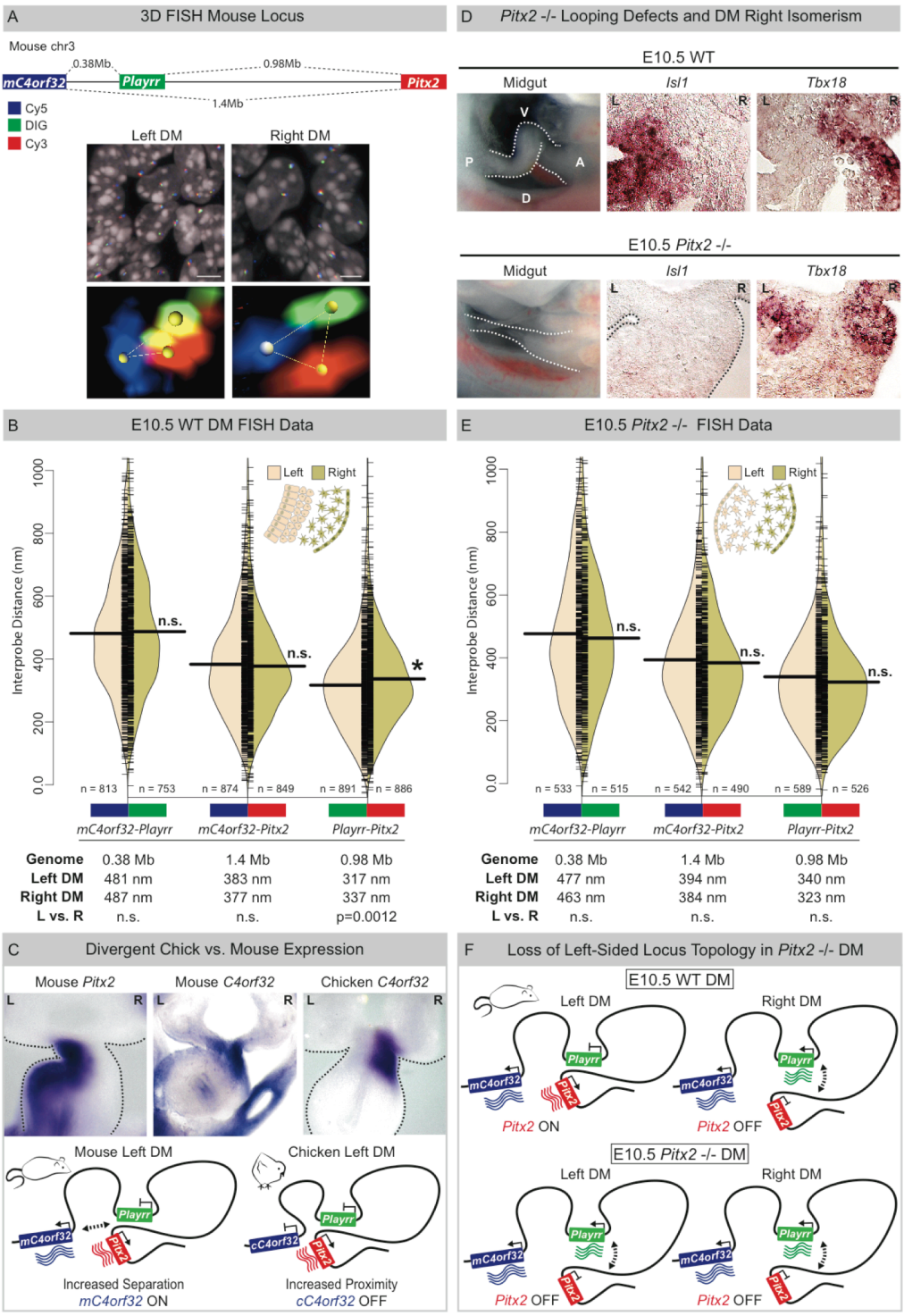

Figure 5. Spatial proximity of *Playrr* and *Pitx2* are a conserved feature of locus topology and is dependent on Pitx2. (A) Cy5, DIG, and Cy3 mouse DNA probe labeling scheme akin to chicken was used to analyze the mouse Pitx2 locus. (B) Split bean plots of WT E10.5 left and right DM. Summary table below plots shows distance separating each probe pair in the genome or nucleus. (C) Divergent chicken vs. mouse C4orf32 expression accompanies increased separation of *mC4orf32* (arrow) from *Playrr* and *Pitx2* in mice. (D) Altered midgut looping and right-isomerized DM in *Pitx2*-null embryos is evidenced by loss of left-specific *Isl1* and bilateral Tbx18 expression. (E) Split bean plots of FISH analysis in *Pitx2*-null DM. (F) Model of *Pitx2* locus organization and resulting gene expression in nuclei of the left or right mouse WT and Pitx2-null DM. Scale bars in A, 2.0mm.

nuclei on the left is associated with preferential *Pitx2* transcription (Fig. 4.5B, Table 1B). In contrast, we found that the position of *mC4orf32* relative to both *Playrr* and *Pitx2* is farther than observed in chicken and not different in nuclei on the left vs. right (Fig. 4.5BF, Table 4.1B). Thus, L-R asymmetry in the proximity of *Playrr* with *Pitx2* is a conserved feature of *Pitx2* locus topology.

4.4.8 Changes in spatial gene expression across species accompany differences in Pitx2 locus topology

The genomic expansion of the mouse vs. chicken *Pitx2* locus is uniform across the locus and not biased towards intervals separating either *mC4orf32-Playrr* or *Playrr-Pitx2*. This suggests that differences in the topology of the locus in mouse are due to a change in the position of the proximal gene desert (i.e. *mC4orf32*) relative to the overall conserved 3D topology of the locus. To assess the possible regulatory significance of this difference, we analyzed the expression of *mC4orf32* in the mouse DM. In contrast to the exclusive right-sided expression of *cC4orf32* in the chicken DM, *mC4orf32* was weakly expressed in the left DM of E10.5 mouse embryos, in addition to its robust expression on the right side (Fig. 4.5C). This is in contrast to highly conserved left-sided *Pitx2* expression (Shiratori et al. 2006) or expression of *Playrr*, which was strictly right-sided in both chicken and mouse DM (Fig. 4.3C). Thus, while complementary L-R *Pitx2* locus gene expression is conserved, differences in nuclear architecture observed between chicken and mouse involving relative proximity to *Pitx2* in the left or right DM correlate with changes in spatial gene expression between these species.

4.4.9 Pitx2 locus topology is invariant across diverse cell types

Previous experiments have shown that some chromatin loops exist in a constitutive 3D configuration that can be used in any cell type, in contrast to loops that are triggered de novo at the time of transcriptional activation (Drissen et al. 2004; Shopland et al. 2006; van de Werken et al. 2012; Montavon et al. 2011; Jin et al. 2013; de Laat and Duboule 2013). To determine whether the *Pitx2* locus shares similar 3D topology in different cell types, we first analyzed *Pitx2* locus topology in cells of the chicken and mouse neural tube (HH21 and E10.5, respectively). Remarkably, although neuroectodermal cells of the neural tube and mesodermal cells of the DM represent distinct lineages separated early during gastrulation, we found that in both chicken and mouse the *Pitx2* locus shares a consistent 3D topology as seen in the DM (Fig. 4.6A, Table 1DE). Furthermore, species-specific differences in the relative proximity of *cC4orf32* vs. *mC4orf32* to *Playrr* and *Pitx2* were also maintained in the neural tube (Fig. 4.6A).

Next, we analyzed *Pitx2* locus topology in mouse embryonic stem cells (mESCs). RNA Pol II ChIP-seq data (Kagey et al. 2010) demonstrate that mESCs exclusively express the asymmetric *Pitx2c* isoform associated with L-R patterning (Fig. 4.6B). Moreover, p300 and Mediator binding indicate that activation of the asymmetric ASE enhancer accompanies *Pitx2c* expression in these cells (Fig. S4.5) (Creyghton et al. 2010). Additionally, *mC4orf32* is expressed at very low levels while *Enpep* and *Playrr*, the other right-sided genes, are not expressed at all. Hence, mESCs mimick the expression profile of the *Pitx2* locus in the left DM.

We found that the 3D organization of the *Pitx2* locus in the nuclei of mESCs is nearly identical to that of the DM and neural tube of the mouse, where *Playrr-Pitx2* are in closest proximity and *mC4orf32-Playrr* are furthest separated (Fig. 4.6A, Table 4.1F). These findings support a model of preassembled regulatory topology of the *Pitx2* locus, where a similar pattern of long-range chromatin looping across the gene desert is a constitutive feature 3D configuration of the locus in diverse cell types (Fig.4. 6D).

4.4.10 Altered L-R patterning disrupts asymmetric Pitx2 locus topology

In mice lacking *Pitx2*, the left DM fails to condense, all L-R DM asymmetry is lost and stereotypical gut looping is randomized (a 'double-right' phenotype) (Fig. 4.5D) (Davis et al. 2008; Kurpios et al. 2008). On a molecular level, *Pitx2*-null embryos exhibit a loss of left-specific expression of *Pitx2* target genes, such as *Islet1* (Fig. 4.5D) and show bilateral expression of right-sided genes, such as *Tbx18* (Fig. 5D) and *Playrr* (Fig. 4.3C). To investigate whether such molecular and cellular defects due to loss of *Pitx2* impact the subtle L-R differences of locus topology, we performed FISH on *Pitx2*-null mouse DM. As expected, we found that the global organization of the locus was not impacted by loss of *Pitx2* (Fig. 4.5E, Table 4.1C). Importantly, the conserved proximity of *Playrr* and *Pitx2* in the left WT DM was lost in *Pitx2*-null embryos (Fig. 5E, Table 1C). Hence, in the absence of *Pitx2*, *Playrr* and *Pitx2* are significantly farther apart in the left DM compared to the WT left DM, and indistinguishable from the interprobe distance in the WT right DM (Fig. 4.5BE, Fig. S4.4, Table 4.1BC). Thus, a double-right phenotype of the *Pitx2*-null DM is accompanied by isomerized nuclear architecture of the *Pitx2* locus (Fig. 4.5F). These

Table 1. Mean FISH Interprobe Distances (nm)

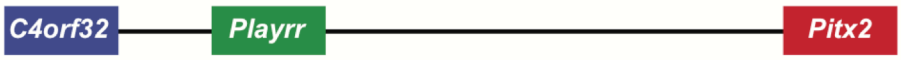

A	**Chick DM**					
	cC4orf32-Playrr		*cC4orf32-Pitx2*		*Playrr-Pitx2*	
	L	R	L	R	L	R
	452 ± 5	469 ± 6	292 ± 4	314 ± 5	325 ± 5	342 ± 6
	n = 757	n = 629	n = 829	n = 699	n = 642	n = 555
	p = 0.0634		**p = 0.0016**		**p = 0.0288**	
B	**Mouse WT DM**					
	mC4orf32-Playrr		*mC4orf32-Pitx2*		*Playrr-Pitx2*	
	L	R	L	R	L	R
	481 ± 7	487 ± 7	383 ± 6	377 ± 6	317 ± 5	337 ± 5
	n = 813	n = 753	n = 874	n = 849	n = 891	n = 886
	p = 0.5827		p = 0.4181		**p = 0.0012**	
C	**Mouse Pitx2 -/- DM**					
	mC4orf32-Playrr		*mC4orf32-Pitx2*		*Playrr-Pitx2*	
	L	R	L	R	L	R
	477 ± 9	463 ± 9	394 ± 8	384 ± 8	340 ± 7	323 ± 7
	n = 533	n = 515	n = 542	n = 490	n = 589	n = 526
	p = 0.3661		p = 0.2835		**p = 0.1010**	
D	**Chick NT**					
	cC4orf32-Playrr		*cC4orf32-Pitx2*		*Playrr-Pitx2*	
	455 ± 5		294 ± 4		348 ± 5	
	n = 1047		n = 1277		n = 947	
E	**Mouse NT**					
	mC4orf32-Playrr		*mC4orf32-Pitx2*		*Playrr-Pitx2*	
	490 ± 9		397 ± 7		362 ± 7	
	n = 585		n = 660		n = 555	
F	**Mouse WT ESC**					
	mC4orf32-Playrr		*mC4orf32-Pitx2*		*Playrr-Pitx2*	
	546 ± 19		443 ± 17		412 ± 17	
	n = 164		n = 164		n = 148	
G	**Mouse ESC CTCF shRNA**					
	mC4orf32-Playrr		*mC4orf32-Pitx2*		*Playrr-Pitx2*	
	461 ± 41		607 ± 59		614 ± 76	
	n = 39		n = 29		n = 18	
	p = 0.0232		**p = 0.0159**		**p = 0.053**	

data indicate that whereas *Pitx2* is dispensable for the global architecture of the locus it is required for subtle asymmetries involving the position of individual loci with respect to the overall locus topology (Fig. 5F).

4.4.11 CTCF is essential for maintaining the global topology of the Pitx2 locus

CCCTC-binding factor, CTCF, is a sequence-specific architectural protein known to be involved in long-range loop formation and constitutive chromatin organization (Splinter et al. 2006; Phillips-Cremins et al. 2013). We hypothesized that CTCF is essential for maintaining the global topology of the *Pitx2* locus. Indeed, CTCF ChIP-seq data from mESCs identifies several significant CTCF binding peaks across the region spanned by *mC4orf32* and *Playrr* at the proximal end of the gene desert (Fig. 6B) (Kagey et al. 2010).

To directly test the role of CTCF in *Pitx2* locus organization, we used lentiviral shRNA to knockdown CTCF in mESCs (Fig. 6C). Compared to control ESCs, knockdown of CTCF abrogated long-range looping across the gene desert and disrupted chromatin organization of the locus (Fig. 6A, Table 1FG). These data demonstrate that CTCF mediated chromatin looping is essential for maintaining the invariant global topology of the *Pitx2* locus, a prerequisite for subsequent *Pitx2*-dependent regulatory interactions across the L-R axis.

4.5 Discussion

Spatiotemporal *Pitx2* expression controls transcriptional regulatory programs essential for normal development and the establishment of asymmetric organ morphology. In the DM, left-sided *Pitx2* regulates molecular and cellular asymmetry required to initiate intestinal looping and gut vasculogenesis (Davis et al. 2008; Kurpios et al. 2008; Welsh et al. 2013; Mahadevan et al. 2014). Remarkably, we show

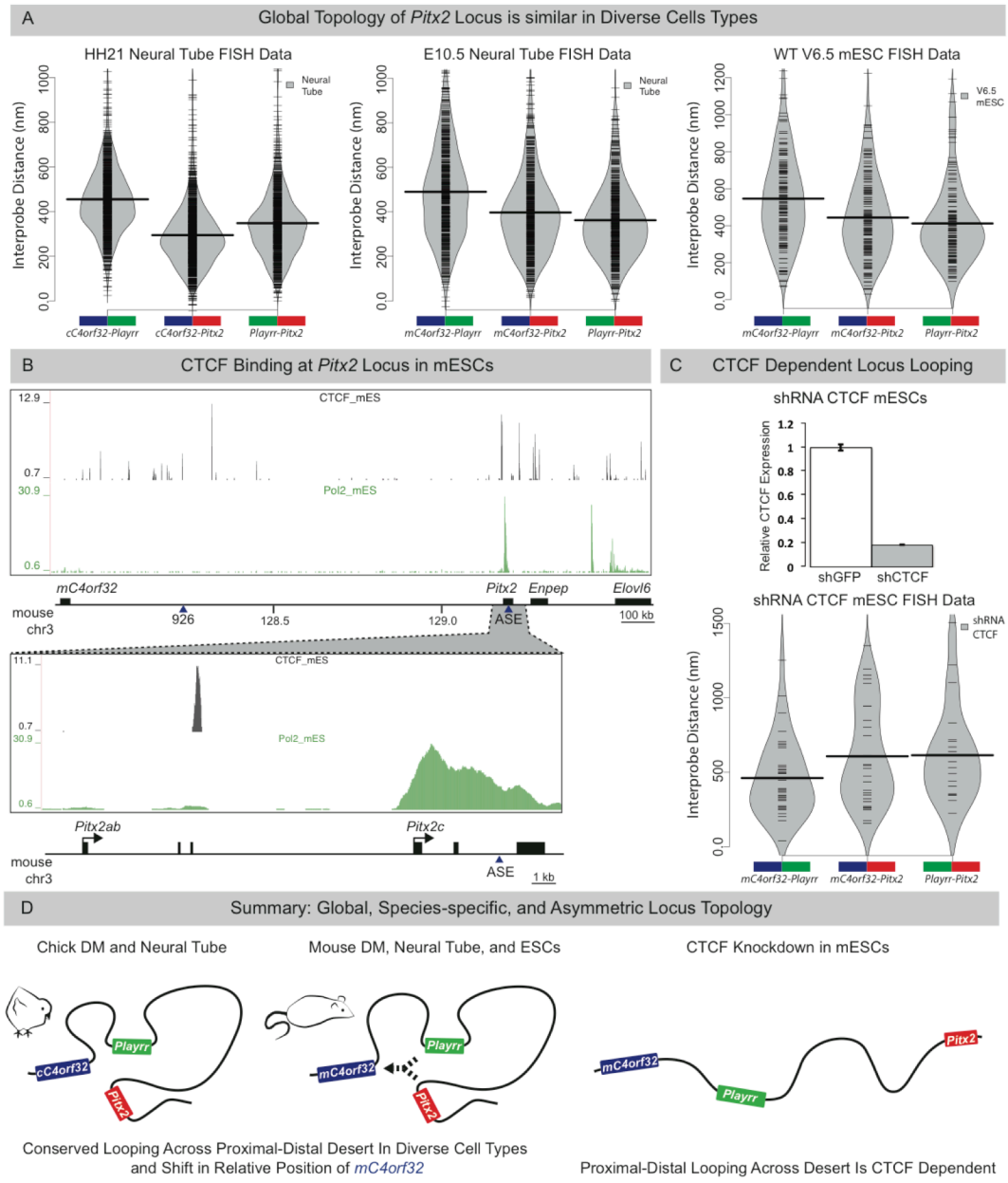

Figure 6. *Pitx2* locus topology is invariant across diverse cell types and is dependent on CTCF. (A) FISH analysis of locus topology in cells of chicken and mouse neural tube and mESCs. (B) CTCF ChIP-seq data from mESCs, shows several strong CTCF binding at the proximal desert and downstream of *Pitx2ab* specific exon while RNA Pol II ChIP-seq demonstrates mESCs express the asymmetric *Pitx2c* isoform. (C) shRNA mediated knockdown of CTCF in mESCs (top) abrogates long-range looping across the gene desert detected by FISH (bottom). (D) Summary of *Pitx2* locus topology across cell types in chicken and mouse and upon knockdown of CTCF (mESc).

here that the binary L-R organization of the DM at the tissue level is mirrored in the binary transcriptional output and chromatin level organization of the Pix2 locus in the left and right DM (Fig. 7).

Leveraging the organization of the DM, our 3D tissue FISH analysis characterizes how the large conserved chromosome interval harboring the *Pitx2* locus is organized within the 3D space of the nucleus in order to effect L-R patterning and asymmetric gene expression. The 3D topology of the *Pitx2* locus, as measured optically by a common set of 3 reference points, demonstrates both global and local scale organizational principles. We establish that in chicken and mouse tissue, long-range chromatin looping across a large gene desert is a constitutive feature of locus organization dependent on CTCF. Conversely, consistent with L-R differences in cis-regulatory interactions within this invariant 3D topology, we show that complementarily expressed genes are in closer proximity in the left DM where *Pitx2* is preferentially expressed but positioned further from *Pitx2* in the right DM where right-specific genes are expressed and *Pitx2* is not (Fig. 7). While L-R differences in locus topology, as measured by mean interprobe distance, are notably small, these differences are highly reproducible across biological replicates. Moreover, in the absence of *Pitx2,* mean *Playrr*-*Pitx2* interprobe distance in the left DM is similar to that in the right DM of both Pitx2-/- and WT mice, supporting that small L-R differences are *Pitx2*-dependent and hence biologically meaningful. Finally, our FISH analysis only marks the relative position of asymmetrically expressed genes in the left or right DM and it is likely that the subtle L-R proximity differences are actually secondary to interactions between promoters and sequences that we have not labeled.

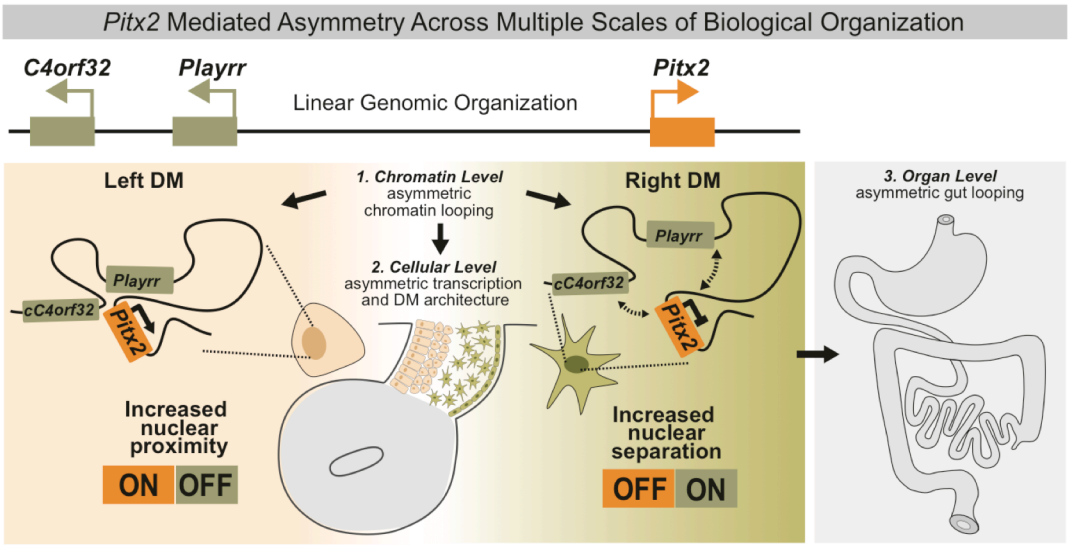

Figure 4.7. Summary Model: *Pitx2* mediated asymmetry across multiple scales of biological organization.

Alternative assays of chromatin topology, such as chromosome conformation capture (3C), although not always concordant with FISH data, may assist in identifying additional interactions across the locus that are the primary basis for L-R differences in *Pitx2* locus topology and will be integral to defining mechanisms that regulate L-R transcription (Williamson et al. 2014).

The preassembly of constitutive long range chromatin looping necessary for proper spatial expression has been documented at other critical developmental loci (Shopland et al. 2006; Montavon et al. 2011; Jin et al. 2013; de Laat and Duboule 2013). Such preassembly of permissive regulatory topologies has been suggested to poise cells for rapid changes in expression. For example, simple shifts in regulatory contacts, analogous to allosteric conformational changes that alter protein activity, may promote transcriptional activation via release of paused RNA Pol II (Liu et al.

2013; Ghavi-Helm et al. 2014; de Laat and Duboule 2013). This suggests that L-R differences in *Pitx2* vs. *Playrr* transcription may be achieved by regulating the position of their promoters and associated REs within nuclear foci containing RNA Pol II and tissue-specific co-factors that target release of paused RNA Pol II already assembled at their promoters (Razin et al. 2011; Schaukowitch et al. 2014). Implementation of such regulatory strategy, where 3D topology facilitates efficient RNA Pol II trafficking, may provide a mechanism for robust establishment of asymmetric expression in response to very transient Nodal signaling critical for *Pitx2* induction (Shiratori and Hamada 2006).

Supporting this hypothesis, our microarray and RNA in situ hybridization data demonstrate the exclusive expression of Mllt3 in the left DM, a transcriptional co-activator associated with rapid establishment of cell fate and lineage commitment (data not shown) (Flajollet et al. 2013; Pina et al. 2008). Significantly, Mllt3 directly interacts with and activates P-TEFb, a kinase targeting Ser2 in the C-terminal domain (CTD) of RNA Pol II, a critical step for release of paused RNA Pol II and transcriptional elongation (Shim et al. 2002; Biswas et al. 2011; Bitoun et al. 2007). Mllt3 also complexes with Dot1L, a developmentally essential histone methyltransferase that interacts with the phosphorylated CTD of RNA Pol II and is solely responsible for histone H3K79 methylation at active enhancers and transcribed genes. Interestingly, we observed H3K79 methylation flanking the ASE enhancer in mESCs expressing *Pitx2c* (Fig. S5) (Steger et al. 2008; Kim et al. 2012; Jones et al. 2008; Bonn et al. 2012) further supporting the involvement of Mllt3 at the *Pitx2* locus.

Invariance in the global organization of a locus across a range of cellular contexts is a defining characteristic of topologically associating domains (TADs), a feature of genomic structure that emerges at the megabase scale characterized by preferential association of long-range chromatin interactions (Phillips-Cremins et al. 2013; Nora et al. 2013). The structure of TADs correlate with blocks of genomic synteny and thus changes in their structure are likely evolutionarily constrained (Dixon et al. 2012; Nora et al. 2013). The boundaries of TADs are enriched for binding of CTCF (Dixon et al. 2012) and we show here that CTCF is required for maintenance of the megabase scale topology of the *Pitx2* locus in mESCs. High-resolution long-range chromatin interaction maps provided by HiC analysis of mESCs (Shen et al. 2012) support the presence of a TAD extending proximally from *Pitx2* across the gene desert that span the region that we have characterized via 3D FISH (Fig. S6A).

However, we observed changes in spatial gene expression between chicken and mouse consistent with significant differences in positioning of the proximal but not distal gene desert. Interestingly, in mESCs, binding of CTCF downstream of exon 3 of the bilaterally expressed *Pitx2a* isoform in the absence of Mediator, overlaps a conserved CTCF recognition sequence in chicken and suggests a conserved role in constitutive chromatin looping for CTCF binding this site (Fig. 6B, Fig. S5) (Phillips-Cremins et al. 2013). In contrast, CTCF binding proximally in the vicinity of *cC4orf32*/*mC4orf32* appears to lack conservation or are potentially divergent. Interestingly, although the gene desert is conserved in zebrafish, they lack an ortholog of *C4ORF32*, further supporting evolutionary divergence of the proximal gene desert

(Fig. S6B) (Volkmann et al. 2011). Finally, we also observe a loss of *Enpep* expression in the mouse DM in comparison to its right-sided expression in chicken. Consistent with this finding, the HiC interaction map of mESC shows a very distinct interaction boundary separating *Pitx2* from *Enpep*, suggesting these adjacent genes are partitioned into separate TADs (Fig. S6A). Thus, while the *Pitx2* locus in chicken and mouse exhibits conserved 3D chromatin architecture, species-specific differences in this architecture have consequences on spatial gene expression and may result from the acquisition or turnover of CTCF binding.

Characterization of distal regulatory elements in the genome and identification of their target promoters is requisite for advancing our understanding of genomic regulatory logic. This study demonstrates the utility of combining GRO-seq with dREG analysis in vivo to characterize nascent transcription and identifying the activity of REs within a single sample. An unanticipated finding from this approach was the identification of *Playrr* as a novel, asymmetrically expressed lncRNA derived from the conserved e926 sequence element. Rather than matching the left-specific enhancer activity of e926 observed in transgenic embryos, we show that *Playrr* is exclusively expressed in the right DM. Thus, mapping of active REs in situ via dREG analysis avoids potentially confounding data that may arise from testing putative cis-regulatory sequences in isolation of their endogenous context (Marinić et al. 2013).

A coherent understanding of the biological roles of lncRNAs is still lacking, although a role in transcriptional regulation is an emerging theme. Studies demonstrate that lncRNAs can function either locally at their site of transcription or at distal sites in either cis or trans in order to control gene expression (Rinn and Chang 2012; Vance

and Ponting 2014). Recent analysis of the trans-acting lncRNA Fendrr, which interacts with the polycomb repressive complex 2 (PRC2), establishes a role for lncRNAs in regulation of *Pitx2* developmental expression (Grote et al. 2013). Although the impact on L-R patterning was not addressed, mutation of Fendrr causes loss of *Pitx2* silencing and altered differentiation of the lateral mesoderm, resulting in an embryonic lethal phenotype consistent with *Pitx2* misexpression (Grote et al. 2013; Grote and Herrmann 2013). It is therefore interesting to speculate whether *Playrr* function provides a regulatory contribution to asymmetric expression of locus genes during development. The role of *Playrr* function during organogenesis is currently being addressed in our laboratory using CRISPR/Cas9 genome editing.

Pitx2 is expressed in dynamic spatial patterns essential for normal development and individual *Pitx2* isoforms play distinct dosage dependent roles in diverse tissues (Liu et al. 2001; Waite et al. 2013). Consistent with such pleiotropic function, mutations of human *PITX2* result in a spectrum of serious birth defects associated with Axenfeld-Rieger Syndrome and predispose otherwise healthy individuals to cardiac fibrillation and arrhythmia (Semina et al. 1996; Tao et al. 2014; Wang et al. 2014). Conservation of the expansive gene desert at the locus and the number of noncoding mutations identified in human ARS patients likely represent the considerable regulatory demand necessary to orchestrate complex *Pitx2* expression. Therefore, identification of mechanisms that direct precise spatiotemporal expression of *Pitx2* is as critical as defining its downstream regulatory targets. The binary L-R organization of the DM, accessible for both targeted and whole animal genetic manipulation, combined with the unique pattern of asymmetric gene expression

mirrored by L-R 3D chromatin organization of the *Pitx2* locus, represents a powerful experimental system to advance understanding of the integrated regulation and essential function of the evolutionarily conserved *Pitx2*. Furthermore, our work begins to shed light on the cis-regulatory mechanisms and etiology of ARS and offers unprecedented potential for developing mouse models of this important human disease.

4.6 Material and Methods

Animals

Mouse embryos were collected from timed matings with the morning of the plug defined as E0.5. *Pitx2* mutant mice, *Pitx2*^{hd} allele (Lu et al., 1999), were used for analyses. Fertile eggs (White Leghorn) obtained from the Cornell Poultry Research Farm were incubated at 38°C and staged (Hamburger and Hamilton, 1992). Experiments adhered to guidelines of the Institutional Animal Care and Use Committee of Cornell University, under the Animal Welfare Assurance on file with the Office of Laboratory Animal Welfare.

Histology

Embryos were dissected in PBS and fixed in 4% PFA/PBS or Bouin's fixative overnight, dehydrated in ethanol and embedded in paraffin, sections were collected on Superfrost Plus slides. 6mm paraffin sections were stained with Hematoxylin &Eosin and included a brief wash with 1% HCl/70% EtOH followed by NH_4OH.

RNA in situ hybridization

250mm thick embryo slices for whole mount RNA in situ hybridization (ISH) were collected with a McIlwain tissue chopper (Campden Instruments), fixed in 4% PFA/PBS ON, dehydrated, and stored in 100% methanol prior to processing. Whole mount ISH followed standard protocols as previously described (Welsh et al. 2013).

Statistical analysis

Measurement data were analyzed with R and Mann–Whitney–Wilcoxon test was used to compare interprobe distances in FISH experiments, and data was plotted with the beanplot package in R (Kampstra 2008). Box plots of FISH data in supplemental figure 4 were generated using JMP Pro 11.

L-R GRO-seq and dREG analysis

Whole embryos (n=250) were chopped into 250mm transverse slices using a McIlwain tissue chopper, followed by manual microdissection of the left and right DM. Collected tissues were pooled, snap frozen in liquid nitrogen and stored at -80°C until processing for GRO-seq as previously described (Core et al. 2008). We also performed GRO-seq on whole embryos (HH21, n=2), on embryonic heads (HH12, n=250) and on the left and right hemisected embryos (HH12, n=250), to monitor enrichment of asymmetric reads and further define the regulatory landscape of the *Pitx2* locus across several developmental contexts. dREG analysis of all GRO-seq data sets was implemented in R and is available via GitHub (https://github.com/Danko-Lab/dREG).

Cloning, plasmids, and oligonucleotides

Full-length cDNAs and probes for RNA ISH were cloned using TA cloning (Invitrogen) and oligo-dT primed cDNA reverse transcription (Superscript III, Invitrogen) from RNA pooled from HH19 and HH21 whole chicken, or from E8.5-18.5 whole mouse embryos. Cloned DNA was sequence-verified.

Quantitative reverse-transcriptase PCR (qRT-PCR)

Embryonic tissue was isolated in cold PBS, and stored in RNAlater until RNA was extracted with a Qiagen RNeasy miniprep kit. For cultured cells, RNA was extracted using 4-6 x 10^6 cells. 2mg of RNA was reverse transcribed using the ABI high-capacity cDNA archive kit and diluted to 20ng/ml. The CTCF (Mm00484027_m1) and GAPDH (Mm99999915_g1) TaqMan gene expression assays were used for relative quantification using an ABI7500 realtime PCR system using 20ng of template for each sample, GAPDH as the endogenous control.

3D DNA fluorescent in situ hybridization (FISH)

The following BACs spanning either the chicken or mouse *Pitx2* locus were used to generate FISH probes targeting *Pitx2* locus genes: chicken – CH261-95I8, CH261-66N5, CH261-187K8, CH261-34B16, CH261-110J5, CH261-91C24, CH261-134M23; mouse – RP23-306C6, RP23-328J13, RP23-225C17, RP24-98F15, RP23-266N9, RP23-106J9, RP23-150F9, RP24-156B21, RP24-100G2, RP23-307L21. Restriction enzyme digestion or PCR amplification using purified BAC DNA was

used to subclone 15-20kb DNA templates for FISH probe production. Probes were labeled with either dUTP-Cy3, -Cy5, or -DIG, via nick translation of 1mg of DNA (Roche).

3D FISH on embryonic tissue was previously described. Briefly, embryos were fixed overnight in 4% paraformaldehyde and embedded in paraffin following standard protocol. 6mm sections were collected on Suprerfrost plus slides, dried overnight at 37^{o}C, baked at 60^{o}C for 20 minutes, cooled, and then dewaxed in xylene with 2 washes for 10 minutes each, followed by 2 washes in 100% ethanol, and 1 wash in 70% ethanol, 5 minutes each. Sections were then treated for 5 minutes with 0.2N NaOH in 70% ethanol to remove RNAs, washed twice in 70% ethanol, rehydrated, and washed 10 minutes in 0.1M citrate buffer at 80^{o}C. Sections were washed in water, equilibrated in 2X SSC for 5 minutes, denatured for 2.5 minutes at 79^{o}C in 70% formamide/2X SSC. Sections were hybridized overnight 37^{o}C with 50ng of probe, 10mg species specific Cot-1 DNA, 10mg salmon sperm DNA, and 10mg tRNA. The following day sections were washed with 2X SSC/50% formamide at 37^{o}C, 2X SSC 37^{o}C, 1X SSC at room temperature, for 15 minutes each. DIG labeled probes were detected with AF488 anti-DIG conjugated antibodies diluted 1:500 in 4X SSC/1% BSA.

For FISH on cultured V6.4 mouse ESCs cells were seeded onto coverslips, fixed in 4% paraformaldehyde, then permeabilized following published protocols (Kurz et al., 1996). Hybridization followed the same protocol with the exception that the citrate unmasking step was omitted.

Image acquisition and analysis for 3D FISH

Slides were imaged on a Zeiss 710 scanning laser microscope using a 63X/1.4 NA Plan-APOCHROMAT oil immersion objective and Z-series data were acquired using the optimal step size. Imaris image analysis software (Bitplane) was used to quantify interprobe distances. Following thresholding, FISH signals were identified and defined as spot objects and measurements between the center of mass for each signal was determined.

Lentiviral production and transduction

293FT cells were transfected with pLKO.1 lentiviral plasmids containing either shRNAs targeting CTCF or GFP (control), along with the packaging plasmids pLP1, pLP2, and pLP/VSV-g, using Lipofectamine 2000. The following day, media was replaced with ES media minus LIF and cells were incubated overnight. Viral media was collected and centrifuged at 3000 rpm to pellet debris and then filtered through a 0.45mm PVFD filter and frozen until use. Virus containing media was supplemented with additional FBS, LIF, and 6mg/ml polybrene, prior to use.

WT V6.4 ES cells, expanded on gamma irradiated feeder cells, were trypsinized, plated for 30 minutes onto gelatin-free tissue culture plates to remove feeders prior to transduction. Following seeding ES cells at 2 x 10^6 cells/100mm plate and incubation for 24 hours, media was exchanged with ES media supplemented with 6mg/ml polybrene and plates were incubated for an additional15 minutes at 37^{o}C prior to exchanging media with virus containing ES media. After transduction, media was exchanged for normal ES cell media and cells were incubated for an additional 24

hours prior to selection with 2mg/ml puromycin. After 3 days of selection, surviving ES cells were trypsinized and plated for FISH or collected for RNA.

4.7 Acknowledgements

We thank Dr. Len Pennacchio and the VISTA enhancer browser (http://enhancer.lbl.gov) for providing archived transgene positive whole embryos for further histological analysis, Dr. Stephen Dalton for generously sharing shRNA lentiviral constructs, David Gludish for technical advice regarding shRNA experiments, and Dr. John Schimenti for helpful discussions and stocks of V6.5 ES cells. Jason Crossley, Michelle Miller, and Sriharsha Ponna provided technical assistance. We also thank Cornell University Biotechnology Resource Center (BRC) Imaging Facility (NIH 1S10RR025502-01) and Carol Bayles for assistance with confocal microscopy.

REFERENCES

Anderson E, Devenney PS, Hill RE, Lettice LA. 2014. Mapping the Shh long-range regulatory domain. *Development*. **141**(20):3934-3943.

Attanasio C, Nord AS, Zhu Y, Blow MJ, Li Z, Liberton DK, Morrison H, Plajzer-Frick I, Holt A, Hosseini R, et al. 2013. Fine tuning of craniofacial morphology by distant-acting enhancers. *Science* **342**: (6157):1241006.

Biswas D, Milne TA, Basrur V, Kim J, Elenitoba-Johnson KSJ, Allis CD, Roeder RG. 2011. Function of leukemogenic mixed lineage leukemia 1 (MLL) fusion proteins through distinct partner protein complexes. *Proc Natl Acad Sci* **108**: 15751–15756.

Bitoun E, Oliver PL, Davies KE. 2007. The mixed-lineage leukemia fusion partner AF4 stimulates RNA polymerase II transcriptional elongation and mediates coordinated chromatin remodeling. *Hum Mol Genet* **16**: 92–106.

Bonn S, Zinzen RP, Girardot C, Gustafson EH, Perez-Gonzalez A, Delhomme N, Ghavi-Helm Y, Wilczyński B, Riddell A, Furlong EEM. 2012. Tissue-specific analysis of chromatin state identifies temporal signatures of enhancer activity during embryonic development. *Nat Genet* **44**: 148–156.

Cajiao I, Zhang A, Yoo EJ, Cooke NE, Liebhaber SA. 2004. Bystander gene activation by a locus control region. *EMBO J* **23**: 3854–3863.

Core LJ, Martins AL, Danko CG, Waters CT, Siepel A, Lis JT. 2014. Analysis of nascent RNA identifies a unified architecture of initiation regions at mammalian promoters and enhancers. *Nat Genet* **46**: 1311–1320.

Core LJ, Waterfall JJ, Lis JT. 2008. Nascent RNA sequencing reveals widespread pausing and divergent initiation at human promoters. *Science* **322**: 1845–1848.

Creyghton MP, Cheng AW, Welstead GG, Kooistra T, Carey BW, Steine EJ, Hanna J, Lodato MA, Frampton GM, Sharp PA, et al. 2010. Histone H3K27ac separates active

from poised enhancers and predicts developmental state. *Proc Natl Acad Sci U S A* **107**: 21931–21936.

Danko CG, Hyland SL, Core LJ, Martins AL, Waters CT, Lee HW, Cheung VG, Kraus WL, Lis JT, Siepel A. 2015. Identification of active transcriptional regulatory elements from GRO-seq data. *Nat Meth* **12**: 433–438. http://dx.doi.org/10.1038/nmeth.3329.

Davis NM, Kurpios NA, Sun X, Gros J, Martin JF, Tabin CJ. 2008. The Chirality of Gut Rotation Derives from Left-Right Asymmetric Changes in the Architecture of the Dorsal Mesentery. *Dev Cell* **15**: 134–145.

De Laat W, Duboule D. 2013. Topology of mammalian developmental enhancers and their regulatory landscapes. *Nature* **502**: 499–506.

Dixon JR, Selvaraj S, Yue F, Kim A, Li Y, Shen Y, Hu M, Liu JS, Ren B. 2012. Topological domains in mammalian genomes identified by analysis of chromatin interactions. *Nature* **485**: 376–380.

Drissen R, Palstra R-J, Gillemans N, Splinter E, Grosveld F, Philipsen S, de Laat W. 2004. The active spatial organization of the beta-globin locus requires the transcription factor EKLF. *Genes Dev* **18**: 2485–2490.

Duboc V, Röttinger E, Lapraz F, Besnardeau L, Lepage T. 2005. Left-right asymmetry in the sea urchin embryo is regulated by nodal signaling on the right side. *Dev Cell* **9**: 147–158.

Flajollet S, Rachez C, Ploton M, Schulz C, Gallais R, Métivier R, Pawlak M, Leray A, Issulahi AA, Héliot L, et al. 2013. The Elongation Complex Components BRD4 and MLLT3/AF9 Are Transcriptional Coactivators of Nuclear Retinoid Receptors. *PLoS One* **8**(6):e64880.

Flomen RH, Vatcheva R, Gorman PA, Baptista PR, Groet J, Barišić I, Ligutic I, Nižetić D. 1998. Construction and Analysis of a Sequence-Ready Map in 4q25: Rieger Syndrome Can Be Caused by Haploinsufficiency ofRIEG, but Also by Chromosome Breaks ≈90 kb Upstream of This Gene. *Genomics* **47**: 409–413.

Franco D, Campione M. 2003. The role of Pitx2 during cardiac development: Linking left-right signaling and congenital heart diseases. *Trends Cardiovasc Med* **13**: 157–163.

Ghavi-Helm Y, Klein FA, Pakozdi T, Ciglar L, Noordermeer D, Huber W, Furlong EEM. 2014. Enhancer loops appear stable during development and are associated with paused polymerase. *Nature*. **512**(7512):96-100.

Grote P, Herrmann BG. 2013. The long non-coding RNA Fendrr links epigenetic control mechanisms to gene regulatory networks in mammalian embryogenesis. *RNA Biol* **10**: 1579–1585.

Grote P, Wittler L, Hendrix D, Koch F, Währisch S, Beisaw A, Macura K, Bläss G, Kellis M, Werber M, et al. 2013. The Tissue-Specific lncRNA Fendrr Is an Essential Regulator of Heart and Body Wall Development in the Mouse. *Dev Cell* **24**: 206–214.
Hamburger V, Hamilton HL. 1951. A series of normal stages in the development of the chick embryo. *J Morphol* **88**: 49–92.

Jin F, Li Y, Dixon JR, Selvaraj S, Ye Z, Lee AY, Yen C-A, Schmitt AD, Espinoza C a, Ren B. 2013. A high-resolution map of the three-dimensional chromatin interactome in human cells. *Nature* **503**: 290–294.

Jones B, Su H, Bhat A, Lei H, Bajko J, Hevi S, Baltus GA, Kadam S, Zhai H, Valdez R, et al. 2008. The histone H3K79 methyltransferase Dot1L is essential for mammalian development and heterochromatin structure. *PLoS Genet* **4**(9):e1000190.

Kagey MH, Newman JJ, Bilodeau S, Zhan Y, Orlando DA, van Berkum NL, Ebmeier CC, Goossens J, Rahl PB, Levine SS, et al. 2010. Mediator and cohesin connect gene expression and chromatin architecture. *Nature* **467**: 430–435.

Kampstra P. 2008. Beanplot : A Boxplot Alternative for Visual Comparison of Distributions. *J Stat Softw* **28**: 1–9.

Kikuta H, Laplante M, Navratilova P, Komisarczuk AZ, Engström PG, Fredman D, Akalin A, Caccamo M, Sealy I, Howe K, et al. 2007. Genomic regulatory blocks

encompass multiple neighboring genes and maintain conserved synteny in vertebrates. *Genome Res* **17**: 545–555.

Kim SK, Jung I, Lee H, Kang K, Kim M, Jeong K, Kwon CS, Han YM, Kim YS, Kim D, et al. 2012. Human histone H3K79 methyltransferase DOT1L methyltransferase binds actively transcribing RNA polymerase II to regulate gene expression. *J Biol Chem* **287**: 39698–39709.

Kurpios NA, Ibañes M, Davis NM, Lui W, Katz T, Martin JF, Belmonte JCI, Tabin CJ. 2008. The direction of gut looping is established by changes in the extracellular matrix and in cell:cell adhesion. *Proc Natl Acad Sci* **105** : 8499–8506.

Lettice LA, Horikoshi T, Heaney SJH, van Baren MJ, van der Linde HC, Breedveld GJ, Joosse M, Akarsu N, Oostra BA, Endo N, et al. 2002. Disruption of a long-range cis-acting regulator for Shh causes preaxial polydactyly. *Proc Natl Acad Sci U S A* **99**: 7548–7553.

Liu C, Liu W, Lu MF, Brown NA, Martin JF. 2001. Regulation of left-right asymmetry by thresholds of Pitx2c activity. *Development* **128**: 2039–2048.

Liu W, Ma Q, Wong K, Li W, Ohgi K, Zhang J, Aggarwal AK, Rosenfeld MG. 2013. Brd4 and JMJD6-associated anti-pause enhancers in regulation of transcriptional pause release. *Cell* **155**: 1581–1595.

Logan M, Pagán-Westphal SM, Smith DM, Paganessi L, Tabin CJ. 1998. The transcription factor pitx2 mediates situs-specific morphogenesis in response to left-right asymmetric signals. *Cell* **94**: 307–317.

Lu MF, Pressman C, Dyer R, Johnson RL, Martin JF. 1999. Function of Rieger syndrome gene in left-right asymmetry and craniofacial development. *Nature* **401**: 276–278.

Mahadevan A, Welsh ICC, Sivakumar A, Gludish DWW, Shilvock ARR, Noden DMM, Huss D, Lansford R, Kurpios NAA. 2014. The Left-Right Pitx2 Pathway Drives Organ-Specific Arterial and Lymphatic Development in the Intestine. *Dev Cell* **31**: 690–706.

Marinić M, Aktas T, Ruf S, Spitz F. 2013. An Integrated Holo-Enhancer Unit Defines Tissue and Gene Specificity of the Fgf8 Regulatory Landscape. *Dev Cell* **24**: 530–542.

Melgar MF, Collins FS, Sethupathy P. 2011. Discovery of active enhancers through bidirectional expression of short transcripts. *Genome Biol* **12**:(11):R113.

Montavon T, Soshnikova N, Mascrez B, Joye E, Thevenet L, Splinter E, De Laat W, Spitz F, Duboule D. 2011. A regulatory archipelago controls hox genes transcription in digits. *Cell* **147**: 1132–1145.

Nobrega MA, Ovcharenko I, Afzal V, Rubin EM. 2003. Scanning Human Gene Deserts for Long-Range Enhancers. *Sci* **302** : (5644):413.

Nora EP, Dekker J, Heard E. 2013. Segmental folding of chromosomes: A basis for structural and regulatory chromosomal neighborhoods? *BioEssays* **35**: 818–828.

Phillips-Cremins JE, Sauria MEG, Sanyal A, Gerasimova TI, Lajoie BR, Bell JSK, Ong CT, Hookway TA, Guo C, Sun Y, et al. 2013. Architectural protein subclasses shape 3D organization of genomes during lineage commitment. *Cell* **153**: 1281–1295.

Pina C, May G, Soneji S, Hong D, Enver T. 2008. MLLT3 Regulates Early Human Erythroid and Megakaryocytic Cell Fate. *Cell Stem Cell* **2**: 264–273.

Rainger JK, Bhatia S, Bengani H, Gautier P, Rainger J, Pearson M, Ansari M, Crow J, Mehendale F, Palinkasova B, et al. 2014. Disruption of SATB2 or its long-range cis-regulation by SOX9 causes a syndromic form of Pierre Robin sequence. *Hum Mol Genet* **23**(10):2569-2579.

Razin S V., Gavrilov AA, Pichugin A, Lipinski M, Iarovaia O V., Vassetzky YS. 2011. Transcription factories in the context of the nuclear and genome organization. *Nucleic Acids Res* **39**: 9085–9092.

Reis LM, Tyler RC, Volkmann Kloss BA, Schilter KF, Levin A V, Lowry RB, Zwijnenburg PJG, Stroh E, Broeckel U, Murray JC, et al. 2012. PITX2 and FOXC1 spectrum of mutations in ocular syndromes. *Eur J Hum Genet*. **20**(12): 1224-1233.

Rinn JL, Chang HY. 2012. Genome Regulation by Long Noncoding RNAs. *Annu Rev Biochem* **81**: 145–166.

Ryan AK, Blumberg B, Rodriguez-Esteban C, Yonei-Tamura S, Tamura K, Tsukui T, de la Peña J, Sabbagh W, Greenwald J, Choe S, et al. 1998. Pitx2 determines left-right asymmetry of internal organs in vertebrates. *Nature* **394**: 545–551.

Schaukowitch K, Joo J-Y, Liu X, Watts JK, Martinez C, Kim T-K. 2014. Enhancer RNA Facilitates NELF Release from Immediate Early Genes. *Mol Cell* **56**: 29–42.

Semina E V, Reiter R, Leysens NJ, Alward WL, Small KW, Datson NA, Siegel-Bartelt J, Bierke-Nelson D, Bitoun P, Zabel BU, et al. 1996. Cloning and characterization of a novel bicoid-related homeobox transcription factor gene, RIEG, involved in Rieger syndrome. *Nat Genet* **14**: 392–399.

Shen Y, Yue F, McCleary DF, Ye Z, Edsall L, Kuan S, Wagner U, Dixon J, Lee L, Lobanenkov V V., et al. 2012. A map of the cis-regulatory sequences in the mouse genome. *Nature* **488**: 116–120.

Shim EY, Walker AK, Shi Y, Blackwell TK. 2002. CDK-9/cyclin T (P-TEFb) is required in two postinitiation pathways for transcription in the C. elegans embryo. *Genes Dev* **16**: 2135–2146.

Shiratori H, Hamada H. 2006. The left-right axis in the mouse: from origin to morphology. *Development* **133**: 2095–2104.

Shiratori H, Sakuma R, Watanabe M, Hashiguchi H, Mochida K, Sakai Y, Nishino J, Saijoh Y, Whitman M, Hamada H. 2001. Two-step regulation of left-right asymmetric expression of Pitx2: Initiation by nodal signaling and maintenance by Nkx2. *Mol Cell* **7**: 137–149.

Shiratori H, Yashiro K, Shen MM, Hamada H. 2006. Conserved regulation and role of Pitx2 in situs-specific morphogenesis of visceral organs. *Development* **133**: 3015–3025.

Shopland LS, Lynch CR, Peterson KA, Thornton K, Kepper N, Von Hase J, Stein S, Vincent S, Molloy KR, Kreth G, et al. 2006. Folding and organization of a contiguous chromosome region according to the gene distribution pattern in primary genomic sequence. *J Cell Biol* **174**: 27–38.

Spitz F, Gonzalez F, Duboule D. 2003. A global control region defines a chromosomal regulatory landscape containing the HoxD cluster. *Cell* **113**: 405–417.

Splinter E, Heath H, Kooren J, Palstra RJ, Klous P, Grosveld F, Galjart N, De Laat W. 2006. CTCF mediates long-range chromatin looping and local histone modification in the ??-globin locus. *Genes Dev* **20**: 2349–2354.

Steger DJ, Lefterova MI, Ying L, Stonestrom AJ, Schupp M, Zhuo D, Vakoc AL, Kim J-E, Chen J, Lazar MA, et al. 2008. DOT1L/KMT4 recruitment and H3K79 methylation are ubiquitously coupled with gene transcription in mammalian cells. *Mol Cell Biol* **28**: 2825–2839.

Sutherland H, Bickmore WA. 2009. Transcription factories: gene expression in unions? *Nat Rev Genet* **10**: 457–466.

Tao Y, Zhang M, Li L, Bai Y, Zhou Y, Moon AM, Kaminski HJ, Martin JF. 2014. Pitx2, an atrial fibrillation predisposition gene, directly regulates ion transport and intercalated disc genes. *Circ Cardiovasc Genet* **7**: 23–32.

Van de Werken HJG, Landan G, Holwerda SJB, Hoichman M, Klous P, Chachik R, Splinter E, Valdes-Quezada C, Öz Y, Bouwman BAM, et al. 2012. Robust 4C-seq data analysis to screen for regulatory DNA interactions. *Nat Methods* **9**: 969–972.

Vance KW, Ponting CP. 2014. Transcriptional regulatory functions of nuclear long noncoding RNAs. *Trends Genet* **30**: 348–355.

Visel A, Minovitsky S, Dubchak I, Pennacchio LA. 2007. VISTA Enhancer Browser - A database of tissue-specific human enhancers. *Nucleic Acids Res* **35** (Database issue):D88-92.

Volkmann BA, Zinkevich NS, Mustonen A, Schilter KF, Bosenko D V., Reis LM, Broeckel U, Link BA, Semina E V. 2011. Potential novel mechanism for Axenfeld-Rieger syndrome: Deletion of a distant region containing regulatory elements of PITX2. *Investig Ophthalmol Vis Sci* **52**: 1450–1459.

Waite MR, Skidmore JM, Micucci JA, Shiratori H, Hamada H, Martin JF, Martin DM. 2013. Pleiotropic and isoform-specific functions for Pitx2 in superior colliculus and hypothalamic neuronal development. *Mol Cell Neurosci* **52**: 128–139.

Wang J, Bai Y, Li N, Ye W, Zhang M, Greene SB, Tao Y, Chen Y, Wehrens XHT, Martin JF. 2014. Pitx2-microRNA pathway that delimits sinoatrial node development and inhibits predisposition to atrial fibrillation. *Proc Natl Acad Sci U S A* **111**: 9181–9186.

Watanabe H, Schmidt HA, Kuhn A, Hoger SK, Kocagoz Y, Laumann-Lipp N, Ozbek S, Holstein TW. 2014. Nodal signalling determines biradial asymmetry in Hydra. *Nature* **515** (7525):112-115

Welsh IC, Thomsen M, Gludish DW, Alfonso-Parra C, Bai Y, Martin JF, Kurpios N a. 2013. Integration of left-right Pitx2 transcription and Wnt signaling drives asymmetric gut morphogenesis via Daam2. *Dev Cell* **26**: 629–644.

Williamson I, Berlivet S, Eskeland R, Boyle S, Illingworth RS, Paquette D, Dostie J, Bickmore WA. 2014. Spatial genome organization: contrasting views from chromosome conformation capture and fluorescence in situ hybridization. *Genes Dev* **28** : 2778–2791.

Zorn AM, Wells JM. 2009. Vertebrate endoderm development and organ formation. *Annu Rev Cell Dev Biol* **25**: 221–251.

Zuniga A, Michos O, Spitz F, Haramis A-PG, Panman L, Galli A, Vintersten K, Klasen C, Mansfield W, Kuc S, et al. 2004. Mouse limb deformity mutations disrupt a global control region within the large regulatory landscape required for Gremlin expression. *Genes Dev* **18**: 1553–1564.

CHAPTER 5

SUMMARY AND FUTURE PERSPECTIVES

5.1 SUMMARY

Genetic information is the code script for life, and over evolutionary time scales, this code script has been expanded upon, edited, and permuted as a means to identify adaptive novelty, exploit niche resources, and ultimately ramify the complexity of life produced via that code script's potential. For example, the transition from unicellular to multicellular life represents a significant advance in the cellular specialization, biological complexity, and adaptive potential achievable from the manifestation of a single genome. Developmental genomics seeks to understand how genetic (and epigenetic) information is accessed and deployed in an integrated manner to robustly regulate the temporally ordered specification, differentiation, and spatial organization of cells and tissues necessary to generate functional organs and species-specific morphology. Morphogenesis arguably represents the most critical and dynamic utilization of genomic information in the life history of an organism and thus a powerful system for advancing our understanding of genomic regulation and function. A key challenge in pursuit of this goal is establishing *in vivo* models to provide a cellular context where the causal relationships between the expression of key morphoregulatory genes and the downstream transcriptional targets and morphogenic cellular behaviors that they control are easily determined, quantifiable, and amenable to experimental manipulation.

The preceding chapters represent efforts to establish GRN models involved in key aspects of embryonic development, namely craniofacial and asymmetric organ morphogenesis. Although these GRNs are provisional, in that the network

connectivity between genes has not been made explicit and fully validated at the level of cis-regulatory sequence, they do represent a first critical step. The process of producing a fully validated GRN is not trivial and requires considerable time and effort on the part of multiple labs with varying expertise. The nascent GRN models presented here provide key resources for both hypothesis generation and curation of data as it becomes available (for example Tao et al. 2014). The following sections summarize some key findings and identify avenues for further research.

5.2 The Rugae Growth Zone and the Complexity of Craniofacial Development

Formation of the vertebrate face is a critical and notably complex process requiring the coordinated outgrowth and fusion of multiple paired prominences. Accordingly, clefting of the lip and palate are among the most common human birth defects. Defects may be isolated or part of a number of syndromes involving the malformation of multiple structures (Jugessur and Murray 2005) underscoring that common developmental pathways and components are utilized repeatedly throughout morphogenesis. How morphogenetic domains are integrated to coordinate craniofacial development is an important question, and while a number of genes and pathways important for palate development have been identified, an understanding of how these signals are organized and integrated to achieve precise control of craniofacial development has been lacking.

The identification of the previously unappreciated the rugae growth zone (RGZ) provides a novel and much needed reference frame from which to study the integrated activity and spatial organization of genes controlling palate development.

Such insight is required to significantly advance our understanding of the etiology of an important class of birth defects, clefting of the lip and palate. Prior to publication of this work, the bulk of gene expression analysis to investigate palate development was performed on frontal sections of the developing palate, which increased the challenge of fully appreciating the pattern of gene activity related to 3 dimensional growth of the palatal shelves. Indeed expression of Shh was initially reported in the palatal rugae a decade earlier (Bitgood and McMahon 1995). However, the dynamic spatiotemporal pattern of this expression was not appreciated until analyzed via whole mount in situ hybridization was employed (Welsh et al. 2007). The localized production of Shh expressing epithelial stripes within the RGZ and subsequent rostral displacement provides anatomically referenced landmarks for appreciating regionalized patterns of directional growth that would not otherwise be apparent. Moreover, the sequential formation of these landmarks provides a means to more accurately compare the temporal stage of palate samples and interpret altered spatial expression patterns resulting from genetic and experimental perturbations.

An additional significant finding has been the identification that segmental organization for gene expression along the anterior-posterior axis of the palatal shelves is not limited to the expression of Shh. Strikingly, many genes exhibit one of two complementary segmented expression patterns along the length of the developing palate. These genes are either expressed in thin stripes representing the palatal rugae or in broader bands that correspond to domains between the rugae. The localized expression of several developmentally important signaling genes and transcription factors in addition to *Shh* (e.g. *Fgf9*, and *Bmp4*) to the regions of thickened epithelium

that constitute the rugae suggested that the periodic formation and modular organization of rugae signaling domains provides a distributed system of common instructional cues that maintain growth of the secondary palate in proper registration with the surrounding elements of the upper jaw. In light of this hypothesis it is notable that species-specific variation in rugae number range from 3-4 in human, 8 in mouse, and 18 in the horse, and that this variation correlates with striking differences in the rostral extension of the face and the underlying skeletal elements (Fig. X). The data presented in this work provides testable hypotheses regarding the mechanisms that allow for evolutionary variation in facial form while maintaining overall coordination of craniofacial development.

Following the publication of Welsh and O'Brien 2009, further genetic analysis and computational modeling by other researchers have leveraged the RGZ model to established clear experimental evidence for a reaction-diffusion type mechanism at play in the establishment of the striped organization of Shh expression in the palate (Economou et al. 2012). Such a patterning mechanism was initially proposed in the 1950s by Alan Turing, however few bona fide examples and genetically tractable models have since been established (Turing 1952; Green and Sharpe 2015). Thus the RGZ provides a rigorously

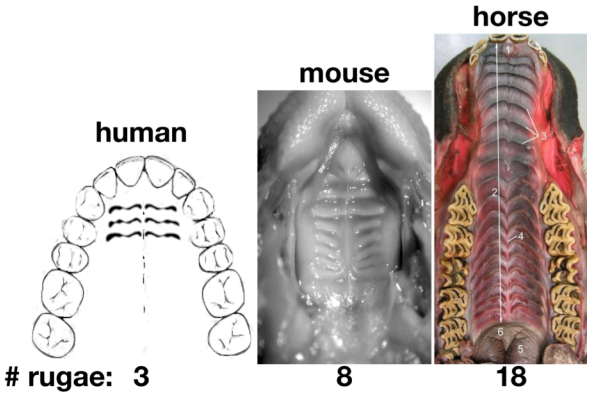

Fig. 5.1. Species-specific differences in rugae number and the extent of rostral outgrowth of the palate.

established example of one of the foundational concepts in modern developmental biology.

5.3 Tissue level integration of left-right patterning and intercellular signaling to direct asymmetric intestinal morphogenesis

The dorsal mesentery (DM), which suspends the gut tube from the dorsal body wall, is critical for establishing normal left-right asymmetry of the elongating gastrointestinal (GI) tract (Davis et al. 2008; Kurpios et al. 2008). Failure to achieve proper intestinal chirality can have serious consequences for neonatal health, including midgut volvulus (Applegate et al. 1999; Applegate 2009). Left-right differences in cell shape and behavior within the DM are downstream of the left-specific transcription factor *Pitx2* and play a central role in the transfer of asymmetric patterning information from the lateral plate mesoderm (LPM) to the developing gut tube. In the Kurpios lab I have leveraged a laser capture microdissection (LCM) and microarray screen comprehensively cataloging the molecular signatures defining each mesenteric compartment, as a means to address how *Pitx2* patterning is physically translated into the asymmetric cellular architecture of the DM (Welsh et al. 2013).

This work represents a considerable advance in efforts to identify the transcriptional targets of *Pitx2* and cellular mechanisms that contribute to asymmetric organ growth. The central finding of this work was the identification of both extra- and intracellular components of the noncanonical WNT5A signaling as downstream targets of *Pitx2* as a means to stabilize cell-cell adhesion and effect mesenchymal condensation observed in the left DM. Key genes within the DM network that this

work has assembled are each associated with gut malrotation when mutated in human (Pilia et al. 1996; Lu et al. 1999). The resulting model highlights regulation of asymmetric intercellular signaling potential as a conserved mechanism through with Pitx2 manifests differential cellular behavior to achieve asymmetric organ growth. Interestingly, recent work from the Kurpios lab suggests such intersection of Pitx2 L-R patterning with intercellular signaling pathways may be a common theme of Pitx2 regulation (Mahadevan et al. 2014). Therefore, continued analysis of this DM network will provide a mechanistic model for the control of cell shape changes underlying asymmetric organ development in higher vertebrates as well as make more genetically tractable an important class of birth defects.

The noncanonical ligand *Wnt5a* is critically required for intestinal morphogenesis but is not expressed within the DM (Cervantes et al. 2009). However, its expression in the adjacent gut mesenchyme does provide a source of directional signaling potential that could allow cells in the DM to orient condensation. Thus an outstanding question regarding our model of *Pitx2* and *Wnt5a* regulation of cellular dynamics in the DM, is what mechanisms provide for transfer of WNT5A from the gut mesenchyme? Extracellularly, noncanonical WNT signaling is positively regulated by *Glypican 3* (*Gpc3*), a heparin sulfate proteoglycan (HSPG) that stabilizes receptor-ligand interactions (Filmus et al. 2008; Song and Filmus 2002) and mutation of human *GPC3* can cause gut malrotation (Pilia et al. 1996; Neri et al. 1998).

The availability of WNT in the extracellular space can be dynamically regulated by the balance of: 1) preferential ligand binding to HS chains on HSPGs which can sequester WNT proteins to increase local concentration (O'Connell et al. 2009; Häcker et al. 2005) and 2) enzymatic activity of HS-specific 6-O sulfatases such as *Sulf1* that diminish WNT affinity for HS and release Glypican bound ligands to activate WNT signaling (Ai et al. 2003; Dhoot et al. 2001). Additionally, genes involved in posttranslational processing of *Gpc3*, such as *Pcsk5* and *Notum*, are required for *Gpc3* function or release from the cell surface to modulate WNT gradients in a tissue (Giráldez et al. 2002; Traister et al. 2008, and collaboration in progress with the Seidah lab). Importantly, in addition to *Gpc3*, the expression of *Hs6t1*, *Sulf1*, *Notum*, and *Pcsk5* also exhibit dynamic left specific expression in the DM and are downstream targets of Pitx2 (unpublished). Therefore, modulation of *Gpc3* and its 6-O sulfation status in the ECM is likely to be an important determinant of WNT signaling dynamics in the DM regulated by Pitx2 (Fig.X).

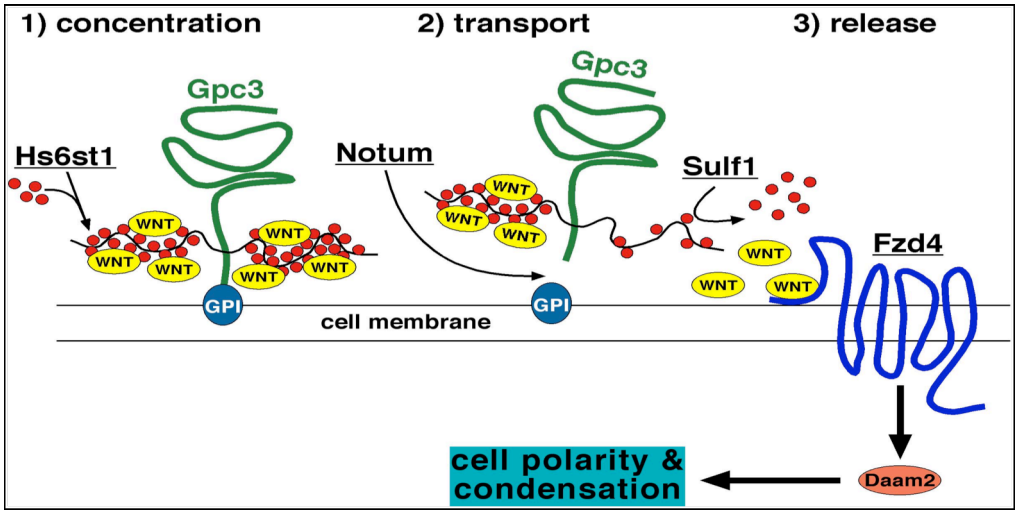

Fig.5.2: Regulation of WNT signaling through Gpc3 processing. 1) The 6-O sulfation (red circles) of *Gpc3* by *Hs6st1* generates high affinity interaction with WNTs to increase local concentration. 2) cleavage of the GPI anchor by *Notum* can facilitate transport of *Gpc3* bound WNTs. 3) Removal of sulfate from *Gpc3* can release WNTs to activate local signaling levels.

5.4 Chromatin structure and directing asymmetric gene expression

Asymmetric *Pitx2* expression is initially induced via very transient asymmetric expression and signaling of the Tgf-β signaling gene *Nodal* and the persistent *Pitx2* expression until the onset of organogenesis serves as the molecular and genetic memory of this early step in patterning the left-right axis (Shiratori and Hamada 2006). In addition to asymmetric expression, vertebrate *Pitx2* encodes multiple isoforms whose expression plays non-redundant dosage dependent roles during development, indicating the need for complex cis-regulatory inputs (Skidmore et al. 2008; Waite et al. 2013). Finally, mutation of human *PITX2* results in Axenfeld-Rieger Syndrome (ARS) and patients with ARS have been identified with no coding mutations but who carry deletion or translocation breakpoints in adjacent noncoding sequence (Volkmann et al. 2011). Therefore, equally important as identifying the transcriptional targets of *Pitx2*, is defining the mechanisms that provide for precise and robust asymmetric expression of *Pitx2* itself.

Stemming from the unexpected finding that genes physically linked to *Pitx2* in chicken and mouse exhibit right-specific expression in domains complementary to left-specific *Pitx2*, work presented in chapter 4 represents the first analysis of long-range chromatin organization in relation to asymmetric gene expression. A defining feature of the *Pitx2* locus is the presence of an evolutionarily conserved gene desert, flanked proximally by the uncharacterized human gene *C4orf32* (orthologous to *5730508B09Rik* or *Loc422694* in mouse or chicken, respectively) and *Pitx2* distally. In chick, the complementary right-sided expression of genes at the locus included

Loc422694 at the proximal end of the desert, Enpep the distal neighbor of *Pitx2*, and *Elovl6* located adjacent to *Enpep*. Analysis of nascent transcription in the chicken DM via GRO-seq also led to the identification of a long noncoding RNA (lncRNA) we have named *Playrr* (Pitx2 locus asymmetric regulated RNA) located just distal to *Loc422694*. Interestingly, in mouse the phenomenon of complementary right-sided expression was limited to the lncRNA *Playrr*. Significantly, loss of normal left-right patterning due to *Pitx2* mutation resulted in bilateral *Playrr* expression in the DM, indicating negative feedback by *Pitx2* on right sided expression of *Playrr* and consistent with conserved *Pitx2* binding sites within in its promoter region.

Extensive characterization of the 3-dimensional topology of the locus in nuclei of embryos and cultured cells using fluorescent in situ hybridization (FISH) establishes that there exists a constitutive, cell-type invariant topology of the *Pitx2* locus. In the nuclei of cells in vivo and in vitro, looping across the gene desert brings the proximal and distal ends in closer proximity than would be expected given the length of the intervening genomic sequence, nearly 600kb in chicken and 1Mb in mouse. The presence of this long-range constitutive association is supported by chromatin interaction maps detected by HiC analysis in mouse embryonic stem cells (mESCs) (Shen et al. 2012).

Within this invariant topology, analysis in both chicken and mouse found that for genes exhibiting complementary asymmetric in the DM, there is subtle but statistically significant differences in their proximity in the nuclei of the left vs. right DM. Specifically, it was found that in the left DM where *Pitx2* is expressed, *Playrr* is in closer proximity to *Pitx2*, while in the right DM absence of *Pitx2* expression and an

increased separation was associated with right specific expression of *Playrr*. Right isomerism of the DM due to Pitx2 mutation also results in the loss of asymmetry of Playrr-Pitx2 proximity in nuclei of the DM, supporting the biological relevance of the small differences in proximity.

While, the functional significance of these small differences in proximity represents an enigmatic finding, the nature of the labeling scheme used in the analysis is important to bear in mind. Other than the ASE enhancer embedded in the last intron of *Pitx2* itself, the analysis of the locus to date has not identified strictly noncoding regulatory elements with asymmetric activity. Therefore, the FISH probes used in this study all target transcribed genes and locus topology has been defined by the relative position of these genes to each other rather than in reference to enhancers with validated asymmetric activity which would be more likely to reveal asymmetric regulatory topology of the locus in nuclei of the left or right DM. The small differences in mean separation of genes in the left of right DM is accompanied by rather broad distribution of measured interprobe distances measured which may also be reflective of the challenge of defining an asymmetric regulatory topology for the locus in the absence of additional asymmetric enhancer elements to provide spatial reference. Alternatively, the ASE element may be the only enhancer at the locus with asymmetric activity in the context of the endogenous locus and other regulatory elements may simply provide transcriptional enhancement but not spatial specificity. Indeed this is the case for recently analyzed regulatory sequence from the locus that were assayed in the context of atrial fibrillation and cardiac function dependent of *Pitx2* expression (Aguirre et al. 2015).

Hence, a key priority for advancing the understanding of regulatory logic and the role of chromatin topology in directing asymmetric *Pitx2* locus expression is further annotation of regulatory potential distributed across the locus. The left vs. right DM GRO-seq data and dREG analysis provides one avenue for identifying additional regulatory elements. A number of dREG peaks appear to be differential between the left and right DM. Unfortunately, efforts to validate these sequences via electroporation of reporter constructs to the chicken DM have so far been unsuccessfully. However, attempts to electroporate know enhancers as positive controls have also failed, suggesting either a technical issue with the reporter constructs or that the DM is refractory to such assays. Transient transgenesis assays in mouse embryos provide an alternative avenue for dREG predicted enhancer validation, however such experiments are currently prohibitively expensive.

Fortunately the lab of Francois Spitz has TRACER mice representing an alternative pathway to regulatory annotation of defined chromosomal intervals (Ruf et al. 2011). TRACER (**T**ransposase and **R**ecombinase-**A**ssociated **C**hromosomal **E**ngineering **R**esource) utilizes a LacZ reporter for detecting regulatory activity in the vicinity of the integration site in combination with Sleeping Beauty transposon allowing controlled remobilization and local hoping to survey the regulatory landscape in the region of the initial integration. Additionally, loxP sites incorporated into the Sleeping Beauty vector are also propagated by transposition and provide the means to engineered chromosomal rearrangements such as deletions and inversions (Hérault et al. 1998; Spitz et al. 2005). Therefore, a single integrant represents a resource for both regulatory annotation and functional dissection of a defined chromosomal region.

Importantly, mouse stocks harboring a *Pitx2* locus TRACER integrated within the gene desert have been identified and received from the Spitz lab and are awaiting release to our animal facility from quarantine and acclimation.

Finally the complementary asymmetric expression of the lncRNA *Playrr* represents the most conserved aspect of both locus expression and topology between chicken and mouse. Although a complete understanding of lncRNA function and biology is still emerging, a common theme appears to be transcriptional regulation (Rinn and Chang 2012; Vance and Ponting 2014). Therefore, defining the function of *Playrr* in vivo will also be critical. Interestingly, targeted negative regulation of *Pitx2* expression by the lncRNA Fendrr has recently been documented (Grote et al. 2013; Grote and Herrmann 2013), however, to our knowledge *Playrr* represents the first lncRNA with demonstrated asymmetric expression. Whether this is a secondary consequence to mechanisms controlling *Pitx2* expression or if right-specific *Playrr* expression influences expression from the locus is a key question.

Using CRISPR/Cas9 mediated genome editing we have generated a series of deletions and targeted disruptions of the *Playrr* locus, and the phenotypic analysis of these mutant mice is currently underway. Interestingly, although full validation of the targeted disruption of *Playrr* is still needed, initial qRT-PCR analysis indicates that *Playrr* homozygotes exhibit elevated *Pitx2* expression levels in the developing visceral organs, suggesting reciprocal negative feedback between Pitx2 and Playrr expression and consistent with the negative regulation of *Pitx2* expression by the lncRNA *Fendrr* (Grote et al. 2013; Grote and Herrmann 2013).

REFERENCES

Aguirre LA, Alonso ME, Badía-Careaga C, Rollán I, Arias C, Fernández-Miñán A, López-Jiménez E, Aránega A, Gómez-Skarmeta JL, Franco D, et al. 2015. Long-range regulatory interactions at the 4q25 Atrial Fibrillation risk locus involve PITX2c and ENPEP. *BMC Biol* **13**: 26. http://www.biomedcentral.com/1741-7007/13/26 (Accessed April 29, 2015).

Ai X, Do A-T, Lozynska O, Kusche-Gullberg M, Lindahl U, Emerson CP. 2003. QSulf1 remodels the 6-O sulfation states of cell surface heparan sulfate proteoglycans to promote Wnt signaling. *J Cell Biol* **162** : 341–351. http://jcb.rupress.org/content/162/2/341.abstract.

Applegate K. 2009. Evidence-based diagnosis of malrotation and volvulus. *Pediatr Radiol* **39**: 161–163. http://dx.doi.org/10.1007/s00247-009-1177-x.

Applegate KE, Goske MJ, Pierce G, Murphy D. 1999. Situs Revisited: Imaging of the Heterotaxy Syndrome. *RadioGraphics* **19**: 837–852. http://dx.doi.org/10.1148/radiographics.19.4.g99jl31837.

Bitgood MJ, McMahon AP. 1995. Hedgehog and Bmp genes are coexpressed at many diverse sites of cell-cell interaction in the mouse embryo. *Dev Biol* **172**: 126–138.

Cervantes S, Yamaguchi TP, Hebrok M. 2009. Wnt5a is essential for intestinal elongation in mice. *Dev Biol* **326**: 285–294.

Davis NM, Kurpios NA, Sun X, Gros J, Martin JF, Tabin CJ. 2008. The Chirality of Gut Rotation Derives from Left-Right Asymmetric Changes in the Architecture of the Dorsal Mesentery. *Dev Cell* **15**: 134–145.

Dhoot GK, Gustafsson MK, Ai X, Sun W, Standiford DM, Emerson CP. 2001. Regulation of Wnt signaling and embryo patterning by an extracellular sulfatase. *Science* **293**: 1663–1666.

Economou AD, Ohazama A, Porntaveetus T, Sharpe PT, Kondo S, Basson MA, Gritli-Linde A, Cobourne MT, Green JBA. 2012. Periodic stripe formation by a Turing mechanism operating at growth zones in the mammalian palate. *Nat Genet* **44**: 348–351.

Filmus J, Capurro M, Rast J. 2008. Glypicans. *Genome Biol* **9**: 224.

Giráldez AJ, Copley RR, Cohen SM. 2002. HSPG modification by the secreted enzyme Notum shapes the Wingless morphogen gradient. *Dev Cell* **2**: 667–676.

Green JBA, Sharpe J. 2015. Positional information and reaction-diffusion: two big ideas in developmental biology combine. *Dev* **142** : 1203–1211. http://dev.biologists.org/content/142/7/1203.abstract.

Grote P, Herrmann BG. 2013. The long non-coding RNA Fendrr links epigenetic control mechanisms to gene regulatory networks in mammalian embryogenesis. *RNA Biol* **10**: 1579–1585. http://www.ncbi.nlm.nih.gov/pubmed/24036695.

Grote P, Wittler L, Hendrix D, Koch F, Währisch S, Beisaw A, Macura K, Bläss G, Kellis M, Werber M, et al. 2013. The Tissue-Specific lncRNA Fendrr Is an Essential Regulator of Heart and Body Wall Development in the Mouse. *Dev Cell* **24**: 206–214.

Häcker U, Nybakken K, Perrimon N. 2005. Heparan sulphate proteoglycans: the sweet side of development. *Nat Rev Mol Cell Biol* **6**: 530–541.

Hérault Y, Rassoulzadegan M, Cuzin F, Duboule D. 1998. Engineering chromosomes in mice through targeted meiotic recombination (TAMERE). *Nat Genet* **20**: 381–384.

Jugessur A, Murray JC. 2005. Orofacial clefting: Recent insights into a complex trait. *Curr Opin Genet Dev* **15**: 270–278.

Kurpios NA, Ibañes M, Davis NM, Lui W, Katz T, Martin JF, Belmonte JCI, Tabin CJ. 2008. The direction of gut looping is established by changes in the extracellular matrix and in cell:cell adhesion. *Proc Natl Acad Sci* **105** : 8499–8506. http://www.pnas.org/content/105/25/8499.abstract.

Lu MF, Pressman C, Dyer R, Johnson RL, Martin JF. 1999. Function of Rieger syndrome gene in left-right asymmetry and craniofacial development. *Nature* **401**: 276–278.

Mahadevan A, Welsh ICC, Sivakumar A, Gludish DWW, Shilvock ARR, Noden DMM, Huss D, Lansford R, Kurpios NAA. 2014. The Left-Right Pitx2 Pathway Drives Organ-Specific Arterial and Lymphatic Development in the Intestine. *Dev Cell* **31**: 690–706. http://www.cell.com/article/S1534580714006959/fulltext (Accessed December 11, 2014).

Neri G, Gurrieri F, Zanni G, Lin A. 1998. Clinical and molecular aspects of the Simpson-Golabi-Behmel syndrome. In *American Journal of Medical Genetics*, Vol. 79 of, pp. 279–283.

O'Connell MP, Fiori JL, Kershner EK, Frank BP, Indig FE, Taub DD, Hoek KS, Weeraratna AT. 2009. Heparan sulfate proteoglycan modulation of Wnt5A signal transduction in metastatic melanoma cells. *J Biol Chem* **284**: 28704–28712.

Pilia G, Hughes-Benzie RM, MacKenzie A, Baybayan P, Chen EY, Huber R, Neri G, Cao A, Forabosco A, Schlessinger D. 1996. Mutations in GPC3, a glypican gene, cause the Simpson-Golabi-Behmel overgrowth syndrome. *Nat Genet* **12**: 241–247.

Rinn JL, Chang HY. 2012. Genome Regulation by Long Noncoding RNAs. *Annu Rev Biochem* **81**: 145–166.

Ruf S, Symmons O, Uslu VV, Dolle D, Hot C, Ettwiller L, Spitz F. 2011. Large-scale analysis of the regulatory architecture of the mouse genome with a transposon-associated sensor. *Nat Genet* **43**: 379–386.

Shen Y, Yue F, McCleary DF, Ye Z, Edsall L, Kuan S, Wagner U, Dixon J, Lee L, Lobanenkov V V., et al. 2012. A map of the cis-regulatory sequences in the mouse genome. *Nature* **488**: 116–120.

Shiratori H, Hamada H. 2006. The left-right axis in the mouse: from origin to morphology. *Development* **133**: 2095–2104.

Skidmore JM, Cramer JD, Martin JF, Martin DM. 2008. Cre fate mapping reveals lineage specific defects in neuronal migration with loss of Pitx2 function in the developing mouse hypothalamus and subthalamic nucleus. *Mol Cell Neurosci* **37**: 696–707.

Song HH, Filmus J. 2002. The role of glypicans in mammalian development. *Biochim Biophys Acta - Gen Subj* **1573**: 241–246.

Spitz F, Herkenne C, Morris MA, Duboule D. 2005. Inversion-induced disruption of the Hoxd cluster leads to the partition of regulatory landscapes. *Nat Genet* **37**: 889–893.

Tao Y, Zhang M, Li L, Bai Y, Zhou Y, Moon AM, Kaminski HJ, Martin JF. 2014. Pitx2, an atrial fibrillation predisposition gene, directly regulates ion transport and intercalated disc genes. *Circ Cardiovasc Genet* **7**: 23–32.

Traister A, Shi W, Filmus J. 2008. Mammalian Notum induces the release of glypicans and other GPI-anchored proteins from the cell surface. *Biochem J* **410**: 503–511.

Turing AM. 1952. The Chemical Basis of Morphogenesis. *Philos Trans R Soc London B Biol Sci* **237**: 37–72. http://rstb.royalsocietypublishing.org/content/237/641/37.abstract.

Vance KW, Ponting CP. 2014. Transcriptional regulatory functions of nuclear long noncoding RNAs. *Trends Genet* **30**: 348–355. http://www.sciencedirect.com/science/article/pii/S0168952514000869.

Volkmann BA, Zinkevich NS, Mustonen A, Schilter KF, Bosenko D V., Reis LM, Broeckel U, Link BA, Semina E V. 2011. Potential novel mechanism for Axenfeld-Rieger syndrome: Deletion of a distant region containing regulatory elements of PITX2. *Investig Ophthalmol Vis Sci* **52**: 1450–1459.

Waite MR, Skidmore JM, Micucci JA, Shiratori H, Hamada H, Martin JF, Martin DM. 2013. Pleiotropic and isoform-specific functions for Pitx2 in superior colliculus and hypothalamic neuronal development. *Mol Cell Neurosci* **52**: 128–139.

Welsh IC, Hagge-Greenberg A, O'Brien TP. 2007. A dosage-dependent role for Spry2 in growth and patterning during palate development. *Mech Dev* **124**: 746–61. http://www.pubmedcentral.nih.gov/articlerender.fcgi?artid=2043129&tool=pmcentrez&rendertype=abstract (Accessed April 1, 2014).

Welsh IC, Thomsen M, Gludish DW, Alfonso-Parra C, Bai Y, Martin JF, Kurpios N a. 2013. Integration of left-right Pitx2 transcription and Wnt signaling drives asymmetric gut morphogenesis via Daam2. *Dev Cell* **26**: 629–44. http://www.ncbi.nlm.nih.gov/pubmed/24091014 (Accessed March 27, 2014).

APPENDIX

Supplementary Figures Related to Chapters 3 & 4

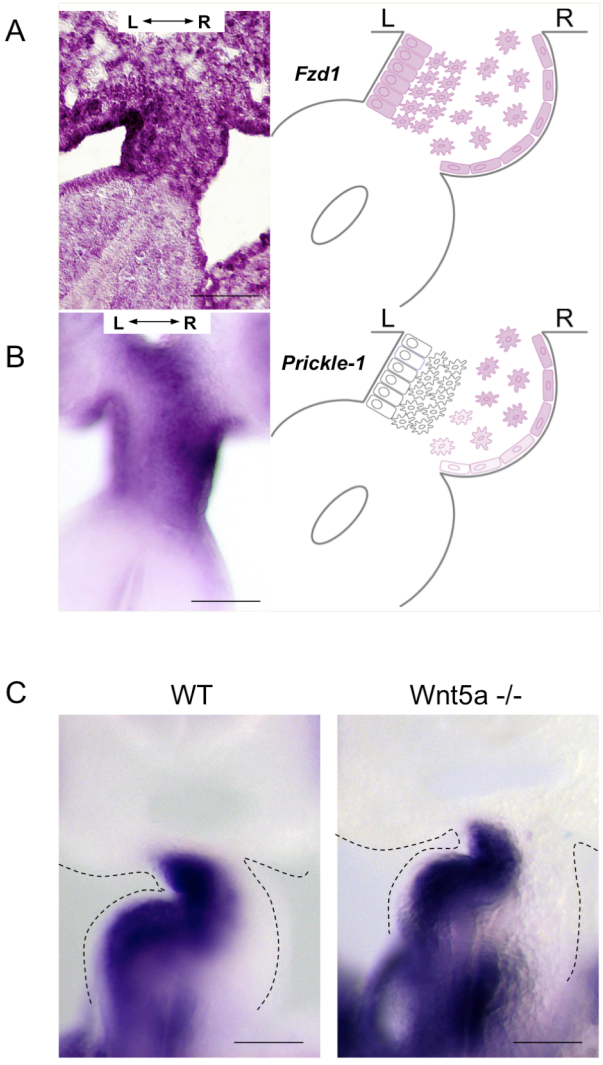

FIGURE S3.1. Asymmetric organization of a Wnt signaling network across the L-R DM. **A** Bilateral expression of *Fzd1* in the DM at HH21. **B** Right-to-left expression gradient of *Prickle-1* in the DM at HH21 (**related to Fig. 1**). **C** Expression of Pitx2 in WT and Wnt5a-null mouse embryos at E10.75 (**related to Fig. 7**). Scale bars: **AB** (100 μm); **C** (50 μm).

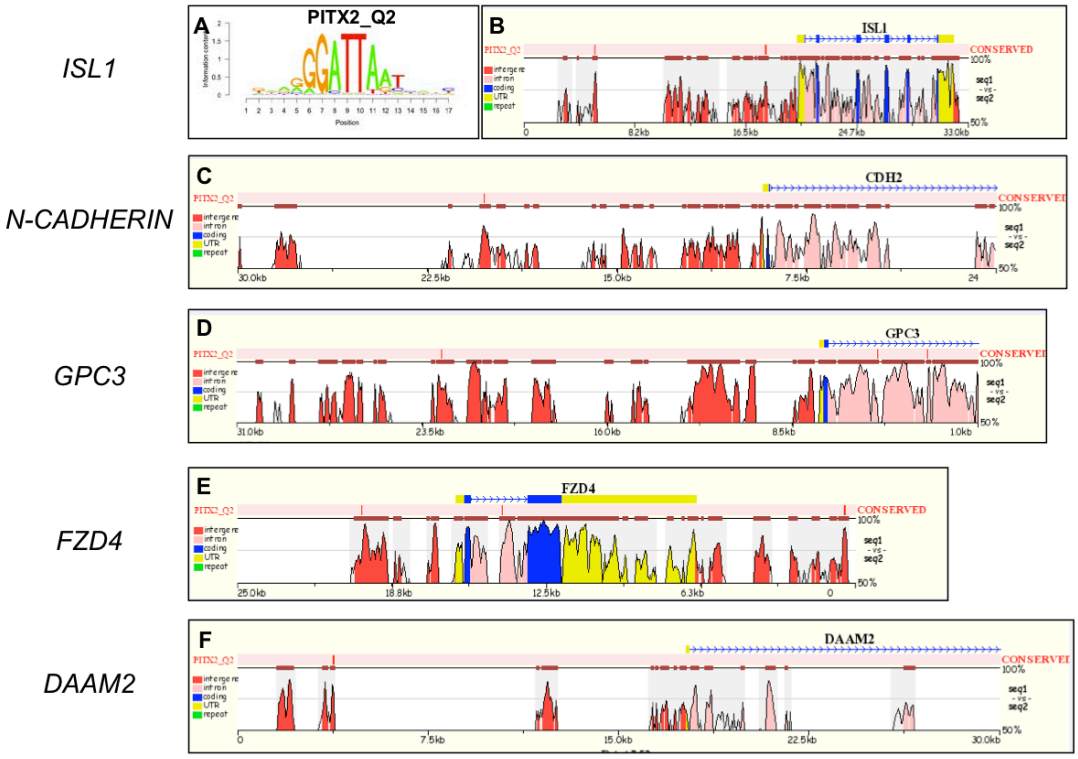

FIGURE S3.2. Computational sequence analysis to identify Pitx2 recognition sites conserved between human and mouse (related to Fig. 2). A Logo representation of the PITX2_Q2 position weight matrix used to search loci for possible Pitx2 binding sites. **B-F** rVista plots showing promoter proximal regions of known (*ISL1*, B and *N-CADHERIN*, C) and potential (D-F) Pitx2 targets that our work has identified. Sequences conserved between human and mouse (>70% over 100bp) are displayed as peaks color coded with respect to their genomic annotation (*red*: intergenic, *pink*: intronic, *yellow*: UTR, *blue*: coding, *green*: repetitive) and the direction of transcription is indicated by blue arrowheads in the gene model. The position of conserved Pitx2 binding site predictions are indicated by a *red* tic above the corresponding conserved peak. Consistent with a role in positive regulation of Wnt signaling, we have predicted conserved Pitx2 binding sites at genes known to either potentiate Wnt signaling such as *GPC3* (D), or in the case of *FZD4* (G) and *DAAM2* (H) to directly mediate its influence on cells.

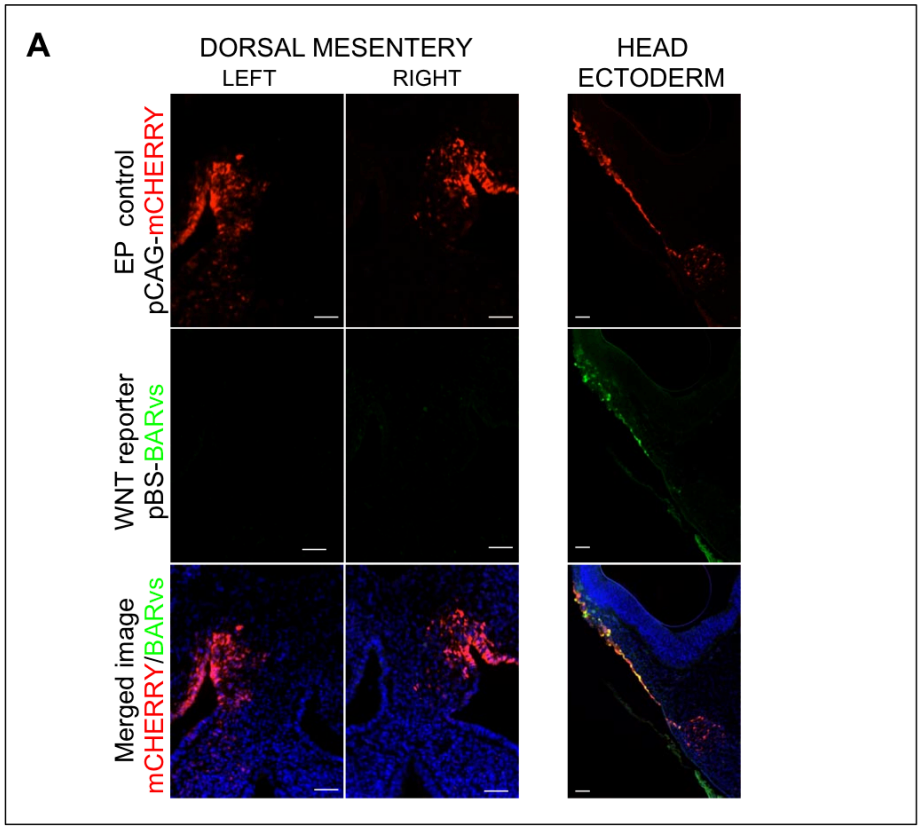

FIGURE S3.3. Lack of pBS-BARvs and BAT-GAL activity in the chick and mouse DM, respectively (related to Fig. 3). A In ovo electroporation of the canonical Wnt reporter construct pBS-BARvsTOP-dsRED (*green*) into the left and right DM (*left*) or the head ectoderm (*right*). mCHERRY (*red*) identifies electroporated cells. *Blue* is DAPI. **B** Two midgut sections isolated from E10.5 transgenic BAT-GAL mouse embryos reporting β-galactosidase activity (blue) in the gut mesenchyme only; boxes highlight the DM which lacks β-galactosidase activity, consistent with the pBS-BARvsTOP-dsRED data in ovo. As a positive control, a section of the neural tube from the same embryo shows high β-galactosidase activity. Scale bars: **AB** (50 μm).

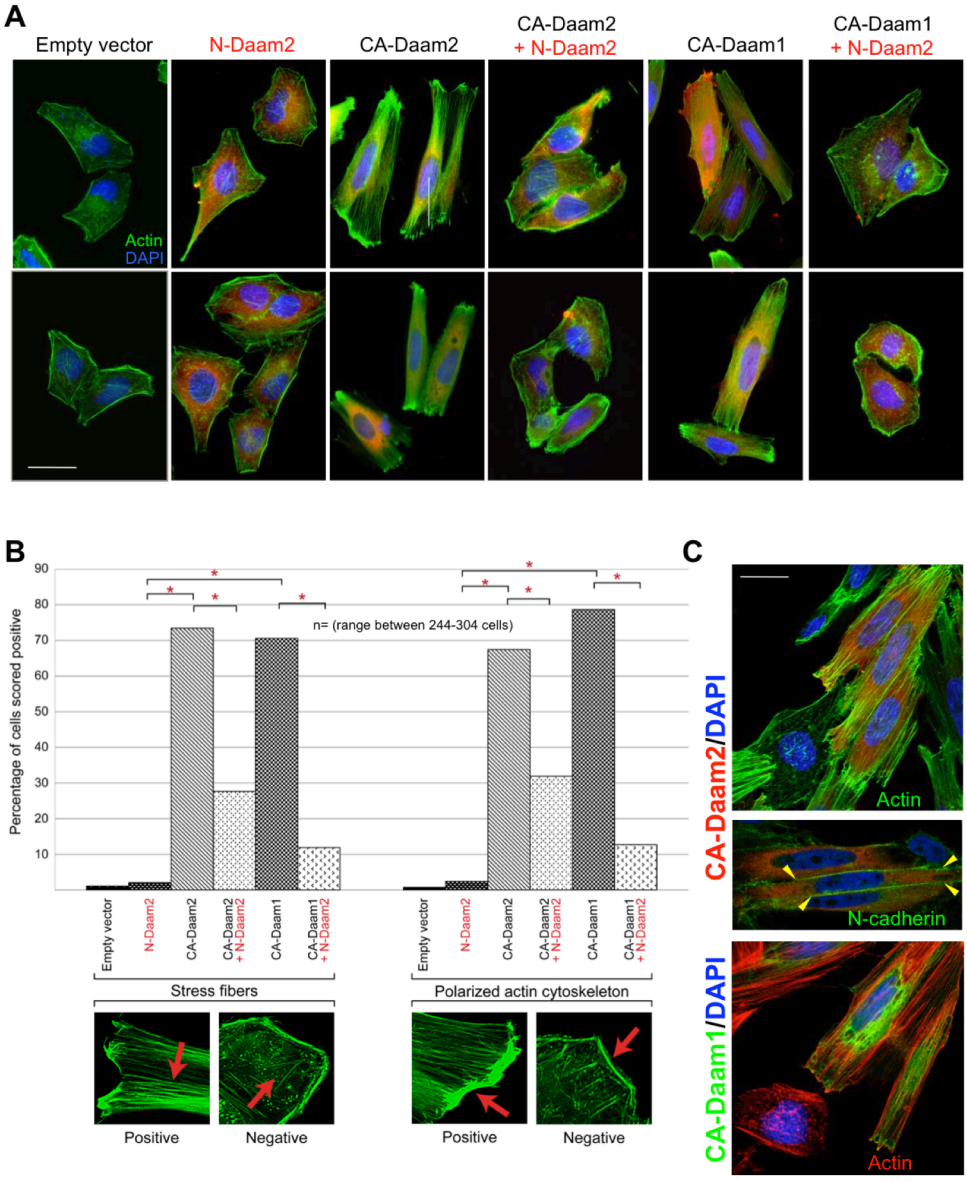

FIGURE S3.4. N-Daam2 rescues CA-Daam2 activation phenotype in cultured HeLa cells (related to Fig. 4). A Cultured HeLa cells 48 hours post-transfection with the indicated constructs; two representative fields shown for each construct (top and bottom rows). N-Daam2 ablates polarized stress fiber formation when co-transfected with CA-Daam2 or CA-Daam1. **B** Quantification of (**A**): multiple 20x fields were scored for stress fibers or polarized cytoskeletal elements using Phalloidin-488 (scoring phenotypes inset). Significance was established using the chi-squared test (n=244-304 cells). **C** CA-Daam2 overexpression in HeLa cells, stained for actin stress fibers (**C**, *top* panel) and N-cadherin (**C**, *middle* panel), which is organized specifically at the junctions between neighboring cells.

Comparable activation phenotype is evident with CA-Daam1 (**C**, *bottom* panel). Scale bars: **A** (20 μm); **C** (15 μm).

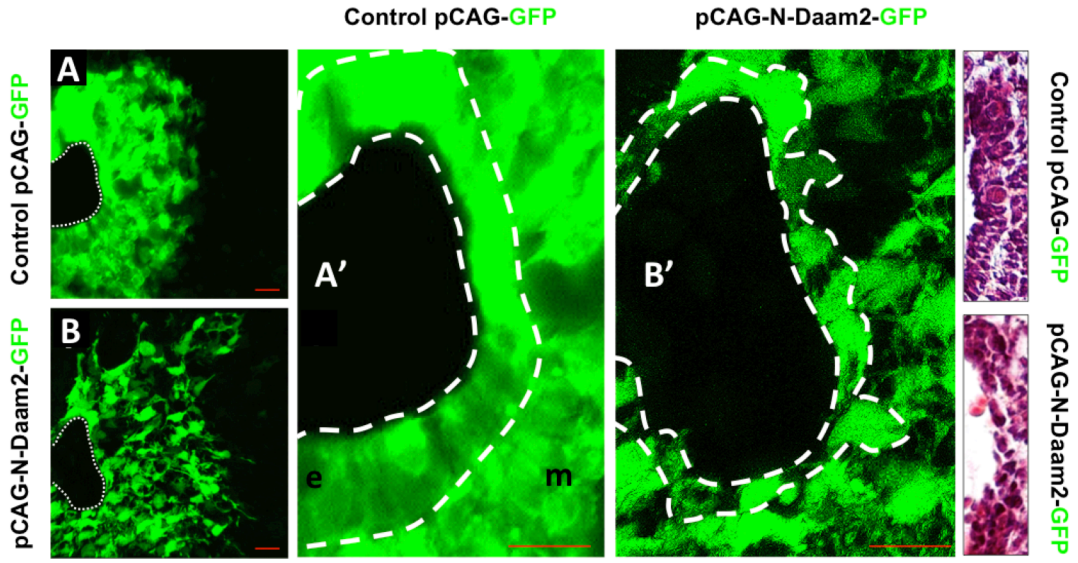

FIGURE S5. Left-sided N-Daam2 electroporation perturbs the integrity of columnar epithelial cells in the DM (related to Fig. 4). GFP epifluorescence images of embryos electroporated with pCAG-GFP control **(A)** or pCAG-CA-Daam2 **(B)**, with corresponding H&E images (far right, taken from Figure 3) to highlight the effect of pCAG-N-Daam2 on the integrity of the epithelial compartment of the DM. Panels A' and B' are higher magnification of A and B, respectively. **H&E images**, *top*: WT left epithelium; *bottom*: pCAG-N-Daam2 electroporated epithelium. Epithelial (e) and mesenchymal (m) compartments are labeled. Scale bars: (15 μm).

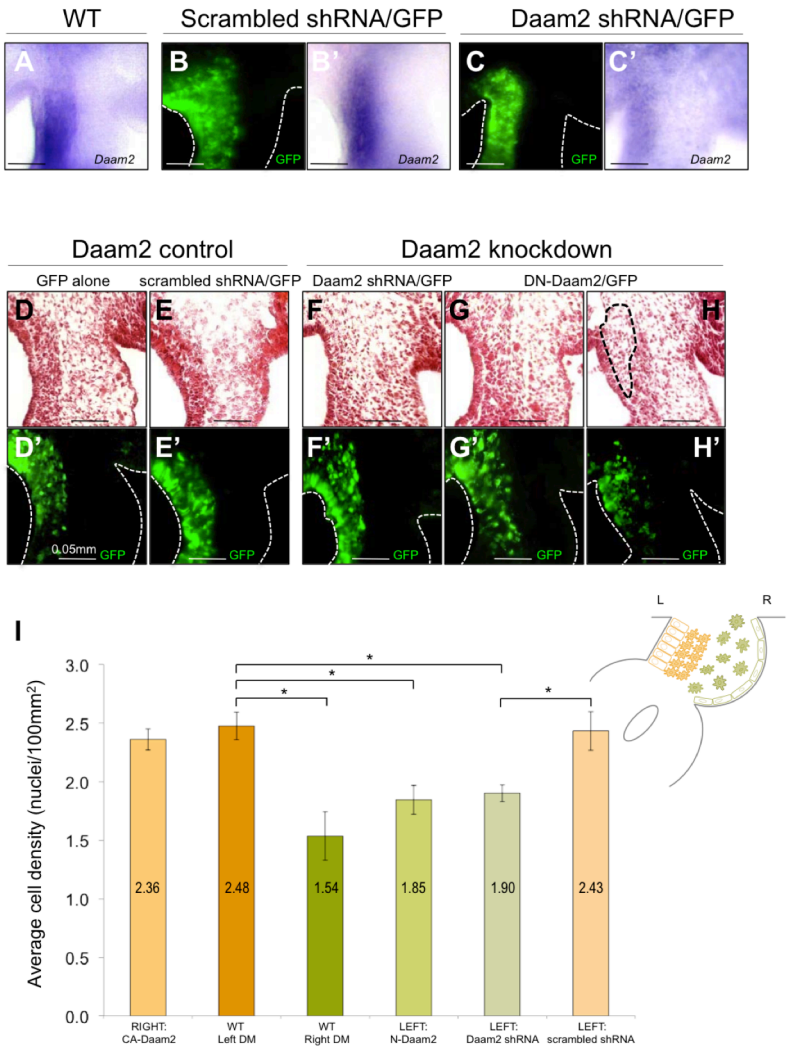

FIGURE S3.6. Daam2 shRNA electroporation in the left DM impairs mesenchymal compaction and mirrors the effects of N-Daam2 (related to Fig. 4). A-C' The effect of knockdown of endogenous Daam2 using electroporated RCAS-Daam2-shRNA **(CC')** was verified using ISH compared to either WT embryos **(A)** or to a mutant shRNA scrambled control (**BB'**). **D-H'** Electroporation of RCAS-Daam2-shRNA disrupts mesenchymal condensation (compare **EE'** to **FF'**) and this phenotype is comparable to N-Daam2-electroporated mesenchyme (compare **FF'** to **G-H'**). Specificity of the Daam2 knockdown was confirmed with scrambled shRNA (compare **EE'** to **FF'**) and with GFP electroporation (**EE'** vs. **DD'**). **I** Morphometric analysis of mesenchymal cell density of WT and electroporated tissue sections as measured by the number of nuclei per 100 μm^2. For **WT Left**: mean 2.476, S.E.M 0.119, n=4; for **WT Right:** mean 1.536, S.E.M. 0.208, n=4; for **N-Daam2**: mean 1.846, S.E.M. 0.124, n=3; for **RCAS-Daam2-shRNA**: mean is 1.902, S.E.M. 0.072, n=6; for **scrambled shRNA**: mean is 2.266, S.E.M. 0.159, n=3. For pairwise statistical analysis: $p<0.0078$ for **WT Left vs. WT Right**; $p<0.0056$ for **CA-Daam2 Right vs. WT Right**; $p<0.0155$ for **N-Daam2 Left vs. WT Left**; $p<0.0023$ for **WT Left vs. RCAS-Daam2-shRNA Left**; $p<0.0441$ for **scrambled shRNA Left vs. RCAS-Daam2-shRNA Left**; $p<0.688$ for **N-Daam2 Left vs. RCAS-Daam2-shRNA Left**; and $p<0.839$ for **WT Left vs. scrambled shRNA Left**. Scale bars: **A-H'** (50 μm).

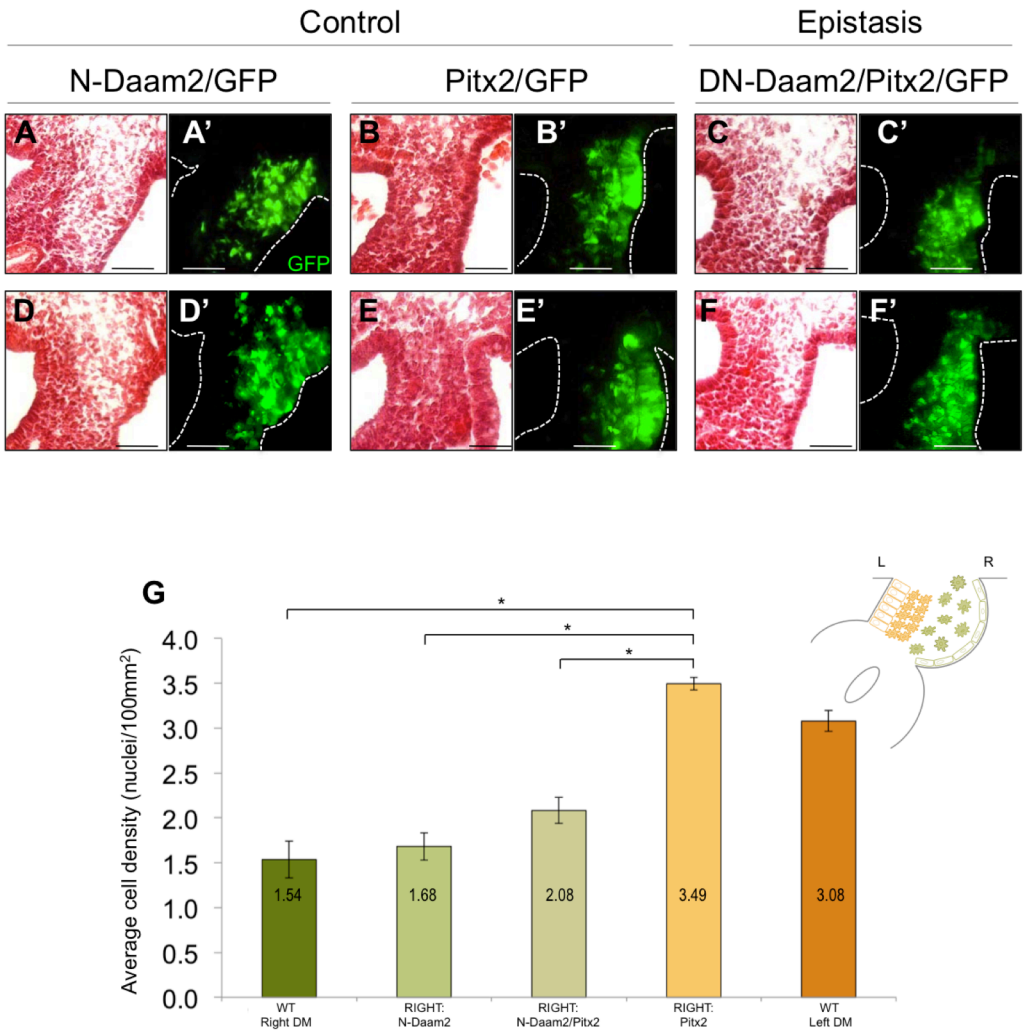

FIGURE S3.7. N-Daam2 rescues the effects of Pitx2 in the DM as demonstrated by an epistasis experiment using co-electroporation (related to Fig. 4). A-D' Electroporation of N-Daam2 alone on the right side of the DM had no significant effect on cell behaviors. **B** Electroporation of Pitx2 alone on the right side of the DM induced mesenchymal condensation and epithelial cell shape change. **C-F'** Co-electroporation of N-Daam2 and Pitx2 significantly impaired the ability of Pitx2 to induce mesenchymal condensation and epithelial cell shape change in the right DM. **G** Morphometric analysis of mesenchymal cell density of WT and electroporated tissue sections as measured by the number of nuclei per 100 um^2. For **WT Left:** mean 3.079, S.E.M. 0.115, n=6; for **WT Right:** mean 1.536, S.E.M. 0.208, n=4; for **N-Daam2 Right:** mean 1.682, S.E.M. 0.154, n=3; for **Pitx2 Right:** mean 3.495, S.E.M. 0.068, n=2; for **N-Daam2/Pitx2 Right**: mean 2.082, S.E.M. 0.144, n=3. For statistical analysis: $p<0.0078$ for **WT Left vs. WT Right**; $p<0.622$ for **WT Right vs. N-Daam2 right**; $p< 0.003$ for **WT Right and Pitx2 Right**; $p<0.103$ for **WT Right and N-Daam2/Pitx2 Right**; and $p<0.005$ for **Pitx2 Right and N-Daam2/Pitx2 Right**. Scale bars: **A-F'** (50 µm).

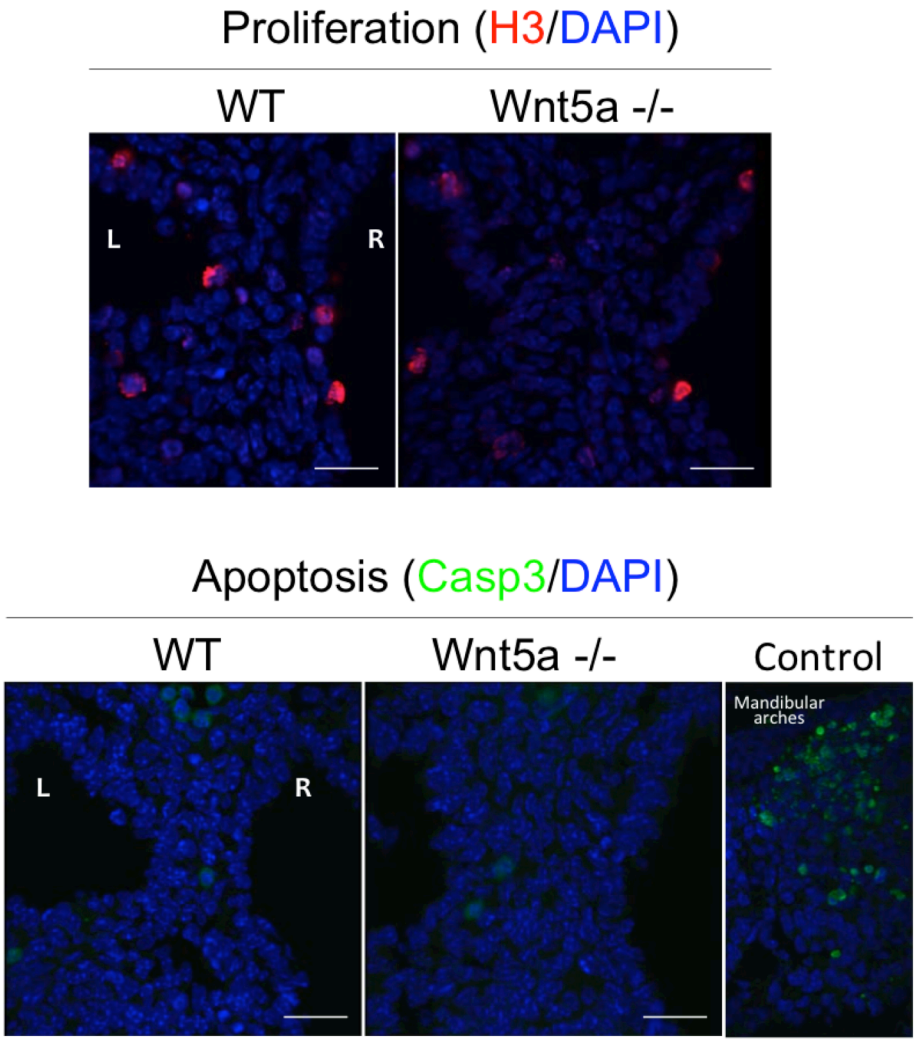

FIGURE S3.8. Loss of Wnt5a has no effect on cell proliferation or death in the DM (related to Fig. 7). *Top*: proliferation assay using phosphorylation of histone H3 (anti-H3, *red*). *Bottom*: cell death assay using anti-caspase-3 (*green*). *Blue* is DAPI. Apoptotic cells (positive for anti-caspase-3) normally present in mandibular arches were used as a positive control. Scale bars: (25 μm, proliferation; 50 μm, apoptosis).

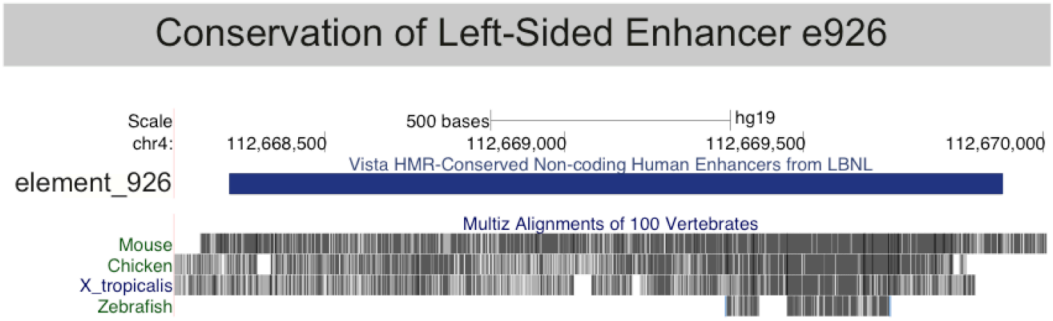

Figure S4.1. Multiz alignment showing conservation of human enhancer element e926 (Vista, blue bar) in mouse, chicken, frog, and fish.

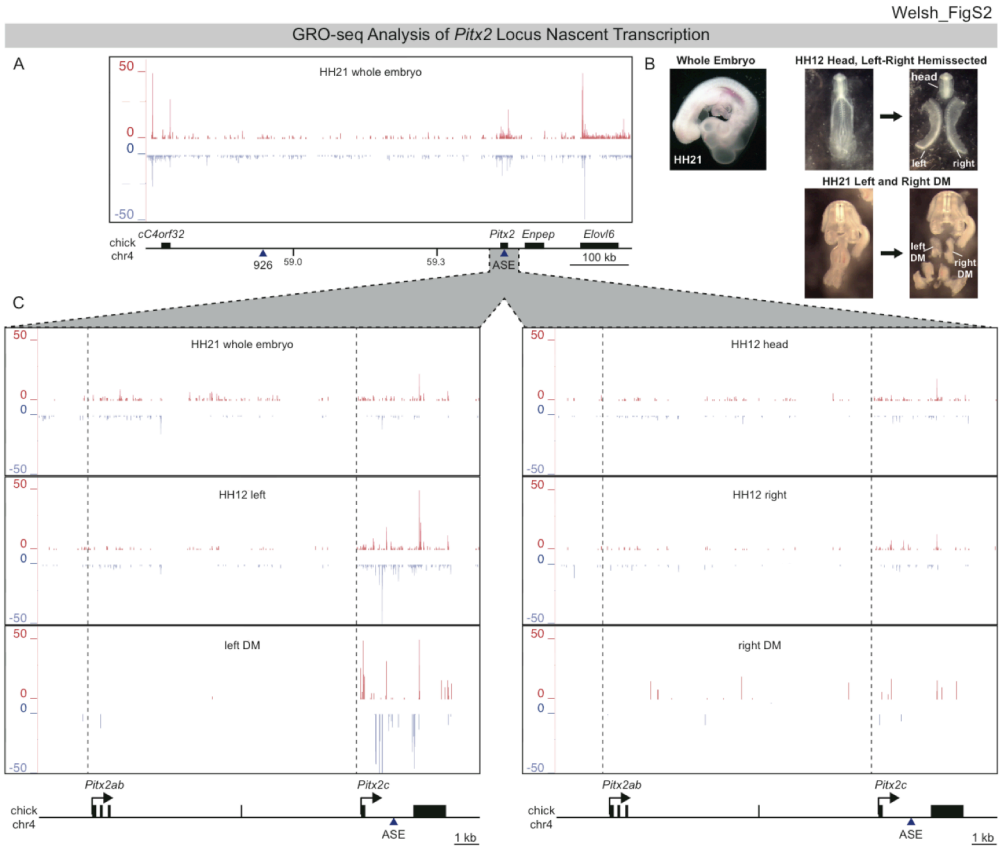

Figure S4.2. Annotation of asymmetric *Pitx2* locus transcription in vivo. (A) GRO-seq of HH21 whole embryo characterizes nascent transcription across the *Pitx2* locus. (B) Whole embryo, HH12 head, and HH12 left & right hemisected samples were collected in addition to HH21 left and right DM samples to monitor enrichment and specificity of asymmetric transcription. (C) Transcription of bilaterally expressed *Pitx2ab* isoforms is observed in HH21 whole embryo and HH12 head. Elevated *Pitx2* expression is observed in the HH12 left hemisected sample compared to the right, while only the left DM sample detects exclusive *Pitx2c* expression. Dashed vertical lines mark *Pitx2ab* and *Pitx2c* TSS.

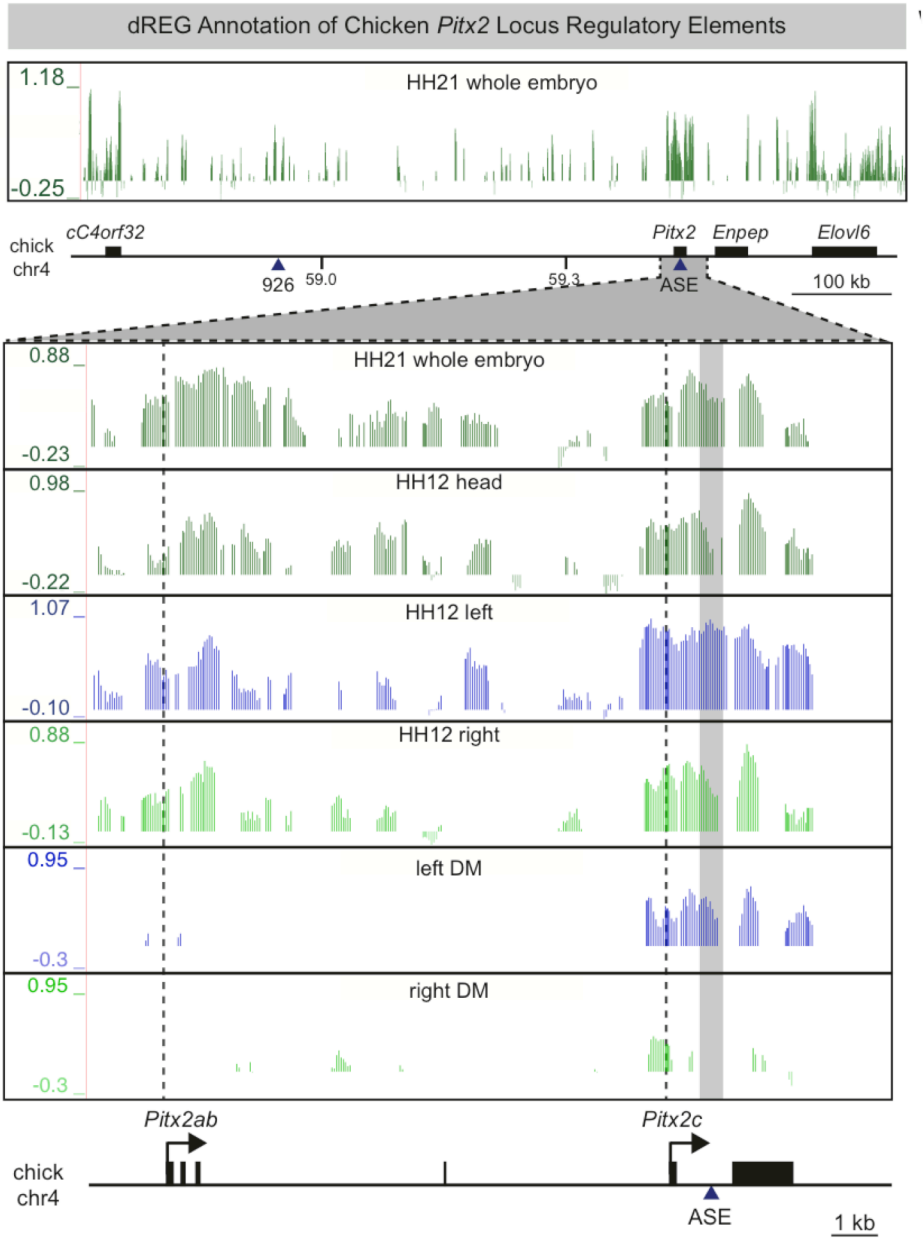

Figure S4.3. In vivo annotation of active regulatory elements at the *Pitx2* locus. (Top) dREG annotation of the *Pitx2* locus from GRO-seq of HH21 whole embryo sample identifies a considerable number of distal regulatory elements distributed across the gene desert in addition to peaks more closely associated with coding genes. (Bottom) dREG peaks in the left DM sample demonstrates enrichment of asymmetric *Pitx2c* specific peaks and in the right DM shows absence of ASE activity. Dashed vertical lines mark *Pitx2ab* and *Pitx2c* TSS and grey box marks the ASE for reference.

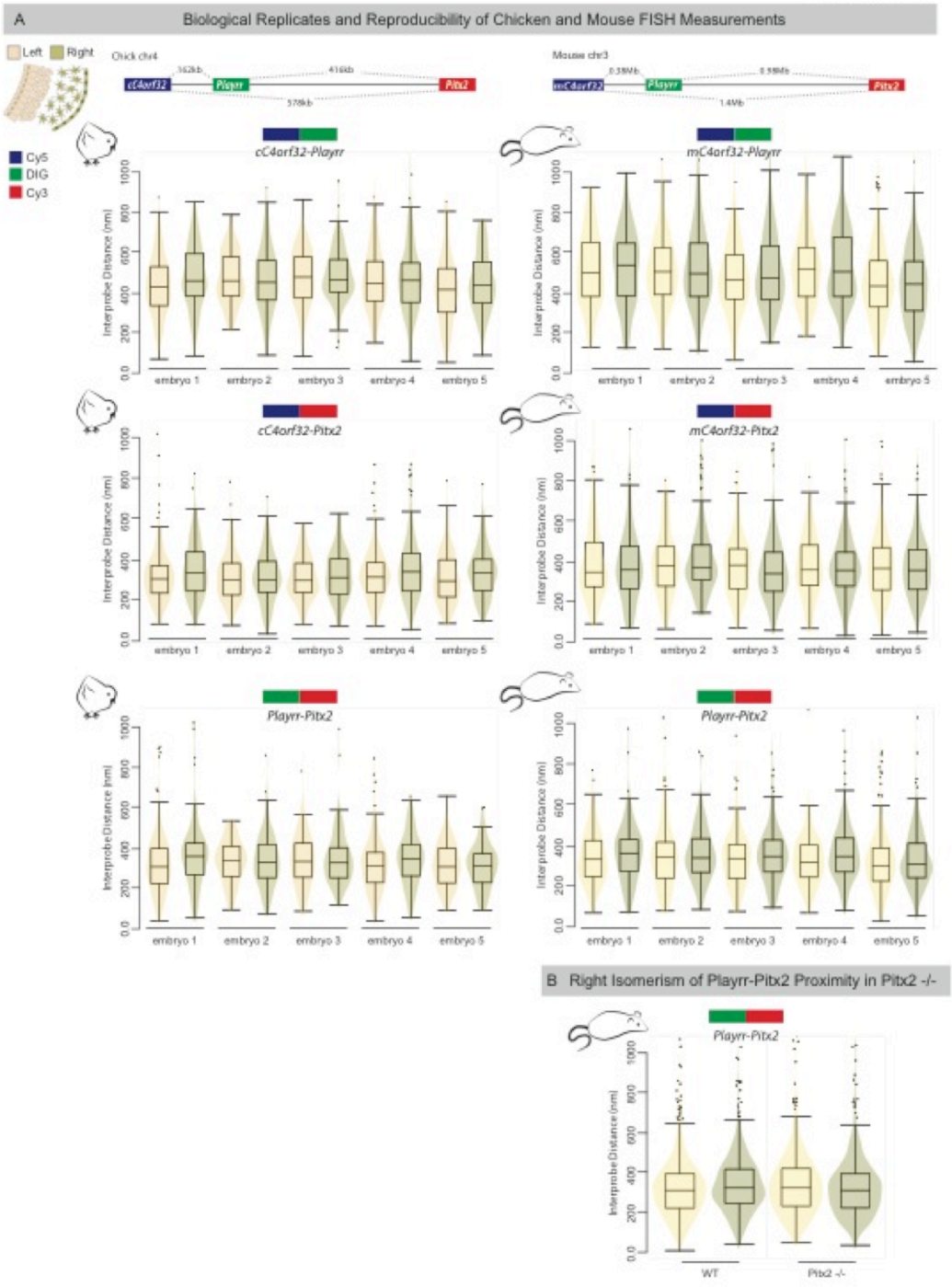

Figure S4.4. Reproducible L-R differences in chicken and mouse FISH data (A) Increased proximity in the left DM between *cC4orf32-Pitx2* and *Playrr-Pitx2* in chicken, or *Playrr-Pitx2* in mouse, is highly reproducible across biological replicates. Box plots show the lower quartile, median, upper quartile, and whiskers show ±1.5 times the interquartile range. Contour plotting the density of the underlying distribution of the data are color coded for left (tan) and right (green) DM (B) Box plots showing *Playrr-Pitx2* interprobe distances in the left DM of *Pitx2* -/- embryos is indistinguishable from the right DM of WT embryos.

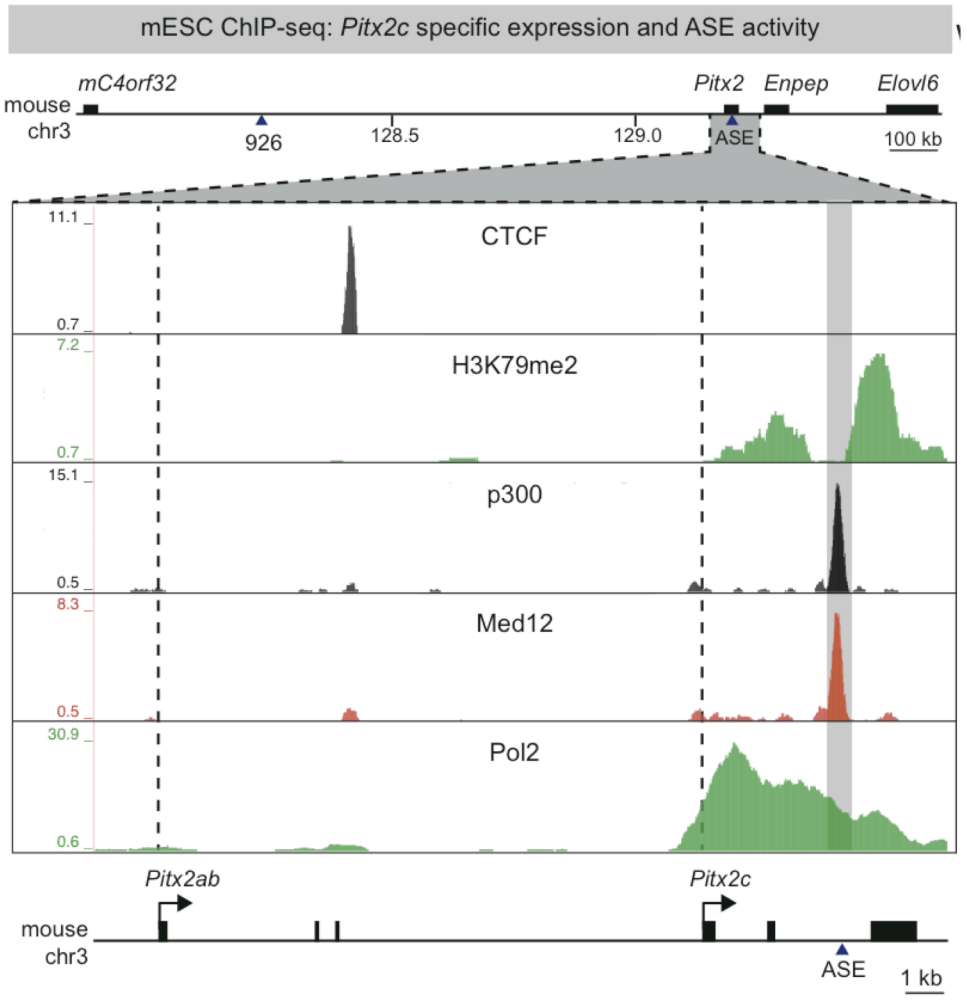

Figure S4.5. ChIP-seq analysis of mouse embryonic stem cells (mESCs). RNA Pol II ChIP-seq data demonstrate that exclusive expression of the asymmetric *Pitx2c* isoform in mESCs is accompanied by binding at the ASE enhancer by positive regulators of transcriptional activation such as Mediator (Med12), p300 and chromatin marks including H3K79 methylation deposited by the DOT1L transcriptional elongation complex via association with RNA Pol II.

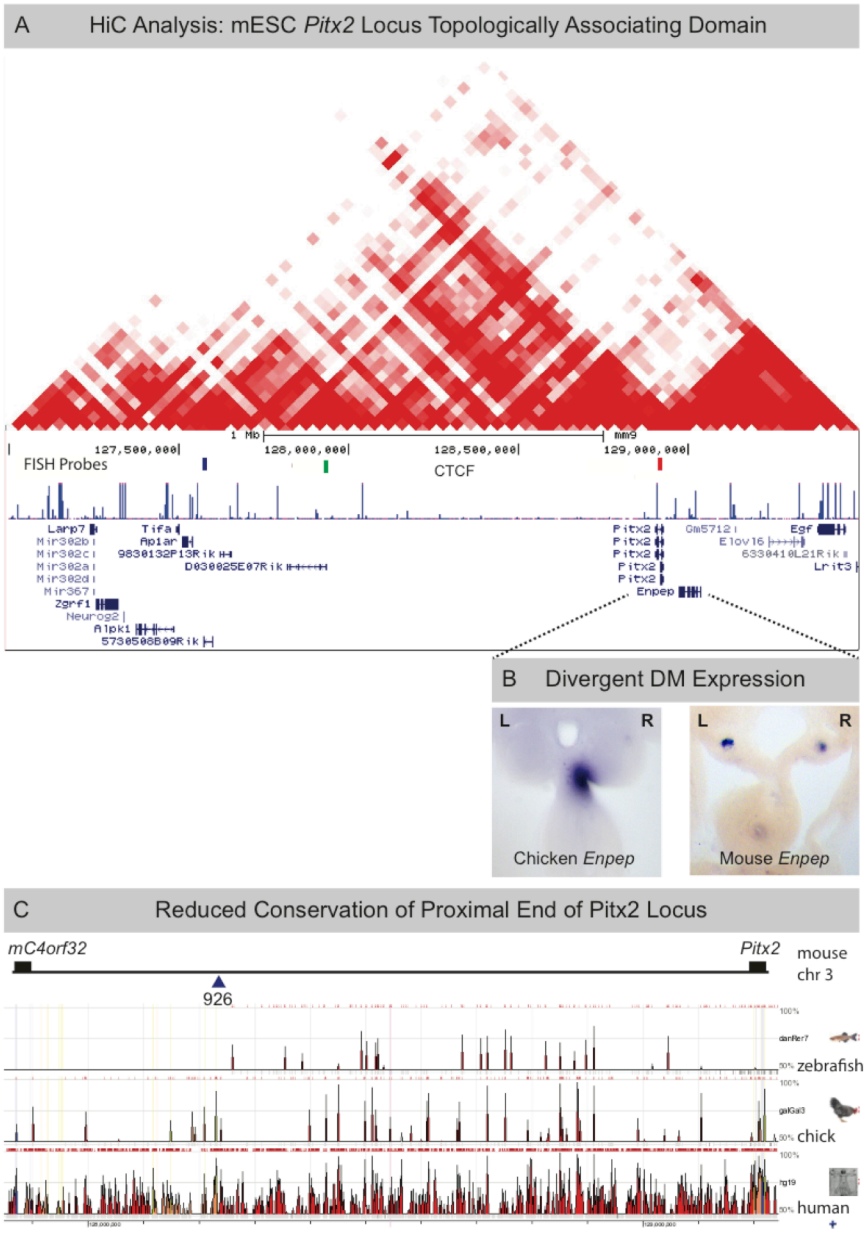

Figure S4.6. Chromatin contact map and evolutionary divergence of the *Pitx2* locus (A) HiC analysis of chromatin contacts in mESCs (Shen et al. 2012; http://yuelab.org/hi-c/) demonstrates preferential contacts spanning the *Pitx2* locus consistent with the presence of a topologically associating domain (TAD) spanning the interval we have analyzed in the current study. Position of mouse FISH used is indicated above CTCF ChIP-seq track. (B) The TAD structure of the *Pitx2* locus in mESCs suggests that *Pitx2* and *Enpep* are positioned within separate regulatory domains is supported by loss of *Enpep* expression in the DM of mouse. (C) Comparison of conserved sequences from the mouse *Pitx2* locus with zebrafish, chicken, and human, supports that evolutionary divergence is greatest at the proximal end of the gene desert. Zebrafish lack an ortholog of *C4ORF32*, and e926 is only minimally conserved (see also Fig. S1).